



HAL
open science

Spatiotemporal properties of sensory integration in the mouse barrel cortex

María Eugenia Vilarchao

► **To cite this version:**

María Eugenia Vilarchao. Spatiotemporal properties of sensory integration in the mouse barrel cortex. Human health and pathology. Université Sorbonne Paris Cité, 2015. English. NNT : 2015USPCB108 . tel-01535987

HAL Id: tel-01535987

<https://theses.hal.science/tel-01535987>

Submitted on 9 Jun 2017

HAL is a multi-disciplinary open access archive for the deposit and dissemination of scientific research documents, whether they are published or not. The documents may come from teaching and research institutions in France or abroad, or from public or private research centers.

L'archive ouverte pluridisciplinaire **HAL**, est destinée au dépôt et à la diffusion de documents scientifiques de niveau recherche, publiés ou non, émanant des établissements d'enseignement et de recherche français ou étrangers, des laboratoires publics ou privés.



Université Paris Descartes

Faculté de Médecine
École doctorale 474 - Frontières du Vivant



Thèse de doctorat de Neurosciences

Spatiotemporal properties of sensory integration in the mouse barrel cortex

Propriétés spatiotemporelles de l'intégration sensorielle dans le cortex à tonneaux de la souris

Par María Eugenia Vilarchao

Dirigée par Daniel Shulz et Isabelle Férézou

Présentée et soutenue publiquement le 27 Novembre 2015, devant un jury composé de :

Laurent	Bourdieu	École Normale Supérieure, Paris	Examineur
Randy	Bruno	Columbia University, New York	Rapporteur
Frédéric	Chavane	Institut de Neurosciences de la Timone, Marseille	Rapporteur
Valentina	Emiliani	Université Paris Descartes, Paris	Examinatrice
Daniel	Shulz	UNIC, Gif-sur-Yvette	Directeur de thèse

Unité de Neurosciences, Information et Complexité (UNIC, CNRS FRE-3693)

Abstract

While rodents explore their environment they actively contact surrounding objects with their array of whiskers, resulting in a complex pattern of multiwhisker deflections. Despite this complexity, the whisker system is able to extract relevant information from the spatiotemporal sequence of deflections to generate touch-dependent behavior. The question that arises is: *How is global multiwhisker information encoded?*

Whiskers are mapped onto layer 4 of the primary somatosensory cortex (S1) as discrete units named “barrels”. Each barrel-related vertical column processes information coming primarily from its corresponding principal whisker (PW). Previous experiments in our lab done with extracellular recordings have revealed that neurons in the rat S1 and thalamus not only show a preferred direction for the local deflection of the PW but also for the direction of a global motion across the whisker pad.

To further understand how the cortical network processes global tactile scenes, we built a set-up that enables to perform voltage sensitive dye imaging of the mouse barrel cortex while applying precise tactile stimuli using a 24-multi-whisker stimulator. We further developed a technical method to map the recorded functional data onto the cortical structure.

We first studied whether local direction selectivity is spatially distributed within the barrel-related column. Responses to different directions were slightly segregated on space close to the barrel center, but the distribution differed from the one previously described in rat S1, namely a pinwheel-like structure.

We then showed that global direction selectivity is spatially organized in the barrel cortex. Columns related to rostral whiskers were more selective to the global direction than columns related to caudal whiskers. Moreover, the columns related to dorsal whiskers preferred ventral global directions, while the columns related to ventral whiskers preferred caudal global directions. Overall the responses to the caudo-ventral global directions were the strongest in average for all the columns.

We showed that the spatial distribution of the global direction selectivity can be explained neither by the high salience of the starting position of the deflections on the whiskerpad (a border effect), nor by the linear summation of the responses to deflections of several whiskers. Responses to the global motion of the whisker array are indeed highly sublinear independently of the direction of stimulation.

In conclusion, we show here that stepping aside from the classical view of the whisker-to-barrel cortex system allows a better understanding of how different features of complex stimuli are processed and how the emergent properties of the cortex, like the global direction selectivity, are built-up.

Résumé

Lorsque les rongeurs explorent leur environnement, ils contactent activement les objets environnants avec leurs vibrisses qui sont ainsi défléchies selon des séquences spatiotemporelles complexes. Le système vibrissal est néanmoins capable d'extraire des informations pertinentes de ces stimulations pour générer un comportement tactile-dépendant. Une question se pose alors: *Comment l'information multivibrissale globale est-elle encodée?*

La représentation corticale des vibrisses au sein du cortex somatosensoriel primaire (S1) du rongeur est dotée de structures anatomiquement remarquables, nommées "tonneaux", au niveau de la couche IV, qui sont organisées de la même manière que les vibrisses sur le museau de l'animal. A chaque "tonneau" correspond une colonne corticale, unité de traitement de l'information, qui reçoit en priorité les informations provenant la vibrisse principale (VP) correspondante. Des enregistrements extracellulaires réalisés dans notre équipe chez le rat ont révélé que les réponses des neurones du cortex S1 et du thalamus sont non seulement sensibles à la direction de déflexion locale de leur VP, mais aussi à la direction d'un mouvement global de l'ensemble de leurs vibrisses.

Afin de mieux comprendre la manière dont le réseau cortical traite ces scènes tactiles globales, nous avons construit un poste expérimental permettant d'enregistrer en temps réel l'activité du cortex S1 chez la souris par imagerie sensible au potentiel, tout en appliquant des stimuli tactiles complexes à l'aide d'une matrice de 24-stimulateurs vibrissaux. Nous avons de plus développé une méthode permettant d'aligner les données fonctionnelles ainsi obtenues par rapport la carte cytoarchitecturale du réseau cortical sous-jacent.

Nous avons ainsi étudié premièrement la distribution spatiale de la sélectivité à la direction de déflexion locale d'une vibrisse au niveau d'une colonne corticale. Les réponses aux différentes directions étaient localisées de manière légèrement distincte, autour du centre de la colonne, mais selon une organisation différente de celle précédemment décrite chez le rat. Nous avons montré par la suite que la sélectivité à la direction globale est spatialement organisée dans le cortex "en tonneaux" à l'échelle supra-colonnaire. Les colonnes correspondant aux vibrisses rostrales étant plus sélectives à la direction globale que les colonnes associées aux vibrisses caudales. En outre, les colonnes correspondant aux vibrisses dorsales répondent préférentiellement aux directions globales ventrales, tandis que les colonnes associées aux vibrisses ventrales répondent préférentiellement aux directions globales caudales. Enfin, les réponses induites par des directions globales caudo-ventrales étaient en moyenne les plus fortes pour toutes les colonnes.

Nous avons montré que la répartition spatiale de la sélectivité à la direction globale peut être expliquée ni par la saillance prédominante de la position de départ de la séquence de stimulation multivibrissale (effet de bord), ni par la sommation linéaire des réponses aux déflexions de quelques vibrisses. Les réponses aux stimulations globales de l'ensemble des vibrisses sont en effet fortement sous-linéaires, indépendamment de la direction de la stimulation.

Brièvement, nous montrons ici que sortir de la vision classique du système vibrissal permet une meilleure compréhension de la façon dont les différentes caractéristiques des stimuli complexes sont traitées et de la manière dont les propriétés émergentes du cortex, comme la sélectivité à la direction globale, sont construites.

Remerciements

As Jacques Derrida wrote in his book 'Le monolinguisme de l'autre': « *Je n'ai qu'une langue, ce n'est pas la mienne* ». I am lucky to have three; however, none can express what I feel now. So, as I have been doing all these years, I will move from one language to another, to try to thank you in the one that my heart feels more comfortable with.

Firstly, I would like to express my sincere gratitude to Randy Bruno and Frédéric Chavane. I am honoured that you agreed to be the rapporteurs of this work, and together with Valentina Emiliani and Laurent Bourdieu, I would like to thank you for taking part in my examining committee. Je voudrais remercier à mes tuteurs, Laurent Bourdieu et Daniel Pressnitzer, et aussi à Jean-François Léger, pour tous les bons conseils que vous m'avez donnés pendant ces années de thèse.

My sincere thanks also go to Ehud Ahissar and Ilan Lampl for receiving me in their teams at Weizmann Institute in Israel. Especially to Boaz Mohar, Sebastian Haidarliu and Knarik Bagdasarian, who taught me a lot of things about the brainstem, from surgery to histology.

And what to say about UNIC? The time here was simply amazing. Merci à Yves Frégnac for directing an institute that combines excellent scientific research with an exceptional human quality. Merci aux belles secrétaires: Aline et Justine pour votre énorme patience et aide (et oui, j'ai fini d'écrire!). Merci à Paul et Roland pour l'aide informatique, et à Patrick Parra et Jean-Yves Tiercelin pour l'assistance technique. Un énorme merci à Aurélie, Guillaume et Gérard pour toute l'aide que vous m'avez apportée avec mes manips.

I thank all the UNIC members for the stimulating discussions, endless trips in the RER, conferences, and for all the fun we have had. In particular I would like to thank some UNICs with whom I have shared a little more time outside the lab (i.e. museums, cinema, dinners, trips, picnics): merci Xoana, Jan, Domenico, Yann, Gilles et Francesca (and of course to Daniel, Tanja and Assunta).

Special thanks to Evan and Mati, who arrived at the lab in my worst moment (writing time), and suffered all my "thesis crisis". Thank you for your support, patience and the shared "mates", oh, and for all the boring football talks (you too Yannick!). Thanks to Luc, especially for the help you gave me when I was building the matrix, and for sharing the first and last months of my PhD. And Zuzanna, thanks for your advice regarding my scientific career and also for all the interesting talks about literature.

Pauline, on est arrivée au labo presque au même moment, et donc on a partagé beaucoup de choses ensemble dans le labo et aussi des bons moments dehors, dans les meetings, les conférences, picnics, bars, etc. Merci pour tout ça et pour ton sourire continu!

Also I thank Valérie, for the very useful bibliography that I've extensively cited in this thesis, for being always so open, nice and willing to help. And of course, thanks for sharing your supernatural culinary skills. Mil gracias Valeria!

I would also like to thank Lidia Szczupak, my MSc thesis supervisor at Universidad de Buenos Aires, not only for being an inspiration but also for helping me to find a PhD abroad. And it was at UNIC where I met other two exceptional researchers that are now also an inspiration for me: Dan and Isabelle.

Dan, mil gracias por tu apoyo durante estos años de tesis. It was a big responsibility to be the first Argentinian student in your team, and I hope I represented well the country! Thank you for your advice, and especially for taking care not only of my scientific development in the lab, but also of my career. It is an inspiration for me, the energy and motivation that you put in all your projects, and how you manage the team always looking beyond. Thank you for your guidance!

Isabelle, je n'ai pas des mots pour te remercier. You taught me lots of things, from technical to analytical, regarding writing, presenting results, critical thinking, etc. It was great to share these years with you in the lab, I enjoyed a lot our many talks in the office, at the canteen, during the experiments, the ones about science, about politics, society. As I mentioned before you are an inspiration because you are not only an excellent researcher, but also a nice person and a great supervisor. Thanks for your constant encouragement!

On the personal side, I would like to thank all the great people I met during these years in Paris, especially those who have been here since the beginning: Camila, Marina, Silvia, Wail and Rafaela. You put some sunshine on the cloudy Parisian days, merci!

Y por último quiero agradecer a ese grupo heterogéneo de personas que considero fundamental para mi vida, los que estuvieron siempre dándome fuerzas, de uno y otro lado del charco: a mis amigas de toda la vida, a Flor y Juan, a Poly, a Mai, a mis "padres adjuntos", a Hugo y a Lau mi hermana del corazón, a mi familia de Argentina y de España.

Especialmente gracias a esas cuatro personitas que son los pilares de mi vida: mi hermano, mi tía, mi mamá y mi papá, que siempre me apoyaron en todos mis proyectos, aunque incluyeran irme a 11000 km de Buenos Aires. Y sobre todo gracias a mi mamá, por contenerme y darme la energía que necesité en cada momento de la tesis, y especialmente para terminar esta etapa, siguiendo tu consejo, como me decías siempre: "sin prisa, pero sin pausa". Por eso esta tesis te la dedico a vos.

Acknowledgements

This thesis was possible thanks to the doctoral school “Frontières du Vivant” part of the “Programme Bettencourt” created and funded by the “Bettencourt-Schueller Foundation”. I would also like to gratefully acknowledge the funding received during my PhD from: FACETS-ITN - European Union Seventh Framework Program (FP7/2007–2013) no. 269921 (BrainScaleS), UPR CNRS 3293, Lidex NeuroSaclay and Lidex iCODE.

Table of Contents

TABLE OF FIGURES.....	14
ABBREVIATIONS.....	15
FOREWORD.....	17
PART I – INTRODUCTION TO THE WHISKER-TO-BARREL CORTEX SOMATOSENSORY PATHWAY	21
CHAPTER 1: THE VIBRISAL SYSTEM OF RODENTS	23
I.1.1 THE VIBRISAE: A SENSORIMOTOR ORGAN.....	24
I.1.1.1 The use of vibrissae: whisking and perception.....	24
i. Nocturnal and subterranean activity of rodents.....	24
ii. General description of vibrissal movements.....	25
I.1.1.2 The vibrissae as tactile sensorimotor organs	28
i. Morphological description of the mystacial pad	28
ii. Anatomy of the vibrissa: the follicle-sinus complex	30
iii. Mechanical transduction by the sensory receptors	30
I.1.2 FROM WHISKERS TO SOMATOSENSORY CORTEX.....	33
I.1.2.1 General description of the neuronal relays.....	33
I.1.2.2 Different pathways to reach the cortex	34
I.1.2.3 Somatotopy at each neuronal relay.....	36
CHAPTER 2: THE BARREL CORTEX	39
I.2.1 SOMATOTOPIC MAPS	39
I.2.1.1 The somatosensory homunculus.....	39
I.2.1.2 The “mouseunculus”	40
I.2.2 THE BARREL CORTEX: AN IDENTIFIABLE CORTICAL STRUCTURE	41
I.2.2.1 General architecture	41
I.2.2.2 Cellular components	45
I.2.2.3 Receptive fields.....	49
I.2.3 CONNECTIVITY IN THE BARREL CORTEX	51
I.2.3.1 Afferent connections.....	51
I.2.3.2 Intracortical connectivity.....	52
I.2.3.3 Efferent connections	53
I.2.4 BEYOND THE CLASSICAL VIEW.....	56

CHAPTER 3: FUNCTIONAL CORTICAL MAPS	59
I.3.1 DIRECTIONAL TUNING IN THE SOMATOSENSORY PATHWAY	59
I.3.1.1 Local direction selectivity in the subcortical structures.....	60
I.3.1.2 Local direction selectivity in the barrel cortex	64
I.3.2 “TOPY” OF DIRECTION SELECTIVITY IN THE BARREL CORTEX	65
I.3.3 EMERGENT PROPERTIES OF SPATIOTEMPORAL COMPLEX STIMULI	69
AIM OF THE THESIS	79

PART II – CONTROLLING THE INPUT – READING THE OUTPUT.....81

CHAPTER 1: OPTICAL IMAGING OF CORTICAL SPATIOTEMPORAL DYNAMICS	83
II.1.1 BEYOND THE ELECTRODES: OVERVIEW AND ADVANTAGES OF OPTICAL IMAGING	83
II.1.2 VOLTAGE-SENSITIVE DYE IMAGING	85
1.2.1 Description of the technique.....	85
1.2.2 What are we seeing?	89
II.1.3 VSDI IN THE BARREL CORTEX	91
CHAPTER 2: COUPLING MATRIX-VSD	95
II.2.1 A MULTIWHISKER STIMULATOR: THE MATRIX.....	95
II.2.2 BUILDING THE SET-UP	98
II.2.3 ANATOMO-FUNCTIONAL MAPPING OF THE BARREL CORTEX	100
Article: “An automated workflow for the anatomic-functional mapping of the barrel cortex”	103

PART III – CORTICAL PROCESSING OF SOMATOSENSORY INPUTS115

CHAPTER 1: DIRECTION SELECTIVITY TO SINGLE WHISKER DEFLECTION	117
III.1.1 Materials and methods	117
• <i>Animals and Surgery</i>	117
• <i>Voltage-Sensitive Dye Imaging</i>	118
• <i>Whisker Stimulation</i>	118
• <i>Image analysis</i>	119
• <i>Histology</i>	119
• <i>Quantification of VSD responses</i>	119
• <i>Direction selectivity</i>	119
• <i>Statistical Tests</i>	120

III.1.2	Results	121
	• <i>Highly reproducible location of afferent responses within the barrel columns</i>	121
	• <i>Rostral and caudal deflections evoke the highest responses in the C2 barrel column</i>	121
	• <i>Direction selectivity is spatially distributed within the C2 column</i>	123
CHAPTER 2: CORTICAL REPRESENTATION OF MULTIVIBRISSAL STIMULATIONS.....		127
III.2.1	Materials and Methods	127
	• <i>Animals and Surgery</i>	127
	• <i>Voltage-Sensitive Dye Imaging</i>	128
	• <i>Whisker Stimulation</i>	128
	• <i>Multiwhisker global motion protocol</i>	128
	• <i>Multiwhisker moving/static bar protocol</i>	129
	• <i>Image analysis</i>	129
	• <i>Histology</i>	129
	• <i>Quantification of VSD responses</i>	130
	• <i>Direction selectivity</i>	130
	• <i>Statistical Tests</i>	130
III.2.2	Results	132
	• <i>Voltage sensitive dye imaging of depolarizing responses evoked by multiwhisker stimuli spread across the barrel cortex</i>	132
	• <i>At each column evoked responses depend on the spatio-temporal context of the multiwhisker deflections</i>	132
	• <i>Barrels corresponding to the most rostral whiskers show significant direction selectivity towards caudoventral global angles</i>	135
	• <i>Global direction selectivity map is juxtaposed with the somatotopic map</i>	137
	• <i>Cortical responses to a moving bar are highly sublinear</i>	139
	• <i>Global direction selectivity cannot be explained by the linear summation model</i>	143
	• <i>Despite of the high salience of the starting position of the moving bar, it is not enough to explain the global direction selectivity</i>	143
PART IV – DISCUSSION		145
IV.1	VSD IMAGING: SOME ASPECTS TO KEEP IN MIND.	147
IV.2	INTRACOLUMNAR SPATIAL ORGANIZATION OF DIRECTION SELECTIVITY IN THE MOUSE BARREL CORTEX.....	151
IV.3	POSSIBLE MECHANISMS FOR THE EMERGENCE OF GLOBAL DIRECTION SELECTIVITY	155
IV.4	READ-OUT: ADVANTAGES OF DIRECTION SELECTIVITY MAPS?	161
IV.5	SENSORY EXPECTATIONS	167
IV.5.1	Direction selectivity in the awake mouse	168
IV.5.2	Why a directional anisotropy?	168
IV.6	CONCLUSION	171
BIBLIOGRAPHY		173

Table of Figures

Figure 1: Whisking behavior in rodents.	27
Figure 2: The mystacial pad of the rodents.....	29
Figure 3: Structure of the whisker follicle.	31
Figure 4: Muscles controlling whisker movement.....	32
Figure 5: Parallel pathways to the cortex.....	35
Figure 6: Preserved somatotopy through the somatosensory pathway.	37
Figure 7: Somatotopic maps.....	41
Figure 8: Anatomy of the barrel cortex.....	42
Figure 9: Correspondence between whiskers and barrels.....	44
Figure 10: Dendritic morphology of excitatory neurons in the rat barrel cortex.	48
Figure 11: Axonal arborizations of cortical inhibitory neurons.....	48
Figure 12: Scheme of parallel cortical microcircuits in the barrel cortex.	55
Figure 13: Direction selectivity in two well-tuned units of the trigeminal ganglion.	62
Figure 14: Direction selectivity in the trigeminal nuclei and thalamus.	63
Figure 15: Transformation in directional tuning along the whisker pathway.....	65
Figure 16: Review of the spatial distribution of local direction selectivity.....	68
Figure 17: Representation of the starting position of a moving bar.	71
Figure 18: Cortical responses selective to the direction of global motion.	74
Figure 19: Possible explanations for the global direction selectivity.	75
Figure 20: Voltage-sensitive dye RH1691 and the origins of the VSD signal.	88
Figure 21: VSD imaging the barrel cortex of anaesthetized mice.	93
Figure 22: The second generation matrix. Probing with natural stimuli.	97
Figure 23: VSD imaging responses to multidirectional stimulation of whisker C2.	122
Figure 24: Spatial distribution of the early responses to different local directions of deflection of the C2 whisker.	125
Figure 25: Analysis of the spatial distribution of the early responses.....	126
Figure 26: VSD imaging of cortical responses to multiwhisker stimulation.....	131
Figure 27: Responses depend on the spatio-temporal context of the multiwhisker deflections.	134
Figure 28: Spatial distribution of direction selectivity to global motion.	136
Figure 29: Averaged spatial distribution of global direction selectivity	138
Figure 30: Global direction selectivity controls.	139
Figure 31: Cortical responses to a moving bar and to a static bar.	141
Figure 32: Cortical responses to a moving bar are highly sublinear.....	142
Figure 33: Global direction selectivity is neither explained by the linear prediction nor the starting position of the moving bar.	144
Figure 34: Relationship between feature mapping and coding in the visual cortex of the rodent and cat	165

Abbreviations

AW	adjacent whisker
CO	cytochrome oxidase
CT	corticothalamic
DI	direction index
Dpref	preferred direction
EEG	electroencephalogram
FOV	field of view
FSU	fast spiking unit
GABA	γ -Aminobutyric acid
GEVI	genetically-encoded voltage indicators
IADI	interarc deflection interval (same as IWI)
IT	intratelencephalic
IWI	interwhisker interval
L	cortical layer
PFA	paraformaldehyde
PMBSF	posteromedial barrel subfield
POm	posteromedial nucleus of the thalamus
PrV	rostral principal nucleus of the brainstem
PSTH	peristimulus time histogram
PT	pyramidal tract
PW	principal whisker
RF	receptive field
ROI	region of interest
RHR	ramp-hold-ramp stimulus
RSU	regular spiking unit
S1	primary somatosensory cortex
S2	secondary somatosensory cortex
SpV	caudal spinal nucleus of the brainstem
St	Straddler
StA	Straddler Alpha (α)
StB	Straddler Beta (β)
StC	Straddler Gamma (γ)
StD	Straddler Delta (δ)
SW	surround whisker (same as AW)
V1	primary visual cortex
VPM	ventro posteromedial nucleus of the thalamus
VSD	voltage-sensitive dye

Foreword

« The body is our general medium for having a world »

Maurice Merleau-Ponty – Phenomenology of Perception

What is reality? How do we perceive “reality”? Is the world inside our mind an accurate model of the outside physical world? Is our perception a true representation of it? Philosophers, psychologists and neuroscientists, among many others, have been asking these questions for many centuries. Surprisingly we do not have a unique answer yet, but several theories have been developed to try to explain our perceptual experiences.

The theory of direct realism, first described by Aristotle but mainly developed by the American psychologist James J. Gibson, claims that we perceive the world through our senses in a direct way, i.e. we perceive the world as it really is. One of the main beliefs of this theory is that the properties we perceive on the objects are independent of our perception, thus the objects retain these properties even when we are not perceiving them. Then what if we look at an object but instead of using our eyes we look at it with the eyes of a snail? Or, would we claim that a surface is “soft” if we perceive it with the mouse whiskers instead of using our fingers? In both cases our perception of the object would be different, as the sensory receptors and their sensitivity differ. It is hard to support this theory if we consider that we do not perceive directly, there is something that mediates the reality and our perception, our body. Other arguments against this theory are the illusions and the hallucinations, where we perceive physical properties that the object does not have.

On the other hand, the representational realism theory – also called indirect realism – claims that our conscious perception is not coming from the real world, but of an internal representation of it. This theory, whose main supporters had been Locke and Descartes, goes in the opposite direction than the direct realism, as it claims that our ideas of the world are interpretations of sensory inputs derived from the external world, agreeing with the saying: “We don’t see things as they are; we see them as we are”. Thus, in order to understand the world we should start by understanding ourselves.

In this sense it is essential to focus on how our body functions in order to understand perception. Our perception is mediated by our body and thus it is constrained by our physiology, from the sensitivity and organization of the sensory receptors to the complex neuronal networks that process these stimuli.

Sensory perception constitutes the first step of acquisition of information coming from the environment. A large amount of information coming from different sensory modalities enters through the sensors in order to create a percept of the world. This requires to integrate complex signals coming from different pathways and to analyze them in the order of a few milliseconds. In the mammalian nervous system this high velocity is guaranteed by the existence of a neuronal network that is optimized in the cortical areas with a given anatomical and functional organization.

With this thesis, we want to contribute to the understanding of the physiological mechanisms of perception, in particular to the tactile perception. For this we considered that it is important to step aside of the classical view of the neocortex as a juxtaposition of independent columnar units, and move to a more holistic view, which allows studying how different features of the stimuli are processed, and how emergent properties of the cortex are built-up. Particularly, we focused on the spatial organization of global direction selectivity in L2/3 of the mouse barrel cortex.

This thesis is divided in four parts as follow:

In the **Part I** we start by giving a general introduction to the canonical view of the rodent whisker to barrel cortex sensory pathway: a general presentation of the whiskers as sensorimotor organs specialized in the detection and discrimination of objects is evoked together with the anatomical and functional organization of the whisker-to-cortex pathway, followed by a description of the barrel cortex and its connectivity pattern. We further propose another view of the system, where the cortical column is not an isolated functional unit of the cortex. We describe then the functional cortical maps and present the state-of-the-art in the coding of selectivity to the direction of deflection of the vibrissae in the barrel cortex. From there we depict the primary aims of this thesis.

Part II addresses the scientific question of how we can study the emergent properties of the cortex. We describe the set-up that we have built to this aim and the technical challenges that have been raised. We comment on the advantages of the voltage-sensitive dye technique and discuss the origins of these signals. Then we present the technical method we have developed to map recorded functional data onto the cortical structure, which resulted in an article (Perronnet, Vilarchao et al., *Journal of Neuroscience Methods*, 2015).

Part III is dedicated to the central subject of the thesis: the processing of complex tactile scenes. It is divided in two chapters that follow the same structure, starting with our motivation to explore the subject, followed by the description of the protocols we used and the results obtained. In the first chapter we analyze the spatial intracolumnar organization of the direction selectivity to the local deflection of a single whisker. In the second chapter we show that the direction selectivity to the global deflection of the whiskers is spatially distributed in the mouse barrel cortex, and we further characterize the dynamical properties of the responses to such complex multiwhisker stimuli.

Finally, in a general **discussion** (Part IV) of the results, we consider how revisiting the classical view of the whisker-to-barrel cortex system allows to better understand the neuronal bases of emergent properties of the cortex, like global direction selectivity.

Part I – Introduction to the whisker-to-barrel cortex somatosensory pathway

The cerebral cortex is the key brain structure that sets apart mammals from other animals and humans from other mammals. This fascinating structure covers our cerebral hemispheres and is known to be the place where the highest cognitive processes occur: consciousness, awareness, attention, memory, language, calculations, judgment, emotions, abstraction, generation of motor commands, and processing of sensory information. Maybe one of the most amazing things that happened during the evolutionary expansion of the cerebral cortex is that it made the human brain capable of understanding itself. The human brain is then a brain that asks about its own processing properties, that is able to formulate hypothesis about its own working mechanisms and to develop technology to see its own functioning; in essence, a brain that wants to study itself.

Studying the cortical processing of sensory information is one of the most straightforward ways to explore the integrative properties of the cerebral cortex, since it can be done in animal models by applying a variety of controlled external stimuli while recording cortical activity with high resolution techniques.

Within this thesis we will use the somatosensory cortex of the mouse as a model to study cortical processing, focusing on a region of the rodent primary somatosensory cortex: the barrel cortex. Our interest is to study the existence of a functional organization of the sensory information, in particular of the direction of movement of the vibrissae, within the barrel cortex.

In this first part we will briefly introduce the vibrissal system, the different whisker-to-cortex pathways, followed by a more detailed anatomical and functional description of the barrel cortex. We will finish by reviewing the up-to-date studies on coding of direction for single and multiwhisker stimuli, which have motivated us to do this thesis.

Chapter 1: The Vibrissal System of Rodents

« As Gregor Samsa awoke one morning from uneasy dreams he found himself transformed in his bed into a gigantic insect. » Franz Kafka, *The Metamorphosis*

It is hard to imagine how it would feel like to wake up one day and, like Gregor Samsa, find ourselves converted into something else, a mouse. The change in our sensory modalities would be, I imagine, the first thing that we will notice. Our eyes giving us a blurred image of our room; our sense of smell discriminating all the ingredients that our neighbor, who is two stores apart, is using to cook breakfast; many sounds will come from things we always thought silent; but the most striking thing we might experience is the extreme sensitivity of the big hairs coming out from our face, the whiskers. We will have to learn to perceive in this new whisker space; to learn the feeling of an air flow coming from the open window and slowly moving our whiskers, the feeling of contacting an object. We will learn how to actively move ourselves and our whiskers in order to optimize the extraction of information with this new sensory modality. And of course we will learn how it feels to touch with our whiskers our own body.

Even if we push our imagination, it is hard to know how whiskers feel like, as we are one of the few mammal species that do not have whiskers, and we do not even have an equivalent organ. Our fingers seem to have the same sensitivity (Carvell and Simons, 1990), but the system structure and the way we gather information is quite different, and even if we tried to reproduce it (Saig et al., 2010), we still have no intuition of the use of this sensory organ. For studying the whisker system, then, we must step out of the Kafkian nightmare and try to understand first how do the rodents live and how do they use their whiskers and process this information.

I.1.1 The vibrissae: a sensorimotor organ

I.1.1.1 The use of vibrissae: whisking and perception

i. Nocturnal and subterranean activity of rodents

Rats and mice are subterranean animals that live in dark tight burrows. Their life, breeding, eating, sleeping, mating, exploring, happens in underground tunnels, and – as they are nocturnal animals – it happens at night. Therefore, their somatosensory system is adapted for tactile exploration, from the shape of the whiskers to their movements. In other words:

« Eyes may be 'the window to the soul' in humans, but whiskers provide a better path to the inner lives of rodents. » Sofroniew and Svoboda, 2015.

More than one century ago it was published the first study demonstrating that whiskers are behaviorally important for the rats while navigating in a maze (Vincent, 1912). When mice and rats are in an open-field or walking along a tunnel, they present thigmotactic behavior (i.e. wall scanning behavior); their whiskers are in constant contact with the walls. A unilateral “vibrissotomy” makes the rats to position more often their intact vibrissae in order to scan a wall (Milani et al., 1989) while unilateral barrel cortex lesion contralateral thigmotaxis in mice (Luhmann et al., 2005).

Using only their whiskers, rodents are able to detect distance, shape and texture of objects (Guić-Robles et al., 1989). But these are not the only uses of the whiskers. Recently, the group of Michael Brecht shed light on the social relevance of the whiskers. Tactile responses to social touch of another rat are bigger than the responses obtained when touching an object (Wolfe et al., 2011; Bobrov et al., 2014). They also showed that barrel cortex neurons vary their activity with sex and sexual status of the conspecifics, and they described an anticipatory pre-contact depolarization of the membrane potential of these neurons (Lenschow and Brecht, 2015). The natural use of the mechanosensitive whiskers involves a broad repertoire of complex behaviors, as these social interactions also involve changes in the position of the whiskers and their active movement.

ii. General description of vibrissal movements

Even though all mammals (but us) have whiskers, there is a major difference among them: some whisk and others do not. Whisking is an active rhythmic movement of the whiskers in the rostro-caudal axis at 5-25 Hz in rats (Berg and Kleinfeld, 2003), and 14-24 Hz in mice (Jin et al., 2004). Differences between the whisking frequency spectra of mice and rats are shown in Figure 1A-B.

Once rats and mice encounter an object or an obstacle, they actively use their whiskers to scan and discriminate it (Kleinfeld and Deschênes, 2011). During the discrimination period, which normally lasts from 1 to 10 s, the respiration, head and whisker movements are synchronized (Welker, 1964; Wineski, 1983; Semba and Komisaruk, 1984; Cao et al., 2012). The tight synchronization between sniffing and whisking suggests that breath rhythm constitutes a common clock in the integration of olfactory and tactile cues, thus playing a role in the generation of a global percept (Deschênes et al., 2012; Kleinfeld et al., 2014).

Humans have behaviors analogue to whisking for tactile discrimination, which consist in scanning an object or a surface with the tip of the fingers with the aim of better perceiving its texture (Gamzu and Ahissar, 2001). The non-whisking animals perceive with their whiskers as with any tactile hair, and their sensibility has been described to be comparable to the sensitivity of the eyelashes in the human (Fitzgerald, 1940).

When the animal is quiet or sleeping, its whiskers are in a retracted position. Once the animal is alert, the whiskers deploy thus occupying a larger volume. During the whisking exploratory behavior, rats and mice move their vibrissae in the rostro-caudal axis, creating a functional asymmetry between rows and arcs: whiskers in the same row will tend to contact an object successively, whereas whiskers in the same arc either will contact the object nearly simultaneously, or might not all contact the object. Both extrinsic and intrinsic muscles that surround the follicle are arranged in the rostro-caudal direction, allowing fine-scale positioning of all the whiskers or an individual whisker during tactile exploration. The mouse whisking has an average frequency of 20 Hz, an average amplitude of 55°, with a higher velocity for the retraction (2400°/s) than the protraction (2000°/s) (Jin et al., 2004). Once the whiskers contact an object, the little vibrissae that are more rostral are protracted and stay this way without losing the contact with the surface, while the bigger caudal vibrissae

continue to whisk (Carvell and Simons, 1990). These movements of retraction and protraction move both sides of the whisker pad in a synchronized manner and are finely controlled by the motor cortex (Wineski, 1983; Gao et al., 2001). However, depending on the situation they can move their whiskers in an independent way directing their attention towards a particular point in space (Sachdev et al., 2002). By moving the head and also by asymmetrically moving the whiskers, they can bring a larger number of whiskers in contact with the object or surface that called their attention (Mitchinson et al., 2007).

Rodents change their whisker strategy depending on their behavior. When exploring a new environment, rodents deploy their whiskers forward and whisk (Arkley et al., 2014). The rhythmic whisking is coupled to running: the faster they run, the faster they whisk, and the further they protract their whiskers (Figure 1). When turning they move their whiskers asymmetrically, protracting the whiskers in the side of the turn, as a way of anticipating the exploration of the space they are about to enter (Towal and Hartmann, 2006; Grant et al., 2009). When the animals become familiarized with the environment or the object, they reduce the whisking amplitudes and the whiskers are more retracted. Although there is an identified whisking pattern generator in the brainstem (Moore et al., 2013), both S1 and the primary motor cortex seem to be involved in the fine control of whisker position (Matyas et al., 2010; Petersen, 2014).

All the experiments done in awake-behaving animals provided the researchers with a valuable estimation of the natural conditions of stimulation of the whiskers. Nonetheless, the information that the animal extracts from a whisker deflection is not reduced to a contact/non-contact binary form. On the contrary, the animal is capable of using precise features (i.e. direction, velocity, amplitude) of the deflection of the whiskers that are first acquired by the mechanoreceptors on the base of the vibrissae, and then encoded and enriched by integrating information through the pathway up to the cortex. We dedicate the next section to briefly describe the mechanisms of sensory transduction of tactile stimuli in the rodents' vibrissal system.

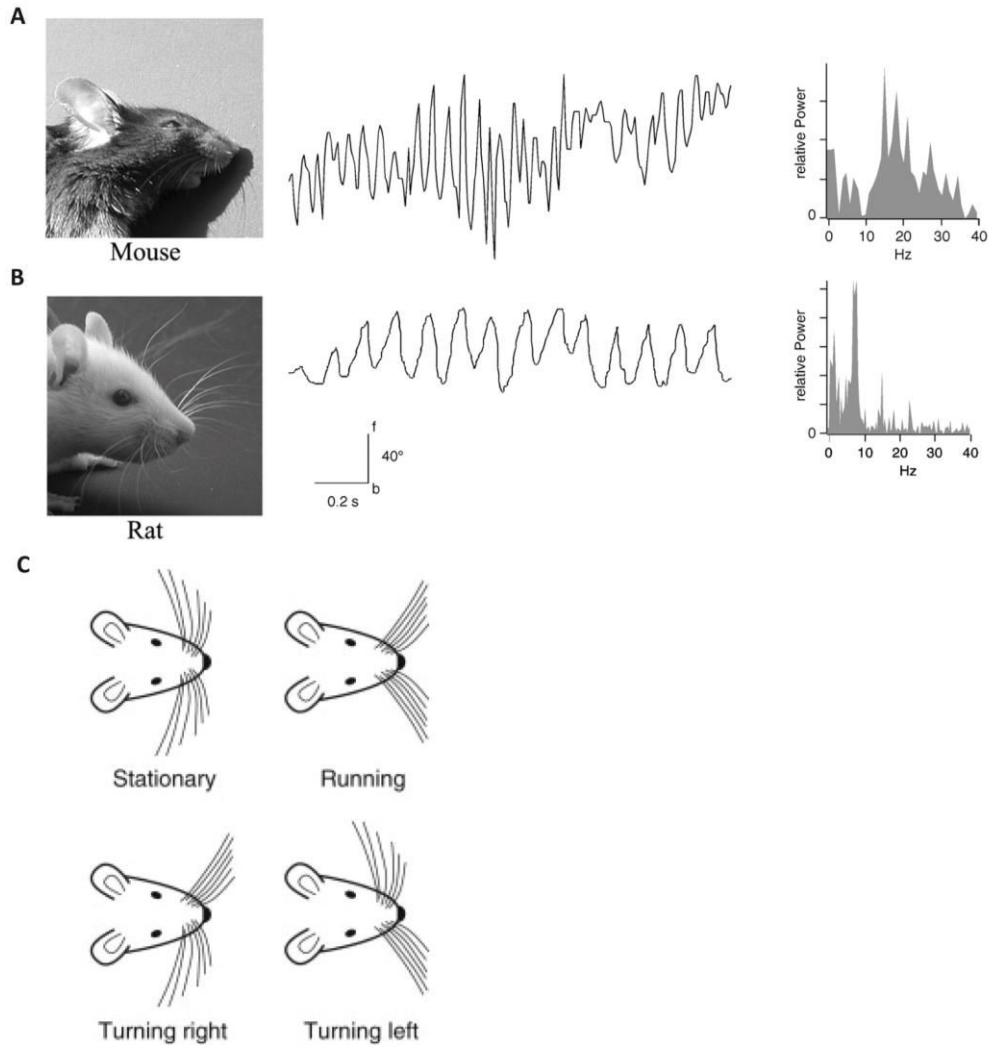


Figure 1: Whisking behavior in rodents.

A: Left, side view of a mouse head and whiskers. Middle, Back (b) and forth (f) movements (angular positions) of whisker C2 of a mouse during a whisking episode. Right, Power spectrum of the movement trace.

B: Rat snout (same as in A).

C: Whiskers' position in the behaving rodent.

A-B from (Jin et al., 2004); C from (Sofroniew and Svoboda, 2015).

1.1.1.2 The vibrissae as tactile sensorimotor organs

i. Morphological description of the mystacial pad

The mouse has over the upper lips, at both sides of the snout, a group of 30 to 35 specialized hairs emanating from follicles that are densely packed with nerve endings, and which are considered “mystacial” (Welker and Van der Loos, 1986). This number varies depending on the mouse line and different criteria to evaluate a mystacial vibrissae like the length of the hair, the presence of follicular muscle, the number of axons that innervate the follicle, and so on (Haidarliu and Ahissar, 1997). However, mice also have additional vibrissae below the jaws, over the eyes, and below the lips. Figure 2A-B shows a scheme of the snout of rodents.

The mouse mystacial vibrissae are organized in a matrix of 5 rows named from A to E in the dorso-ventral direction, and about 7 principal arcs numbered from 1 to 7 in the caudo-rostral direction (Figure 2C shows the most caudal arcs). Each whisker has its specific length and thickness, but the caudal vibrissae are longer than the rostral ones; the length decays exponentially from caudal to rostral arcs (Brecht et al., 1997). Four vibrissae named with greek letters (α , β , γ and δ) form an additional arc in the caudal part of the mystacial matrix. They are found aligned between the rows, and are therefore called “straddlers”.

The macrovibrissae have a conical shape and base diameter of 100 μm that narrows gradually to only a few micrometers at the tip. The conical shape allows better sensing the distance of an object, since the bending moment required to produce a change in the whisker curvature is proportional to the fourth power of the whisker diameter (Hires et al., 2013). This shape is also useful for sweeping along rough surfaces as the stiffer base can push the narrower tip to get out of traps.

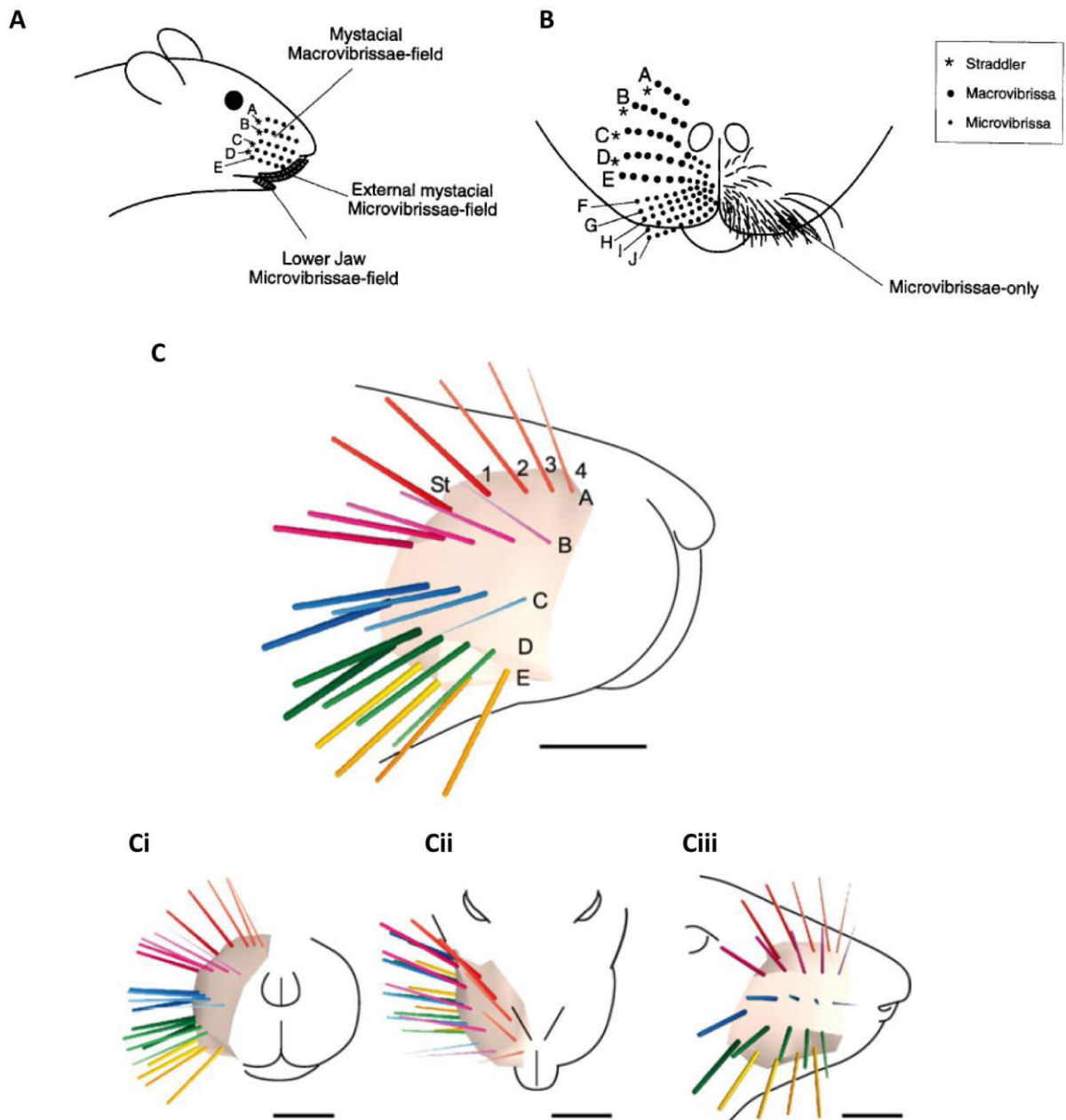


Figure 2: The mystacial pad of the rodents.

A: Macro- and microvibrissae in the rat. Side view of the mystacial pad.

B: Magnified schematic frontal view. On one side only the follicles are represented, on the other, only the microvibrissae.

C: 3D reconstruction of the 24 right macrovibrissae of a Wistar rat, 7 mm of each whisker are shown. Ci, front view; Cii, top view; Ciii, lateral view. Whiskers rows A, B, C, D, and E are color coded. St, straddlers.

A-B from (Brecht et al., 1997); C from (Jacob et al., 2010).

ii. Anatomy of the vibrissa: the follicle-sinus complex

Similar to any other hair in the mammal, a vibrissa comes out from an invagination of the epidermis called “follicle”. Nevertheless, the vibrissae have some singular properties that make them different: the size of the hair is bigger, connective tissue isolates the follicle, the follicle receives significant irrigation, striate muscles surround the follicle, and every follicle has multiple innervations (Figure 3). Due to its anatomical complexity, this whole structure is named the “follicle-sinus complex”. Briefly, this complex has an oval shape and is formed by two pockets one inside the other. The inside pocket originates from the epidermis and the external pocket from the dermis, and both are separated by a cavity called “sinus”. The complex is associated to striate muscle that is attached at the base and wraps around the follicle (Dörfl, 1982). A detailed review of the musculature associated to the follicle-sinus complex can be found in the Scholarpedia article curated by Dr. Haidarliu (Haidarliu, 2015). The movements of the whiskers are generated by two types of muscles: intrinsic and extrinsic (Figure 4). The intrinsic muscle surrounds the deep base of the follicle and attaches to the upper part of the immediately posterior follicle, generating protraction of the whisker when it contracts. On the other hand, the extrinsic muscles nasolabialis and maxillolabialis attach to the bone and act superficially, so when they contract the whiskers are retracted. When the whisker contacts an object, the follicle is stretched by the mechanical interaction, activating the mechanoreceptors that are in charge of the transduction of the mechanical stimulus into neural signals.

iii. Mechanical transduction by the sensory receptors

In the somatosensory system, the peripheral receptors of the skin can be found in different forms of mechanoreceptors: hair follicle receptors, proprioceptors, thermoreceptors, and nociceptors. Mechanoreceptors transduce different stimulus properties to neural signals and channel the information as parallel streams, although our tactile perception of the stimuli is unique. The site of mechanical transduction in the vibrissal system is the follicle-sinus complex, where many different types of mechanoreceptors are present (Figure 3).

Every follicle-sinus complex is innervated by a deep alpha nerve and a more superficial beta nerve (Vincent, 1913). Both nerves also innervate the skin between the whiskers, and project to the trigeminal ganglion via the infra-orbital nerve. The superficial nerve has its

endings at the superior section of the follicle-sinus complex, namely in the epidermis surrounding the aperture of the follicle. The nerve endings can be free, lanceolate or Merkel's type. The deep vibrissal nerve has several endings types, like the Merkel's, Ruffini's, reticular's, lanceolate's, and free endings. All of them terminate surrounding the sinus cavity (Dörfl, 1985). There are also some nerve endings in the dermic papilla at the base of the hair.

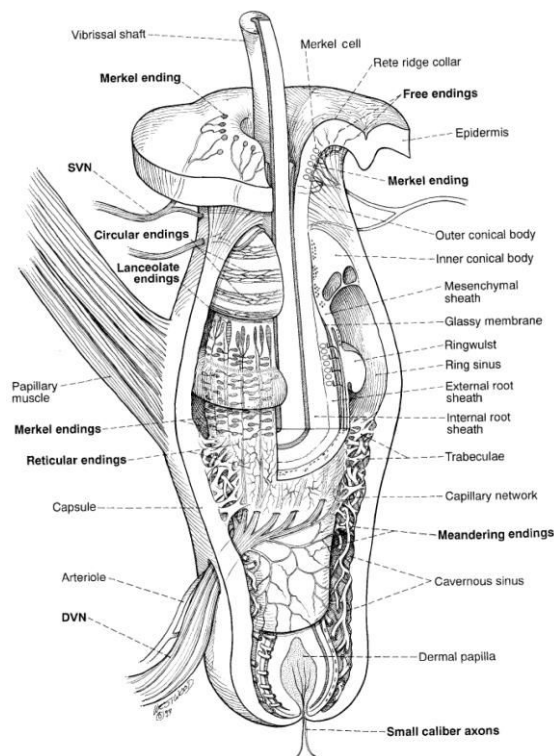


Figure 3: Structure of the whisker follicle.

Diagram showing the structure and innervation of a rat follicle. SVN, superficial vibrissae nerve; DVN, deep vibrissae nerve.

From (Rice et al., 1993).

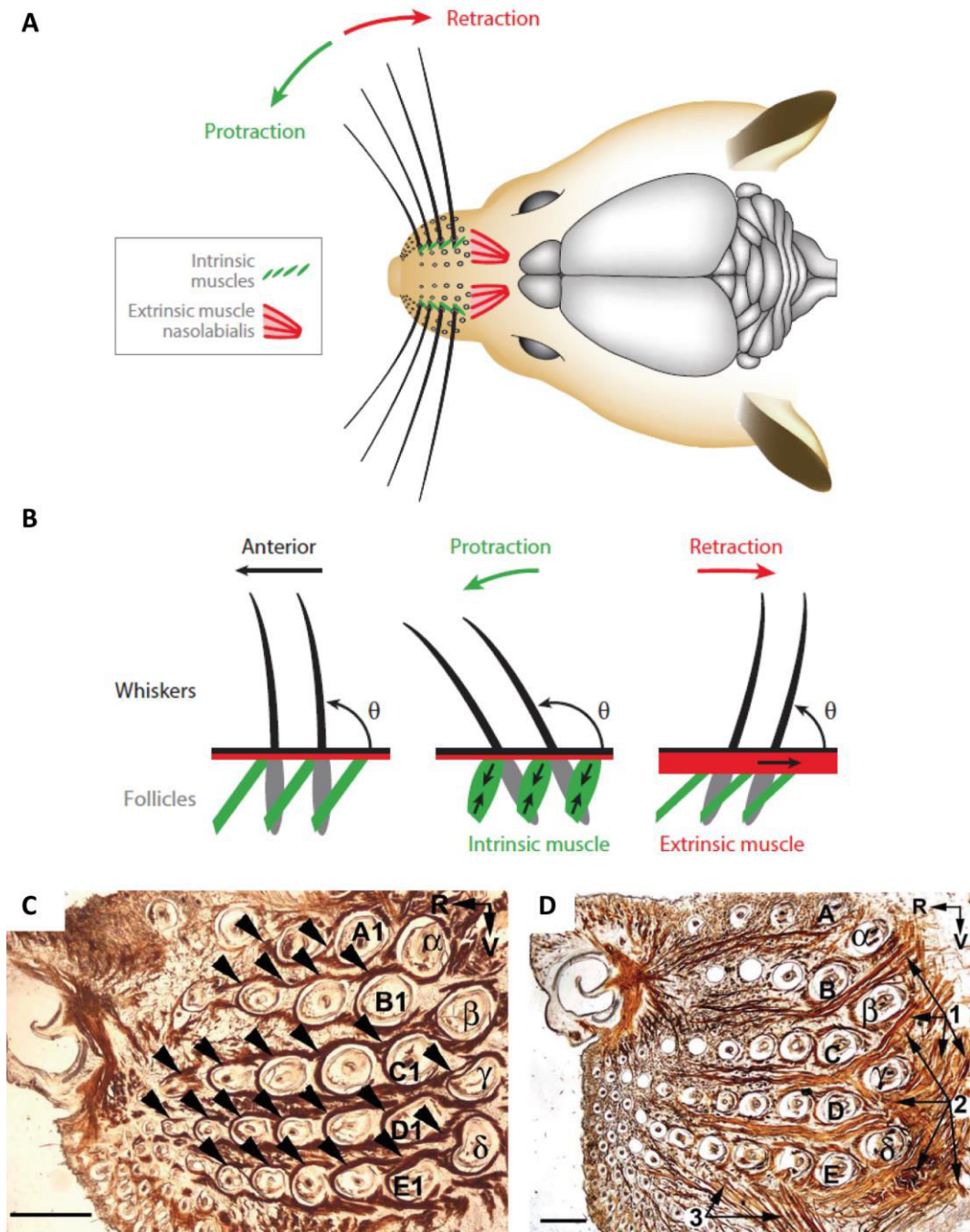


Figure 4: Muscles controlling whisker movement.

A: Most important whisker movements: forward (protraction) and backward (retraction).

B: Intrinsic muscles generate protraction and extrinsic muscles retraction of the whiskers.

C: Intrinsic muscles (arrow heads) in tangential slices of an adult mouse. Slices were stained for cytochrome oxidase (CO) activity. Scale bar = 1 mm.

D: Extrinsic muscles (M) in tangential slices of an adult mouse with CO staining. (1) M. nasolabialis; (2) M. maxillolabialis; (3) pars orbicularis of the M. buccinatorius.

Scale bar = 1 mm.

A-B from (Petersen, 2014); C-D from (Haidarliu et al., 2015)

I.1.2 From whiskers to somatosensory cortex

The basic ascending sensory pathway scheme includes afferents from the receptors in the periphery that terminate in the spinal cord or brainstem, from there second-order neurons convey the information to the thalamus, and projections from the thalamic nuclei go to the primary sensory area of the neocortex. Sensory information is also relayed to other cortical and subcortical structures. We will describe in the next sections the neuronal relays and the different pathways that exist in the whisker system of the rodent.

I.1.2.1 General description of the neuronal relays

The mechanical movements of the vibrissae are transduced in a highly reliable way into nervous influx by the different receptors that innervate the follicles (Jones et al., 2004). The cell bodies of these first-order neurons form the trigeminal ganglion, where information has a very similar representation of the characteristics of the stimulus (Szwed et al., 2003, 2006). Primary central afferents that form the trigeminal tract project to the brainstem where the cell bodies of the second-order neurons are located.

The brainstem trigeminal complex is divided into two nuclei: the rostral principal nucleus (PrV) and the caudal spinal nucleus (SpV), depicted in Figure 5A. The latter is subdivided into the oralis, interpolaris, and caudalis regions (SpVo, SpVi, SpVc, respectively). This is the first processing stage in the vibrissal system. Upon entering the brainstem, the primary afferent axons bifurcate into ascending and descending branches. Both nuclei, in particular the PrV and SpVi, send efferent projections to the contralateral thalamus.

The thalamic relay of tactile sensory information is also divided into two main nuclei: the ventral posteromedial (VPM) nucleus and the posteromedial (POm) nucleus (Figure 5B). The VPM receives projections coming from PrV and SpVi nuclei of the brainstem (Veinante et al., 2000; Deschênes et al., 2003; Arsenault and Zhang, 2006), while the POm receives projections mainly from the SpVi (Pierret et al., 2000; Veinante et al., 2000). Finally, thalamic neurons from both structures project to the region of the primary somatosensory cortex (S1) devoted to process whisker information, the barrel cortex.

Briefly, similar to other sensory cortices, the barrel cortex is composed of six layers (L) named L1 to L6, which present different cellular types and connectivity patterns. The barrel cortex also has a columnar organization, and owes its name to the presence of characteristic neuronal clusters in the L4 whose shapes resemble a barrel of wine (see Chapter 2). The space between the barrels is called “septa”.

1.1.2.2 Different pathways to reach the cortex

There are three different anatomical pathways from the brainstem to the cortex: the lemniscal, paralemniscal and extralemniscal (Figure 5C).

The lemniscal pathway goes through the nucleus PrV of the brainstem and projects to the dorsomedial section of VPM (VPMdm) in the thalamus, and finally arrives to the L4 of S1, and also to the L5b and L6a (Bernardo and Woolsey, 1987; Jensen and Killackey, 1987). The lemniscal pathway regroups the axons of big diameter ensuring a fast transmission of sensory inputs (Ahissar et al., 2000; Diamond et al., 1992). This pathway conveys information about the whisker movement (whisking) and the object location (touch), to the barrel cortex (Yu et al., 2006).

On the other hand, the paralemniscal pathway goes through the rostral region of the nucleus SpVi of the brainstem, projecting to the nucleus POm of the thalamus and the zona incerta (ZI; Veinante et al., 2000). The POm sends projections to the septal region between the barrels of L4, and to L1 and L5a of S1. In addition, it projects to S2 and to the primary motor cortex (M1; Koralek et al., 1988; Lu and Lin, 1993; Alloway, 2008; Wimmer et al., 2010). The paralemniscal pathway carries mainly information relative to whisker motion (Yu et al., 2006).

A third pathway, called the “extralemniscal” pathway, projects from the caudal region of the SpVi to the ventrolateral region of the VPM (VPMvl) and then sparsely projects to the septa between the L4 barrels of S1, in addition to L3 and L6. Furthermore, SpVi sends strong projections to the L4 and L6 of the secondary somatosensory cortex (S2; Pierret et al., 2000; Bokor et al., 2008). This pathway conveys only “touch” information to S1 and S2 (Yu et al., 2006).

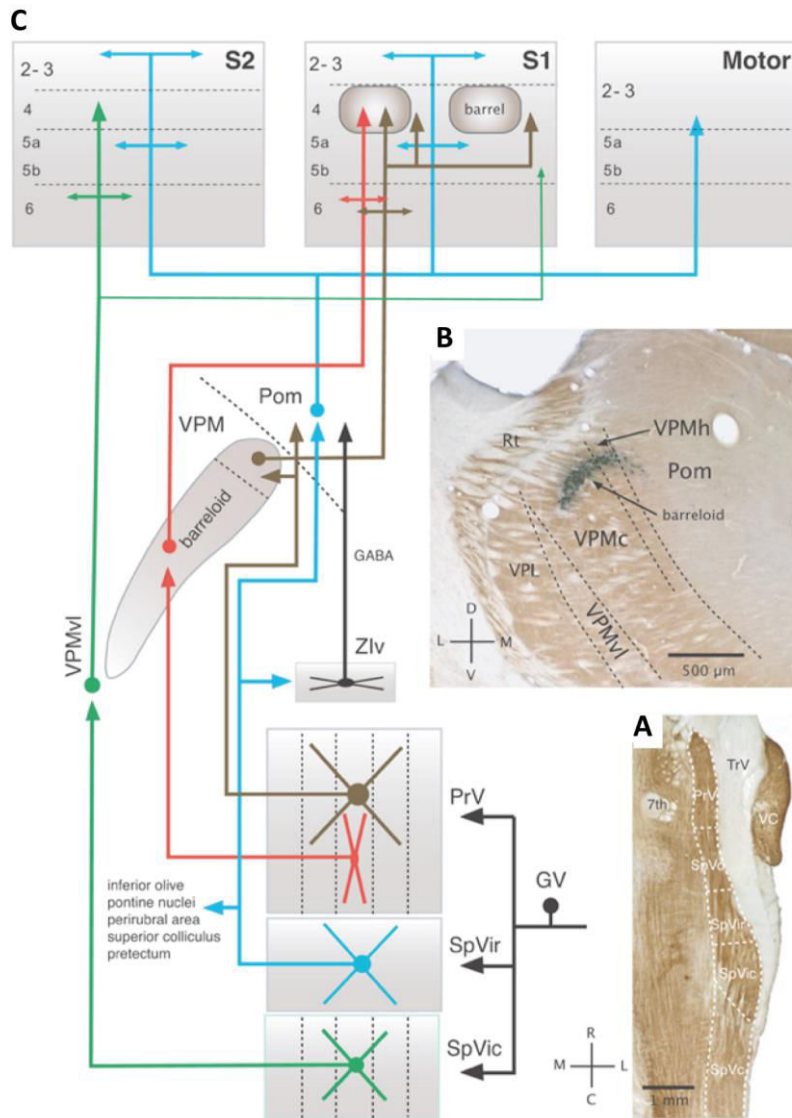


Figure 5: Parallel pathways to the cortex.

A: Trigeminal subnuclei that give rise to the ascending pathways are outlined in the horizontal section of the brainstem (CO staining); R, C, M, L, stand for rostral, caudal, medial, and lateral, respectively.

B: Thalamic regions that serve as relay stations for each ascending pathway are delineated by dashed lines in the CO-stained section. A barreloid was labeled by Fluorogold injection into barrel C2; D, V, M, L stand for dorsal, ventral, medial, and lateral, respectively.

C: Different cortical areas and different layers in the same cortical area, receive the thalamic afferents through distinct pathways. The wiring diagram shows each of these pathways: lemniscal pathway, red; paralemniscal pathway, blue; extralemniscal pathway, green. A second lemniscal pathway is depicted in brown.

From (Deschenes, 2009).

I.1.2.3 Somatotopy at each neuronal relay

The discrete aspect inherent to the vibrissae is remarkably conserved over the whole afferent pathway from the whiskers to the cortex: one vibrissa has its respective “barrelette” in the brainstem, a “barreloid” in the thalamus and finally a “barrel” in S1. Figure 6 shows how somatotopy is conserved along the afferent pathways.

In the trigeminal ganglion the cell bodies of the primary afferents are organized in a dorsal-to-ventral somatotopic way, meaning that the neurons innervating distinct rows can be distinguished by their location, however this is not the case for the neurons innervating distinct arc (Leiser and Moxon, 2006). In addition, Leiser and Moxon showed that there are more cells that respond to the caudal whiskers than to the more rostral ones, suggesting a gradient of representation, where the bigger whiskers are more represented than the smaller ones in this stage.

The brainstem is the first level where the facial maps and whisker representations are formed. Indeed, as described before, the primary afferent fibers coming from the first-order neurons of the trigeminal ganglion are projecting to the brainstem trigeminal nuclei. Among those, only the PrV, SpVi and SpVc nuclei have a clear sensory somatotopic representation. Such map could not be revealed by histological means in the nucleus SpVo (Ma, 1991). The sensory input of each whisker is relayed and somatotopically mapped into structures called “barrelettes” that can be clearly visible, after staining with cytochrome oxidase, as rostrocaudally-oriented rods (Ma and Woolsey, 1984). The PrV nucleus is dominated by single whisker receptive field neurons and 75% of them project to VPM (Minnery and Simons, 2003). The different nuclei of the brainstem are interconnected, with the exception of the SpVo, which is not projecting to PrV (Jacquin et al., 1990; Furuta et al., 2008).

At the thalamic level, we can find a clear somatotopy in the VPM nucleus where each vibrissa is represented anatomically as a cytoarchitectonic distinct unit called “barreloid” (Van Der Loos, 1976; Land and Simons, 1985). Thus, along the lemniscal pathway the information from each vibrissa stays segregated and the somatotopy is respected while the paralemniscal is much more diffuse, which explains the absence of barreloids in the thalamic POm nucleus. Multiwhisker responses are found in the trigeminal nuclei of the brainstem (Veinante and Deschênes, 1999) as well as in the thalamic nuclei that project their axons to the cortex, including the VPM (Armstrong-James and Callahan, 1991).

The VPM projects to the L4 of S1, in particular the VPMdm send its thalamic buttons at the center of the barrel through the lemniscal pathway and the VPMvl project to the septa between barrels through the extralemniscal pathway. In addition, other synaptic buttons can be found in L5b and L6a, an area related, but not exclusively, with the cortico-thalamic feedback (Chmielowska et al., 1989; Lu and Lin, 1993; Bureau et al., 2006; Brecht, 2007; Alloway, 2008; Constantinople and Bruno, 2013).

A recent study showed that the cortical somatotopic map of the facial whiskers is maintained in the reeler mouse, a reelin mutant without cortical lamination, suggesting that the functional map does not depends on the cortical layers (Guy et al., 2015).

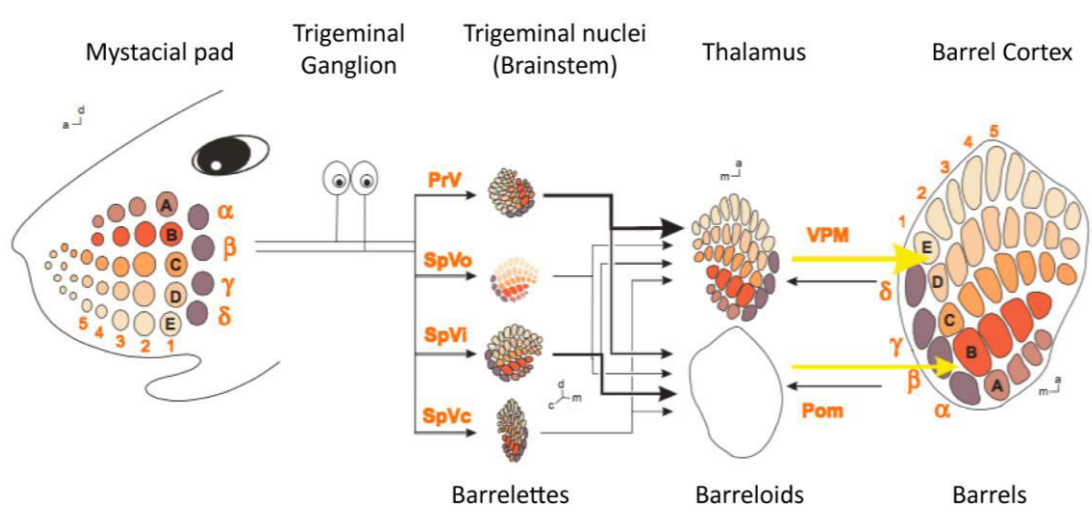


Figure 6: Preserved somatotopy through the somatosensory pathway.

Schematic diagram summarizing the major stages of the rodent barrel pathway. Sensory information from the mystacial whiskers reaches the trigeminal nuclei in the brain stem, the thalamus, and the barrel cortex. Each vibrissa is associated with a brainstem “barrelette”, a thalamic “barreloid”, and a cortical “barrel”.

PrV, nucleus principalis of the trigeminus; SpVo, spinal nucleus of the trigeminus pars oralis; SpVi, spinal nucleus of the trigeminus pars interpolaris; SpVc, spinal nucleus of the trigeminus pars caudalis; VPM, ventral posterior medial (ventrobasal) nucleus of the thalamus; and Po, posterior nucleus of the thalamus.

Modified from (Yuste and Simons, 1997).

As a summary, it appears that the rodent vibrissal system acquires tactile information actively, the motor commands being constantly adjusted according to the sensory inputs. Vibrissae are moved collectively against the surrounding objects, thus leading to complex spatiotemporal sequences of deflections. From the vibrissae follicles where the mechanical constraints are transduced into neuronal activity, the tactile sensory information is conveyed to different regions of the barrel cortex through the lemniscal, paralemniscal and extralemniscal pathways that carry different features of the stimulus (Bureau et al., 2006; Yu et al., 2006). These pathways are reviewed in (Petersen, 2007; Diamond et al., 2008). Even though the information is segregated from the vibrissae to the cortex, the perception of the stimulus is unique. This integration of the information might rely on many cortico-cortical projections, both within the barrel column (Lefort et al., 2009) and also through laterals projections from one column to the next (Schubert et al., 2007). We will review the different types of connectivity of the barrel cortex in the following chapter.

Chapter 2: The Barrel Cortex

1.2.1 Somatotopic maps

In the mammalian primary somatosensory cortex (S1) the body surface is represented in a way that adjacent cortical neurons respond selectively to stimuli presented to adjacent locations of the body. This arrangement was first described in the human S1 where the spatial representation of the human body was named “homunculus” (i.e. “little man”).

1.2.1.1 The somatosensory homunculus

The presence of an orderly representation of the body in the brain was first published in 1886 by John Hughlings Jackson, an English physician who studied how the spasms on epileptic patients progress from one part of the body to a neighboring one (Jacksonian march) suggesting that these areas are represented in neighboring regions on the brain. By using electrical stimulation of the cortex in primates, (Leyton and Sherrington, 1917), provided the first detailed map of the motor cortex. However, the existence of such a systematic body representation in the somatosensory cortex has been first evidenced in 1937 by the Canadian neurosurgeon Wilder Penfield who mapped the cerebral cortex of conscious epileptic patients via direct electrical stimulation (Penfield and Boldrey, 1937). The results were represented in a cartoon, which was further developed in the book of Penfield and Rasmussen (1950, Figure 7A).

The homunculus shows the relative amount of cortical space devoted to gather information from each part of the body (Penfield and Boldrey, 1937; Penfield and Rasmussen, 1950). While the accuracy of these first maps has been discussed (Schott, 1993), their importance is unquestionable as they revealed the existence of a spatial organization of the somatosensory cortex; they showed that the somatosensory representation of the hands and face occupy a large cortical space and uncovered the existence of somatotopic discontinuities at the junctions between some body representations (e.g.: junction between feet and genitals). Curiously, only a few studies have been done in human females, and many parts of the “hermunculus” still need to be revealed (reviewed in Di Noto et al., 2013).

Later on, Woosley (1952) and Kaas et al. (1979) depicted somatotopic maps on other primate species, but instead of stimulating the cortex, they measured the electrical responses evoked by the delivery of tactile stimulation to different parts of the body. Virtually, all mammalian species have these homunculi of different shapes as a result of different evolutionary adaptations of their usage of the tactile system (Krubitzer and Seelke, 2012). The somatotopic maps of S1 appear to be a highly conserved organizational principle, but this does not mean that they remain fixed, on the contrary, they are highly plastic at different developmental stages and also, depending on the motor task, they can be dynamically re-organized (Shulz and Ego-Stengel, 2012). Hence, the body parts that have a strong behavioral relevance for the species have more extended cortical representations than the others, as it is the case in the visual system for the fovea area in the retinotopic maps.

1.2.1.2 The “mouseunculus”

The sensory maps of mammals are finely tuned to the animal life style. Rodents are nocturnal animals that live underground, they use their vibrissae to navigate and gather information from the environment (as previously mentioned in Chapter 1). Within the barrel cortex, the representation of the whiskers dominates the somatotopic map (Figure 7B). This region, also called the posteromedial barrel subfield (PMBSF), covers approximately 40 % of the mouse barrel cortex, and it was first described by (Woosley and Van der Loos, 1970). Although this first description of the “mouseunculus” determined by evoked potential techniques has been rectified along the years through the accumulation of anatomic-functional data, it represents a crucial step in the field since it revealed the importance of the whisker’s cortical representation in rodents.

For simplicity purposes, in the thesis, we refer to the “barrel cortex” to designate the PMBSF, since our work was centered on the whisker’s representation within S1.

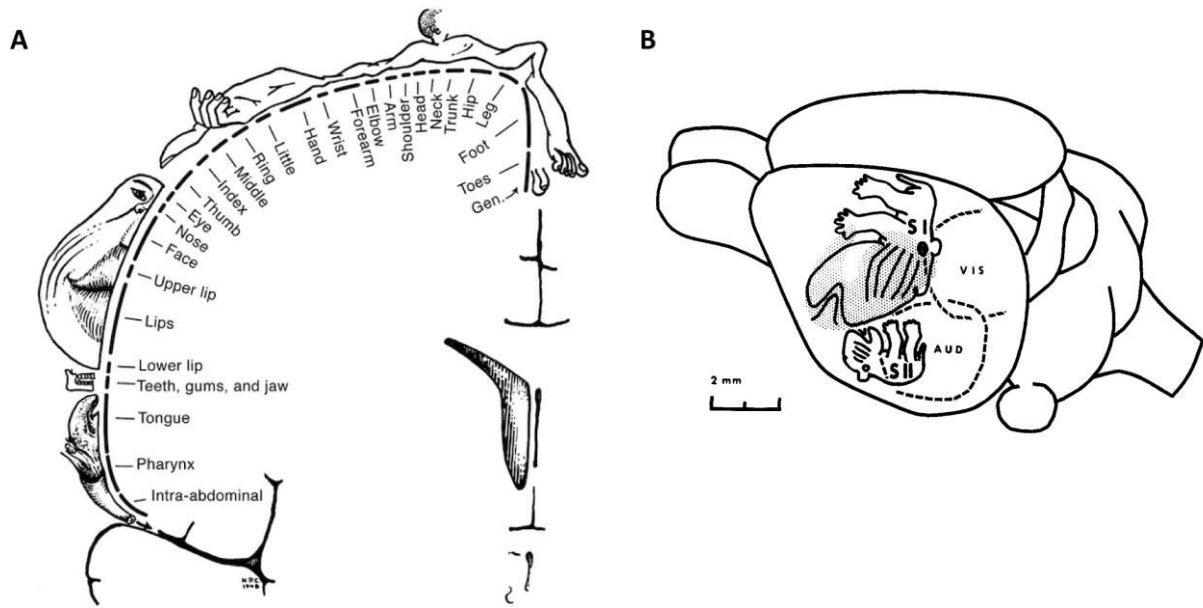


Figure 7: Somatotopic maps.

A: The homunculus, *adapted from* Penfield and Rasmussen (1950)

B: The mouseunculus, *from* Woolsey and Van der Loos (1970)

1.2.2 The barrel cortex: an identifiable cortical structure

Since it was first described by Woosley, Welker, and collaborators, the barrel cortex has become one of the most important models to study cortical processing, mainly due to the tight correspondence between the individual sensors – the whiskers – and the cortical columns – the barrels (Woolsey and Van der Loos, 1970; Welker and Woolsey, 1974; Welker, 1976). Because of its high specialization and clear spatial organization, the barrel cortex is an adequate sensory system to study the relationship between structure and function. The barrel cortex is present in many rodent species and some marsupials; however the majority of the knowledge that has been gathered on this cortical network comes from rats and mice. In the following pages, we will focus our attention on these two species, and especially on the mouse barrel cortex since it was the model chosen for our experimental work.

1.2.2.1 General architecture

Despite primary sensory cortices have different functions; they share some common principles in terms of organization and processing of sensory inputs. One of these principles

is the functional organization in columns. The columnar hypothesis (Mountcastle, 1957, 1997) suggests that the cortical column is the functional unit of the cortex. In the rodent somatosensory cortex, the L4 barrels made the cortical columns clearly visible and constituted a strong argument in favor of the columnar hypothesis. Woolsey and Van der Loos (1970) were the first ones to observe and describe discrete units in the cortical L4 when sectioning the brain in the coronal or transversal plane. They named them “barrels” given their 3D structure resemblance to barrels of wine.

Curiously, in their seminal article, Woolsey and Van der Loos compared this peculiar brain structure with some barrels that appear on a XVIIth century painting of Pieter Bruegel named “The fair of St George’s Day” (Figure 8A). In their own words:

«This 17th century representation of the barrel is a geometrically adequate rendition of the unit. The cortical barrel may have undergone some distortions from Bruegel's model in various places in the field but the basic elements, sides and hollows, are shared by all. The field as a whole (...) may be thought of as being composed of many barrels placed tightly side by side much as, in Bruegelian dimensions, might happen at a brewery».
Woolsey & Van der Loos, 1970.

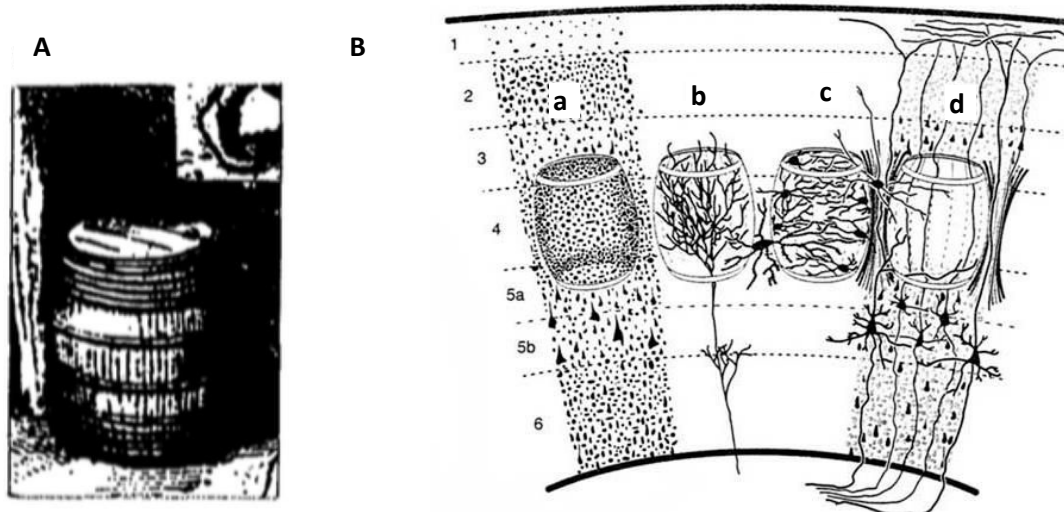


Figure 8: Anatomy of the barrel cortex.

A: The Bruegel’s barrel, from Woolsey & Van der Loos (1970).

B: Neuronal components of a cortical barrel. **a:** the distribution of neural somata as seen with Nissl staining. **b:** an afferent from the ventral posteromedial nucleus of the thalamus ends primarily in the barrel center. **c:** morphology of barrel cells, cell bodies in the walls of the barrel and the dendrites projecting to the center. **d:** apical dendrites of infragranular (mainly layer 5 cells) and axons of supragranular cells pass preferentially through the barrel wall and septum. From (Waite, 2004).

Alike other sensory cortices, the barrel cortex contains six layers named L1 to L6. Each layer is distinguishable by the type and size of its cellular components and thus can be visualized by histochemical staining (such as Cresyl violet or Nissl). The most superficial layer, L1, shows the lowest cell density of all. The L2 and L3 are difficult to dissociate in rodents, and usually referred as L2/3 or “supragranular layers” as they are on top of L4. The L5 and L6 are subdivided in L5a, L5b, L6a, L6b, and they are called “infragranular layers”. As mentioned before, a tangential cut at the depth of L4 reveals a group of ordered cytoarchitectonic structures, the barrels, making L4 the most visible of the cortical layers of S1.

But why we see barrels in L4 of the rodent S1? In this layer many thalamic afferents terminate and form dense discrete clusters at the center of the barrels. In the mouse, cell bodies tend to be dense in the barrel wall and sparser in the center (Woolsey and Van der Loos, 1970; Welker and Woolsey, 1974). The cells in the wall (between 2 to 3 layers of cells) tend to project their dendrites towards the center (Simons and Woolsey, 1984) where they pick up synaptic contacts from the thalamic afferents (Figure 8B). Following a histological staining with cytochrome oxidase (CO) the barrels become clearly visible (Figure 9). CO is a mitochondrial enzyme, and mitochondria are particularly dense at synapses, so we can see a stronger staining in the center of the barrel where the thalamic inputs arrive. L4 is characterized by a high density of spiny stellate cells, also named granule cells, and this layer is then referred as the “granular layer”. Barrels are surrounded by septa that can be seen as clearer areas with CO staining since they are poorer in cell bodies.

The architecture of S1 is globally conserved from one individual to the other. The somatotopic organization of the barrel cortex can be easily visualized on tangential sections by CO staining (Figure 9). Barrel subfields dedicated to specific parts of the body can be distinguished such as the forepaw, hindpaw and lower jaw subfields. The larger posterior medial and anterior lateral barrel subfields correspond to the cortical representation of the macro-vibrissae, and the micro-vibrissae, respectively (Land and Erickson, 2005). The spatial distribution of the barrels in the PMBSF reflects the organization of the whiskers on the snout of the animal. The barrels are arranged from row A to E and the five bigger arcs numerated from 1 to 4 (assigning a greek letter to the most caudal arcs corresponding to the whiskers “straddlers”). It can also be observed in Figure 9B that the barrels present different

shapes: the ones of the posterior arc (greek letters) and the ones of the middle row (row C) being the largest ones (Meyer et al., 2013). In the mouse, the barrels tend to be narrower along the rows than in the orthogonal axis along the arcs, and measure in average about 300 μm (Lefort et al., 2009). Indeed, the most central barrel (C2) counts about 1700 excitatory neurons and 140 GABAergic interneurons, while the entire cortical column which contains this C2 barrel counts in total 5730 excitatory neurons for 740 inhibitory interneurons (Lefort et al., 2009). Note that the same anatomically defined region (the C2 barrel-related column) of the rat barrel cortex contains, three times more neurons: 17200 excitatory neurons for 2500 inhibitory interneurons (Meyer et al., 2013).

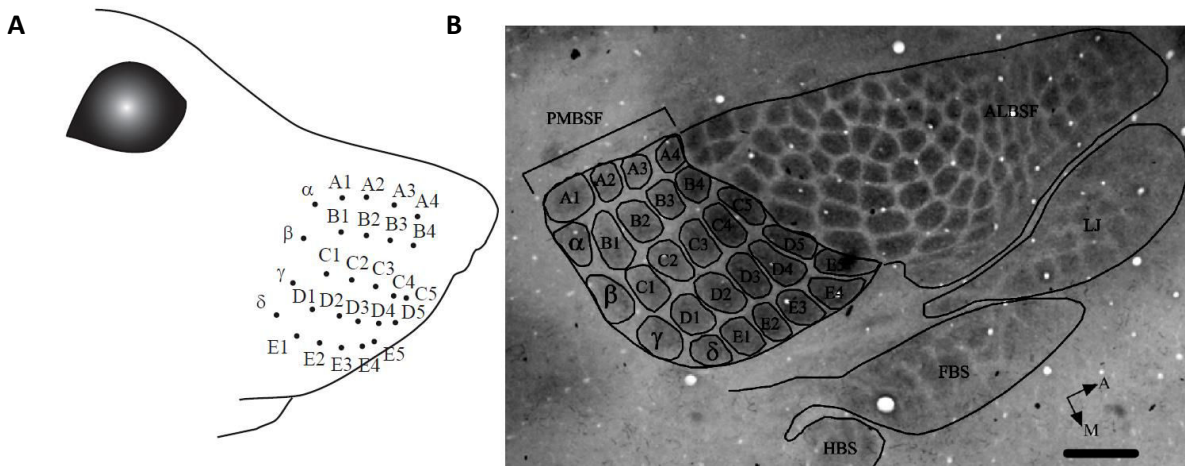


Figure 9: Correspondence between whiskers and barrels.

A: Disposition of the whiskers on the snout of the mouse.

B: Cytochrome oxidase stained barrel field in a mouse with a drawing superimposed showing prominent barrel subfields: PMBSF, posterior medial barrel subfield; ALBSF, anterior lateral barrel subfield; LJ, lower jaw; FBS, forepaw barrel subfield; HBS, hindpaw barrel subfield. Individual PMBSF barrels are outlined and labeled. Five prominent rows of barrels (A to E) can be seen. In addition, four posteriorly located straddler barrels (α , β , γ , δ) can be also seen. Scale 500 μm . *Adapted from* (Jan et al., 2008).

1.2.2.2 Cellular components

The barrel cortex contains a majority (about 80% or more) of excitatory cells that are glutamatergic and localized in all the layers from L2 to L6, but preferentially in L2/3 and L5/6 (Feldmeyer et al., 2002; Lefort et al., 2009). This neuronal population is mainly composed by pyramidal cells, which are characterized by the triangular shape of their soma, a prominent apical dendrite that extends vertically to the surface of the cortex, and basal dendrites that emerge laterally from the base of their cell body. Beyond these common morphological properties, the pyramidal neurons can be divided into different populations according to their post-synaptic targets (Figure 10). One can distinguish the intratelencephalic (IT) neurons, found in L2-6 and whose targets are located within the telencephalon (including the contralateral cortex); the pyramidal tract (PT) neurons, essentially located in L5b that project to subcerebral targets (such as the brainstem, midbrain, but also send branches to the ipsilateral cortex); and the corticothalamic (CT) neurons, found in L6 that project primarily to the ipsilateral thalamus (Harris and Shepherd, 2015). In addition to the pyramidal cells, excitatory neurons of the barrel cortex comprises the spiny stellate cells, which are specially located in L4 where they collect afferent information from the center of the barrel and distribute it to the upper layers within the column, mainly to L3 (Lübke et al., 2000; Markram et al., 2004; Staiger et al., 2004).

The barrel cortex contains also inhibitory interneurons present within all layers. These neurons are GABAergic non-pyramidal cells with low spine density, and have short axons that project within the cortical column and to direct neighboring columns. Barrel cortex interneurons are likely to cover all possible types of inhibitory interneurons that occur in the neocortex (Markram et al., 2004; Helmstaedter et al., 2009a, 2009b). Indeed, these cells present highly diverse morphological, biochemical, and electrophysiological properties (Figure 11). This diversity has led to several classifications that aimed at identifying populations of interneurons relevant from a functional point of view. However, the restriction of the classification criteria, due, at least in part, to technical limitations, makes difficult the comparison of the defined neuronal populations (Ascoli et al., 2008; DeFelipe et al., 2013).

We describe here the interneurons depending on their post-synaptic target, which strongly impacts the function of these cells. Markram and collaborators published a review of the inhibitory interneurons based on this classification criterion (Markram et al., 2004). The basket cells make synapses on the soma and proximal dendrites of pyramidal cells and interneurons; chandelier cells form synapses in the initial segment of pyramidal cell axons and might silence their output without affecting the processing of the input, and also prevent the back-propagation of action potentials; and a third class of cells target the dendrites of pyramidal cells like the double bouquet, bitufted, bipolar, Cajal-Retzius, neurogliaform, and Martinotti cells. Large basket cells together with Martinotti cells have axons that project over a wider area than a single barrel column, providing a substrate for cross-columnar inhibition. Given that they project to the soma and dendrites, they might inhibit excitatory inputs on pyramidal cells, for example projections coming from the thalamus or back projections from other cortical areas.

As mentioned before, L1 shows the lowest cell density of all layers and it is considered that virtually all L1 cells are GABAergic interneurons in the adult (Ren et al., 1992; Beaulieu, 1993; Hestrin and Armstrong, 1996). One hypothesis is that these inhibitory interneurons directly regulate the feedforward information coming from the thalamus (Galazo et al., 2008) and the feedback from “higher” cortical areas which could co-innervate these neurons as well as the terminal tufts of pyramidal cells arborizing in L1 (Vogt, 1995; Zhu and Zhu, 2004).

Glial cells, and in particular astrocytes, have an important role in the brain function, not only for their classical “housekeeping” properties, but also because they dynamically interact with neurons (Sims et al., 2015). These cells actively participate in the synaptic communication as they surround with their multiple processes the synapses between neurons, having a close contact with the pre- and post-synaptic cells. Astrocytes sense the same synaptic inputs as neurons and despite they are electrically non-excitabile, they respond with intracellular calcium changes that might trigger the release of gliotransmitters. In particular in the barrel cortex, *in vivo* studies showed that the astrocyte release of D-serine promotes plasticity (Takata et al., 2011), and the release of glutamate facilitates the remodeling of somatosensory maps during the critical period (Takasaki et al., 2008).

Astrocytes within barrels are preferentially coupled via gap junctions to each other, following the same arrangement in L4 as the anatomical defined neuronal structure (Houades et al., 2008).

In the following sections, we will explore the functional properties of the neuronal actors of the barrel cortex and their connectivity.

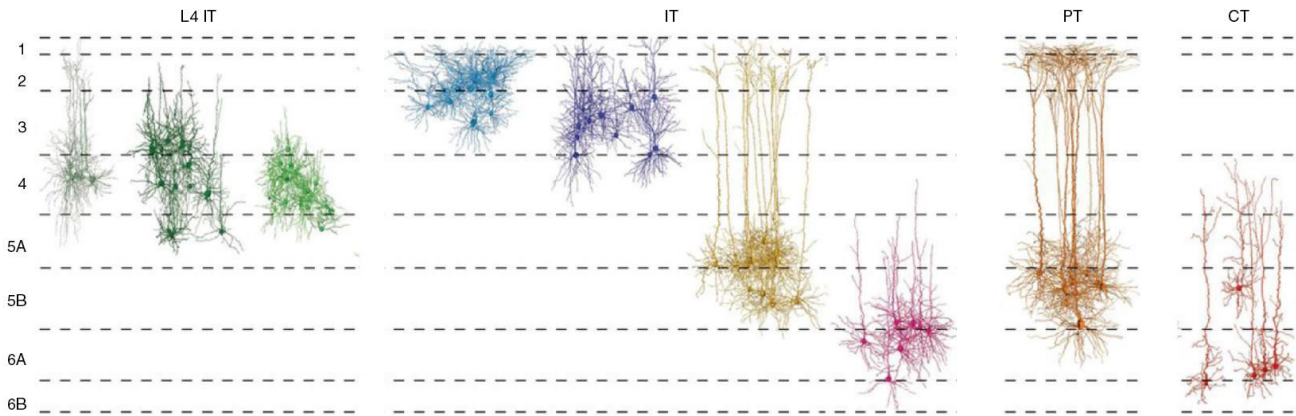


Figure 10: Dendritic morphology of excitatory neurons in the rat barrel cortex.

L4 IT: three morphological classes of L4 intratelencephalic (IT) neurons: pyramidal, star pyramidal and spiny stellate cells. **IT:** other intratelencephalic neurons of L2, L3, 5A/B and 6. **PT:** pyramidal tract neurons of L5B. **CT:** corticothalamic neurons of L6.

From (Harris and Shepherd, 2015)

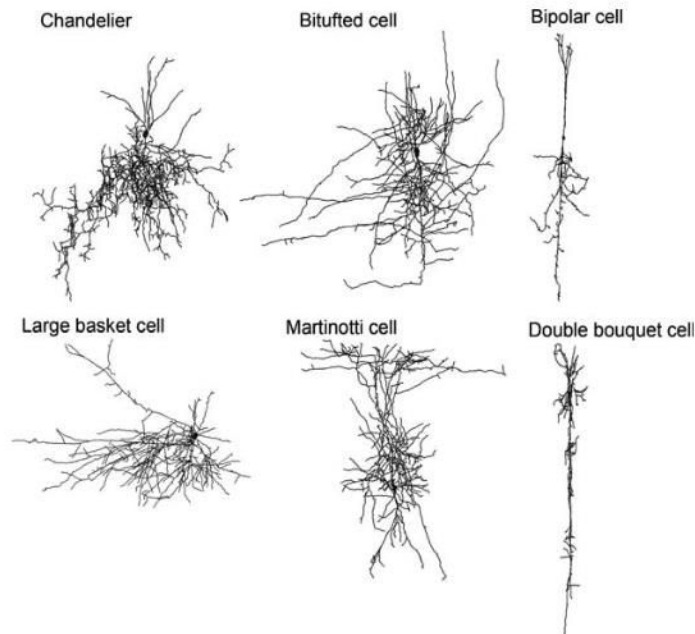


Figure 11: Axonal arborizations of cortical inhibitory neurons.

From (Fox, 2008) p.41.

1.2.2.3 Receptive fields

The term “receptive field” (RF) was first defined by Sherrington in 1906, as the area of the body surface where a stimulus can elicit a reflex. Later on, in 1938, Hartline extended the use of the term to sensory neurons in the visual system. He re-defined “receptive field” as the restricted region of the visual space where a luminous stimulus could elicit an electrical response in a retinal ganglion cell. Afterwards, the notion of RF was further extended to other neurons on the visual pathway, and to other sensory modalities. Hubel and Wiesel provided the first characterization of the RFs of neurons in the primary visual cortex, and they were the first ones to classify cells based on the RFs (Hubel and Wiesel, 1959, 1962). A broader definition of RF describes it as the portion of the sensory space that can elicit a neuronal response when stimulated. The neuronal response can be quantified by measuring the spiking activity (firing rate of the neuron) or the subthreshold (excitatory post synaptic potential) activity evoked by the stimulus. The sensory space can be composed of one or multiple dimensions.

In S1, the RF of a neuron that encodes tactile information is primarily defined as the region of the body that, after stimulation, elicits a response. Regarding the whisker barrel cortex, the RFs of neurons are multidimensional as these cells are selective not only to the identity of the stimulated whisker, but also to the direction of the whisker deflection (Simons, 1978; Swadlow and Gusev, 2002; Kida et al., 2005; Andermann and Moore, 2006; Puccini et al., 2006). In this sense, the barrel cortex neurons have RFs that share many characteristics with the visual RFs.

As we have seen in a previous section, the barrel cortex is characterized by anatomofunctionally well-defined columns. These columns are arranged in an anatomic map of body representation (Figure 9). When a whisker is deflected there is a chain of activation of the afferent neural pathway, from the peripheral receptors to the cortex, where information arrives mainly at the level of the corresponding barrel in L4. The cortical column associated to this whisker is activated, and then the adjacent columns are subsequently activated (Petersen et al., 2003a; Ferezou et al., 2006). The “principal whisker” (PW) of a neuron is the whisker that elicits the strongest response with the shortest latency. In addition, every neuron in the barrel cortex responds to the stimulation of several whiskers (Simons, 1978; Armstrong-James and Fox, 1987; Zhu and Connors, 1999; Brecht and Sakmann, 2002). These

are called the “adjacent whiskers” (AW), and they elicit responses that have smaller amplitude and longer latency than the response to of the PW. However, the principal whisker paradigm is not that straightforward, as defining a RF is not trivial. Many functional properties of the barrel cortex neurons are not integrated in the picture; for instance, it has been shown by our team that the structure of the RFs varies according to the direction of the local whisker deflections (Le Cam et al., 2011). One factor that will influence the estimation of the RF is then the type of whisker stimulation. Moreover, non-linear summations of responses to the stimulation of AWs were also observed in many studies (Simons, 1985; Simons and Carvell, 1989; Brumberg et al., 1996; Shimegi et al., 1999; Ego-Stengel et al., 2005). It is also important to consider that RF might change dynamically: early responses can condition responses to input arriving late to surround whiskers (Armstrong-James and Fox, 1987). It is also known that the RF size depends on the type and level of anesthetics used. Under deep anesthesia, RFs were larger than under light anesthesia both when using pentobarbital or urethane (Ito, 1981; Brecht and Sakmann, 2002; Jacob et al., 2008); similar responses have been reported in the thalamic VPM nucleus (Friedberg et al., 1999).

Within the L4, the neurons that are located in the septa between the barrels have receptive fields much larger and diffuse than the barrel neurons (Armstrong-James and Fox, 1987; Brecht and Sakmann, 2002). This result suggests that there are two cortical maps that coexist in the L4: the one of the barrels and the one of the septa. In the non-granular layers, the cortical domains associated to the stimulation of one vibrissa are larger than the anatomical cortical column –the barrel – and overlap each other (Armstrong-James and Fox, 1987; Brecht et al., 2003; Petersen et al., 2003a).

The receptive field properties of a given neuron directly depend on its synaptic inputs; exploring the cortical connectivity within the barrel cortex is therefore a key step to further understand the processing of tactile sensory information.

1.2.3 Connectivity in the barrel cortex

1.2.3.1 Afferent connections

All layers in the barrel cortex receive excitatory synaptic inputs from the thalamus (Alloway, 2008; Meyer et al., 2010; Oberlaender et al., 2012; Constantinople and Bruno, 2013).

As already mentioned, the projections from the barreloids of the VPM thalamic nucleus end mainly in L4, at the center of its corresponding barrel without trespassing its borders (Bernardo and Woolsey, 1987; Jensen and Killackey, 1987). However this is just a simplification, as 5 % of the neurons that project to one barrel are in fact coming from an adjacent barreloid (Land et al., 1995). About 10-20% of the synapses received by an excitatory neuron of L4 come from the thalamus (Benshalom and White, 1986; Schoonover et al., 2014), which means that intracortical connections considerably outnumbered them. Both excitatory and inhibitory neurons are innervated by thalamocortical projections in the L4 barrel (Keller and White, 1987; Porter et al., 2001; Bruno and Simons, 2002), although the majority of synapses are with excitatory neurons since they outnumber the L4 interneurons by far (8% inhibitory vs 92% excitatory)(Lefort et al., 2009; Meyer et al., 2011).

Afferent projections coming from the VPM also innervate pyramidal cells and inhibitory GABAergic interneurons in L3, L5b and L6a (Meyer et al., 2011; Oberlaender et al., 2012), as it is schematized in Figure 12A.

Thalamic afferents coming from P0m end mainly in the septa between the barrels of the L4, in the L1, L2/3 and L5a (Herkenham, 1980; Koralek et al., 1988; Chmielowska et al., 1989; Lu and Lin, 1993). In L5a, P0m afferents probably establish synaptic contacts with basal dendrites of L5a pyramidal neurons (Petreanu et al., 2009), while in L1 and upper L2 they target the apical dendrites of L2, L3 and L5 pyramidal neurons, in addition to L1 and L2 interneurons (Figure 12B).

As VPM and P0m inputs afferent connections end in different subareas of the barrel cortex, they are supposed to be the key elements for distinct pathways: the “barrel column” and the “septal column” (Alloway, 2008).

Even though the vertical feed-forward flow in a barrel column is strong, there is a high degree of horizontal and transcolumar synaptic connections together with reciprocal intracolumar synapses.

1.2.3.2 Intracortical connectivity

The intracortical circuitry is dominated by two sources: local intralaminar connections (intracolumnar and transcolumnar), and translaminar input.

Excitation arriving from the VPM recruits mainly L4 spiny stellate cells. These cells have very confined connections within the barrel column, but they principally project vertically to L2/3 and present smaller vertical projections to L5a (Lübke et al., 2000). Both projections tend to keep the topography, as they do not spread much to other columns. Also it has been shown that both spiny stellate neurons and star pyramidal neurons of L4 project to L6 pyramidal cells as part of the corticothalamic feedback (Qi and Feldmeyer, 2015).

The excitatory pyramidal cells from L2/3 have a big volume; in particular, their axons can extend horizontally for several millimeters within this layer covering numerous columns (Gottlieb and Keller, 1997). These horizontal connections between the columns have been confirmed by many histological techniques, showing in addition an asymmetry on their distribution. The connections are more common between the barrel columns from the same row towards the barrel columns of the rostral vibrissae (Hoeflinger et al., 1995), and to the most ventral row (Bernardo et al., 1990a). Electrophysiological studies of these cells showed that they do synaptic contacts with other pyramidal cells mainly in the L2/3 and in L5 (Reyes and Sakmann, 1999). This suggests that after the initial excitation of the L4, the cells of the supragranular layers are in charge of spreading the activity all along the column. The circuits of L2/3 can then be interpreted to link ongoing tactile information processing in S1 with the related activity of a multitude of afferent and efferent columns, and different functional cortical areas outside S1.

In the L5/6, especially in the L5, the pyramidal cells send one apical dendrite up to L1, and the basal dendrites extend over an area corresponding to several barrels within L5/6 (Ito, 1992; Lübke et al., 2000). These cells are also in charge of collecting information from all layers of the cortical column and from several barrel columns. Also, it has been shown that all the cortical layers send connections to L5 (Schubert et al., 2001), confirming the integrative role of these neurons.

Both L2/3 and L5 pyramidal cells show a strong and prominent horizontal projection domain, projecting across the entire barrel field (Bruno et al., 2009; Oberlaender et al., 2011;

Narayanan et al., 2015). These projections might help integrating whisker-touch induced synaptic excitation in different barrel columns.

Finally, the cells in the septal region form a wide mesh of connections with septal regions several barrels apart. These cells have been reported to receive thalamic input from the POm and the VPMvl (Koralek et al., 1988; Bokor et al., 2008). Unlike the barrel cells, they receive callosal input from the barrel field in the other hemisphere (Sehara et al., 2012).

All these connections are further detailed in the Scholarpedia review article by Feldmeyer: S1 microcircuits (Feldmeyer, 2015).

1.2.3.3 Efferent connections

In the barrel cortex, only the pyramidal cells project their axon (and its multiple collaterals) towards other cortical areas or subcortical structures. The projections to the sub-cortical structures come from neurons located in the L5/6: thalamus (L5b/L6); striatum (L5a); spinal cord, pons and inferior colliculi (L5b).

The pyramidal cells from both supragranular (L2/3) and subgranular (L5/6) layers send projections to S2 and M1, generally in a non-overlapping manner (Chakrabarti and Alloway, 2006; Mao et al., 2011).

The projections to S2 are topographic and form a mirror image of the S1 map. One barrel of S1 projects to a strip of S2, and neighboring barrels project to the same strip overlapping each other. Barrels from different rows project to different strips (Benison et al., 2007).

Both calcium imaging (Chen et al., 2013; Clancy et al., 2015) and targeted patch-clamp experiments (Yamashita et al., 2013) have revealed that within S1 supragranular layers, the pyramidal cells projecting to M1 or S2 have distinct properties. They are indeed characterized by different intrinsic membrane properties, they exhibit markedly different membrane potential dynamics during behavior, and even more importantly, they respond differently to whisker stimuli. M1-projecting neurons exhibits large receptive fields and strong responses although rapidly adapting; therefore, they are likely to play a role in contact detection, object localization, and optimization of motor commands to adapt whisker movements. In contrast, S2-projecting neurons present narrow receptive fields and

robustly signal sensory information during repetitive touch; they are more likely to be involved in object feature discrimination (Chen et al., 2013; Yamashita et al., 2013; Clancy et al., 2015).

As we previously mentioned, L5b and L6a have an important role in the cortico-thalamic (CT) feedback (Figure 12C). Alitto and Usrey reviewed the role of this loop in the top-down modulation of the ascending sensory information (Alitto and Usrey, 2003). The corticothalamic neurons have both excitatory and inhibitory effects on the thalamic neurons that send ascendant sensory afferents to the cortex. The excitatory influence of the cortex is made by monosynaptic connections, while the inhibitory is made polysynaptically via GABAergic interneurons within the thalamus or via GABAergic neurons of the reticular nucleus (RTN) of the thalamus (Bourassa et al., 1995; Cox et al., 1997; Golshani et al., 2001; Lam and Sherman, 2010). In a recent article Crandall and collaborators showed that corticothalamic feedback influences the thalamus by dynamically changing the balance between excitation and inhibition (Crandall et al., 2015). During low-frequency activity, CT effects are mainly suppressive, while during high-frequency activity the balance shifts having enhancing effects.

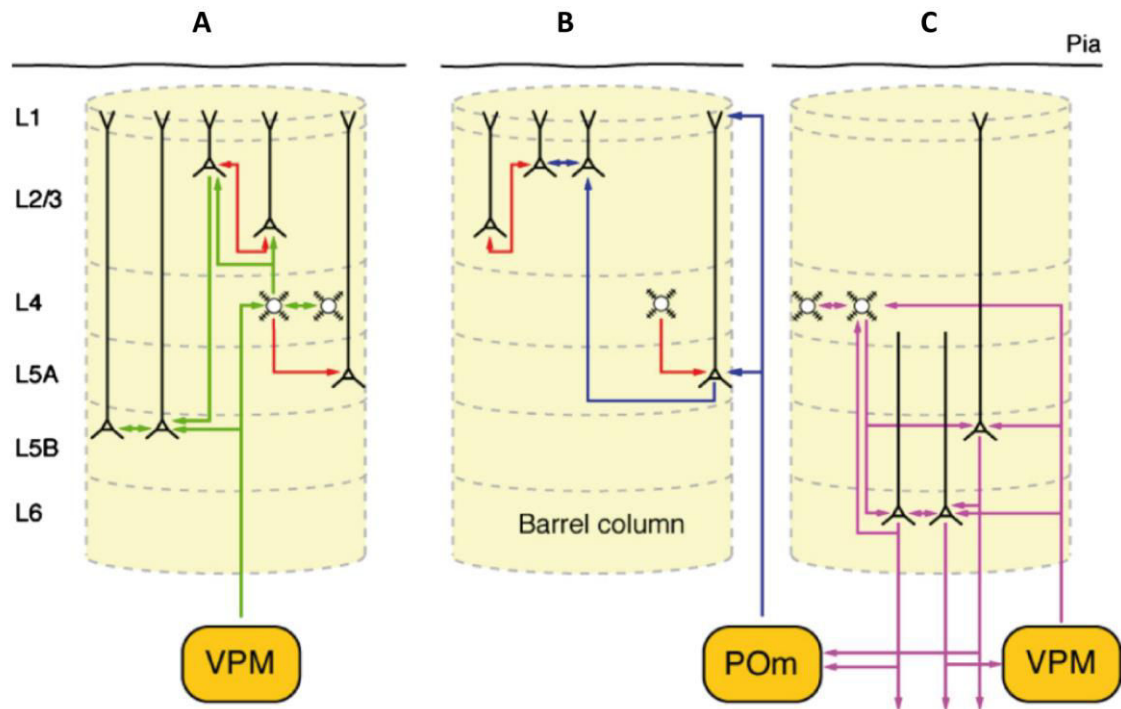


Figure 12: Scheme of parallel cortical microcircuits in the barrel cortex.

A: Cortical microcircuits receiving thalamic afferents from the VPM (lemniscal pathway) predominantly in L4 (and to a lesser degree in L5B).

B: Intracortical microcircuit receiving thalamic afferents from the POm (paralemniscal pathway) in L5a pyramidal neurons.

C: Synaptic connections involved in the thalamo-cortico-thalamic feedback circuit between L4 spiny neurons, L5b and L6 pyramidal cells, and the thalamic nuclei.

From (Feldmeyer et al., 2013).

1.2.4 Beyond the classical view

The classical view of the whisker system consists of several information relays from the follicle to the cortex, in which information is simply wired by the subcortical structures to the barrel cortex, being the cortex the only level where multiwhisker processing occurs. In addition, the anatomical and electrophysiological data suggests that the functional connectivity of the barrel cortex has the shape of a sandglass: restricted to one barrel in L4 and horizontally extended towards neighboring columns in the supragranular and infragranular layers (Bernardo et al., 1990b). Similarly to other sensory cortices, we can predict the dominant flow of cortical activity: starting in L4, ascending to L2/3, and then propagating to the whole cortical column and extending towards neighboring columns in the supra- and infragranular layers. The tight link between cortical structure and spatial organization of the periphery made the barrel cortex a popular model to study the cortical column. In particular, many studies were focused on the C2 column, as C2 is the whisker located in the center of the whiskerpad, with experimental approaches from *in vitro* to awake behaving animal (Crochet and Petersen, 2006; Ferezou et al., 2006, 2007; Poulet and Petersen, 2008; Lefort et al., 2009; Gentet et al., 2010; Crochet et al., 2011).

On the contrary to this canonical view of the whisker system, multiwhisker responses can be found already in the subcortical nuclei, both at the level of the trigeminal nuclei (Veinante and Deschênes, 1999), and at the VPM (Armstrong-James and Callahan, 1991). In addition, the three pathways that convey information to the cortex (lemniscal, paralemniscal and extralemniscal) have different temporal filtering and spatial integration properties, and, as previously described, they project to different regions of the barrel cortex where they are integrated through cortico-cortical connections.

Despite the fact that the classical view of the barrel cortex agrees with the columnar hypothesis, many of the functional properties of the barrel cortex neurons failed to be integrated into this big picture. The sensory information coming from one whisker is not treated in an independent way only by its corresponding cortical column. The idea that the thalamic inputs coming from one barreloid influence only the activity of the neurons within one barrel is not an actualized one.

Nonlinear summation of the responses to the stimulation of adjacent whiskers have been reported in many studies (Simons, 1985; Simons and Carvell, 1989; Brumberg et al., 1996; Goldreich et al., 1998; Shimegi et al., 1999; Ego-Stengel et al., 2005). In addition, it has been shown that a large proportion of barrel cortex neurons are tuned to the direction of deflection of the whisker (Simons, 1985; Brecht and Sakmann, 2002; Wilent and Contreras, 2005). Thus, the functional map is not totally equivalent to the anatomical map.

Even more complex is the scenario when giving multiwhisker stimulation. The experiments done in our lab (Jacob et al., 2008; Ego-Stengel et al., 2012) showed that some neurons in the barrel cortex are able to extract more information than only the one of its PW or AWs. In fact, neurons are able to extract emergent properties of the multiwhisker stimulation, such as the direction of the global motion of deflection of all the whiskers. Furthermore, additional experiments (Ego-Stengel et al., 2012) showed that these properties were already present at the thalamic level and revealed the importance of the corticothalamic loop on the global direction selectivity.

Moreover, in 2013 the group of Dr. Randy Bruno showed that neurons in L5/6 receive directly thalamocortical sensory-evoked inputs (Constantinople and Bruno, 2013). This study showed that L4 is not the only hub for distributing sensory-evoked activity, suggesting that there are at least two strata working independently in the barrel cortex.

Another argument against the classical view of the system is that cortical responses strongly depend on the behavioral context and the whisking activity of the awake-behaving rodent (Fanselow and Nicolelis, 1999; Ferezou et al., 2007). Other reports indicate that the level of attention and motivation of the animal can also affect the sensory responses in the barrel cortex (Ganguly and Kleinfeld, 2004; Pantoja et al., 2007).

In addition, the extent of lateral connectivity is much larger than previously thought. A recent study (Narayanan et al., 2015), showed that the majority of the intracortical axons project horizontally beyond the anatomical principal column, and this study also showed the existence of two orthogonal horizontal projection patterns of the supragranular and infragranular layers, which improve the integration and coding of multiwhisker information.

To sum up, if the barrel cortex is an attractive model by its apparent stereotypic organization, a closer view into it reveals a dense, highly interconnected network of heterogeneous neuronal components whose organizing principles are still being under exploration through constantly progressing techniques. Indeed, the evolution from pioneering studies based on electrophysiological recordings in anesthetized animals of neuronal activity evoked by deflections of one or two whiskers, to the most recent works relying on awake recordings, neuronal population imaging, or controlled stimulation of many whiskers, has revealed increasing levels of complexity. Hence, taking in account this complexity, it is hard to think the barrel cortex as a straightforward mirror of the whiskerpad. In the next chapter we will further discuss the existence of functional maps in the barrel cortex.

Chapter 3: Functional Cortical Maps

Maps are an organizing principle of the mammalian brain, and in particular functional maps relate function to anatomy. One type of functional organization is the topographic maps: such as the retinotopic, tonotopic or somatotopic. This type of representation persists from the receptor surface up to the cortex. Other functional maps like the orientation preference maps of the visual system originate first in the cortex.

The different dimensions of the stimulus can be mapped in different areas of the sensory cortices or share the same cortical volume. For instance, in the cat visual cortex the retinotopic map and the ocular dominance map are overlaid in the same cortical area. Multiplexing might be then a strategy for coding several features of the stimulus in a limited cortical volume. For a recent review on cortical mapping, see (Rothschild and Mizrahi, 2015).

As already mentioned, in the whisker system of the rodents, somatotopy is present from the ganglion cells to the cortex. We are interested in how other dimensions of the stimulus might be coded in the barrel cortex, in particular the direction of deflection of the whiskers. Within this chapter we will first review how directional tuning is coded along the whisker-to-cortex system; secondly, we will describe the controversy around the existence of an intracolumnar functional map for the direction selectivity; and finally, we will focus on the coding of multiwhisker features and their possible spatial distribution within the barrel cortex.

1.3.1 Directional tuning in the somatosensory pathway

Sensory neurons can code specific features of a stimulus like: position, direction, frequency, velocity. Direction selectivity, the preference of a neuron for a specific direction of motion of the stimulus, has been extensively studied in the visual system. It was first described in the cat's primary visual cortex (V1) by Hubel and Wiesel (Hubel, 1959; Hubel and Wiesel, 1959, 1962). When a luminous bar of a given orientation goes through the receptive field of a cortical cell in different directions, the neuronal response is often stronger to one of these directions of movement. This selectivity might be explained by the organization of the RFs

with ON/OFF subfields: when a stimulus goes from an OFF to an ON subfield, it produces simultaneously an excitation due to the entry on the ON zone and a disinhibition due to the exit from the OFF subfield. However, this synergy does not take place when moving on the opposite direction, thus the neuron will show a stronger response to the first direction. Nevertheless, this rationale of linear summation cannot be generalized to the entire cortical network given the complexity of the RFs of the different cell types and the strong interactions with other cortical sub-areas.

The following sections will briefly describe the local direction selectivity at different stages of the vibrissal pathway finishing by the cortex, and further discuss the potential origin of this selectivity.

1.3.1.1 Local direction selectivity in the subcortical structures

Eighty percent of the first-order whisker afferents present in the trigeminal ganglion are selective to a direction of deflection of the corresponding whisker (Zucker and Welker, 1969; Gibson and Welker, 1983; Lichtenstein et al., 1990). Figure 13 shows two representative units recorded extracellularly from the ganglion. The rapidly adapting (RA) cell responded transiently to stimulus onsets and offsets at all deflection angles, while the slowly adapting (SA) cell responded selectively to rostral deflections, whether occurring at the onset of the offset of the whisker displacement. In general, SA neurons are more selective than RA cells and this might be due to different mechanoreceptor endings and their relationship with the follicle structure (Zucker and Welker, 1969).

Neurons with local direction selectivity can be also found both in the lemniscal and the paralemniscal pathways (Minnery et al., 2003; Furuta et al., 2006). Figure 14A shows the neuronal responses in both the PrV trigeminal nucleus and the VPM when deflecting a whisker in different directions. The majority of cells in both the PrV and VPM show sensitivity to the direction of whisker deflection, with a similar degree of directional tuning (Figure 14B), suggesting that the directional properties of the stimulus are preserved across the trigeminothalamic synapse. Local direction selectivity, therefore, is present at all the levels of the lemniscal pathway, from PrV to S1 (Waite, 1973; Simons, 1978; Minnery and Simons, 2003).

Direction selectivity is also present in the paralemniscal pathway since an anisotropic organization of the receptive fields has been reported in the neurons of the interpolaris nucleus of the spinal trigeminal complex (SpVi, Figure 14 C-D), which project to the POM of the thalamus (Furuta et al., 2006).

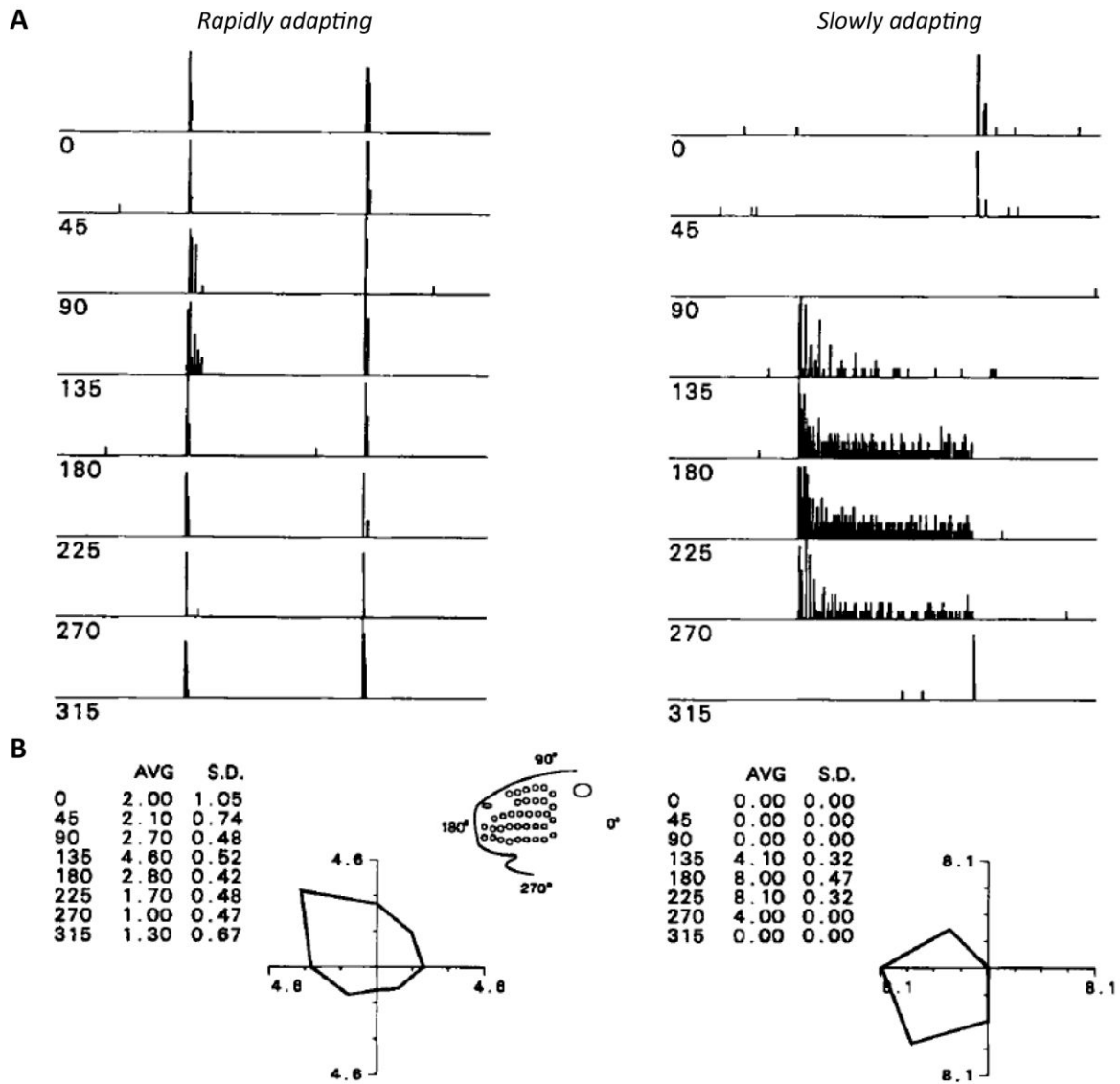


Figure 13: Direction selectivity in two well-tuned units of the trigeminal ganglion.

A: PSTHs of accumulated response to 10 deflections at eight different angles. PSTH duration of 500 ms; bins: 1 spike/ms.

B: Polar plots of responses to stimulus onset. Mean discharge and SD in spikes/stimulus onset are indicated for each angle.

Modified from (Lichtenstein et al., 1990)

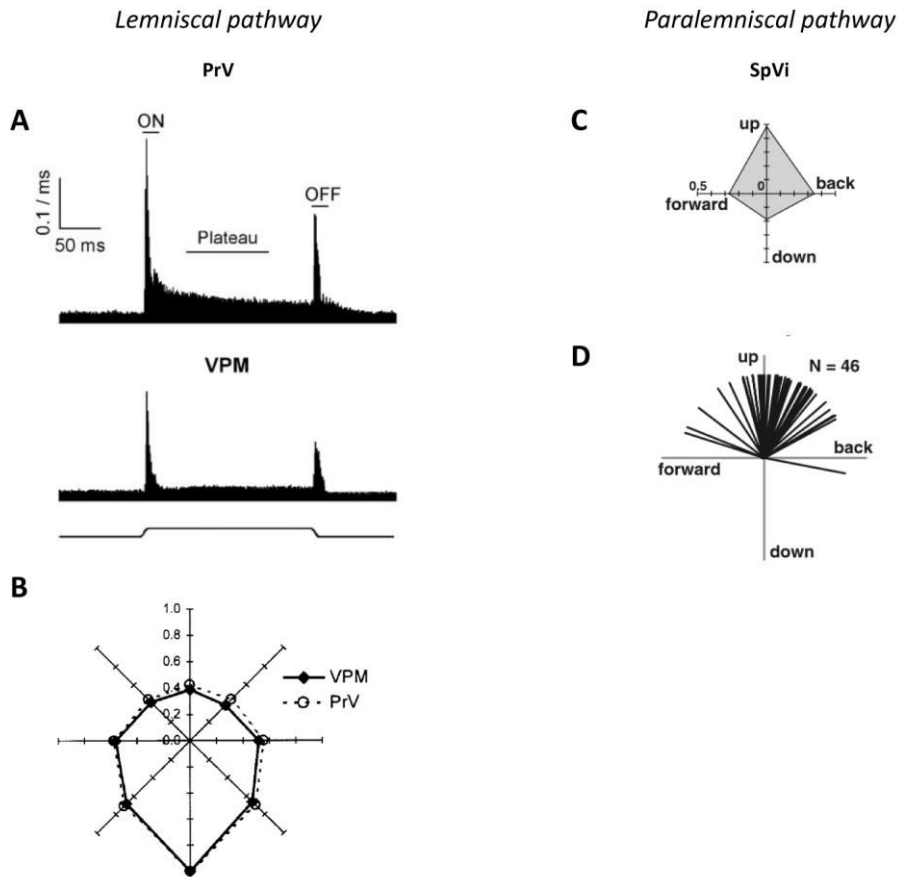


Figure 14: Direction selectivity in the trigeminal nuclei and thalamus.

A-B: Lemniscal pathway. *Modified from* (Minnery et al., 2003)

A: PSTHs of PrV and VPM population responses to PW deflections (n=72 cells; 5,760 deflections and n=77 cells; 9,760 deflections, respectively). Line under PSTH depicts stimulus waveform.

B: Directional tuning responses superimposed for VPM and PrV. Individual polar plots were rotated so that maximally responsive angles were aligned in a common direction and normalized to the maximally responsive angle. An average response at each angle was then calculated based on the entire population. These population polar plots for PrV and VPM reveal similar degree of ON response tuning within both populations.

C-D: Paralemniscal pathway. *Modified from* (Furuta et al., 2006)

C: Angular tuning of vibrissal responses in the SpVi. Mean normalized responses in all directions of SpVir (n= 341 vibrissae) and SpVic cells (n= 169 vibrissae). By computing the vector sum of all vibrissa-associated vectors within the receptive field of a cell, a grand vector was obtained that represents the ensemble direction tuning of that cell.

D: Distributions of grand vectors of angular preference for SpVi.

1.3.1.2 Local direction selectivity in the barrel cortex

Neurons of the barrel cortex are also selective to the direction of stimulation of a single whisker (Simons, 1978; Wilent and Contreras, 2005; Puccini et al., 2006; Andermann and Moore, 2006; Jacob et al., 2008). However, the percentage of cells strongly selective to the direction decreases from the trigeminal ganglion (80%) to the cortex (27%) (Bruno and Simons, 2002). Figure 15 shows the transformation of the direction tuning through the whisker pathway.

We might suppose then that the direction selectivity in the barrel cortex is inherited from the thalamic inputs. In fact, applying bicuculline (GABA_A antagonist) to the cortex induces cortical cells to present sensitivity towards all directions (Kyriazi et al., 1996), showing that local direction selectivity depends in part of the underlying local inhibition. This suggests that the cortical direction selectivity emerges through the intrinsic connectivity of the network. In addition, Wilent and Contreras showed that the selectivity is generated by a difference in the timing of the synaptic inputs between excitatory and inhibitory afferents (Wilent and Contreras, 2005).

Direction selectivity is coded by the neurons all along the vibrissal pathway, from the ganglion cells to the barrel cortex. Then, the following question arises: is it spatially distributed across the cortical space? This question will be addressed in the next section.

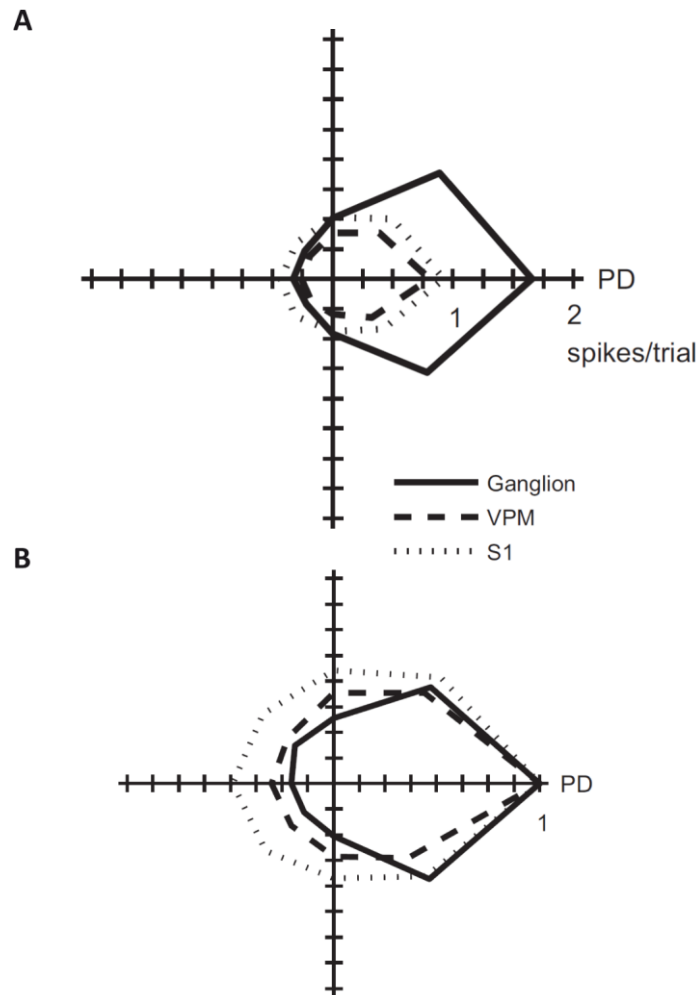


Figure 15: Transformation in directional tuning along the whisker pathway.

A: Tuning curves aligned by preferred direction (PD) and averaged over units.

B: Aligned tuning curves normalized by firing rate in the PD and averaged over units.

Modified from (Bale and Petersen, 2009)

1.3.2 “Topy” of direction selectivity in the barrel cortex

The representation of multiple features of a stimulus within the same cortical area potentially allows sensory systems to perform more optimized computations and processing of the external information. Some efforts have been made to extract the organizing principles of such representations within the barrel cortex of rodents (Petersen, 2007).

Some morphological evidences for subdivisions within the large L4 barrels of the rat barrel cortex have been reported (Land and Erickson, 2005), although they were not

observed in the mouse barrels. Furthermore, the description of a clear angular tuning preference mapping at the level of the VPM thalamic barreloids (Timofeeva et al., 2003), strongly suggests the possible existence of such a direction mapping at the cortical level.

However, the existence of a map for preferred direction at the subcolumnar scale in the barrel cortex has been an object of controversy. The group of Simons was the first to report the existence of mini-columns of neurons that shared the same angle of direction selectivity in the rat barrel cortex (Simons, 1978; Bruno et al., 2003). Nonetheless, they did not report any spatial distribution of these mini-columns.

In contrast, Andermann and Moore described in 2006 an anatomical organization of the local direction selectivity within the barrel column (Andermann and Moore, 2006). By doing extracellular recordings of the L2/3 on the rat, they described that, within the barrel column, the direction selectivity is organized in a pinwheel-like form centered near the column center (Figure 16A).

In 2007, Kerr and collaborators used 2-photon calcium imaging experiments to tackle this question. However, while imaging the responses of L2/3 neurons in young rats, they could not distinguish any direction selectivity map (Kerr et al., 2007), see Figure 16B. Later on, Tsytsarev and collaborators, by imaging intrinsic optical signals (Tsytsarev et al., 2010a) and VSD signals (Tsytsarev et al., 2010b) in the rat barrel cortex, aimed to reveal a mapping of orientation preference in supragranular layers although their results are difficult to interpret due to the lack of proper quantifications.

Finally, in 2011, Kremer and collaborators decided to run 2-photon calcium imaging experiments with two groups of rats of different ages (Kremer et al., 2011). They confirmed the presence of the map on the older group of rats, but not on the younger, suggesting that the direction selectivity maps emerge during the post-natal development (Figure 16C).

Recently, the group of Feldman studied coding in the mouse barrel cortex L2 with 2-photon calcium imaging (Clancy et al., 2015). They found that neurons in L2 are not somatotopically organized; indeed, they show a very sparse salt-and-pepper organization of the somatopy. These results reopen the controversy, as they suggest that the neurons within this layer might neither present a spatial organization of the direction selectivity. Unluckily they did not test this.

As an attempt of contributing to solve this argument, and given that up to the moment no study has been done to test the existence of this directional selectivity intra-barrel pinwheel in the mouse S1, we studied the spatial organization of the responses to multidirectional stimuli of the whisker C2. Our experimental protocols and results can be found in Part III – Chapter 1.

To sum up, neurons in the barrel cortex have a preferred direction of deflection of a single whisker, and this selectivity might be spatially distributed in the cortical space (addressed in Part III). Given the multiwhisker RFs of the cortical neurons, one might ask if global features of the stimuli are also coded, for example whether the barrel cortex neurons also have a preferred direction for stimuli involving all the whiskers deflected in given spatiotemporal sequences.

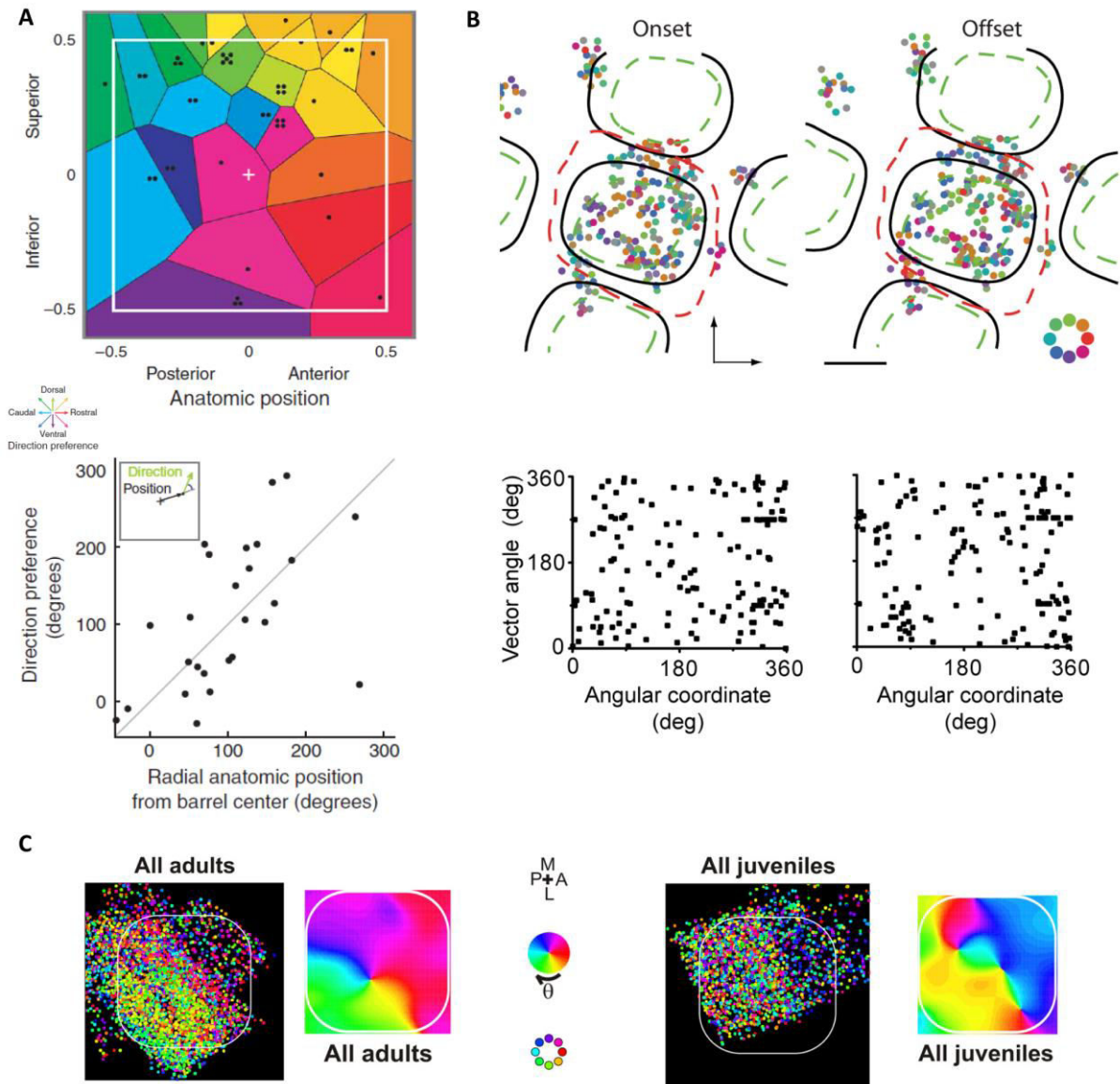


Figure 16: Review of the spatial distribution of local direction selectivity.

A: Direction preference map made from single-unit recordings from L2 to L4 shown relative to barrel coordinates (white box indicates barrel borders). When several single units were recorded within a penetration (indicated by multiple dots), direction preferences were averaged. Below is the scatter plot showing the relation between direction preference and the radial anatomic position of the recording site (without smoothing). *From (Andermann and Moore, 2006).*

B: The maximal-response direction of each neuron was color coded (color scale, bottom right) and plotted on an averaged barrel-centered map for deflection onset (left) and offset (right). Below the angle of directional tuning vector as a function of angular anatomic coordinate for all PW-related neurons. *From (Kerr et al., 2007).*

C: Superposition of all recorded neurons in normalized barrel coordinates and direction selectivity smoothed maps for juvenile rats (right) and for adult rats (left). White contour lines indicate normalized barrel borders. *From (Kremer et al., 2011).*

1.3.3 Emergent properties of spatiotemporal complex stimuli

When exploring the environment rats and mice contact the objects using multiple whiskers. The complex spatiotemporal pattern of deflections of the different whiskers must be integrated within the whisker system. The principal candidates for doing this integration are neurons with multiwhisker RFs of the barrel cortex. It has been shown that in the supra- and infragranular layers of the barrel cortex single neurons receive inputs from the PW and from several whiskers that surround it (Moore and Nelson, 1998; Zhu and Connors, 1999; Brecht and Sakmann, 2002; Brecht et al., 2003; Manns et al., 2004). And, as already mentioned, the structure of these multiwhisker RFs has been shown to vary according to the direction of the local whisker deflections (Le Cam et al., 2011). Moreover, the barrel cortex has a wide array of modulations of responses through the cortico-cortical network that might have profound effects on the neuronal RFs and the spread of subthreshold activity. For example, some studies have revealed an anisotropy towards within-row connectivity in the intracortical circuitry (Simons, 1978; Kim and Ebner, 1999; Petersen et al., 2003a). Furthermore, cortical neurons receive multiwhisker thalamic input, which is also a potential substrate for complex nonlinear interactions. Therefore, the somatosensory cortex is likely to have specific mechanisms to extract information of the complex tactile stimuli; we hypothesized that cortical neurons should be able to extract information about the global direction of movement of the vibrissae from the spatiotemporal sequence of individual whisker deflections while the animal is exploring the environment. In this case, the tactile discrimination capabilities rely strongly on the ability of the system to encode different levels of inter-whisker correlations.

The responses of a sequential deflection of two neighboring whiskers have been broadly studied, showing cross-whisker suppression (Simons, 1985; Simons and Carvell, 1989; Kleinfeld and Delaney, 1996; Brumberg et al., 1996; Shimegi et al., 1999, 2000; Higley and Contreras, 2003, 2005; Ego-Stengel et al., 2005; Civillico and Contreras, 2006; Benison et al., 2006). This suppression is maximal 20 ms after the adjacent whisker (AW) deflection, delay that is likely to occur during natural whisking. In contrast, when stimulating near simultaneously more whiskers within a row/arc responses sum either supralinearly (Ghazanfar and Nicolelis, 1997; Shimegi et al., 1999, 2000; Staba et al., 2005; Ego-Stengel et al., 2005) or sublinearly (Simons, 1985; Mirabella et al., 2001).

In addition, it has been shown that extended temporal sequences of tactile stimuli can generate complex nonlinear responses (Boloori and Stanley, 2006; Webber and Stanley, 2006). Of particular interest is the work of Drew and Feldman, in which they explored how sequential deflections of individual whisker arcs moving progressively on the whisker array (they referred to this as “wavefronts”, we will use “moving bar”) are represented in the rat barrel cortex (Drew and Feldman, 2007). They made extracellular recordings in L2/3, L4 and L5, while using a multiwhisker stimulator of 3x3 or 3x4 whiskers in urethane anesthetized rats. The starting position, direction and velocity of the moving bar varied. They showed that neurons responded strongly when the moving bar starts on their PW, as it can be seen in Figure 17, if not, the responses were suppressed by 90% (IWI= 20 ms), and this suppression was independent of the direction of the moving bar, except for L2/3. The suppression reported there is greater than the 70% suppression typically elicited when deflecting just one AW (Simons and Carvell, 1989; Higley and Contreras, 2005). This is expected, as a larger number of whiskers will nonlinearly recruit suppressive mechanisms (Brumberg et al., 1996). Therefore, this approach was not sufficient to characterize the emergent properties of the complex spatiotemporal stimulations, as they could not stimulate all the macrovibrissae.

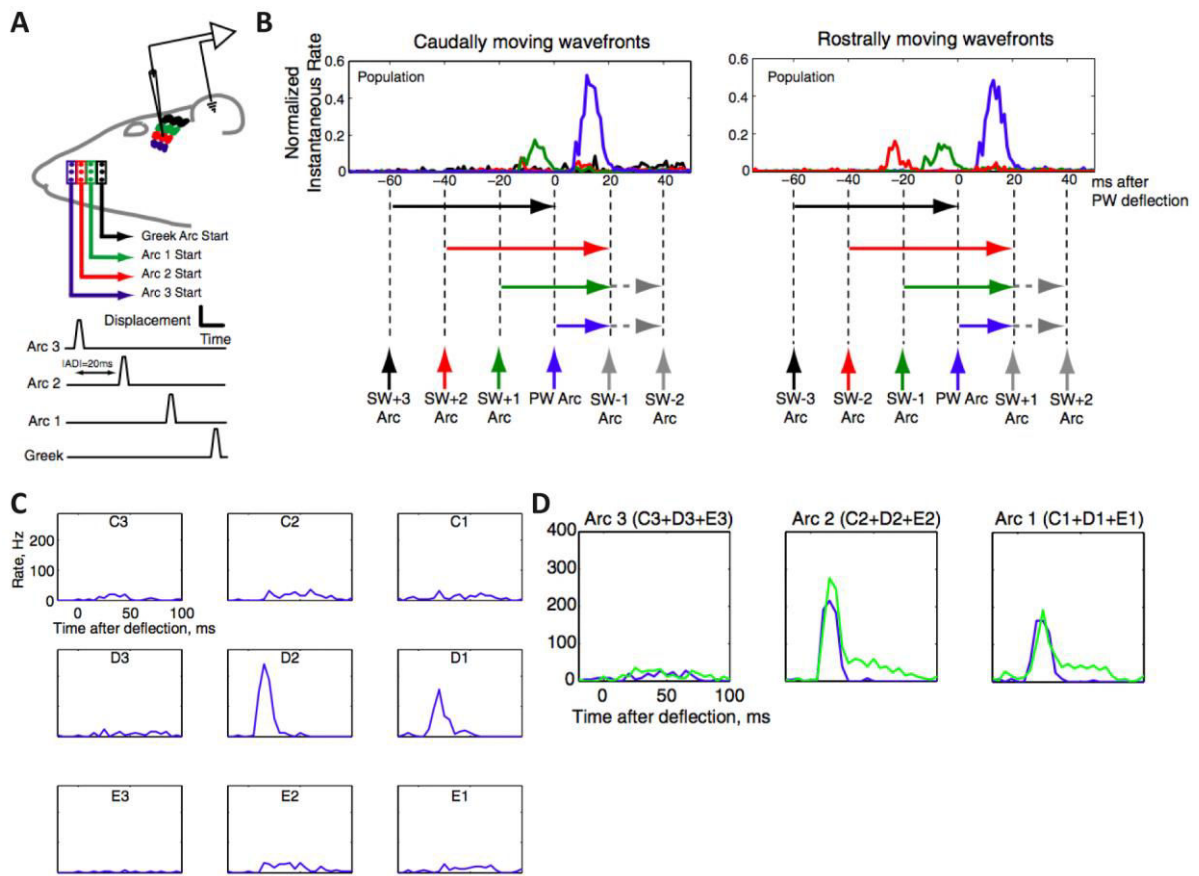


Figure 17: Representation of the starting position of a moving bar.

A: Caudally moving wavefronts generated by sequential deflection of arc 3, 2, 1, and the Greek arc. Each arc deflection is composed of synchronous deflection of 3 whiskers within rows C, D, and E of that arc. The interarc deflection interval (IADI) was 20 ms.

B: Mean PSTHs for responses to caudally or rostrally moving wavefronts across all multiunit recording sites. Before averaging, responses at each site were normalized to the highest 1 ms bin and temporally aligned to deflection of the PW arc.

C: Example single unit recorded from L2/3 showing response to deflection of single whiskers. D2 was the PW; bin size = 5 ms.

D: Measured responses to simultaneous deflection of 3 whiskers within each arc are shown in blue, and summed responses to deflections of individual component whiskers (predicted response) are shown in green. Comparing both responses within 5-25 ms after deflection, the summation is sublinear for Arc 3 and 2 and nearly linear for Arc 1.

Modified from (Drew and Feldman, 2007)

At the same time our team was developing a 24-whisker stimulator, which enabled us to apply complex spatiotemporal patterns of whisker deflections during electrophysiological recordings in the rat barrel cortex (Jacob et al., 2008). This matrix of stimulation, described in Part II – Chapter 2 and in (Jacob et al., 2010), allowed the exploration of the cortical responses to stimulations of the whisker array that resemble spatiotemporal sequences of deflections occurring in natural conditions. In particular, my colleagues studied whether the cortical neurons could extract information about a global feature like the direction of stimulation of the whole mystacial vibrissa array. They designed a “global motion” protocol in which sequences of whisker deflections collectively generated a moving bar spanning eight different directions (Figure 18A). The local deflection of each vibrissa was invariant in the rostro-caudal direction. During these stimuli, whiskers with perpendicular alignment to global motion were deflected simultaneously and those aligned in parallel were deflected sequentially with a delay of 10 ms for horizontal and vertical motion, and 7.1 ms for oblique directions.

If the recorded neurons add up linearly the responses, given that for each sequence the whiskers are deflected one time and with the same local direction, the integrated response for each global direction should be equal, giving an isotropic global direction tuning curve. In contrast, it has been found that around 70% of the single units recorded in the C2-column showed statistically significant global direction selectivity (75% granular layer; 63% infragranular layers). Figure 18B-C shows two representative examples of anisotropic tuning curves for regular spiking units (RSU) and fast spiking units (FSU) of L5. The distribution of the preferred directions was uniform for FSUs and anisotropic for RSUs, with a bias towards the caudoventral directions (circular mean $228 \pm 78^\circ$; Figure 18D-E). Notably, neurons presented similar levels of response to the global motion protocol as to the local deflection of the whisker C2 (Figure 19).

This study further demonstrated that global and local direction selectivity are independent properties of the barrel cortex neurons, since the preferred angle of global motion was not correlated with the preferred angle for local motion of the PW (Figure 19B). It also showed that the global direction selectivity was independent of the direction of deflection of the whiskers (rostro-caudal axis, 180°), by applying the same global motion protocol with a local invariant direction of deflection of the whiskers of 45° (rostro-dorsal).

Another important finding is that the whole whisker pad is implicated in generating selectivity to global motion. The responses in the C2 column when applying the global motion protocol involving all the macrovibrissae, as previously described, were compared to the ones evoked by another “proximal” protocol in which the stimulation was applied to the C2 whisker and to the 8 adjacent whiskers (Figure 19C). The preferred angles obtained from both protocols were uncorrelated (Figure 19D), and in the majority of the cases the direction index for the global protocol was larger than for the proximal one, even though the level of response was the same for both. This explains the results of Drew and Feldman, indeed, when stimulating only the PW and the immediate surrounding whiskers they found no direction selectivity. These results suggest that the stimulation of whiskers far from the center of the RF also sharpens the response tuning profile of the neurons, thus the selectivity to global motion cannot be explained only by local interactions between the PW and the immediate neighboring whiskers.

This work from Jacob and collaborators (2008) failed to explain the global direction selectivity with a linear summation model of the responses for the stimulation of individual whiskers. The difference between the neuronal responses and the model indicates the presence of nonlinear mechanisms, mainly suppressive, that build up progressively during the stimulation for the preferred and non-preferred directions, in agreement with the work of Drew and Feldman (2007). Different models were tested by Jacob et al. to predict the responses: a threshold-like filter applied to the linear prediction, a model including suppressive interactions between neighboring whiskers, and the same model but also including the spatial asymmetry between the suppressive interactions. None of them could explain satisfactorily the responses, but the latter got closer than the others being able to explain the population preferred angle bias towards the caudoventral direction (Figure 19E).

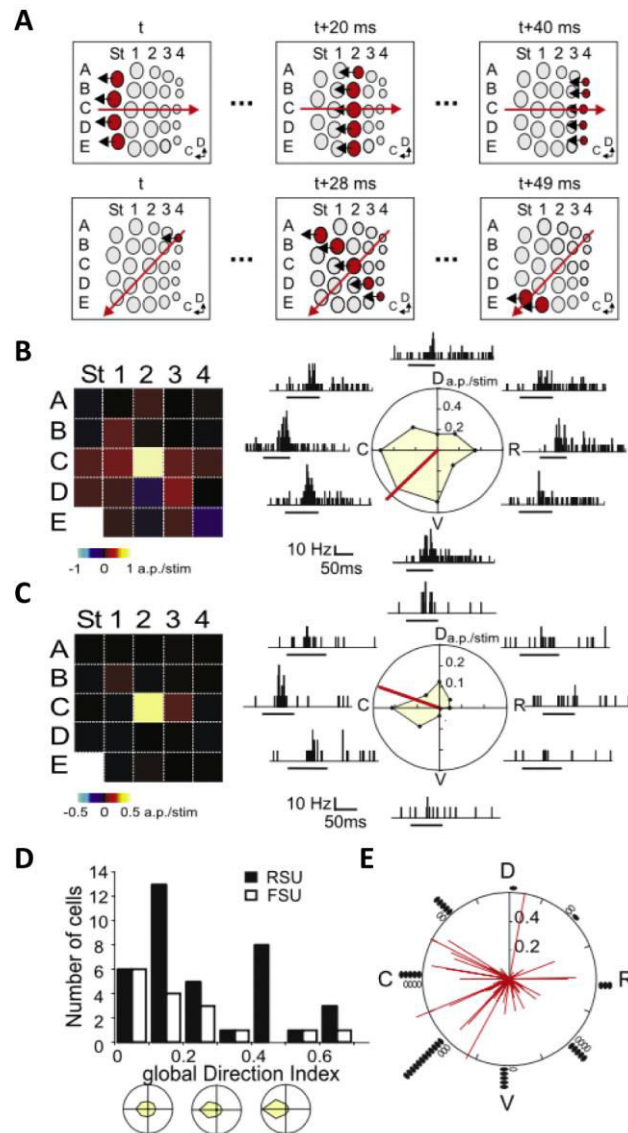


Figure 18: Cortical responses selective to the direction of global motion.

A: Three steps of the global motion protocol for two directions out of eight illustrated on a scheme of the whiskerpad (St, straddlers; C, caudal; D, dorsal). Black arrows show the local whisker movement (rostrocaudal, 180°). Whiskers in red were stimulated simultaneously at the times indicated on top. The red arrow indicated the direction of the global motion.

B: On the left, multiwhisker RF of a L5 RSU cell with a DI=0.24. On the right, polar plot of responses to the eight directions of global motion (spike counts from 25 to 205 ms from stimulus onset). The red line is the vector sum, it points toward the preferred direction. PSTHs of response to the eight directions around the polar plot; bars indicate the duration of the stimulation.

C: Same as in B, but for a L5 FSU cell with a DI=0.41.

D: Population distribution of DI for RSU (black) and FSU (white) units.

E: Distribution of DI vectors. Each vector represents the preferred global direction for a single unit, and its length the DI. The histogram shows the distribution of preferred directions in 45° segments for FSUs (white) and RSUs (black).

Modified from (Jacob et al., 2008).

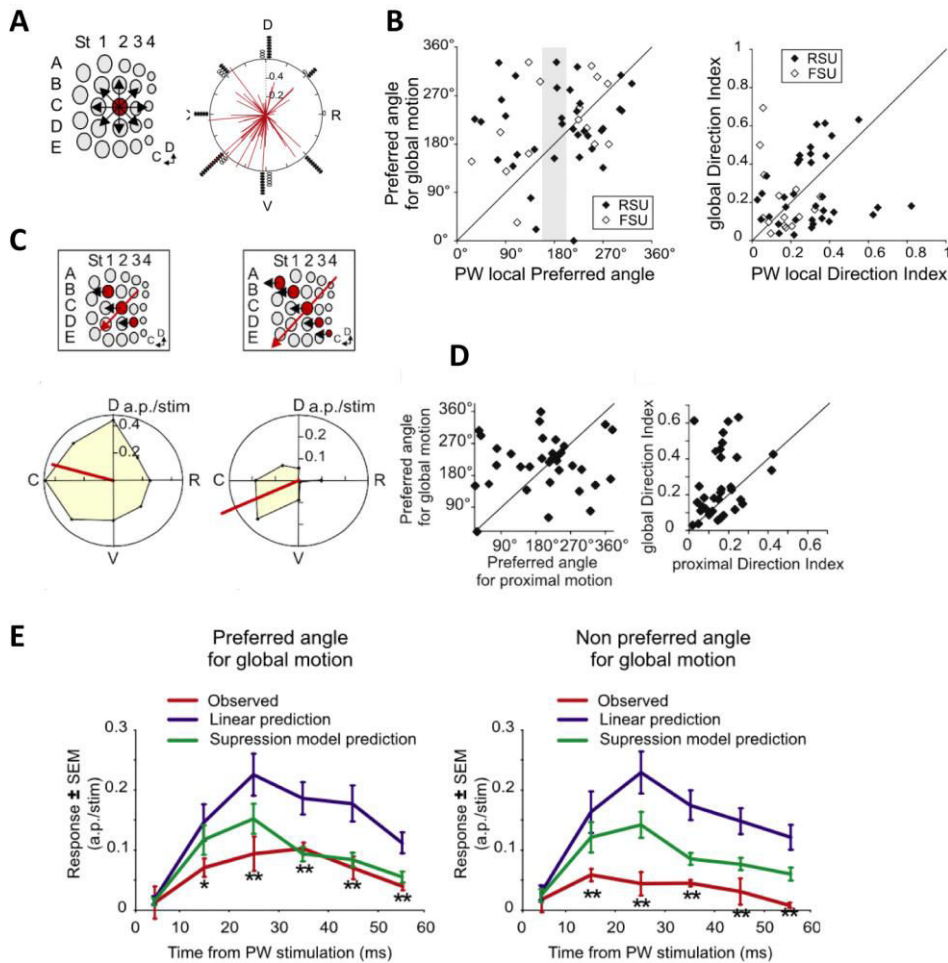


Figure 19: Possible explanations for the global direction selectivity.

A: Local deflection comparison. The PW (red) was deflected in eight directions (arrows on the diagram representing the whisker pad). Distribution of local direction preferences is shown on the right.

B: Local deflection comparison. On the left, the scatter plot of the preferred global direction as function of the preferred local direction. On the right, the scatter plot of the global direction index versus the local direction index. The diagonal shows the unity line (FSUs white, RSU black).

C: Proximal protocol comparison. The insets show one of the eight directions of the proximal (left) and global (right) motion protocols. Polar plots of response of the RSUs are shown below.

D: Proximal protocol comparison. Comparison between the proximal and global protocols for the preferred angle and the direction index (left and right, respectively).

E: Models comparison. Average population responses recorded during stimulation (red) or predicted by the linear model (blue) or the suppression model with asymmetry (green) for the preferred and the non-preferred angle of global motion. Asterisks indicate significant suppression (paired t-test).

Modified from (Jacob et al., 2008).

Taken together, these results suggest that individual neurons in the barrel cortex combine and extract information from the entire whisker pad, supporting the idea that tactile perception relies on neuronal representations of collective features of the stimulus rather than on local independent variables. Nevertheless, a study from (Higley and Contreras, 2007) showed that in the thalamus of isoflurane-anesthetized rats there are strong interactions between the whiskers, suggesting a big contribution of the subcortical structures to the integration of multiwhisker stimuli.

One might hypothesize that this global direction selectivity emerges in subcortical structures and is transmitted in a straightforward manner to the cortex. However, another study achieved in the team (Ego-Stengel et al., 2012) revealed that the global direction selectivity is less important in the VPM than in the cortex, in contrast with the local direction selectivity. This suggests that the selectivity might emerge at the level of the thalamocortical loop and be amplified within the cortical network. To test this hypothesis, they first studied the global direction selectivity of the neurons in the L6 of the barrel cortex, the principal source of cortico-thalamic fibers. Next, the cortex was inactivated to assess the impact of this cortical feedback on the thalamic direction selectivity (Ego-Stengel et al., 2012). Among the cortical neurons from L6 that project to the thalamus, 47 % (n=7/15) have global direction selectivity. The selectivity in L6 was less important than in L4, however the distribution of the preferred angles was similar (L4= $172 \pm 77^\circ$; L6= $202 \pm 88^\circ$; Mann-Whitney, $p = 0.17$), and in 67% of the neurons of L6 the preferred angle was also in the caudo-ventral direction (Ph.D. thesis of Julie Le Cam, Université Pierre et Marie Curie, 2010). After inactivating the cortex by applying 4% Mg^{2+} , 83% of the neurons recorded in VPM (n=10/12) decreased their global direction selectivity, despite the fact that the spontaneous activity of these neurons did not change. Moreover, 25% (n=3/12) of these cells became non-selective during the cortical inactivation (Ego-Stengel et al., 2012). Nonetheless, during the cortical inactivation, the evoked activity significantly increased for all the directions but not for the preferred one. These results suggest that the cortical inactivation produces facilitation of the responses for the non-preferred directions, which induces a reduction of the selectivity of the thalamic cells.

The preferred global angles before and during the cortical inactivation are not correlated neither for the selective nor for the non-selective cells in VPM (Ph.D. thesis of

Julie Le Cam, Université Pierre et Marie Curie, 2010). This suggests that the cortical inactivation induces changes on the preferred direction of the global movement of VPM cells, as it has been also observed in the case of the preferred angle of local whisker deflection (Li and Ebner, 2007).

Given that the integration of multiwhisker information is more important in the cortex and that the cortico-thalamic feedback has a strong influence on the selectivity of the VPM neurons, we can hypothesize that the integration of the multiwhisker information is amplified at the cortical level via the intracortical connectivity.

Although a large part of the global direction selectivity seems to emerge within the cortical network, the mechanical transmission of vibrissa movement through the skin of the snout could also participate in this phenomenon. Extracellular recordings in the trigeminal ganglion have been performed in order to address this question. The trigeminal ganglion contains primary afferents from the vibrissal system and the neurons on this nucleus have monovibrissal receptive fields, hence, they are theoretically incapable of integrating multivibrissal information. None of the six-recorded units presented significant direction selectivity to the global movement (Ph.D. thesis of Julie Le Cam, Université Pierre et Marie Curie, 2010). This finding suggests that the global direction selectivity evidenced in the VPM and the cortex are centrally generated and do not result from mechanical transmission of the vibrissa movement through the skin of the whiskerpad.

In 2010, Wilson and collaborators developed a mechano-computational model of the supragranular layer of the rat S1, in which they predicted that the somatotopic pinwheel maps of whisker local deflections exist and that neurons with similar directional tuning are interconnected in a network of horizontal connections reaching distances of many whisker representations suggesting a suprabarrel organization of the direction selectivity in L2/3 (Wilson et al., 2010).

In fact, as already mentioned, the work of Jacob et al. (2008) showed that there was a bias towards cuadoventral global directions when recording from the C2 barrel-related column. Preliminary data recorded in the same experimental conditions from the barrel-related columns of the whiskers straddlers Alpha (StA) and Beta (StB) also showed biases

(data not published). The responses of the StA barrel-related column had a bias towards rostroventral global directions, while for StB the bias was towards rostral. Generalizing these biases to the rest of the barrels, we can hypothesize that the global direction selectivity is spatially distributed as a suprapinwheel over the barrel cortex. Part III – Chapter 2 shows how we tested this hypothesis and the results obtained.

Summarizing, in the barrel cortex, cortical neurons might code for both local and global direction selectivity. In Part III we will address the question of whether these features are spatially distributed on the cortical space.

Aim of the thesis

In this thesis we aim to study if and how sensory information is functionally organized in the mouse barrel cortex. We are interested in how the system extracts features of the stimuli, in particular the direction of movement of the vibrissae, and how this information is spatially distributed in the cortex. Based on previous results of our laboratory (Jacob et al., 2008), our hypothesis is that within the confined cortical volume of the barrel cortex, there are multiplexed representations, overlying the barrel map, of at least two functional maps for local and global direction selectivity.

For testing this hypothesis it is necessary firstly to precisely deliver, in a controlled manner, multiwhisker stimulations while recording cortical responses at the mesoscopic scale with good time and spatial resolution. We solved this experimental challenge by building a set-up which combines a piezo-electric multiwhisker stimulation matrix with a voltage-sensitive dye (VSD) imaging system (described in Part II). Secondly, it is necessary to realign the functional VSD images with the L4 barrel map in an accurate manner. For this purpose, we developed an automatized method to easily reconstruct the barrel cortex map, from the histological slices obtained post-hoc, in a more accurate manner and faster than using conventional techniques.

By using this unique experimental approach, we first want to tackle a controversial question in the field: whether there is an intracolumnar spatial organization of the selectivity to the angle of deflection of individual whiskers.

We then want to study how the responses to the direction of stimulation of all the macrovibrissae, called here global direction, are spatially organized in the barrel cortex. Our working hypothesis is that there is a suprabarrel organization for coding multiwhisker properties. We will test this hypothesis by analyzing the spatiotemporal dynamics of cortical activity in supragranular layers evoked by complex tactile stimuli.

Part II – Controlling the input – reading the output

Understanding the neuronal computations is an experimental and theoretical challenge. It is essential to apply precise controlled inputs and to choose a good technique to read the neuronal output. It also requires knowing the origins of the signals obtained in order to do an accurate interpretation of the results.

In this second part we will describe how we dealt with these requirements by building an experimental set-up that allows to apply precise multiwhisker stimuli and to record the cortical responses with a high spatiotemporal resolution. Then we will present a technical method we have developed to map recorded functional data onto the cortical structure.

Chapter 1: Optical Imaging of Cortical Spatiotemporal Dynamics

II.1.1 Beyond the electrodes: overview and advantages of optical imaging

For many years the study of the brain was done *in vitro* by anatomists, like Ramon y Cajal and Golgi at the end of XIXth century, who used staining techniques together with light microscopy to describe cell morphology. These anatomical studies helped to understand the organization of the cells in the brain; however, the dynamical and functional aspects of these cells were missing. Later on, the development of electrical recording techniques allowed measuring the neuronal activity of brain cells. These techniques are still in use nowadays both in *in vitro* and *in vivo* preparations. The functional properties of the neurons, such as the spike patterns or the membrane potential dynamics, can be recorded using extracellular or intracellular electrodes with a submillisecond temporal resolution. Far from being an abandoned field, electrophysiology is actively under development. New electrode arrays allow recording neuronal activity from more than 100 different points in space, as well as from different depths of the tissue; extracellular tetrodes and intracellular techniques, together with more complex analysis strategies, have been adapted to enable acquiring efficient recordings from awake and freely moving animals.

However, for understanding the processing of sensory stimuli, which are spatially distributed on the receptor surface, within the dense cortical network, it is essential to record the cortical dynamics not only with high temporal resolution but also at high spatial resolution. As the number of electrodes one could insert into a living brain is limited, the electrophysiology still suffers from a lack of spatial resolution.

In 1990 the invention of the two-photon excited fluorescence laser scanning microscopy (Denk et al., 1990) was a major breakthrough, as it allows the combined study of morphology and function *in vivo* (Denk, 1994; Svoboda et al., 1997). This is a laser-scanning technique, which needs to focus a laser beam through a microscope objective down to a tinny light spot (on the order of micrometers) to excite the fluorescent molecules. The

spatial information is collected by moving the light spot through the sample, and as in general these microscopes are multifocal they allow collecting data from different laser loci at the same time. There are many strategies to scan the sample, in most of them a 2D image is acquired, and if the sample has volume, the plane-by-plane images can be stacked to recreate the 3D configuration. Three dimensional scanning strategies have also been developed recently (Göbel et al., 2007; Kampa et al., 2011). A key element of the two-photon imaging is the labeling of the cells with a fluorescent anatomical marker or functional probe. The fluorescent labeling can be obtained by introducing a fluorescent dye into the cells, or by genetically encoded fluorescent proteins. Fluorescent molecules come in different colors with emission spectra ranging from blue to near infrared (Livet et al., 2007; Lichtman et al., 2008). This technique enables more accurate and dynamical morphological studies, in addition to the study of functional properties by using activity-dependent probes, like calcium indicators in a technique called “calcium imaging”. Calcium indicators can indirectly probe spiking activity but the temporal resolution is limited by their calcium-binding dynamics. There are many calcium indicators with different affinity; their choice depends on the calcium concentration of the cell type we want to record. Generally synthetic indicators show low photobleaching rates with two-photon excitation and do not present obvious pharmacological side effects aside from adding calcium buffering capacity to the cell. The linkage between calcium influx and electrical excitation is mediated by calcium voltage-dependent channels. When a neuron is excited the fast entrance of calcium can be tracked by the fast change in fluorescence followed by a decay to resting fluorescence due to the removal of calcium from the cytosol. This decay, also called “calcium transient”, has a time constant in the range of a few hundred milliseconds when measured in the soma (Helmchen et al., 1996). One of the drawbacks of this technique is that the temporal precision is slower than the electrical recordings and it is limited to the calcium dynamics that have bigger time constants than the membrane potential of the cells. The instantaneous rate of neuronal spikes (Yaksi and Friedrich, 2006) or in the best cases the single action potentials (Kerr et al., 2005, 2007; Sato et al., 2007), can be indirectly inferred from the fluorescence measurements. Two-photon microscopy has a spatial resolution in the micrometer range, which is good enough to resolve synaptic structures (such as dendritic spines and axonal boutons) or small circuit dynamics, but the cortical area that can be

imaged with a cellular resolution is usually restricted to few hundreds of microns. This might be a limitation for studying functional interactions over several cortical columns.

Optical imaging of intrinsic signals is a useful tool to explore the spatial distribution of neuronal activity over relatively large regions of the cerebral cortex (Grinvald et al., 1986). This method consists in imaging variations of light absorption by the active tissue due to hemodynamic changes which themselves result from underlying neuronal activations. Its main advantage is that it is noninvasive, since such optical signals can be gathered through the intact skull in mice. However, despite this technique can be useful to map defined functions on the cortical surface, it does not relate directly on the electrical activity of the neurons and therefore does not allow exploring neuronal dynamics. To cope with these issues voltage-sensitive dyes (VSDs) have been developed.

II.1.2 Voltage-sensitive dye imaging

1.2.1 Description of the technique

The VSDs are fluorescent molecules that insert into the plasma membrane and change their fluorescence intensity depending on the potential across the lipid bilayer. It is a key factor that these changes in fluorescence correlate with the changes in the membrane potential at the submillisecond time scale (Berger et al., 2007). While calcium imaging signals vary according to spike discharges and are therefore limited to the monitoring of suprathreshold neuronal activity, VSDs allow real time imaging of subthreshold activity.

The first in vivo VSD imaging recordings of sensory processing were obtained in the frog visual tectum (Grinvald et al., 1984), in the rat somatosensory and visual cortex (Orbach et al., 1985), and in the monkey striate cortex (Blasdel and Salama, 1986).

Historically, the main inconvenience of this technique has been the heartbeat artifacts: due to the movement artifacts produced by the physical pulsation of the blood vessels, and because the hemoglobin absorption spectrum changes depending on the oxygenation level, contaminating the recorded responses. To minimize the latter, the group of Grinvald developed fluorescent dyes with absorption and emission spectra in the far red, longer than 600 nm (Shoham et al., 1999; Grinvald and Hildesheim, 2004). These molecules were used

successfully by this group to study spatiotemporal dynamics of visual cortices in anesthetized cat and also in awake behaving monkeys (Arieli et al., 1996; Tsodyks et al., 1999).

RH1961 is one of the dyes from this new series of VSDs that has been probed to work well in the rodent neocortex (Figure 20). It is a water-soluble aromatic oxonol compound based on a vinylogous carboxylate conjugate system; its conformation changes are executed via transferring electrons. It is thought to insert mostly in the lipid bilayer of the plasma membrane of cells where it can be excited by light at ~ 630 nm, and emits fluorescent photons with wavelengths >665 nm. Changes in the membrane potential (on the order of hundreds of millivolts) are linearly related to the measured fluorescence with submillisecond resolution, as it has been reported in the oocyte of *Xenopus* while doing a double patch-clamp recording (Berger et al., 2007). As it can be observed in Figure 20A, voltage-clamp steps are tightly correlated with fluorescence steps, making the interpretation of the signals relatively straightforward.

For doing VSD recordings *in vivo*, a craniotomy must be done over the cortical region of interest (ROI) and the dura mater is usually removed (Arieli et al., 2002; Ferezou et al., 2006). Extreme care should be taken to avoid damaging the cortex, especially while removing the dura. The solution of VSD (for RH1691 normally 1 mg/ml) is applied directly over the craniotomy and within 1 hour diffuses into the cortex. After the removal and the washing of the dye the craniotomy can be covered with agarose, which helps stabilizing the cortex and reduces pulsation-related movements. A coverslip placed on the top forming a sealed chamber prevents agarose from drying during the experiment. Note that an alternative technique consisting in staining the cortex through the intact dura has been reported in rat imaging experiment (Lippert et al., 2007).

For acquiring VSD signals it is necessary to excite the dye with band pass filtered light (630 ± 15 nm for RH1961) typically delivered by a halogen light source. The light is reflected using a 650 nm dichroic mirror and focused on the cortical surface with the lower lens. The emitted light is collected via the same optical pathway except for the reflection on the dichroic. Then it is long-pass filtered (>655 nm), and focused onto the detector via the upper lens.

Different types of detectors can be used to collect the emitted photons: photodiode arrays, CCD (Charge Coupled Devices) or CMOS (complementary metal oxide semiconductor) detectors. The three of them share the same principle: they are composed of semiconductor detectors that convert light into current, and are still in use. The first VSD experiments were done using the photodiode arrays (Grinvald et al., 1984; Lippert et al., 2007). More recent cameras present a better spatial resolution, and can be based on CCD detectors (Kleinfeld and Delaney, 1996) or CMOS sensors (Ferezou et al., 2006; Berger et al., 2007).

With VSD imaging in order to measure 0.1% change in light it is necessary to collect approximately one million photons to detect the small VSD signal from the shot noise. As so much light is applied to the preparation it is important to consider the bleaching of the dye, and correct it offline.

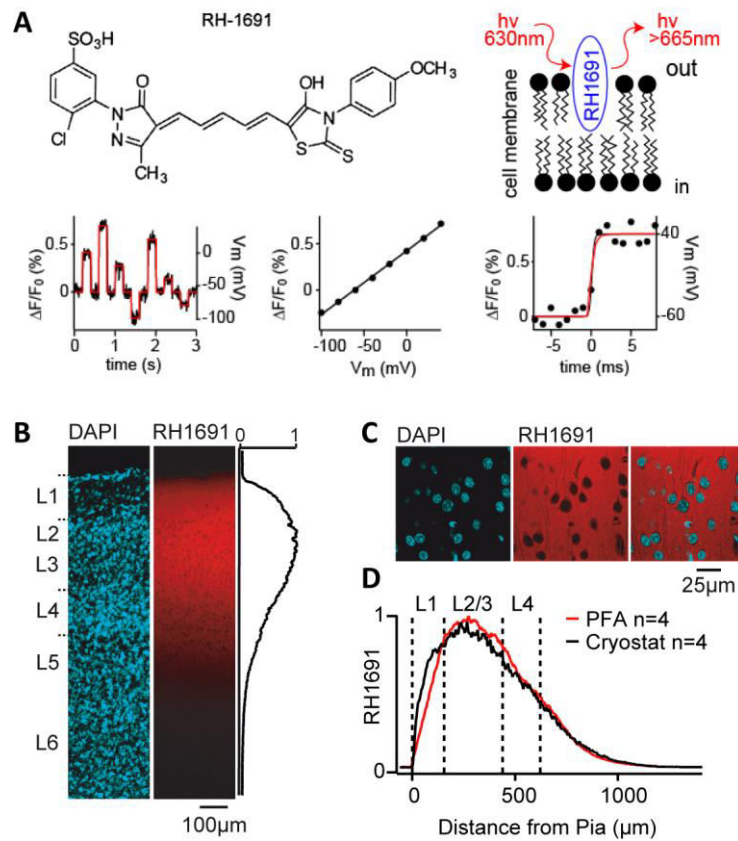


Figure 20: Voltage-sensitive dye RH1691 and the origins of the VSD signal.

A: Chemical structure of the VSD RH1691 (top left), a fluorescent dye excited at ~630 nm and emitting fluorescence >665 nm (top right). The dye is thought to insert primarily into the plasma membrane lipid bilayer and its electrochemical structure depends on the transmembrane field, changing absorption and emission properties of the dye. Below are shown biophysical measurements of RH1691 fluorescence applied to voltage-clamped *Xenopus oocytes*. Changing membrane potential (V_m , red trace) results in well-correlated fluorescence changes (left, $\Delta F/F_0$, black trace). RH1691 fluorescence changes linearly as a function of membrane potential (V_m , central plot). Higher time resolution view of RH1691 fluorescence changes (black data points, black trace shows a sigmoidal fit to the fluorescence data) following voltage changes (solid red line). RH1691 follows membrane potential changes with submillisecond resolution. *From* (Berger et al., 2007).

B: Topical application to the mouse barrel cortex labels mainly supragranular layers. Parasagittal slices (100 μm) from stained barrel cortex, counterstained with DAPI, and observed with confocal microscopy, reveal the highest concentration in L2/3.

C: The dye does not enter inside the cells but rather labels membranes.

D: Quantification across different experiments reveals consistent labelling of supragranular layers, with a peak in L2/3.

B-D from (Ferezou et al., 2006)

1.2.2 What are we seeing?

It is important to ask where the VSD signals are being generated in order to interpret correctly the experimental results. Observation of brain slices following a standard imaging session revealed that the dye RH1691 mainly stains the supragranular layers in both rats (Kleinfeld and Delaney, 1996) and mice (Ferezou et al., 2006)(Figure 20B). The dye can be found in the neuropil, consistent with the hypothesis that it binds the plasma membrane rather than being internalized (Figure 20C). Based on these observations, together with the linear relationship between the fluorescence and the membrane potential, the VSD signals are likely to relate to changes of the membrane potential coming from L2/3 (Figure 20D).

The linear correlation between the membrane potential measured in vivo with whole-cell patch-clamp recordings of a single cell and the VSD signal is remarkable (Petersen et al., 2003a, 2003b; Ferezou et al., 2006; Berger et al., 2007), especially if we keep in mind that in VSD imaging the signal is coming from a population of neurons (Figure 21). We might think then that most neurons within the few hundreds of microns apart have similar dynamics of their subthreshold potentials under anesthesia or in quite wakefulness. Dual whole-cell recordings confirmed this (Petersen et al., 2003a, 2003b; Poulet and Petersen, 2008). Nonetheless, the reasoning does not apply to the suprathreshold activity. Action potentials recorded in whole-cell configuration during the Up state cannot be captured by the VSD signal, although this is not due to a limited time resolution of the technique but rather to the sparse spiking activity in the L2/3, a fact that has been also observed in electrophysiological recordings (Brecht et al., 2003; Petersen et al., 2003a, 2003b; Kerr et al., 2005; de Kock et al., 2007). Because of this sparseness of the spiking activity, thus not synchronized, the VSD signal is almost entirely dominated by subthreshold changes of the membrane potential.

However, a spiking region can be delineated from the VSD signals (Jancke et al., 2004). In this article Jancke and collaborators treated separately the VSD signals separating them into high and low amplitude signals, being the high amplitude the ones corresponding to the spiking zone. They showed that low amplitude activity propagated at the same conduction velocity across horizontal connections, while the high amplitude activity showed no significant lateral extension. The nature of these two VSD signals was confirmed by single-unit recordings, showing that indeed the high amplitude activity area was the spiking area.

But what do we have in the neuropil? It was reported that 80% of the VSD signals originates from dendritic activity of excitatory neurons of the superficial layers (Chemla and Chavane, 2010). As already mentioned in Part I, in the superficial layers of the rodent barrel cortex one can find pyramidal cells, GABAergic interneurons, and glia. The most important afferents come from the L4 spiny stellate excitatory neurons, but it is also important to keep in mind that these layers receive direct thalamic afferents from the three pathways: lemniscal, paralemniscal, and extralemniscal. The supragranular layers integrate information from several barrel columns and from different cortical areas through long-range intracortical connections. In addition, the apical dendrites of the pyramidal cells of L5 are present in these layers. L2/3 pyramidal neurons also project to M1 and S2. A further description of the VSD signal components can be found in the first section of the Discussion.

II.1.3 VSDI in the barrel cortex

As we exposed in Part I of this thesis, the rodent barrel cortex is a great model for studying cortical integration. By doing VSD imaging in anesthetized, awake or behaving rats and mice, it has been possible to correlate behavior, sensory input, and cortical activity.

Carl Petersen and his colleagues have extensively studied the VSD signals in rodents. VSD imaging experiments have been done both in head-restrained anesthetized or awake rats and mice (Petersen et al., 2003a, 2003b; Berger et al., 2007; Ferezou et al., 2007), and in freely moving mice using fiber optic bundles (Ferezou et al., 2006). In such freely moving experiments the spatiotemporal dynamics of cortical activity could be recorded while the mouse was free to move in a restricted area. The fiber used consisted of an array of 300 x 300 individual fibers with 8 μm cores and high numerical aperture (0.6 NA). The fibers were rigid at the ends but loose in the middle allowing flexibility and a reliable image transfer. Even though there were more losses of light than in the direct imaging scenario, the VSD signal resolved cortical dynamics in single trials.

The first characterization of the barrel cortex evoked sensory responses using VSD imaging was done in anesthetized rats after deflecting the whisker C2 (Petersen et al., 2003a, 2003b). A few years later, similar observations have been made on the anesthetized mouse barrel cortex (Ferezou et al., 2006), although with a better signal quality, probably because of the different nature of the animal model, but also thanks to the development of more efficient imaging sensors. There are only three synapses between the whisker deflection and the cortex, sensory information can then reach the cortex with latencies typically around 10 ms. In vivo whole-cell recordings of neurons in the L2/3 show that a brief 2 ms whisker deflection evokes a response lasting for milliseconds (Figure 21A-B). The response is first confined to the corresponding C2 barrel column and over the following milliseconds it spreads over the whole barrel field (Figure 21C). This is in good agreement with the large subthreshold receptive fields measured in the neurons of the L2/3 of the barrel cortex (Brecht et al., 2003; Moore and Nelson, 1998; Zhu and Connors, 1999). These large sensory responses might correspond to a “wake up” call for driving the cortex to an active state.

The good signal-to-noise ratio in the anesthetized VSD imaging experiments allowed recording spontaneous cortical activity (Figure 21D-G). The large membrane potential fluctuations, called “Up and Down states”, were correlated with the VSD signal. Spontaneous Up states appeared as propagating waves of activity that travel as planar waves, spirals or even more complex patterns (Figure 21F). Synchronous spontaneous activity between the somatosensory cortex and the motor cortex of the mouse has been reported (Ferezou et al., 2007). These observations suggest that spontaneous activity imaged under anesthesia is likely to be related to intrinsic properties of the cortical connectivity (Vincent et al., 2007; Mohajerani et al., 2013).

When the animal is awake there are at least two states of the somatosensory-motor system: quiet or whisking. Evoked responses are different depending on the ongoing behavior of the mouse (Faselow and Nicolelis, 1999; Ferezou et al., 2007). During whisking the amplitude of the response to a same stimulus is smaller than during quiet periods, and does not spread. During this “active” whisking brain state the sensory processing can remain confined to highly localized cortical regions.

As in the anesthetized configuration, in the freely moving mouse, the contact of an object evoked activity started on the barrel column and some milliseconds after the responses spread within and beyond the barrel cortex. However, the freely moving technique has the disadvantage of a low experimental control of the whisker deflections. A compromise between the two was developed by some groups: the “freely moving head-restrained” experimental configuration (Dombeck et al., 2007; Sofroniew et al., 2014), where the animal can move and explore a virtual environment but its head remains fixed.

Sensory information is rapidly processed in cortical networks that are distributed on the cortical space. In the rat V1, the velocity of propagation of evoked responses in the upper layers is 50-70 mm/s (Xu et al., 2007; Gao et al., 2012). The major advantage of VSD imaging compared to electrophysiological recordings is the availability to resolve spatiotemporal dynamics of the cortical neurons with a millisecond temporal resolution in vivo preparations. The application of this technique together with precise whisker stimulation on the anesthetized mouse can help to better understand the cortical processing of complex tactile stimuli; particularly, it can help us to answer how some features of the

stimuli like the local or global direction selectivity are spatially organized within the barrel cortex.

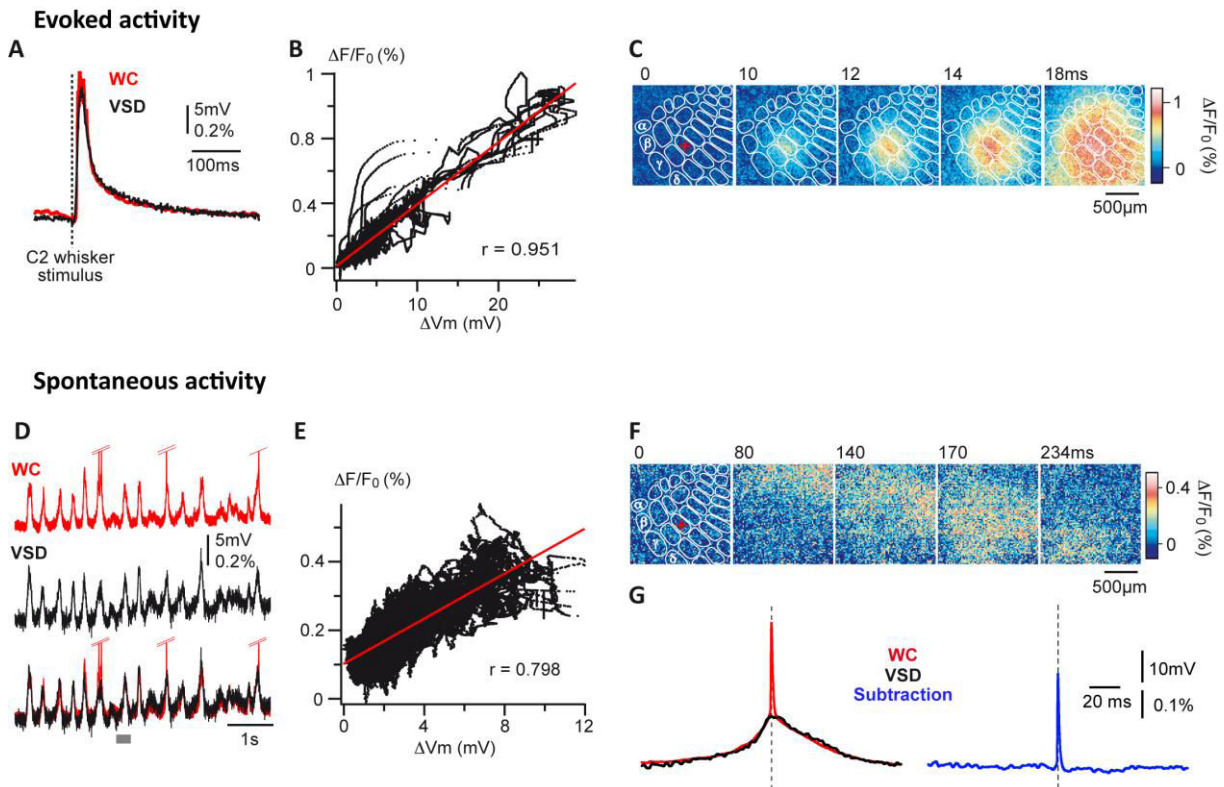


Figure 21: VSD imaging the barrel cortex of anesthetized mice.

A: Responses to C2 whisker deflection. Whole-cell (WC) recording of L2/3 neuron of the C2 column was performed simultaneously with measurement of the VSD fluorescence in anesthetized mouse. Averaged WC recording (red) and VSD signal measured from the C2 column (black) are superimposed ($n=6$ sweeps).

B: VSD signal plotted as function of the change in membrane potential for each individual sweep. Both signals were linearly correlated.

C: Image sequence corresponding to the average cortical responses shown in A.

D: For the same neuron, WC recording of L2/3 neuron of the C2 column was performed simultaneously with measurement of the VSD fluorescence in anesthetized mouse for spontaneous activity.

E: The VSD signal plotted as a function of change in subthreshold membrane potential.

F: VSD images corresponding to a spontaneous depolarization recorded in WC.

G: The VSD signal was aligned to action potentials (APs) recorded in WC. The subtraction shows that AP is missing in the VSD traces.

From (Ferezou et al., 2006)

Chapter 2: Coupling Matrix-VSD

Precise tactile stimulation is essential if we aim to study how specific parameters of the stimulation are coded in the barrel cortex. The anesthetized preparation allows control of the inputs of the whisker system facilitating the correlations between the stimuli and the neuronal responses. Even though the responses of the behaving animal might differ due to different attentional and motivational states, the general processing mechanisms are present in the anesthetized animal and can be more easily studied.

Rodents acquire tactile information through repetitive contacts with multiple whiskers (Carvell and Simons, 1990; Harvey et al., 2001; Sachdev et al., 2001). A multiwhisker stimulator is essential then to understand the integrative properties of the barrel cortex.

II.2.1 A multiwhisker stimulator: the matrix

In the initial studies of the whisker system the macrovibrissae were deflected by hand to trigger functional responses (Welker, 1971). However, shortly after the stimulation of the whiskers started to be done in a controlled way. As the responses in S1 are rather sparse, it is essential to know the precise timing of whisker stimulation in order to average the neuronal responses and to build PSTHs (Axelrad et al., 1976; Simons, 1978; Ito, 1981). Besides the timing, there are other advantages for precise mechanical stimulation: neurons in the barrel cortex respond best to certain features of the stimulus. It was reported that neurons prefer fast whisker stimulations (Arabzadeh et al., 2004; Maravall et al., 2007), and such fast whisker stimulations are only attainable with controlled mechanical stimulation.

Previous attempts to apply multiwhisker stimulation were done on smaller scales; e.g. three/five whiskers in a row (Simons, 1985; Brumberg et al., 1996; Shimegi et al., 1999; Rodgers et al., 2006), nine whiskers in a grid 3x3 (Andermann and Moore, 2006; Drew and Feldman, 2007), 16 whiskers in a 4x4 array (Krupa et al., 2001). The development of the multiwhisker stimulators has been a challenge due to the complex geometry of the whiskerpad (Brecht et al., 1997; Towal et al., 2011).

A stimulation matrix has been developed in our lab that enables to individually deflect each of the 24 caudal macrovibrissae in order to recreate complex tactile scenes that the awake animal produces while exploring its environment (Jacob et al., 2010). The first generation of this matrix consisted of 24 bilayer piezoelectric actuators that could be easily positioned and oriented according to the natural position angle of each whisker on the right side of the snout. These actuators were fixed to a structure rigid enough for limiting the vibrations due to resonance of the stimulators while functioning.

A second generation of the matrix has been developed with some changes, the major ones being: the bidirectional piezoelectric actuators were replaced by multidirectional actuators and the structure of the actuator's holder was redesigned in order to diminish the mechanical ringing artifacts and thus to allow delivering high velocity controlled whisker deflections (Figure 22). Indeed, piezoelectric actuators can give highly precise and reproducible whisker stimulation, as it has been shown in several studies (Simons, 1983; Simons and Carvell, 1989; Andermann and Moore, 2006; Jacob et al., 2008). Their operation principle is based on piezoelectric ceramic blades that when applying an electrical voltage respond by shrinking or expanding. Depending on the spatial distribution of the ceramic blades, the benders can achieve bidirectional or multidirectional whisker deflections. The main drawback of the piezoelectric actuators is their limited range of movement, classically moving on the order of hundreds of microns ($\sim 250 \mu\text{m}$). On the other hand, they are capable of very fast accelerations (more than $1500^\circ/\text{s}$).

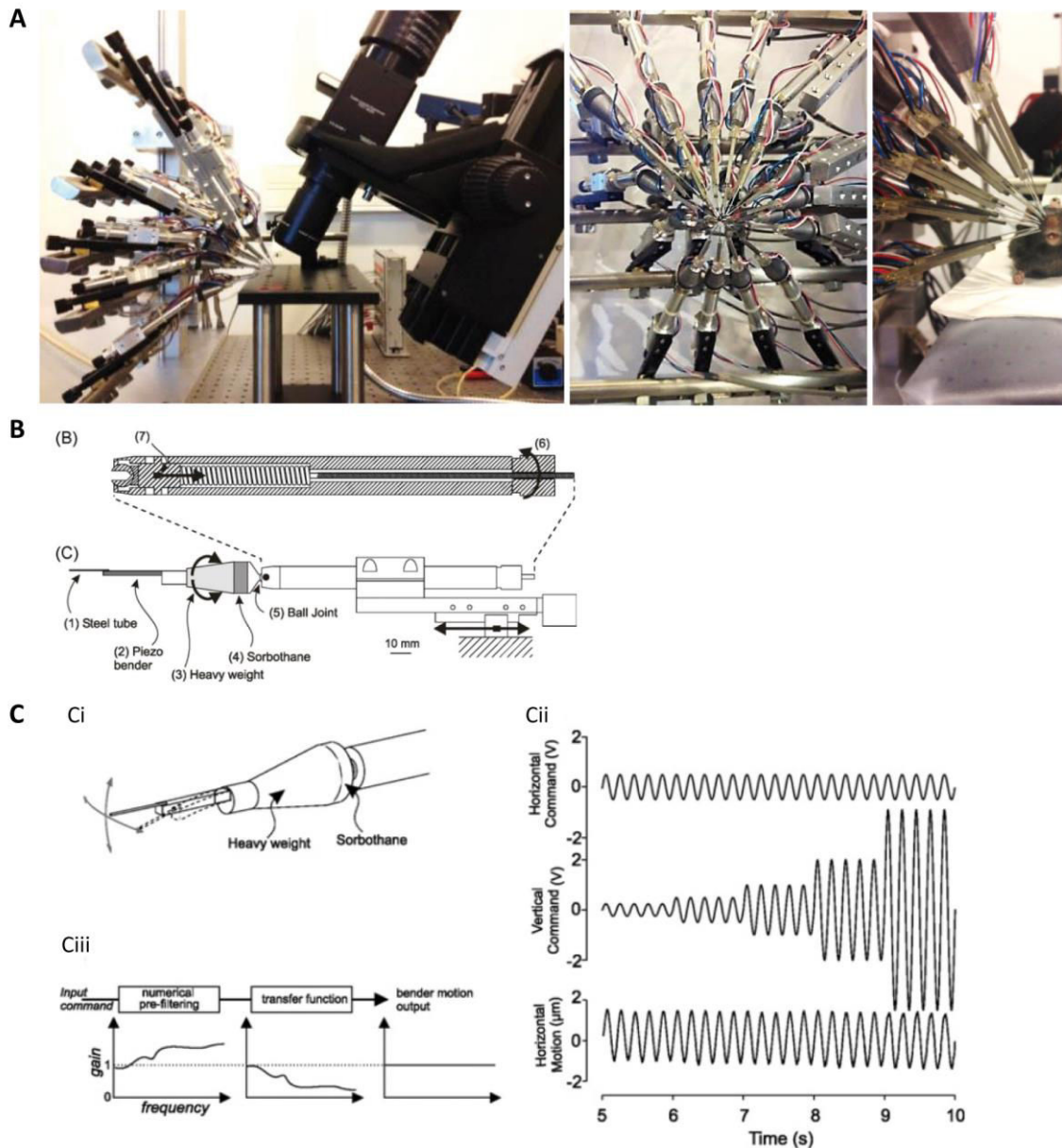


Figure 22: The second generation matrix. Probing with natural stimuli.

A: Left, side view of the stimulation matrix and the VSD imaging camera. Middle, front view of the matrix. Right, zoom in of the stimulator on a side view during the experiment.

B: Schematic drawing of the lever arm. A small steel tube (1) is glued on a multidirectional piezoelectric bender (2), which is held on a heavy weight (3). A sorbothane layer (4) separates this structure from a ball joint (5). The joint can be unclamped (6) by removing the pressure exerted by a spring on the ball (7).

C: Characterization of the stimulator. (Ci) Schematic drawing of the two deflection axes of the piezoelectric bender. (Cii) Test of independence of the two axes. Input command applied to the horizontal (top) and vertical axis (middle). Bottom trace: difference between the motion of the bender in the horizontal plane in response to the vertical axis input command only and to both inputs together. (Ciii) Scheme of the principle of the software correction performed on the bender. For each axis, the transfer function of the bender is computed and its inverse is applied to the input commands. *B-C from (Jacob et al., 2010)*

II.2.2 Building the set-up

The second generation matrix was first build-up at ENS by Luc Estebanez, a PhD student codirected by Daniel Shulz and Laurent Bourdieu, who did there rat experiments coupled with two-photon microscopy (Jacob et al., 2010).

A first step of my work was to build this second generation matrix at UNIC lab in Gif-sur-Yvette (Figure 22A). I proceeded then to adjust it in order to match with the spatial distribution of the whiskers on the snout of the mouse. Indeed, working with mice makes possible to obtain cleaner VSD imaging signals and to couple the whisker stimulation with optogenetics in the future. This stimulator was built with 24-multidirectional piezoelectric actuators (Noliac, Denmark) which had a steel tube (27G, 20 mm length) glued at the tip, where the whiskers can be inserted (Figure 22B). Each actuator was controlled with Elphy software (in-house development, Gérard Sadoc).

When a piezoelectric actuator moves it might also present an uncontrolled movement at its resonance frequency called “ringing”. It is important to correct the ringing as it might trigger unwanted neuronal responses. The gain of the actuators can be calculated by building a linear model of the device, comparing the known inputs and measured outputs. We did this by applying a sinusoidal driving command with constant frequency, but sampling at increasing amplitudes and measuring the displacements of the actuators with a laser telemeter that has a resolution of 1 μm (Micro-Epsilon).

The characterization of the bender’s transfer function can be used – within the linear range – to cancel out deviations from the “perfect transfer function” obtained from an actuator with equal gain and dephasing over a wide range of frequencies (Maravall et al., 2007). There are two methods that are currently used to measure the transfer function of the bender. In Jacob et al. (2010) the transfer function was measured by applying different sinusoidal commands, and or each frequency the gain and phase of the resulting movement were measured. These values across the frequencies provided a good model of the actuators in their linear range and the ringing correction was obtained by filtering the command waveform by the inverse of the transfer function (Figure 22C).

A second method to calculate the transfer function is based on measuring the responses of the benders to infinite Gaussian white noise, which allows then calculating the impulse response of the actuators. The drawback of this technique is that is difficult to deliver infinite white noise, and the quality of noise will determine the precision of the transfer function measurements. Gérard Sadoc developed a software correction for the ringing artifacts with some improvements of this method. A calculation based on the least squares method allows to accept a finite input noise whose quality will not affect the measurement of the impulse response. Once calculated the impulse response, a correction filter was developed to be apply it to the command. After the correction, the ringing was below 5% of the amplitude of the piezoelectric deflection.

As the multiwhisker stimulator was positioned on the right side of the snout, we registered the VSD signals on the left hemisphere (Figure 22A). For this we mounted a high-speed camera MiCam Ultima (SciMedia) that was tilted to make the S1 cortical surface plane parallel to the camera detector (angle of the camera 30°). For exciting the dye (RH1691) we fixed at the camera a fiber optic bundle with a 630 nm filter that was connected to a 100 W halogen lamp controlled by a mechanical shutter (Moritex). We used a 650 nm dichroic to reflect the excitation light onto the cortical surface and a 5x PlanApo objective (Leica) to focus the light onto the cortical surface. The fluorescence can be collected via the same optical pathway, but without reflecting on the dichroic, then is long-pass filtered (>665 nm), and focused via a 1x PlanApo objective (Leica) onto the CMOS detector of the camera. The detector is 100 x 100 pixels, meaning that with the optics described here we had a spatial resolution of 25 $\mu\text{m}/\text{pixel}$ and a field of view (FOV) of 2.5 mm x 2.5 mm, which covers a cortical area that contains the barrel field.

Both the matrix and the camera can be controlled and synchronized via an interface (National Instruments) through stimulation protocols coded in Elphy. With this configuration we can get a temporal resolution of 2 ms, which is fast enough to follow the subthreshold neuronal dynamics. In our set up it is also possible to control the temperature and record the EEG, heartbeat and respiration of the animal. We also adapted the set-up to make possible to use isoflurane anesthesia.

II.2.3 Anatomico-functional mapping of the barrel cortex

In order to combine the VSD signals with the spatio-structural cortical information, it is important to recover the brain after each VSD imaging experiment and do the histological processing. Before recovering the brain the animal is perfused transcardially with saline solution followed with paraformaldehyde (PFA) 4%, which will remove the blood from the vessels and will fix the tissue. After removing it, the brain is kept in PFA overnight to continue the fixation process. Afterwards the brain is cut, in our case by using a vibrotome, in tangential sections of 100 μm thick, which are later stained for cytochrome oxidase (CO) to delineate the barrels.

Next, we need to align the histological barrel maps with the functional signals. This is an important step but very time-consuming. It can be summarized in 4 steps:

1. Pictures of tangential sections of 100 μm thick of the barrel cortex stained for CO are taken under the microscope.
2. The intermediate sections usually contain many orthogonal blood vessels that are used to align subsequent slices. In general, barrels start appearing in sections 3 or 4 and sometimes spread at section 5.
3. Once the slices are aligned the barrel map is reconstructed and drawn.
4. The superficial section contains the tracks of the superficial blood vessels, which are used to align the barrel map reconstruction with the functional images taken in vivo under the VSD set-up.

In collaboration with Dr. Gabriel Peyré (Ceremade, Université Paris-Dauphine), Lorraine Perronnet, a former master student from our laboratories, developed an automated workflow to perform rigid registration of histological sections of the mouse barrel cortex based on sets of detected blood vessels. With this workflow, steps 2 and 3 are automatized, allowing a faster reconstruction of precise barrel maps.

With the aim of assessing the efficiency of the registration method we did two validations: one histological and another functional.

The histological validation consisted in inserting perpendicularly Dil coated electrodes in the barrel cortex of urethane anesthetized mice, before processing the brain for histological procedures. As the penetration was perpendicular to the cortical surface, the Dil

staining traces should be aligned on consecutive cortical sections after a proper registration of the slices. In order to quantify this alignment, the location of Dil traces for different slices were superimposed and traces were not significantly separated confirming the efficacy of the registration method.

In order to validate functionally this automated registration method, we studied the correlation between the functional map and the anatomical map of the mouse barrel cortex. We stimulated individually each of the 24 whiskers while recording the cortical activity by VSD imaging. Each whisker was deflected in 4 cardinal directions (10 trials per direction) and the early responses were averaged (4 to 18 ms post stimulation time). Once the histological reconstruction was done, the peak responses for each whisker were overlaid on the histologically reconstructed barrel field. We found a good match between the functional barrel map and the anatomical one: 86.55% of the maxima of cortical responses were located within the barrel area (further detailed in the article).

Article: “An automated workflow for the anatomo-functional mapping of the barrel cortex”

Perronnet, L.* , Vilarchao, M.E.* , Hucher, G., Shulz, D.E., Peyre, G. and Ferezou, I.

(*Equal contribution to the work)

Journal of Neuroscience Methods 2015, Sep 15. doi:10.1016/j.jneumeth.2015.09.008.

This article presents an automated workflow to perform the registration of histological slices of the barrel cortex followed by the 2D reconstruction of the barrel map from the registered slices. The registration of two successive slices is obtained by computing a rigid transformation to align sets of detected blood vessel cross-sections. This is achieved by using a robust variant of the classical iterative closest point method. A single fused image of the barrel field is then generated by computing a nonlinear merging of the gradients from the registered images.



Basic Neuroscience

An automated workflow for the anatomo-functional mapping of the barrel cortex

Lorraine Perronnet^{a,b,1,2}, María Eugenia Vilarchao^{b,2}, Guillaume Hucher^b, Daniel E. Shulz^b, Gabriel Peyré^a, Isabelle Ferezou^{b,*}

^a CNRS and Ceremade, Université Paris-Dauphine, Place du Maréchal De Lattre De Tassigny, 75775, Paris Cedex 16, France

^b Unité de Neurosciences, Information et Complexité, CNRS FRE 3693, 91198 Gif-sur-Yvette Cedex, France

HIGHLIGHTS

- Here is a new tool to map functional data onto the barrel cortex structure.
- It realigns histological slices and reconstructs the barrel map in 2-D.
- Slice realignment by rigid transformations is computed using detected blood vessels.
- Barrel map reconstruction is obtained by gradient fusion.
- Its application is exemplified for voltage sensitive dye imaging experiments.

ARTICLE INFO

Article history:

Received 17 November 2014

Received in revised form 4 September 2015

Accepted 7 September 2015

Available online xxx

Keywords:

Barrel cortex

Histological sections

Blood vessels

Registration

Robust iterative closest point

Gradient domain fusion

Voltage sensitive dye imaging

ABSTRACT

Background: The rodent barrel cortex is a widely used model to study the cortical processing of tactile sensory information. It is notable by the cytoarchitecture of its layer IV, which contains distinguishable structural units called barrels that can be considered as anatomical landmarks of the functional columnar organization of the cerebral cortex. To study sensory integration in the barrel cortex it is therefore essential to map recorded functional data onto the underlying barrel topography, which can be reconstructed from the post hoc alignment of tangential brain slices stained for cytochrome oxidase.

New method: This article presents an automated workflow to perform the registration of histological slices of the barrel cortex followed by the 2-D reconstruction of the barrel map from the registered slices. The registration of two successive slices is obtained by computing a rigid transformation to align sets of detected blood vessel cross-sections. This is achieved by using a robust variant of the classical iterative closest point method. A single fused image of the barrel field is then generated by computing a nonlinear merging of the gradients from the registered images.

Comparison with existing methods: This novel anatomo-functional mapping tool leads to a substantial gain in time and precision compared to conventional manual methods. It provides a flexible interface for the user with only a few parameters to tune.

Conclusions: We demonstrate here the usefulness of the method for voltage sensitive dye imaging of the mouse barrel cortex. The method could also benefit other experimental approaches and model species.

© 2015 Elsevier B.V. All rights reserved.

1. Introduction

The rodent primary somatosensory cortex is a very convenient model for studying the cortical processing of sensory information because of its well defined structural and functional layout that is invariant from animal to animal (Welker and Van der Loos, 1986; Meyer et al., 2013; Egger et al., 2012). In its layer IV, neurons are gathered into clusters called barrels that respect the same topology as the whiskers on the snout of the animal (Woosley and Loos, 1970). Each barrel is dedicated primarily to the processing of the input coming from its corresponding whisker (Fig. 1A,B). When

* Corresponding author at: Unité de Neurosciences Information et Complexité (UNIC), CNRS FRE 3693, 1 Avenue de la Terrasse, Bât. 32/33, 91198 Gif-sur-Yvette Cedex, France. Tel.: +33 01 69 82 34 02; fax: +33 01 69 82 34 27.

E-mail address: isabelle.ferezou@unic.cnrs-gif.fr (I. Ferezou).

¹ Present address: VISAGES, INRIA, INSERM U746, Université de Rennes 1, CNRS UMR6074, IRISA, campus de Beaulieu, F-35042 Rennes, France.

² These authors contributed equally to the work.

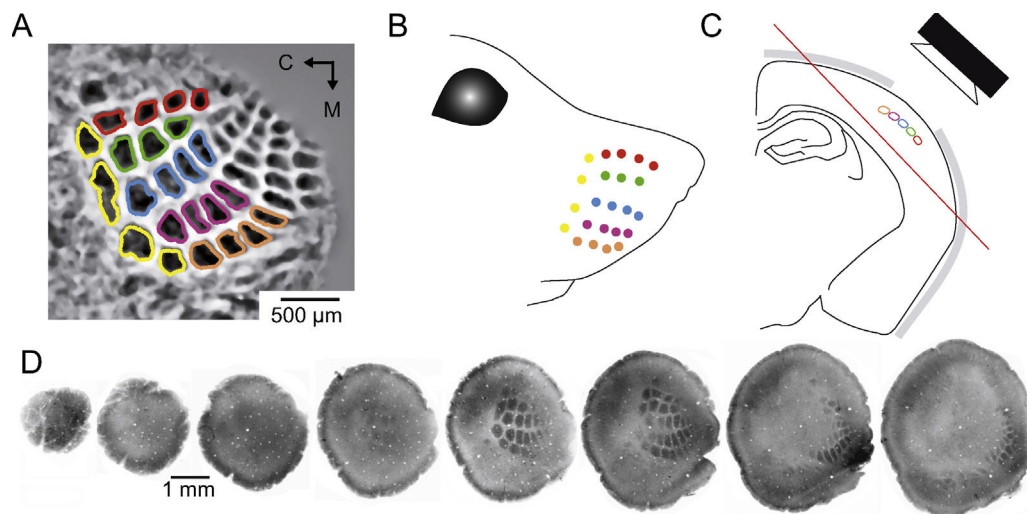


Fig. 1. Cytochrome oxidase staining of tangential sections from the mouse primary somatosensory cortex reveals the structural organization of layer 4 barrels that mirrors the arrangement of the vibrissae on the snout. (A) Following the registration of tangential histological slices and the reconstruction of the barrel map, one can see that the spatial organization of the layer 4 barrels matches the layout of the vibrissae on the snout of the animal (B). (C) Drawing of a coronal section of the left hemisphere of the mouse brain illustrating the position of layer 4 barrels within the primary somatosensory area of the cortex. After *in vivo* imaging of barrel cortex activity, sections are cut tangentially to reconstruct the layer 4 barrel map (cutting plane indicated by the red line). (D) A series of tangential histological slices stained for cytochrome oxidase. On the first slice one can see superficial blood vessels. On the other slices, one can see white circular to elliptical spots that correspond to sections of plunging blood vessels. Depending on the exact axis of the cut, barrels can be spread over several slices.

studying sensory processing in the barrel cortex either with electrophysiological or imaging methods, it is therefore of great interest to superimpose the recorded activity onto the underlying barrel topography, which can be reconstructed from the post hoc alignment of tangential brain slices stained for cytochrome oxidase. In order to optimize this anatomo-functional mapping, which is usually accomplished manually, we developed an automated workflow for the registration of the histological slices of the barrel cortex and the 2-D barrel map reconstruction.

Here we focus our attention on voltage sensitive dye imaging (VSDI) of the mouse barrel cortex to illustrate the usefulness of the approach. However, the method can be extended to the study of the rat barrel cortex and applied to other techniques such as 2-photon calcium imaging.

The traditional first step to recover the map of the barrel cortex after imaging experiments is: brain fixation by perfusing the animal with a solution of paraformaldehyde, followed by the cutting of tangential slices ($\sim 100 \mu\text{m}$ thick, with or without previous flattening of the cortex), which are subsequently stained for cytochrome oxidase using classical histological procedures that reveal the barrel arrangement in layer IV (Fig. 1C and D (Land and Simons, 1985)).

Next, using digital microphotographs of the slices, it is necessary to:

1. register the slices;
2. fuse the registered slices to define a reconstructed barrel image.

In this article we provide an automated solution for these two steps which are the most time-consuming tasks of the workflow when using conventional manual methods. After completing these steps, it is then relatively simple to define the barrel map by segmenting the reconstructed barrel cortex image. The superimposition of the map with the functional data can be finally achieved by using the superficial blood vessels as anatomical landmarks (Fig. 2). The proposed anatomo-functional mapping tool significantly speeds up the overall process and provides more accurate anatomo-functional mapping.

1.1. Registration of histological slices

A typical example of a series of images obtained after the histological process is shown in Fig. 1D. Depending on their depth, the histological sections present different properties: in the first

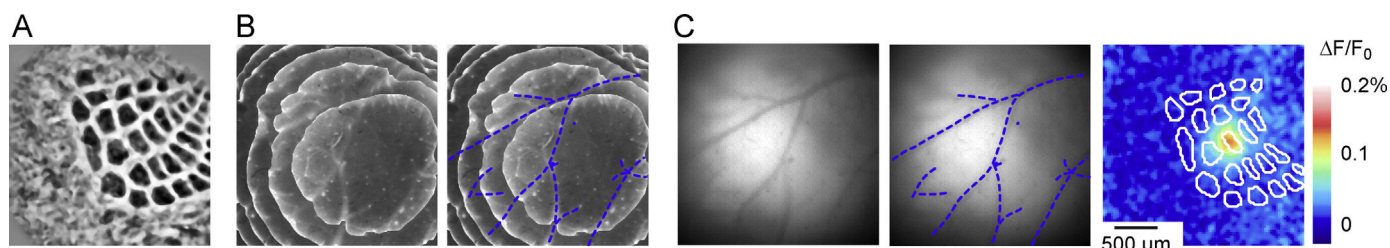


Fig. 2. Alignment of the barrel map with VSDI data using the superficial blood vessels as blueprints. (A) Barrel map reconstructed from the histological slices shown in Fig. 1D, using our anatomo-functional mapping method. (B) Superimposition of the registered histological slices, allowing the delineation of the superficial blood vessels (in blue). (C) The superficial blood vessels also appear *in vivo* on the fluorescent images taken during the VSDI session. The VSDI data can therefore be aligned with the underlying structural map of the barrel cortex using the blood vessels as anatomical landmarks. On the right, the cortical activity is shown imaged at 10 ms following a single C2 whisker deflection with the voltage sensitive dye RH1691 under urethane anesthesia. The barrels outlined from the reconstruction in A are superimposed on the image as white lines.

section, which corresponds to the surface of the cortex, some large superficial blood vessels are visible together with plunging blood vessels. This section is crucial for the whole process since it contains most of the superficial blood vessels that will be used for the final alignment of the histological data with the VSDI data (Fig. 2). The intermediate sections usually contain orthogonal blood vessels (white dots on the slices shown in Fig. 1D) that can be used to align subsequent sections. Barrels start appearing on Section 3 or 4 and can be visualized on up to 5 sections.

We do not use the deeper sections from subgranular layers as they do not contain any useful information for the reconstruction.

Image registration is a classical problem and its solutions find many applications in medical image analysis. Depending on the imaging modality and the specific prior knowledge of the object to register, a wide variety of methods have been considered in the literature (for an overview see (Glocker et al., 2011; Sotiras et al., 2013)). Only a few previous studies explicitly deal with the problem of registering rodent brain histological sections, usually in order to reconstruct a whole brain in 3-D (Ourselin et al., 2001; Ju et al., 2006).

In order to exploit the microscopic-scale information of the histological data, these applications require the precise registration of a large number of histological slices from the whole brain with a method that accounts for global but also local nonlinear deformations due to tissue shrinkage and tearing after histological preparation. Ourselin et al. presented in Ourselin et al. (2001) a block matching strategy to compute local similarities and then estimate the rigid transformation that matches the maximum of similar regions in a robust way. Alternatively (Ju et al., 2006) used a method based on pairwise elastic imaging warps, with the specificity to compute the deformation of each section by considering not only two neighbors for each section, but an extended neighborhood including a group of images.

The specific problem of registering histological sections of the rodent barrel cortex has been rarely addressed in the literature. Egger et al. (2012) proposed a tool for the 3-D reconstruction and standardization of the rat barrel cortex for the precise registration of single neuron morphology. Seventy micrometer thick tangential sections of rat barrel cortex are aligned pairwise by finding the rotation and translation that best superimpose blood vessels of two adjacent sections either manually or automatically, using a tool originally developed for the reconstruction of neuronal processes (Dercksen et al., 2009). Finally the barrels are segmented by using a semi-automated method.

Here we developed a tool to compute the rigid transformations to align sets of detected blood vessels (Fig. 3A), and we decided to focus on a 2-D image fusion using an automated method. The usual approach to perform point cloud registration is the iterative closest point (ICP) algorithm introduced by Besl and McKay (1992). While the initial formulation is not robust to outliers, several approaches explicitly deal with this issue (Chetverikov et al., 2005; Nishino and Ikeuchi, 2008; Stewart et al., 2003; Kaneko et al., 2003; Ma et al., 1999). These approaches are related to re-weighting least squares methods and we propose in Appendix B a unifying presentation and convergence analysis of a robust ICP method.

1.2. Fusion of histological slices

In our framework, the 2-D reconstruction of the barrel maps amounts to perform a fusion of the registered sections (Fig. 3B). The goal is to reconstruct the edges of the barrels that are spread over the slices. Image fusion is classically addressed in the field of image processing and computer vision, to perform for instance image editing and stitching. To reconstruct sharp edges, it is necessary to use

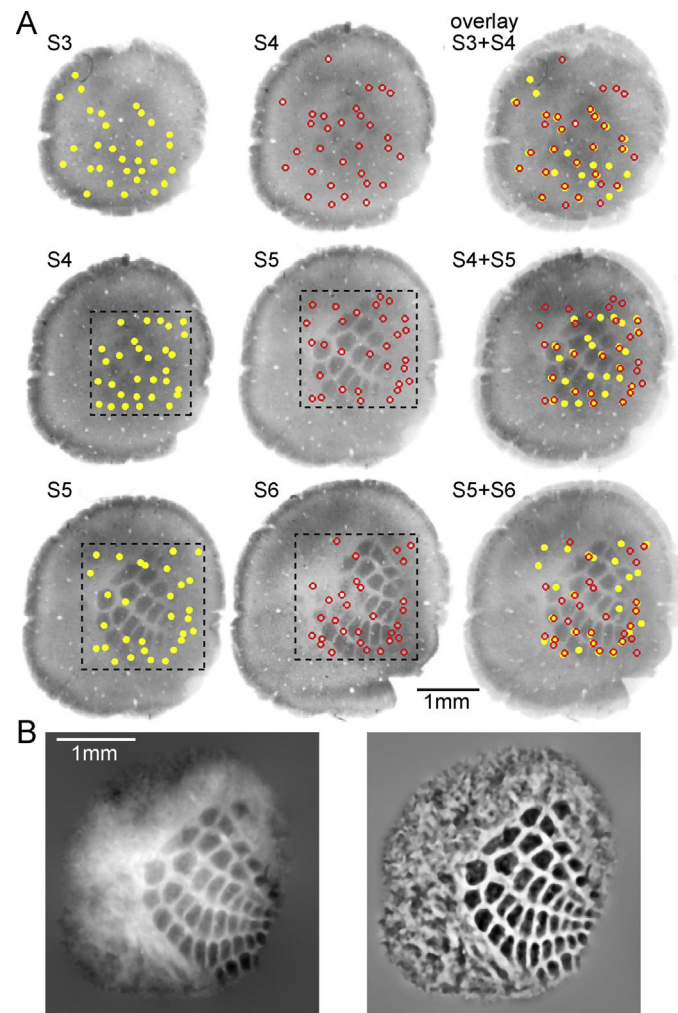


Fig. 3. Registration of histological slices and subsequent barrel map reconstruction. (A) Snapshots extracted from the GUI illustrating the results of the automated detection of blood vessel cross sections on consecutive histological slices (yellow filled circles and red open circles, respectively – S_3 – S_6 previously shown in Fig. 1D). The result of the registration obtained by robust ICP applied on the detected blood vessels is illustrated on the right for each pair of slices. Note that the user can delimit manually a region of interest (black dashed lines) in order to restrict blood vessel detection to the barrel field region. (B) Images from the same experiment obtained by using our automated barrel map reconstruction tool before (left) or after (right) post-processing steps.

non-linear methods, the most popular one being based on gradient-domain blending (Pérez et al., 2003; Raskar et al., 2004). The goal is to generate a novel image by locally keeping the content of the image having the highest local frequency. In this article, we focus on the use of gradient-domain methods, which have the advantage of being simpler and can be easily tuned for the purpose of barrel map fusion.

1.3. Contributions

Our main contribution is a comprehensive pipeline for the 2-D reconstruction of the barrel cortex from tangential histological sections. This pipeline is composed of 2 successive modules that respectively perform: histological section registration and barrel image reconstruction using image fusion. As a side contribution we propose to recast the registration problem using a robust ICP optimization method, and we show that a Majorize-Minimize framework can be applied to provably ensure the convergence of the method. These contributions originate from specific needs

Table 1

Notations used in the paper.

Notation	See
$m \in \{1, \dots, Q\}$	Index of a slice Section 2.2
$\{S_1, \dots, S_Q\}$	Input slices Section 2.2
NCC	Norm. cross correlation Appendix A
\mathcal{X}_m	Set of detected vessels Section 2.2.2
\mathcal{M}	Slices containing barrels Section 2.3.2
T_m	Registration map Eq. (5)
$\{\tilde{S}_1, \dots, \tilde{S}_Q\}$	Registered slices Eq. (5)
$\{\bar{S}_1, \dots, \bar{S}_Q\}$	Inpainted slices Section 2.3.1
S	Fused image Section 2.3.2
\bar{S}	Drift-corrected result Eq. (6)

Table 2

Parameters used in the paper.

Param.	See	Default
τ	NCC threshold Section 2.2.2	0.75
N	Max. number of vessels Section 2.2.2	30
σ_{\max}	Maximum vessel radius Section 2.2.2	4.5
ϵ	ICP robustness parameter Eq. (2)	–
σ^*	Width of debiasing kernel Eq. (6)	10

raised by studies of sensory integration in the barrel cortex, however the histological section registration tool proposed here might be helpful to reconstruct any anatomical tissue in which blood vessels penetrate predominantly orthogonally to the cutting plane of the histological slices.

2. Material and methods

2.1. Overview of the proposed framework

This section details each step of the proposed method. The corresponding Matlab code to reproduce the figures of this article is available online³. This code is packaged as a graphical user interface (GUI) that is helpful to guide the user through the various processing steps, from image loading to the final reconstructed barrel map.

Table 1 reviews the notation introduced in the paper. Table 2 lists the parameters of the method, together with the default values used in our numerical simulations.

The successive steps of the algorithms are:

- Segment the foreground to obtain the input section images $\{S_1, \dots, S_Q\}$ (Section 2.2.1).
- For each $m \in \{1, \dots, Q\}$, compute the list of detected vessel positions \mathcal{X}_m (Section 2.2.2).
- For each $m \in \{1, \dots, Q-1\}$, compute the optimal transform T_m to register S_m with S_{m+1} (Section 2.2.3).
- Apply the transforms to obtain the registered images $\{\tilde{S}_1, \dots, \tilde{S}_Q\}$ (Eq. (5)).
- For each m , inpaint the detected vessel and denoise the resulting images to obtain $\{\bar{S}_1, \dots, \bar{S}_Q\}$ (Section 2.3.1).
- Fuse the relevant maps $\{\bar{S}_m\}_{m \in \mathcal{M}}$ (where $\mathcal{M} \subset \{1, \dots, Q\}$ indexes the maps containing apparent barrels) to obtain the fused map S (Section 2.3.2).
- Remove the low frequency drift to obtain \bar{S} (Section 2.3.3).

³ <https://github.com/gpeyre/2014-NeuroMeth-barrels>.

2.2. Step 1: pairwise registration of histological sections

The input of the algorithm is Q raw images which are digital images with range normalized in $[0, 1]$ (0 being black and 1 white). Fig. 1D shows examples of such images.

2.2.1. Pre-processing

Depending on the configuration of the microscope used to acquire the images, the input images contain 2 or 3 regions:

- In the center of the image, a gray region corresponding to the histological section of the cortex. This is the foreground region.
- A circular white region corresponding to the lens/plate of the microscope and that surrounds the cortex region. It is considered as background.
- In some cases, a black region can also surround the two other regions. It is also considered as background.

We extract the background using a K -means algorithm with $K=3$ regions. The background is then replaced by the value 0 and the resulting images (the so-called “slices” in the following) are denoted $\{S_1, \dots, S_Q\}$.

2.2.2. Vessel detection

Blood vessels which are approximately orthogonal to the cutting plane look like slightly elliptic spots that can be approximated by small Gaussians. To be invariant to local contrast fluctuations, we detect these orthogonal vessels using normalized cross correlations with Gaussian templates of varying standard deviations, assumed to be smaller than σ_{\max} .

For each slice S_m , for $m \in \{1, \dots, Q\}$, we compute its associated normalized cross correlation $NCC(S_m)$ against the set of Gaussian templates, as detailed in Appendix A. Given a threshold $\tau \in [0, 1]$ and a maximum number N of detected vessels, we define the detected vessel centers \mathcal{X}_m to be the set of pixels x satisfying both $NCC(S_m)(x) > \tau$ and $NCC(S_m)(x)$ is among the N largest values of $NCC(S_m)$.

2.2.3. Slice registration by robust ICP

For each m , we now register the slice S_m with the slice S_{m+1} (see Fig. 3A). Registration is obtained by computing an optimal transformation T_m which maps pixels in slice S_{m+1} to pixels in image S_m . We restrict here the computation to rigid transformations, i.e. of the form $T(x) = R(x) + t$ where R is a planar rotation and $t \in \mathbb{R}^2$ is a translation vector.

Variational registration. This optimal deformation is obtained by exploiting the fact that detected orthogonal vessels should have approximately the same position in two consecutive frames. We denote $\mathcal{X}_{m+1} = \{x_i\}_{i \in I}$ and $\mathcal{X}_m = \{y_j\}_{j \in J}$ the two sets of vessel positions. We cast this problem as the optimization of a non-convex functional measure of the goodness of fit between the transformation $T(x_i)$ of each detected vessel x_i in S_m and its closest neighbor y_j in S_{m+1} . T_m is obtained by computing a local minimizer of

$$\min_T \sum_{i \in I} \min_{j \in J} \rho(\|T(x_i) - y_j\|). \quad (1)$$

Here $\rho: \mathbb{R}^+ \rightarrow \mathbb{R}^+$ is a penalty function. The most common choice is a quadratic loss $\rho(r) = r^2$, which assumes some sort of Gaussian distribution of the fitting errors. This choice poorly handles outliers in the detected vessels, which are likely to be present in our datasets. We choose here to use the following robust loss function

$$\rho(r) = \log(\epsilon^2 + r^2), \quad (2)$$

which gives less weight to outliers (large values of r) than a quadratic loss. Small values of ε are used to cope with many outliers. Note that setting $\varepsilon \rightarrow +\infty$ recovers the quadratic loss r^2 which assumes no outliers. Note also that other loss functions could be used as well, as long as they satisfy the hypotheses exposed in Appendix B.

ICP iterations. A classical algorithm to minimize (1) is the iterative closest point (ICP), introduced by Besl and McKay (1992) for the quadratic loss $\rho(r)=r^2$. This algorithm has been extended by several authors to cope with robust loss (see Section 1.1 for more details). We use a similar approach here, and provide more details in Appendix B.

The ICP algorithm iterates between two steps. In the first step, T is known and assumed to be fixed, and one computes a nearest neighbor $z_i=y_j$ for each vessel x_i , where the index j minimizes

$$\min_{j \in I} \rho(\|T(x_i) - y_j\|). \quad (3)$$

In the second step, the optimal T is updated by solving

$$\min_T \sum_{i \in I} \rho(\|T(x_i) - z_i\|). \quad (4)$$

For the quadratic loss $\rho(r)=r^2$, this second step is solved in closed form as detailed in Appendix B.2. For a generic loss ρ , there is no such closed form. We detail in Appendix B.1 a Majorize–Minimize (MM) method to compute a local minimizer. To the best of our knowledge, this presentation, and the corresponding convergence analysis, is new.

Initialization. A major difficulty to solve (2) is that it is highly non-convex, and the ICP algorithm is likely to converge to a local minimizer T . To improve the quality of the result, it is important to test several initializations to obtain a good registration.

Registered images. Once the registration transforms $\{T_1, \dots, T_{Q-1}\}$ have been computed, they can be cascaded to warp the input slice images to obtain the sequence $\{\tilde{S}_1, \dots, \tilde{S}_Q\}$ of sections, all registered with respect to the initial one $S_1 = \tilde{S}_1$ as follow

$$\tilde{S}_m(x) = S_m(T_m(x)) \quad \text{where} \quad T_m = T_1 \circ \dots \circ T_{m-2} \circ T_{m-1}. \quad (5)$$

2.3. Step 2: reconstruction of the barrel image

We now have a set $\{\tilde{S}_1, \dots, \tilde{S}_Q\}$ of registered slices. We fuse them in a single image S , which gathers the edge information of the relevant images to reconstruct the barrel map.

2.3.1. Pre-processing

In order to avoid the amplification of artifacts during the gradient fusion process detailed next, we inpaint (i.e. remove) the orthogonal vessel traces and denoise the resulting image. The inpainting method is detailed in Appendix C. The output of the inpainting is then denoised using a median filter on 3×3 patches. We use this non-linear filter to reduce salt-and-pepper noise instead of a convolution, as it removes noise while preserving edges. We denote the output of this pre-processing \tilde{S}_m .

2.3.2. Slice gradient fusion

We denote $m \in \mathcal{M}$ the set of relevant slices containing partial barrel information. To reconstruct a sharp image, we fuse together the gradient of the input slices $\{S_m\}_{m \in \mathcal{M}}$ by keeping at each pixel the gradient with the largest magnitude. This method is partly inspired by some recent works in computational photography, such as Pérez et al. (2003), Raskar et al. (2004). The details of this method are given in Appendix D. We denote S the output of the fusion process.

2.3.3. Drift removal

The histological sections often present variations in intensity across the barrel cortex that might be due to anatomical reasons. Usually, the anterior lateral barrel subfield (small barrels corresponding to small vibrissae) appears darker than the posterior medial barrel subfield (large barrels corresponding to large vibrissae). This drift is enhanced by the gradient fusion operation that is applied on each pair. As a consequence, the merged image S obtained by the procedure explained above exhibits a strong drift in intensity. We thus filter the merged image with a high-pass filter to remove this low frequency component

$$\bar{S} = S - S \star h_{\sigma^*} \quad (6)$$

where h_{σ^*} is a low-frequency gaussian filter of standard deviation σ^* , and \star is the discrete 2-D convolution.

2.4. In vivo VSDI and Dil staining

Animal preparation and VSDI setup. Experiments were performed in conformity with the French (authorization number: 2012-0068) and European (2010/63/UE) legislations relative to the protection of animals used for experimental and other scientific purposes. VSDI of the cortical activity evoked by single whisker deflections was performed on 6–12 week-old C57Bl6 mice under urethane anesthesia (1.7 mg/g), essentially as previously described in Ferezou et al. (2006). Briefly, the left barrel cortex was exposed and stained for 1 h with the VSD RH1691 (1 mg/ml, in Ringer's solution containing [in mM]: 135 NaCl, 5 KCl, 5 HEPES, 1.8 CaCl₂, 1 MgCl₂). After removal of the unbound dye, the cortex was covered with agarose (0.5–1% in Ringer's) and a coverslip. Cortical imaging was performed through a tandem-lens fluorescence microscope (SciMedia), equipped with one Leica PlanApo 5 \times (objective side) and one Leica PlanApo 1 \times (condensing side), a 630 nm excitation filter, a 650 nm dichroic mirror, and a long pass 665 nm emission filter. The field of view was 2.5 \times 2.5 mm, resulting in a pixel resolution of 25 \times 25 μ m.

Whisker stimulation. Individual deflections of the right 24 posterior macrovibrissae of the mice were performed using a custom built multi-whisker stimulator based on a matrix of 24 multidirectional piezoelectric benders (Jacob et al., 2010). The whiskers were inserted in 27G stainless steel tubes attached to the benders, leaving 2 mm between the tip of the tube and the whisker base. The 24 whiskers were stimulated individually, in the 4 cardinal directions, at 0.1 Hz within pseudo randomized sequences containing extra blank trials (each stimulation being repeated 10 times). Each whisker deflection consisted of a 100 μ m displacement (measured at the tip of the tube), with a 2 ms rising time, a 2 ms plateau and a 2 ms fall (specific filters were used to correct for the mechanical ringing of the stimulators).

Image analysis. Acquisition and data preprocessing were done using in-house software (Elphy, G. Sadoc, UNIC-CNRS), further analyses were made using custom written routines in IgorPro (Wavemetrics). Subtraction of the averaged unstimulated blank trials was used to correct for bleaching artifacts. For each whisker, data corresponding to the 4 directions of deflection were averaged.

Dil in vivo staining. Dil stain (Molecular Probes, LifeTechnologies) was deposited on the shanks of silicon electrodes (DiCarlo et al., 1996) that were inserted in the barrel cortex perpendicularly with a microcontroller (Luigs & Neumann).

2.5. Histological procedures

Following the experiments and the administration of an overdose of urethane, mice were perfused with saline followed by paraformaldehyde (4% in 0.1 M phosphate buffer). After an overnight post-fixation in paraformaldehyde, the brains were cut

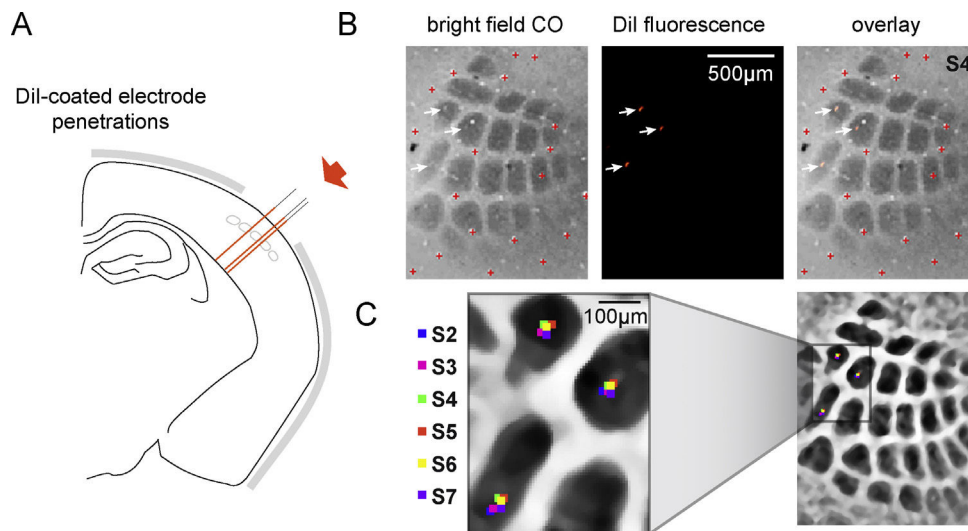


Fig. 4. Histological validation of the registration method. (A) Drawing of a coronal section of the left hemisphere of the mouse brain illustrating the penetration sites of Dil-coated electrodes. (B) The Dil fluorescent staining (middle image) does not interfere with the process of blood vessel detection used on bright field images (left), as shown by the absence of detected spots on the Dil stain (right), arrowheads indicate the Dil stained spots corresponding to electrode tracks. (C) Following the registration of the slices 2–7, we observe a good overlap of Dil spots, indicative of the accuracy of our registration method.

in 100 μm thick tangential sections and stained for cytochrome oxidase.

3. Results

Starting from tangential slices stained for cytochrome oxidase, the reconstructed 2-D barrel map can be obtained in a few clicks by using the provided GUI. The whole procedure takes 7–9 min including 3–5 min of computation that do not require the intervention of the user. The same process using traditional manual methods (with the help of a raster graphics editor such as Adobe Photoshop) takes, for a well-trained person, 16–28 min. Most importantly, our automated approach prevents user dependent variability in the obtained barrel map. In order to assess the accuracy of our registration method, we first carried out histological control experiments, and then used VSD imaging to functionally evaluate the precision of the barrel map obtained following the full reconstruction procedure.

3.1. Histological validation of the registration method

In order to assess the efficiency of our registration method based on automated blood vessel detection and robust ICP, we perpendicularly inserted Dil coated electrodes in the barrel cortex of urethane anesthetized mice ($n=5$ experiments, 3–6 electrode penetrations per experiments), before processing the brain for histological staining of the cytochrome oxidase following our standard procedures. The electrodes being flat, they did not leave any round or elliptic white marks in the tissue and therefore did not interfere with our registration method (Fig. 4). Because the penetration of Dil coated electrodes was perpendicular to the cortical surface, the Dil staining should appear aligned on consecutive cortical sections following proper registration of the slices. In order to control this alignment, the location of Dil spots was reported for each slice on the final fused barrel map image for each section (Fig. 4C). The calculated mean distance between Dil spots from the same electrode penetration ($34.41 \pm 18.93 \mu\text{m}$, mean \pm SD, $n=5$) revealed the subcolumnar resolution of our registration method. These control experiments were further used to evaluate the eventual shrinkage of the cortical tissue due to brain fixation and histological procedures. The distances of 250 μm and 500 μm separating the electrode penetration sites in

vivo, were compared to the distances measured between Dil spots on the slices following histological procedures. Over our 5 control experiments, the observed tissue shrinkage within the $x-y$ plane was minimal (<1.5%).

3.2. Assessment of the barrel map reconstruction tool using VSDI of cortical responses to individual whisker deflections

To finally validate our 2-D barrel map reconstruction method, we confronted its resulting map with the functional organization of the barrel cortex established in vivo by real time imaging of cortical responses to individual whisker deflections under urethane anesthesia ($n=4$ experiments). Using a mechanical multi-whisker stimulator (Jacob et al., 2010), we deflected independently the 24 principal whiskers in a pseudo random order, and imaged the evoked cortical responses in the contralateral barrel cortex using the VSD RH1691. Fig. 5 illustrates the results obtained from one experiment. As previously reported in similar conditions (Ferezou et al., 2006), the earliest responses to whisker deflections were localized to the corresponding barrel-related columns (Fig. 5A). When reporting the 90% contours of the early cortical responses onto the aligned barrel map, we observe a good anatomo-functional match (Fig. 5B). To quantify this match, the distance between the centroid of the anatomically defined barrels and the centroid of the early VSD response (area above a 90% threshold) was measured (Fig. 5C). The mean centroid-centroid distance over the 4 control experiments for all the barrels is $60.5 \pm 21.2 \mu\text{m}$ (34.8–116.5 μm range across the barrel field). We observed slightly higher values for the columns located at the border of the map which might result from the curvature of the cortex, the maxima of cortical responses were located within the corresponding barrel area in the majority of cases (86.55%), attesting to the accuracy of the method.

4. Discussion

We have designed a comprehensive pipeline for the reconstruction of the 2-D barrel map from histological sections. This tool enables a fast reconstruction of a precise barrel map, thus saving a significant amount of time for the experimentalist. Indeed, most of the studies based on optical imaging which required a post-hoc anatomo-functional mapping of the barrel cortex relied

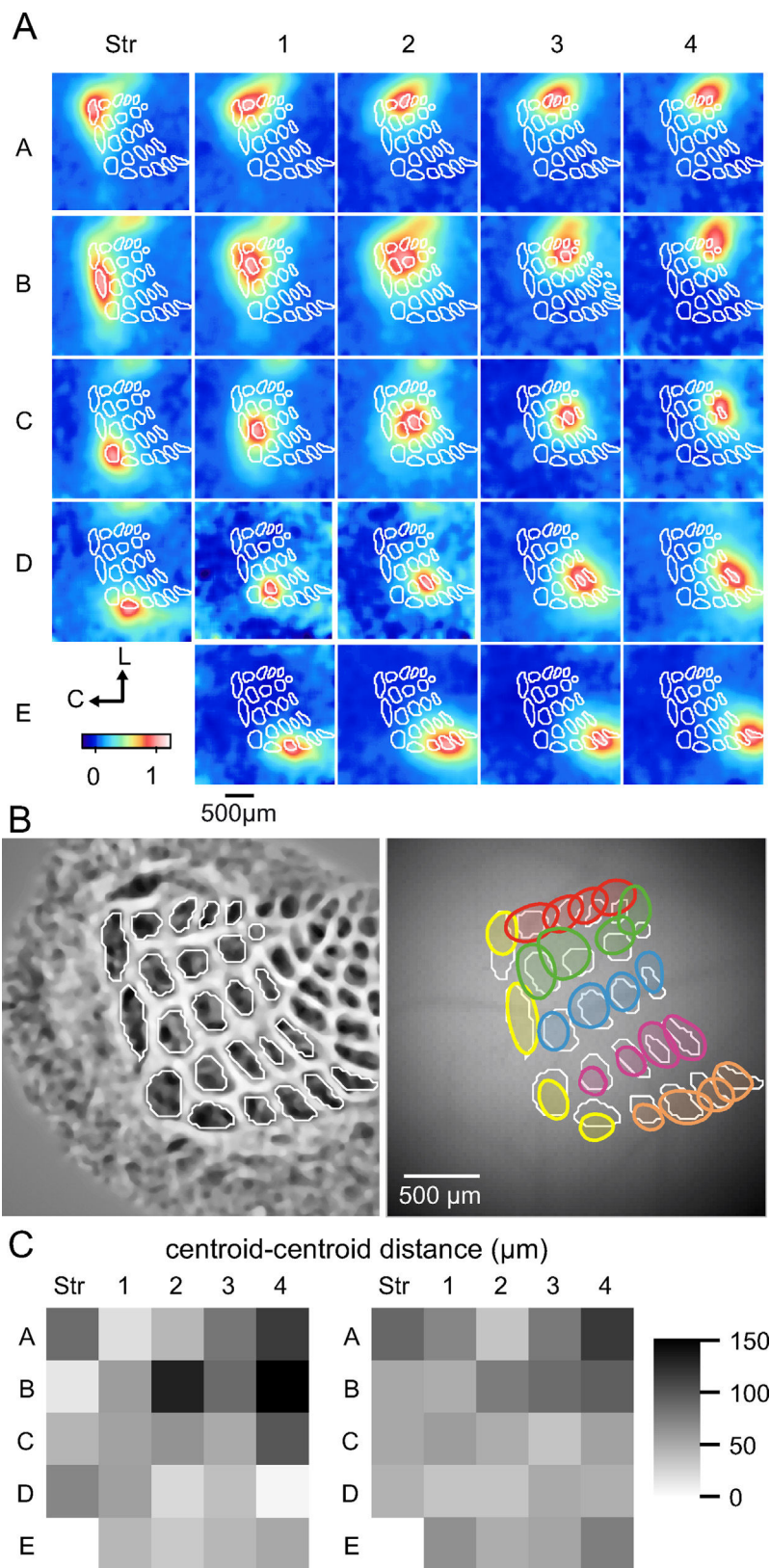


Fig. 5. Functional validation of the registration method. (A) Cortical responses evoked by individual deflections of the 24 principal vibrissae in a urethane anesthetized mouse were imaged using the VSD RH1691. For each whisker, the early cortical response is shown (data averaged from 4 to 18 ms post stimulation time and 40 trials, Gaussian filtered (5×5 pxls), and normalized), together with the aligned barrel map obtained from our reconstruction method (white lines). (B) The barrel map was extracted from the fused barrel field image (left) and overlaid on the VSD reference image (right) together with the early response locations (90% contours of the early responses (in A) are shown in colors) obtained for each whisker. (C) The distance between the centroid of the barrel area and the centroid of the early cortical response (as illustrated in B) was computed, column by column, for the experiment illustrated in A and B (left), and in average for all the control experiments ($n = 4$, right).

on manual reconstruction and alignment of the barrel map with the functional images (Kleinfeld and Delaney, 1996; Takashima and Kajiwara, 2001; Ferezou et al., 2006; Kerr et al., 2007; Tsytsarev et al., 2010; Lustig et al., 2013; Harris et al., 2013). Other studies (Berwick et al., 2004, 2008; Devonshire et al., 2010) used a method based on a warping algorithm described by Zheng et al. (2001). However, the manual detection of the fiducial markers required with this approach remains time-consuming in comparison to the automatic detection of blood vessel cross sections proposed here.

In a recent article, Guy et al. (2014) used a warping algorithm in order to align the layer IV barrel map, reconstructed manually from histological slices of flattened cortex, with the in vivo functional images using sets of fiducial points. Although the algorithm is not described in detail and probably involves manual selection of the fiducial points, it might be an interesting complement to our approach when working with flattened barrel cortex slices, since it allows a compensation for the curvature of the brain and distortion of the tissue. Finally, instead of using the superficial blood vessels as anatomical landmarks to align the barrel map on the functional images, an alternative approach is to use the images of early cortical responses to single whisker deflections as landmarks (Wallace and Sakmann, 2008; Wang et al., 2012; Yang et al., 2013). Using such a method as a standard requires the acquisition of several additional single whisker responses, which might be difficult to implement for instance when working with awake head fixed animals. Note that the tool we propose here to reconstruct the barrel map is valuable whatever solution is chosen in the end to realign the barrel map with the functional images.

On the methodological and mathematical sides, we mainly re-use a set of already existing tools (cross-correlation, ICP and gradient fusion). Our main contribution is to put them together in a coherent processing pipeline. A result of independent interest, that seems to be new, is to show how a family of robust ICP algorithms can be recasted as majorization-minimization algorithms. This in turn allows us to analyze the convergence of these methods.

Obviously the efficacy of the proposed anatomo-functional mapping tool depends upon the quality of the histological slices. Although the preparation of these slices relies on standard protocols which often belong to the daily routines of neurophysiology laboratories, two aspects are essential for the accuracy of the outcome: the quality of the perfusion, and the right thickness of the first (most superficial) slice. Indeed, on the one hand blood vessels have to appear as white circular or elliptical spots on the images to allow the proper registration of consecutive slices and, on the other hand, the superficial blood vessels should be intact to allow the final overlay of the obtained barrel map with the in vivo recordings. When cutting the brain, it is therefore important to set the zero position of the blade with care to ensure a 100 μm thickness to the first slice and thus preserve the integrity of the superficial blood vessels. Finally, although one could deplore that this overlay is a crucial step of the analysis that remains to be achieved manually, we propose here a solution that automatizes the most time-consuming phases of the overall process and thus represents a substantial gain in time and precision. Although its use has been demonstrated successfully for VSDI of the adult mouse barrel cortex, it could be expanded to other experimental model species or to the developing brain. Furthermore, the histological section registration method described here might be helpful to reconstruct any tissue in which a majority of blood vessels are orthogonal to the cutting plane of the slices.

Acknowledgments

We thank Gérard Sadoc for technical expertise, and Aurélie Daret for her experimental assistance. This work was supported by the Centre National de la Recherche Scientifique (France),

the European Research Council (ERC project SIGMA-Vision), the European Union Seventh Framework Programme BrainScaleS (FP7-ICT-2009-6, N 269921), the Agence Nationale pour la Recherche (SensoryProcessing, Transtact).

Appendix A. Feature detection with normalized cross-correlation

We consider a set of Gaussian templates $\{g_k\}_{k \in \mathcal{K}}$,

$$g_k(x) = \frac{1}{Z_k} \exp\left(-\frac{\|x\|^2}{2\sigma_k^2}\right)$$

where Z_k is a constant ensuring a normalization $\sum_x g_k(x)^2 = 1$. The standard deviations σ_k are chosen equally spaced in the range $[0, \sigma_{\max}]$ (note that $\sigma_k = 0$ corresponds to a Dirac, supported on a single pixel).

Given a template g_k , we denote its support as

$$I_k = \{x \ ; \ g_k(x) > \eta\}$$

where $\eta = 10^{-3}$ is a small tolerance threshold. The normalized cross correlation of a section S with the template g_k is then defined as

$$\text{NCC}_k(S)(x) = \frac{\sum_{y \in I_k} S(x+y)g_k(y)}{\left(\sum_{y \in I_k} S(x+y)^2\right)^{1/2}}.$$

The normalized cross correlation with the whole set of filters is the maximum of all the correlations

$$\text{NCC}(S)(x) = \max_{k \in \mathcal{K}} \text{NCC}_k(S)(x). \quad (\text{A.1})$$

A large value of $\text{NCC}(S)(x)$ indicates that a vessel is likely to be present at pixel x . In this case, the value $k = k(x)$ of the maximum appearing in (A.1), i.e. such that $\text{NCC}(S)(x) = \text{NCC}_k(S)(x)$, indicates that the radius of this vessel is approximately σ_k .

Appendix B. Robust iterative closet point

B.1. ICP Step 1 with Majorize–Minimize (MM) iterations

We give here the details of an iterative algorithm to compute a local minimizer (in fact a stationary point) of (3), which reads

$$\min_T \mathcal{E}(T) = \sum_{i \in I} \rho(\|T(x_i) - z_i\|). \quad (\text{B.1})$$

This method is similar to re-weighting ℓ^2 methods often used for robust ICP (see for instance (Bouaziz et al., 2013)), but we integrate it into a Majorize–Minimize framework, which ensures its convergence.

Starting from an initial transform $R^{(0)}$, we compute the iterations as

$$T^{(\ell+1)} \in \underset{T}{\text{argmin}} \tilde{\mathcal{E}}(T, T^{(\ell)}) \quad (\text{B.2})$$

where $\tilde{\mathcal{E}}$ is a so-called surrogate function, which should satisfy

- (H₁) $\tilde{\mathcal{E}}(T, T') - \mathcal{E}(T)$ is a smooth function of T (of class C^1);
- (H₂) for all (T, T') , $\tilde{\mathcal{E}}(T, T') \geq \mathcal{E}(T)$;
- (H₃) for all T , $\tilde{\mathcal{E}}(T, T) = \mathcal{E}(T)$.

Under these conditions, it can be shown that the iterations enjoy some good convergence properties. The sequence $\mathcal{E}(T^{(\ell)})$ is decaying and converges to some value \mathcal{E}^* . If \mathcal{E} is smooth (which is the case here), $\|\nabla \mathcal{E}(T^{(\ell)})\| \rightarrow 0$. Since in our case, the energy \mathcal{E} is coercive, the sequence $T^{(\ell)}$ is bounded, and all its cluster points T^* are stationary (i.e. $\nabla \mathcal{E}(T^*) = 0$) with same energy $\mathcal{E}(T^*) = \mathcal{E}^*$.

The main difficulty in general is to devise a “good” surrogate function $\tilde{\mathcal{E}}$, i.e. such that one can compute the iteration (B.2) in closed form. The following proposition shows that one can actually design such a surrogate function using a quadratic loss.

Proposition 1. *If ρ is $C^1(\mathbb{R})$ and $w(r) = \frac{\rho'(r)}{2r}$ is decreasing, there exists a constant $C(T)$ independent of T so that the functional*

$$\tilde{\mathcal{E}}(T, T') = C(T') + \sum_{i \in I} w_i \|T(x_i) - z_i\|^2 \quad (\text{B.3})$$

where $w_i = w(\|T'(x_i) - z_i\|)$

is a majorizing functional for (B.1) and thus satisfies properties (H_1, H_2, H_3) .

Proof. We rewrite $\tilde{\mathcal{E}}$ as

$$\tilde{\mathcal{E}}(T, T') = \sum_{i \in I} \tilde{\rho}(\|T(x_i) - z_i\|, \|T'(x_i) - z_i\|),$$

where we defined

$$\tilde{\rho}(r, r') = c(r') + w(r')r^2 \quad \text{where} \quad c(r') = \rho(r') - \frac{\rho'(r')}{2}r'.$$

Thanks to the separability $\tilde{\mathcal{E}}$ (it is a summation over i of functions involving independent variables) and the change of variables $r = \|T(x_i) - z_i\|$, it thus suffices to prove that $\tilde{\rho}$ is a surrogate functional for ρ on \mathbb{R}^+ . Hypothesis (H_1) holds because ρ is C^1 , and one verifies that $\tilde{\rho}(r', r') = \rho(r')$ so that (H_3) holds. For any $r' \geq 0$, we consider

$$h(r) = \rho(r, r') - \rho(r) = \rho(r) - \rho(r') + \frac{\rho'(r')}{2r'}r^2 - \frac{\rho'(r')}{2}r'.$$

It satisfies $h(r') = h'(r') = 0$ and $h'(r) = 2r(w(r') - w(r))$. Since w is decaying, r' is the only point where h' is vanishing on \mathbb{R}^+ . This implies that $h \geq 0$, hence (H_2) .

The hypothesis that w is decreasing should be interpreted as the condition that ρ should penalize less than a quadratic loss, which makes sense for a robust penalization. Note that the loss (2) that we use in our method satisfies this condition, and that the weighting function satisfies

$$w(r) = \frac{1}{\varepsilon^2 + r^2}.$$

B.2. ICP Step 2 with weighted quadratic loss

We consider the problem of solving

$$\min_T \sum_{i \in I} w_i \|T(x_i) - z_i\|^2 \quad \text{where} \quad T(x) = R(x) + t$$

where R is a rotation and $t \in \mathbb{R}^2$. This minimization appears in the MM iteration (B.2) when using the majorizing function (B.3). This problem has a closed form solution, as detailed for instance in Maurer et al. (1996). For the sake of completeness, we recall the steps of the method. One first centers the points, for $i \in I$

$$\tilde{x}_i = x_i - \frac{\sum_{k \in I} w_k x_k}{\sum_{k \in I} w_k} \quad \text{and} \quad \tilde{z}_i = z_i - \frac{\sum_{k \in I} w_k z_k}{\sum_{k \in I} w_k}.$$

The optimal rotation is obtained as $R = VU^T$ where (U, V) are the eigenvectors of the correlation matrix

$$\sum_{i \in I} w_i \tilde{x}_i \tilde{y}_i^T = U \Lambda V^T \quad (\text{B.4})$$

(here Λ is the diagonal matrix of eigenvalues). The optimal transformation is then computed as

$$t = \frac{\sum_{i \in I} w_i (\tilde{z}_i - R \tilde{x}_i)}{\sum_{i \in I} w_i}.$$

Appendix C. Inpainting

We consider a registered slice \tilde{S}_m and its associated vessel locations $\mathcal{X}_m = \{x_i\}_{i \in I}$. We denote $\tilde{x}_i = \mathcal{T}_m(x_i)$ the registered vessel locations, where the cumulative transform \mathcal{T}_m is defined in (5). We recall that the cross-correlation minimization (as detailed in Appendix A) outputs at each pixel x the index $k(x)$ of the optimal Gaussian template at this location, which has a radius $\sigma_{k(x)}$.

We define a mask Φ , which is the set of pixels that are at distance smaller than $\sigma_{k(x)}$ from the point \tilde{x}_i . It is thus a union of disks. Pixels in Φ should be discarded and inpainted. This is achieved using a quadratic minimization that seeks a smooth interpolation of missing data

$$\min_S \sum_x \|\nabla S(x)\|^2 \text{ subject to } \forall y \notin \Phi, \quad S(x) = S_m(x), \quad (\text{C.1})$$

where ∇S is a finite difference approximation of the gradient of the image S . The solution of (C.1) corresponds to solving a Poisson equation $\Delta S = 0$ on Φ with Dirichlet boundary conditions given by the constraints. This can be solved using a conjugate gradient method.

Appendix D. Gradient domain image fusion

We consider a set $\{\tilde{S}_m\}_{m \in \mathcal{M}}$ of input images to fuse. At each pixel x , we denote the index of largest gradient magnitude as

$$m(x) = \operatorname{argmin}_{m \in \mathcal{M}} \|\nabla \tilde{S}_m(x)\|$$

where ∇ is a finite differences approximation of the gradient operator.

We design a fused vector field as

$$u(x) = \nabla \tilde{S}_{m(x)}(x) \in \mathbb{R}^2.$$

Since the vector field u is obtained by gluing together gradients from several different images, it is in general not anymore the gradient of an image. We thus reconstruct a valid fused image S using the minimal norm pseudo-inverse, i.e. by computing an image S whose gradient is as close as possible to u

$$\min_S \|u - \nabla S\|^2 = \sum_x \|u(x) - \nabla S(x)\|^2.$$

The solution is obtained by solving a Poisson equation

$$\Delta S = \operatorname{div}(u) \quad (\text{D.1})$$

with adequate boundary conditions, where $\Delta = \operatorname{div} \circ \nabla$ is the Laplacian operator and $\operatorname{div} = -\nabla^*$ is the divergence. When using periodic boundary conditions (which can be used in our case), one solves (D.1) in $O(N \log(N))$ operations (where N is the number of pixels), using an FFT Poisson solver.

References

- Berwick J, Redgrave P, Jones M, Hewson-Stoate N, Martindale J, Johnston D, et al. Integration of neural responses originating from different regions of the cortical somatosensory map. *Brain Res* 2004;1030(2):284–93.
- Berwick J, Johnston D, Jones M, Martindale J, Martin C, Kennerley AJ, et al. Fine detail of neurovascular coupling revealed by spatiotemporal analysis of the hemodynamic response to single whisker stimulation in rat barrel cortex. *J Neurophysiol* 2008;99:787–98.
- Besl PJ, McKay ND. A method for registration of 3-D shapes. *IEEE Trans Pattern Anal Mach Intell* 1992;14(2):239–56.
- Bouaziz S, Tagliasacchi A, Pauly M. Sparse iterative closest point. *Comput Graph Forum* 2013;32(5):113–23.

- Chetverikov D, Stepanov D, Krsek P. Robust euclidean alignment of 3D point sets: the trimmed iterative closest point algorithm. *Image Vis Comput* 2005;23(3):299–309.
- Dercksen VJ, Weber B, Güenther D, Oberlaender M, Prohaska S, Hege HC. Automatic alignment of stacks of filament data. In: *Proc. IEEE int. symp. on biomedical imaging: from nano to macro (ISBI)*; 2009. p. 971–4.
- Devonshire IM, Grandy TH, Dommert EJ, Greenfield SA. Effects of urethane anaesthesia on sensory processing in the rat barrel cortex revealed by combined optical imaging and electrophysiology. *Eur J Neurosci* 2010;32(5):786–97.
- DiCarlo JJ, Lane JW, Hsiao SS, Johnson KO. Marking microelectrode penetrations with fluorescent dyes. *J Neurosci Methods* 1996;64(1):75–81.
- Egger R, Narayanan RT, Helmstaedter M, de Kock CPJ, Oberlaender M. 3D reconstruction and standardization of the rat vibrissal cortex for precise registration of single neuron morphology. *PLoS Comput Biol* 2012;8(12).
- Ferezou I, Bolea S, Petersen CCH. Visualizing the Cortical Representation of Whisker Touch: Voltage-Sensitive Dye Imaging in Freely Moving Mice. *Neuron* 2006;50(4):617–29.
- Glocker B, Sotiras A, Komodakis N, Paragios N. Deformable medical image registration: setting the state of the art with discrete methods. *Annu Rev Biomed Eng* 2011;13:219–44.
- Guy J, Wagener RJ, Mock M, Staiger JF. Persistence of functional sensory maps in the absence of cortical layers in the somatosensory cortex of reeler mice. *Cereb Cortex* 2014, pii:bhu052.
- Harris S, Bruyns-Haylett M, Kennerley A, Boorman L, Overton PG, Ma H, et al. The effects of focal epileptic activity on regional sensory-evoked neurovascular coupling and postictal modulation of bilateral sensory processing. *J Cereb Blood Flow Metab* 2013;33(10):1595–604.
- Jacob V, Estebanez L, Cam JL, Tiercelin J-Y, Parra P, Parésys G, et al. The matrix: a new tool for probing the whisker-to-barrel system with natural stimuli. *J Neurosci Methods* 2010;189(1):65–74.
- Ju T, Warren J, Carson J, Bello M, Kakadiaris I, Chiu W, et al. 3d volume reconstruction of a mouse brain from histological sections using warp filtering. *J Neurosci Methods* 2006;156(1–2):84–100.
- Kaneko S, Kondo T, Miyamoto A. Robust matching of 3D contours using iterative closest point algorithm improved by m-estimation. *Pattern Recogn* 2003;36(9):2041–7.
- Kerr JN, de Kock CP, Greenberg DS, Bruno RM, Sakmann B, Helmchen F. Spatial organization of neuronal population responses in layer 2/3 of rat barrel cortex. *J Neurosci* 2007;27(48):13316–28.
- Kleinfeld D, Delaney KR. Distributed representation of vibrissa movement in the upper layers of somatosensory cortex revealed with voltage-sensitive dyes. *J Comp Neurol* 1996;375(1):89–108.
- Land P, Simons D. Cytochrome oxidase staining in the rat smi barrel cortex. *J Comp Neurol* 1985;238(2):225–35.
- Lustig BR, Friedman RM, Winberry JE, Ebner FF, Roe AW. Voltage-sensitive dye imaging reveals shifting spatiotemporal spread of whisker-induced activity in rat barrel cortex. *J Neurophysiol* 2013;109(9):2382–92.
- Ma B, Ellis RE, Fleet DJ. Spotlights: a robust method for surface-based registration in orthopedic surgery. In: *MICCAI*; 1999. p. 936–44.
- Maurer CR, Aboutanos GB, Dawant BM, Maciunas RJ, Fitzpatrick JM. Registration of 3-d images using weighted geometrical features. *IEEE Trans Med Imaging* 1996;15(6):836–49.
- Meyer H, Egger R, Guest J, Foerster R, Reissl S, Oberlaender M. Cellular organization of cortical barrel columns is whisker-specific. *Proc Natl Acad Sci U S A* 2013;110(47):19113–8.
- Nishino K, Ikeuchi K. Robust simultaneous registration of multiple range images. In: *Digitally Archiving Cultural Objects*. Springer US; 2008. p. 71–88.
- Ourselin S, Roche A, Subsol G, Pennec X, Ayache N. Reconstructing a 3D structure from serial histological sections. *Image Vis Comput* 2001;19(1–2):25–31.
- Pérez P, Gangnet M, Blake A. Poisson image editing. In: *ACM SIGGRAPH 2003 Papers*; 2003. p. 313–8.
- Raskar R, Ilie A, Yu J. Image fusion for context enhancement and video surrealism. In: *Proc. NPAR* 2004; 2004. p. 85–152.
- Sotiras A, Davatzikos C, Paragios N. Deformable medical image registration: a survey. *IEEE Trans Med Imaging* 2013;32(7):1153–90.
- Stewart CV, Tsai C, Roysam B. The dual-bootstrap iterative closest point algorithm with application to retinal image registration. *IEEE Trans Med Imaging* 2003;22(11):1379–94.
- Takashima IT, Kajiwarara RI. Voltage-sensitive dye versus intrinsic signal optical imaging: comparison of optically determined functional maps from rat barrel cortex. *Neuroreport* 2001;12(13):2889–94.
- Tsytsarev V, Pope D, Pumbo E, Yablonskii A, Hofmann M. Study of the cortical representation of whisker directional deflection using voltage-sensitive dye optical imaging. *Neuroimage* 2010;53(1):233–8.
- Wallace DJ, Sakmann B. Plasticity of representational maps in somatosensory cortex observed by in vivo voltage-sensitive dye imaging. *Cereb Cortex* 2008;18(6):1361–73.
- Wang Q, Millard DC, Zheng HJ, Stanley GB. Voltage-sensitive dye imaging reveals improved topographic activation of cortex in response to manipulation of thalamic microstimulation parameters. *J Neural Eng* 2012;9(2):026008.
- Welker E, Van der Loos H. Quantitative correlation between barrel-field size and the sensory innervation of the whiskerpad: a comparative study in six strains of mice bred for different patterns of mystacial vibrissae. *J Neurosci* 1986;6(11):3355–73.
- Woosley T, Loos HVD. The structural organization of layer IV in the somatosensory region (SI) of mouse cerebral cortex: the description of a cortical field composed of discrete cytoarchitectonic units. *Brain Res* 1970;17(2):205–38.
- Yang JW, An S, Sun JJ, Reyes-Puerta V, Kindler J, Berger T, et al. Thalamic network oscillations synchronize ontogenetic columns in the newborn rat barrel cortex. *Cereb Cortex* 2013;23(6):1299–316.
- Zheng Y, Johnston D, Berwick J, Mayhew J. Signal source separation in the analysis of neural activity in brain. *Neuroimage* 2001;13(3):447–58.

Part III – Cortical processing of somatosensory inputs

In the rodent's somatosensory system, each stage of the whisker pathways contains neurons that show selectivity towards one angle of vibrissa deflection (Simons, 1978). We will distinguish the tuning to two sensory dimensions: the preference of a neuron to a certain direction of deflection of a single whisker will be called "local" direction selectivity (discussed in **Chapter 1**); in contrast to the "global" direction selectivity that refers to the preference of a neuron to the angle of a multiwhisker deflection (discussed in **Chapter 2**).

Chapter 1: Direction Selectivity to Single Whisker Deflection

Vibrissa RFs in the barrel cortex can be characterized by their somatotopic tuning and their direction preference. As mentioned in Part I, Andermann and Moore (2006) reported for the first time the existence of systematic map of direction preference organized within the barrel column with a pinwheel-like form centered near the barrel center by performing extracellular recordings. This organization was more recently confirmed by 2-photon calcium imaging experiments performed by Kremer et al. 2011 (but see Kerr et al., 2007). However, none study has been done so far in the mouse barrel cortex to test this.

Our aim is to study the existence of an intracolumnar spatial organization of direction selectivity in the mouse barrel cortex. We will address this question by using VSD imaging recordings coupled with precise multidirectional whisker stimulation.

III.1.1 Materials and methods

- *Animals and Surgery*

Experiments were performed in conformity with the French (authorization number: 2012-0068) and European (2010/63/UE) legislations relative to the protection of animals used for experimental and other scientific purposes. C57BL6J mice aged 6-10 weeks were anesthetized with urethane (1.7 mg/g). Paw withdrawal, whisker movement and eyeblink reflexes were largely suppressed. A heating blanket maintained the rectally measured body temperature at 37°C. The head of the mouse was fixed by a nose clamp. The respiration of the mouse was monitored with a piezoelectric device and its brain state monitored by using two epidural electrodes, one placed above the barrel cortex ipsilateral to the stimulated whiskers and the second one above the frontal cortex on the same hemisphere. A metallic fixation post was implanted on the occipital bone with cyanoacrylate glue and dental cement. An imaging chamber (plastic ring of about 6 mm diameter, 0.5 mm thick) was implanted on the left hemisphere and a 3 x 3 mm craniotomy was made within the chamber, centered on the stereotaxic location of the C2 barrel column (1.5 mm caudal and 3.3 mm

lateral). Extreme care was taken at all times not to damage the cortex, especially during the removal of the dura.

- *Voltage-Sensitive Dye Imaging*

Voltage-sensitive dye RH1691 was dissolved at 1mg/ml in Ringer's solution containing (in mM): 135 NaCl, 5 KCl, 5 HEPES, 1.8 CaCl₂, 1 MgCl₂. This dye solution was topically applied to the exposed cortex and allowed to diffuse into the cortex over 1 hour. After removal of the unbound dye, the cortex was covered with agarose (0.5-1% in Ringer's) and a coverslip. The mouse was then transferred on the recording stage where it was fixed strongly by its metal head fixation post. Cortical imaging was performed through a tandem-lens fluorescence microscope (Sci-Media), equipped with one Leica PlanApo 5x (objective side) and one Leica PlanApo 1x (condensing side), a 630-nm excitation filter, a 650-nm dichroic mirror, and a long-pass 665-nm emission filter. The field of view was 2.5 x 2.5 mm, resulting in a pixel resolution of 25 x 25 μ m.

- *Whisker Stimulation*

Multidirectional stimulation of whisker C2 was performed using the multiwhisker stimulator described in Part II – Chapter 2 (Jacob et al., 2010). All whiskers were trimmed from their base but the right C2 whisker, whose tip was trimmed and painted with nail polish. The right C2 whisker was inserted in 27G stainless steel tubes attached to a multidirectional bender, leaving 2 mm between the tip of the tube and the whisker base. The deflection consisted of a 100- μ m displacement (measured at the tip of the tube), a 2-ms rising time, a 2-ms plateau and a 2-ms fall (specific filters were used to correct for the mechanical ringing of the stimulators). The resulting deflection angle was 2.86° and the deflection velocity 50 mm/s. The whisker was deflected in eight different directions, each sequence was repeated 30 times in a pseudo-randomized way, and intermingled with sequences containing extra blank trials (no stimulation) for correcting the bleaching of the dye. An interval of 15 s was applied between two consecutive stimulations, as previous work showed no adaptation at that frequency of stimulation (Ego-Stengel et al., 2005).

- *Image analysis*

Acquisition and data preprocessing were done using in-house software (Elphy, G. Sadoc, UNIC-CNRS), further analyses were made using custom-written routines in IgorPro (Wavemetrics). Subtraction of the averaged unstimulated blank trials was used to correct for the bleaching artifacts. Variations of the fluorescence signal are expressed as $\Delta F/F_0$, the averaged signal of three frames just preceding the stimulus being used as a reference.

- *Histology*

Following the experiments and the administration of an overdose of urethane, mice were perfused with saline followed by paraformaldehyde (4% in 0.1 M phosphate buffer) at 25°C. After an overnight post-fixation in paraformaldehyde, the brains were cut in 100- μ m thick tangential sections and stained for cytochrome oxidase revealing the layer 4 barrel map. The images of the tangential sections were aligned and the barrel maps drawn using the Matlab routine described in Part I – Chapter 2 (article: Perronet, Vilarchao et al., 2015). The VSD images were aligned with the histological images using the superficial blood vessels as anatomical landmarks.

- *Quantification of VSD responses*

Profiles of fluorescence were computed from ROIs corresponding to the whisker C2 L4 barrels delineated from the post-hoc barrel map reconstruction. Variations of fluorescence from all the pixels included in a barrel were averaged.

- *Direction selectivity*

The response magnitude (R_i) to each direction (θ_i) of stimulation was defined as the integral of such fluorescence profiles on a large time window (-20 to 240 ms relative to the time of stimulation of the corresponding whisker). The preferred direction (D_{pref}) was defined as the circular mean (Fisher, 1995):

$$D_{pref} = \arctan \left[\frac{\sum R_i \sin \theta_i}{\sum R_i \cos \theta_i} \right]$$

To quantify the Dpref, the direction index (DI) was defined as:

$$DI = \sqrt{\left[\sum Ri \sin \theta_i\right]^2 + \left[\sum Ri \cos \theta_i\right]^2} / \sum Ri$$

The DI takes values from 0 (equal responses to all directions) to 1 (complete selectivity to one direction).

- *Statistical Tests*

Rayleigh test of circular uniformity was used to test the significance of the direction selectivity, analyzing the distribution of the Dpref angles for the seven experiments.

III.1.2 Results

- *Highly reproducible location of afferent responses within the barrel columns*

Local direction selectivity was evaluated by stimulating the C2 whisker in eight different directions. Figure 23A shows that the sensory response appears first in the C2 related column and subsequently spreads over the neighboring columns. It has been previously described by many groups, that the deflection of one vibrissa produces depolarization that extends over many cortical columns of S1 with a maximum located near the center of the barrel-related column (Kleinfeld and Delaney, 1996; Ferezou et al., 2006).

- *Rostral and caudal deflections evoke the highest responses in the C2 barrel column*

For each direction, fluorescence profiles ($\Delta F/F_0$) measured from a region of interest (ROI; 5x5 pxls) centered on the C2 column were calculated, together with the corresponding tuning curve, computed by integrating the responses over a large time window (-20 to 240 ms after stimulus onset; Figure 23B). The thick red line is the vector sum of the eight responses in the polar plot, it points toward the preferred direction (D_{pref}), and its length is used to calculate the direction index (DI) by dividing it by the sum of response magnitudes. As it can be observed in this case study, the amplitude of the responses of C2 barrel varied with the different directions of displacement, being bigger in the rostrocaudal axis.

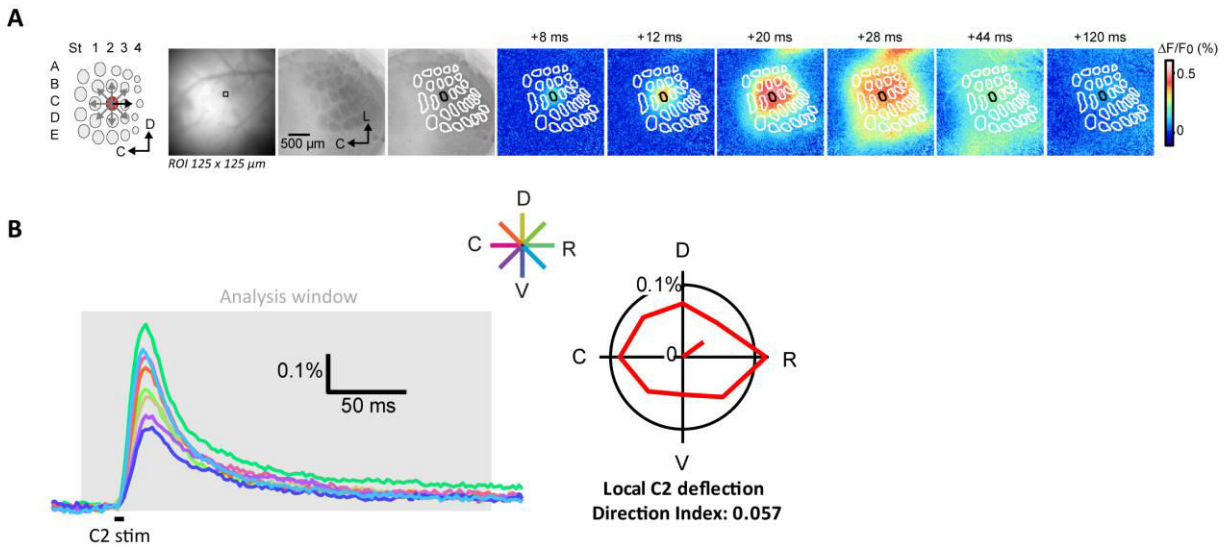


Figure 23: VSD imaging responses to multidirectional stimulation of whisker C2.

A: Local direction selectivity was evaluated by stimulating the C2 whisker in 8 directions as indicated on the diagram on the right, which represents the right whisker pad of the mouse. The superficial blood vessels are visible on the surface of the cortex with the VSD imaging camera. They are used to realign the barrel map obtained by cytochrome oxidase staining (middle black and white image) with the functional VSD images. The black square corresponds to the ROI of 5x5 pxls centered on the C2 barrel that was used to calculate the profiles. On the left are shown the images of the sensory response evoked by rostral stimulation (average of 30 trials) at time 0 ms and the subsequent spread of the activity. The white lines overlaid on the images show the barrel map, the C2 barrel is in black.

B: The fluorescence profiles ($\Delta F/F_0$) measured from a region of interest centered on the C2 column are shown for each direction (left; direction is color coded), together with the corresponding tuning curve (right), computed from a large time window (grey box). The thick red line is the vector sum of the eight responses in the polar plot, it points toward the preferred direction (DPref), and its length is used to calculate the direction index (DI) by dividing it by the sum of response magnitudes.

- *Direction selectivity is spatially distributed within the C2 column*

With the aim of assessing the existence of a particular spatial directional map in the mouse barrel cortex, we computed the location (with respect to the centroid of the C2 barrel-related column) of the peak of the early response (12 ms after whisker deflection) for each direction of stimulation and for 7 experiments. Results are shown in the Figure 24 where it can be observed that responses are close to the center of the column, but seem to follow a specific organizational pattern: e.g. responses to the 315° deflection angle (light blue dots) are all towards the medial region of the column, while responses to the opposite direction (135, orange dots) tend to be located in the towards the lateral subspace of the cortical column.

In Figure 25A we depicted the distribution of the averages peak responses for each direction (filled circles, as in Figure 24) which appears concentrated within the center of the column and in a manner that looks like the mirror image in the vertical axis of the pinwheel observed in rats (Anderman & Moore, 2006; Kremer et al., 2011).

To quantify this spatial distribution we calculated the radial position of the peak and plotted it against the angle of stimulation of the vibrissa (Figure 25B). If the mouse C2 barrel has a similar pinwheel as the rat, meaning that the angle of stimulation of the whisker is the same as the angle where the maximum of activity is found within the barrel, then we would expect to obtain a correlation represented as the unity line (black line). The grey line represents the expected results if the pinwheel was the mirror image in the vertical axis. As it can be observed, preliminary results showed that the latter is more likely to be the case.

Another way of quantifying the spatial distribution is to calculate the angular distance between the angle of the position of the peak and the angle of stimulation (Figure 25C). If these angles were correlated (“perfect pinwheel”) we would expect an angular distance close to 0°, if they were anticorrelated (“inverted pinwheel”) we would expect an angular distance close to 180°, and if there was no correlation at all we would expect an angular distance close to 90°. The results qualitatively show that there is neither a clear correlation nor anticorrelation between these two angles.

To sum up, these results suggest that direction selectivity is spatially distributed in the mouse barrel cortex. However, its organization differs from the one previously reported in the rat. With the limitations of our technique we suggest that in the mouse this spatial

distribution follows a pinwheel organization inverted on the lateral-medial axis. These results will be further discussed in the second section of the discussion.

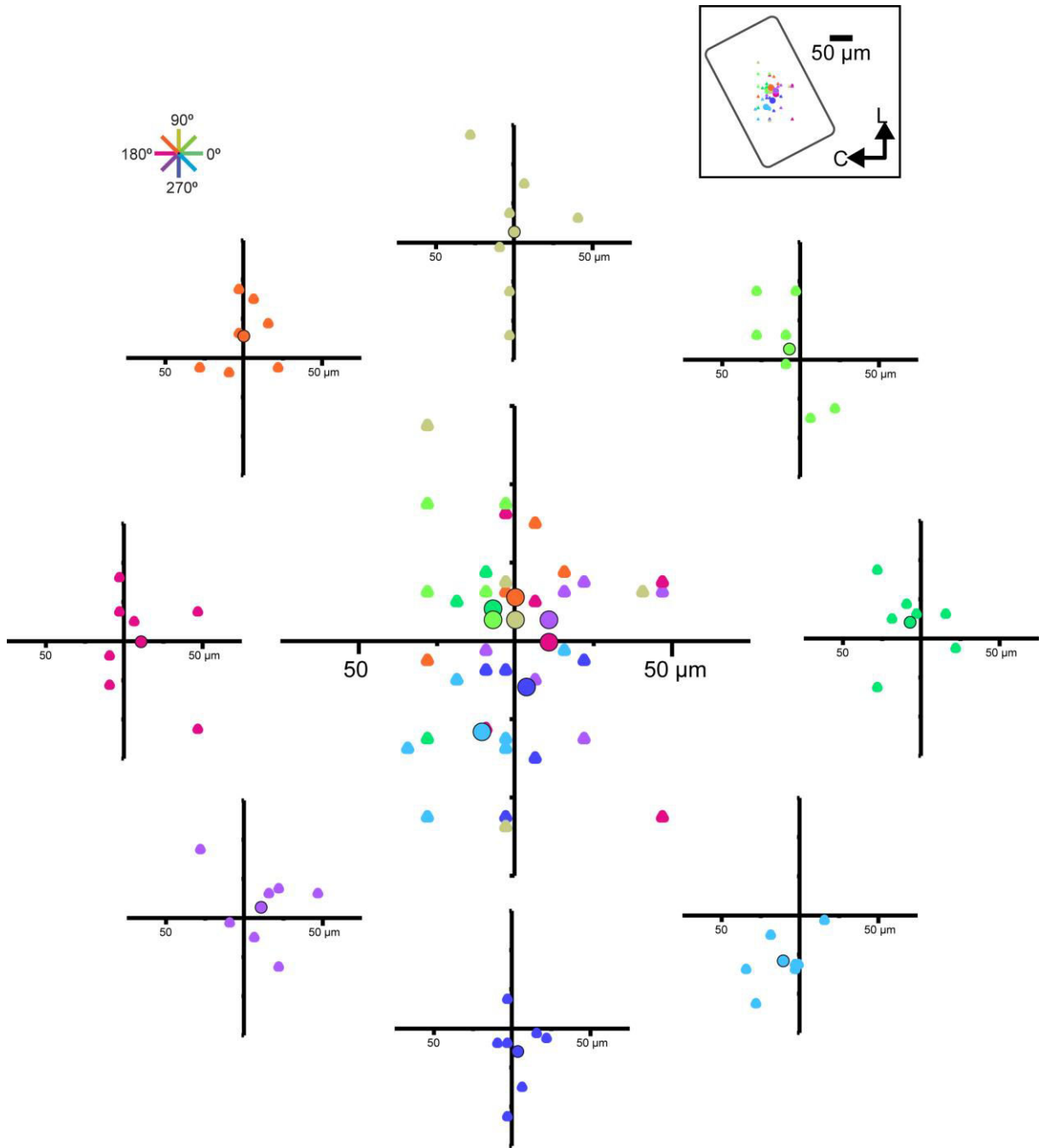


Figure 24: Spatial distribution of the early responses to different local directions of deflection of the C2 whisker.

For each direction (color coded), the location of the peak of fluorescence 12 ms after the C2 deflection ($n=7$ experiments, Δ) is represented in space relative to the center of a virtual C2 barrel (inset). Averaged peak location for each direction is depicted (\bullet).

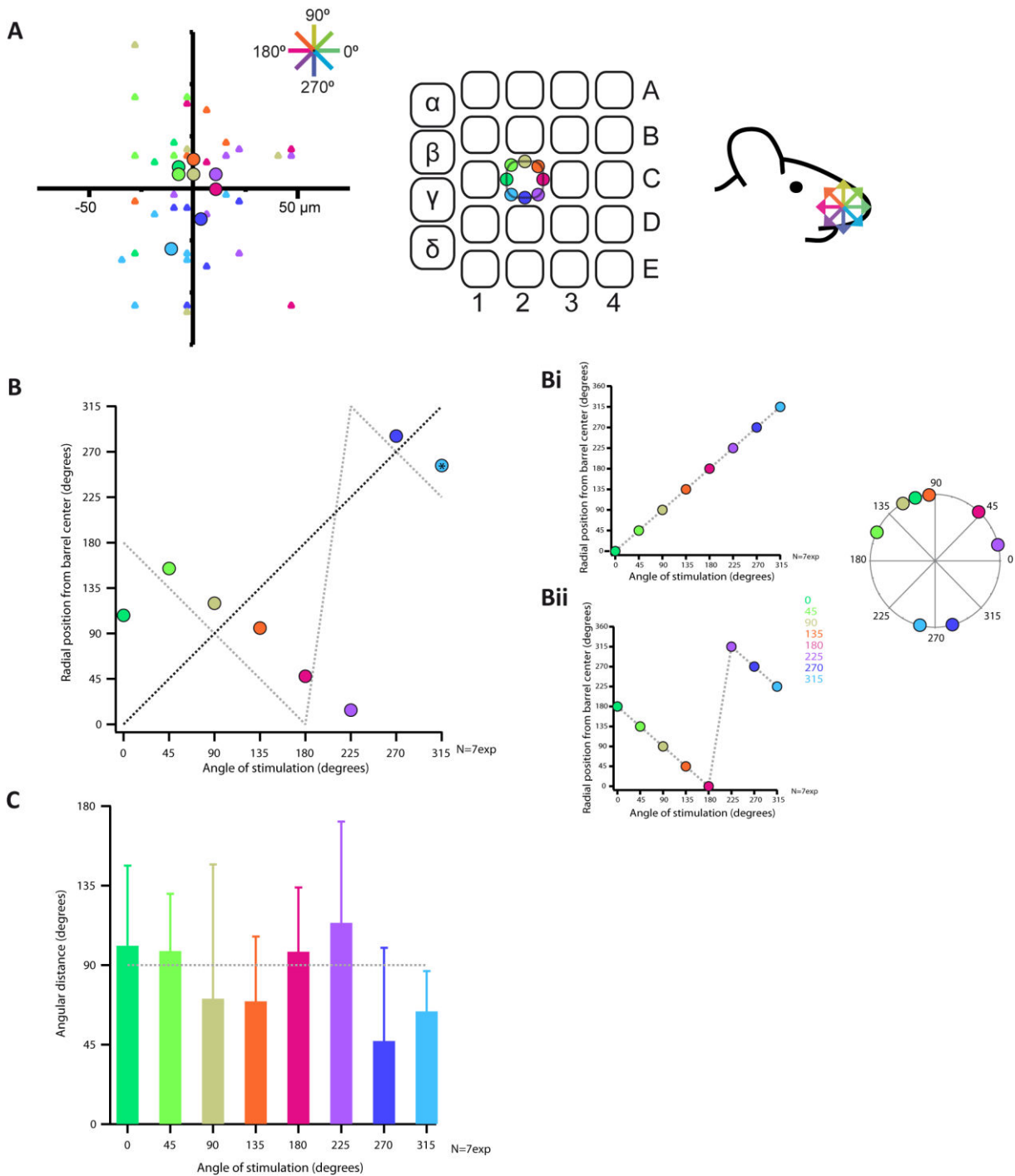


Figure 25: Analysis of the spatial distribution of the early responses.

A: Schematic representation of the 8 directions of C2 stimulation (top) and their corresponding response location within the C2 related column of the contralateral barrel cortex.

B: Angular location of the averages shown in A against the angle of deflection. Unity line represents the expected result if both angles correlate (Bi), the grey line is the expected result if there was a mirror image of a pinwheel in the vertical axis (Bii).

C: Angular distance between the position of the average and the angle of stimulation.

Chapter 2: Cortical Representation of Multivibrissal Stimulations

The representation of multiple features of a stimulus within the same cortical area might allow sensory systems to perform more optimized computations and processing of the external information. Previous results from our team (Jacob et al., 2008) have shown that the direction of sequential deflection of all the whiskers is coded by the cortical neurons of the rat barrel cortex.

Our aim is therefore to look for particular patterns of spatial organization across the mouse barrel field of the global direction selectivity. Multiwhisker stimulation combined with VSD imaging will help us to assess the existence of a directional map specific for the global motion selectivity in the superficial layers of mouse S1.

III.2.1 Materials and Methods

- *Animals and Surgery*

Experiments were performed in conformity with the French (authorization number: 2012-0068) and European (2010/63/UE) legislations relative to the protection of animals used for experimental and other scientific purposes. C57BL6J mice aged 6-10 weeks were anesthetized with urethane (1.7 mg/g). Paw withdrawal, whisker movement and eyeblink reflexes were largely suppressed. A heating blanket maintained the rectally measured body temperature at 37°C. The head of the mouse was fixed by a nose clamp. The respiration of the mouse was monitored with a piezoelectric device and its brain state monitored by using two epidural electrodes, one placed above the barrel cortex ipsilateral to the stimulated whiskers and the second one above the frontal cortex on the same hemisphere. A metallic fixation post was implanted on the occipital bone with cyanoacrylate glue and dental cement. An imaging chamber (plastic ring of about 6 mm diameter, 0.5 mm thick) was implanted on the left hemisphere and a 3 x 3 mm craniotomy was made within the chamber, centered on the stereotaxic location of the C2 barrel column (1.5 mm caudal and 3.3 mm

lateral). Extreme care was taken at all times not to damage the cortex, especially during the removal of the dura.

- *Voltage-Sensitive Dye Imaging*

Voltage-sensitive dye RH1691 was dissolved at 1 mg/ml in Ringer's solution containing (in mM): 135 NaCl, 5 KCl, 5 HEPES, 1.8 CaCl₂, 1 MgCl₂. This dye solution was topically applied to the exposed cortex and allowed to diffuse into the cortex over 1 hour. After removal of the unbound dye, the cortex was covered with agarose (0.5-1% in Ringer's) and a coverslip. The mouse was then transferred on the recording stage where it was fixed strongly by its metal head fixation post. Cortical imaging was performed through a tandem-lens fluorescence microscope (Sci-Media), equipped with one Leica PlanApo 5x (objective side) and one Leica PlanApo 1x (condensing side), a 630 nm excitation filter, a 650 nm dichroic mirror, and a long pass 665 nm emission filter. The field of view was 2.5 x 2.5 mm, resulting in a pixel resolution of 25 x 25 μ m.

- *Whisker Stimulation*

Deflections of the right 24 posterior macrovibrissae of the mice were performed using the multiwhisker stimulator described in Part II – Chapter 2 (Jacob et al., 2010). The experimental set-up is shown in Figure 26A. Whiskers from the left side of the snout were trimmed from their base, while the whiskers on the right side were trimmed at the tip and painted with nail polish. The whiskers were inserted following their natural angles in 27G stainless steel tubes attached to the multidirectional benders, leaving 2 mm between the tip of the tube and the whisker base. Each whisker deflection consisted of a 100- μ m displacement (measured at the tip of the tube), a 2-ms rising time, a 2-ms plateau and a 2-ms fall (specific filters were used to correct for the mechanical ringing of the stimulators). The resulting deflection angle was 2.86° and the deflection velocity 50 mm/s. Figure 26B shows the local whisker deflection of a representative piezoelectric actuator, measured with a laser telemeter (Micro-Epsilon, France).

- *Multiwhisker global motion protocol*

The 24 whiskers were stimulated caudally or rostrally, in spatiotemporal orders that generate global motions in eight different directions (same global motion protocol used in

Jacob et al, 2008). The duration of a sweep in the horizontal and vertical axis was 70 ms (interval between two consecutive stimulated arcs or rows (IWI) = 10 ms), the whisker C2 was deflected 20 ms after the beginning of the sweep. For oblique directions, a sweep lasted 86.6 ms ($IWI = 10/\sqrt{2} = 7.1$ ms) and the whisker C2 was stimulated 28 ms after the beginning of the protocol.

For each direction, each sequence was repeated 30 times in a pseudo randomized way, and intermingled with sequences containing extra blank trials (no stimulation) for correcting the bleaching of the dye. An interval of 15 s was applied between two consecutive sequences, as previous work showed no adaptation at that frequency of stimulation (Ego-Stengel et al., 2001).

- *Multiwhisker moving/static bar protocol*

In this protocol the local deflection of all the whiskers was the same as before, but in all the experiments caudal. For the “Moving Bar” sequences, the 24 macrovibrissae were stimulated in spatiotemporal orders as described before but only in the four cardinal directions (IWI= 10 ms). The “Static Bar” sequences consisted of deflecting simultaneously individual whiskers from one of the 5 arcs or one of the 5 rows. In total, 4 “Moving Bar” and 10 “Static Bar” stimuli were repeated 30 times in a pseudo randomized way, and intermingled with sequences containing extra blank trials (no stimulation) for correcting the bleaching of the dye. An interval of 15 s was applied between two consecutive sequences.

- *Image analysis*

Acquisition and data preprocessing were done using in-house software (Elphy, G. Sadoc, UNIC-CNRS), further analyses were made using custom written routines in IgorPro (Wavemetrics). Subtraction of the averaged unstimulated blank trials was used to correct for the bleaching artifacts. Variations of the fluorescence signal are expressed as $\Delta F/F_0$, the averaged signal of three frames just preceding the stimulus being used as a reference.

- *Histology*

Following the experiments and the administration of an overdose of urethane, mice were perfused with saline followed by paraformaldehyde (4% in 0.1 M phosphate buffer). After an overnight post-fixation in paraformaldehyde, the brains were cut in 100 μm thick

tangential sections and stained for cytochrome oxidase revealing the layer 4 barrel map. The images of the tangential sections were aligned and the barrel maps drawn using the Matlab routine described in Part I – Chapter 2 (article: Perronnet, Vilarchao et al., 2015). The VSD images were aligned with the histological images using the superficial blood vessels as anatomical landmarks.

- *Quantification of VSD responses*

Profiles of fluorescence were computed from ROIs corresponding to the L4 barrels delineated from the post-hoc barrel map reconstruction. Variations of fluorescence from all the pixels included in a barrel were averaged.

- *Direction selectivity*

The response magnitude (R_i) to each direction (θ_i) of stimulation was defined as the integral of such fluorescence profiles on a large time window (-20 to 240 ms relative to the time of stimulation of the corresponding whisker). The preferred direction (D_{pref}) was defined as the circular mean (Fisher, 1995):

$$D_{pref} = \arctan \left[\frac{\sum R_i \sin \theta_i}{\sum R_i \cos \theta_i} \right]$$

To quantify the D_{pref} , the direction index (DI) was defined as:

$$DI = \sqrt{\frac{[\sum R_i \sin \theta_i]^2 + [\sum R_i \cos \theta_i]^2}{\sum R_i}}$$

The DI takes values from 0 (equal responses to all directions) to 1 (complete selectivity to one direction).

- *Statistical Tests*

Rayleigh test of circular uniformity was used to test the significance of the direction selectivity, analyzing the distribution of the D_{pref} angles for the eight experiments in each barrel.

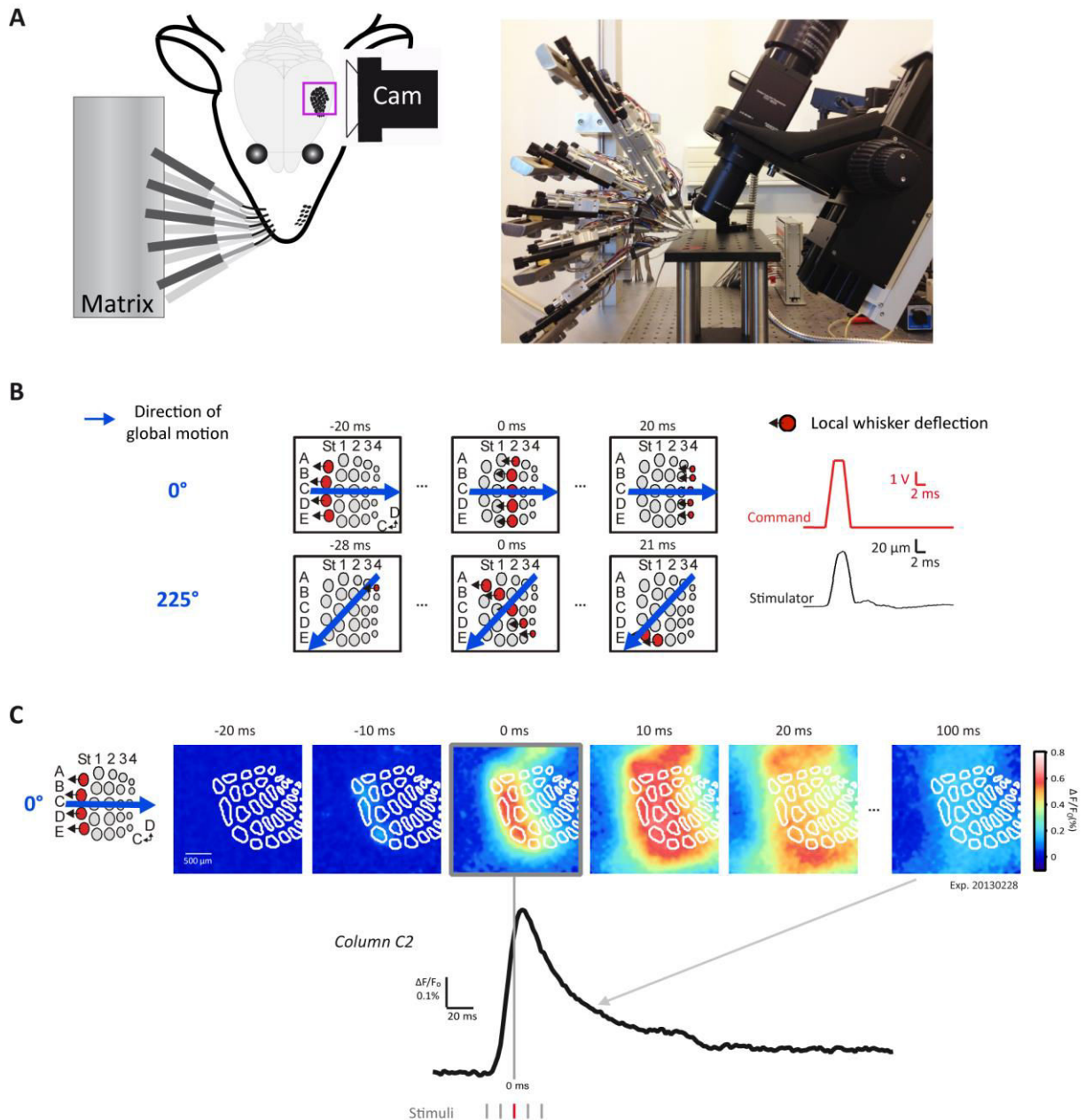


Figure 26: VSD imaging of cortical responses to multiwhisker stimulation.

A: Diagram and photograph of the experimental setup. High-speed imaging system mounted on a multidirectional 24-whisker stimulator placed on the right whisker-pad. The left barrel cortex is imaged while the whiskers on the right side of the snout are stimulated.

B: Three steps of the global motion protocol for two global directions (blue arrow) are illustrated; small black arrows indicate the local motion of each whisker. On the right is shown the command trace for the local whisker deflection (red) and the measured deflection of the actuator (black).

C. Snapshots of the averaged fluorescence signal ($n=30$ trials) for a case study at six different timings relative to the time of deflection of the central C2 whisker for rostral global direction (0°). The profile of activity measured from the C2 barrel region is shown below, where the grey bar represents Straddlers, Arc 1, Arc 3 and Arc 4 deflection times respectively, while the red bar indicates the Arc 2 stimulation time.

III.2.2 Results

- *Voltage sensitive dye imaging of depolarizing responses evoked by multiwhisker stimuli spread across the barrel cortex*

Using a 24-multidirectional whisker stimulator on the mouse right whisker pad, we presented multiwhisker stimuli that were locally invariant – caudal/rostral deflections of each whisker – but globally coherent – spatiotemporal sequences of whisker deflections (Figure 26). The multiwhisker stimulations differed in the resulting direction of the global motion, scanning 8 different directions. We will further refer to this protocol as “Moving Bar”. The multiwhisker stimulator was coupled with a VSD imaging high-speed camera that recorded the cortical activity from the barrel cortex on the left hemisphere.

For each global direction, the spread of activity across the whole barrel cortex correlates with the stimulation of the corresponding whiskers. Figure 26C shows a representative example of the average activity (30 repetitions) for the rostral global direction (0°) at different times relative to the stimulation of the whisker C2. The anatomical map of the barrels from L4 is superimposed to the VSD images to give a spatial reference of the responses. The start of the moving bar protocol is at -20 ms, and 10 ms later it can be observed that activity arrives at the cortical columns that correspond to the first stimulated whiskers (Arc St). After 100 ms the cortical activity goes back close to the baseline level.

Below the figure is shown the profile of activity calculated from a region of interest (ROI) delimited by the anatomical barrel C2. The red bar indicates the time of the stimulation of the whisker C2. As it can be observed, activity spreads to the C2 column even before the whisker C2 is stimulated, and strikingly, this activity is close to the maximum of the response. This shows that the lateral spread of activity in the barrel cortex is faster than the moving bar on the receptive surface, suggesting that the cortical responses to the deflection of the whisker C2 will be conditioned by this spreading activity.

- *At each column evoked responses depend on the spatio-temporal context of the multiwhisker deflections*

Figure 27A shows the responses for the eight global directions at three different timings relative to the stimulation of whisker C2. As we mentioned before, we can observe for some of the global directions a wave of activity that spreads faster than the advancing

front edge of the stimulation. This spread of activity seems different, at least on the amplitude domain, depending on the direction of the global motion. As a consequence, if an adjacent row/arc was stimulated 10 ms before, afferent signals coming from the thalamus might encounter neurons that were recently activated by the cortico-cortical connections, thus their processing might be significantly different. Even though the amplitude of activity across the barrel cortex is not the same for all the directions, the late dynamics of the cortical responses share similar spatial properties (see the panel +10 ms on the right).

The profiles of fluorescence computed from the C2 barrel-related column and aligned on the time of the whisker C2 stimulation are shown in Figure 27B, color-coded for the eight directions of global stimulation. The response of each direction were quantified by calculating the integral from -20 ms to 240 ms, and plotted on a polar graph (Figure 27B-right). The preferred direction was calculated (see Methods) and it is shown as the red vector on the polar plot, which length is the vector sum.

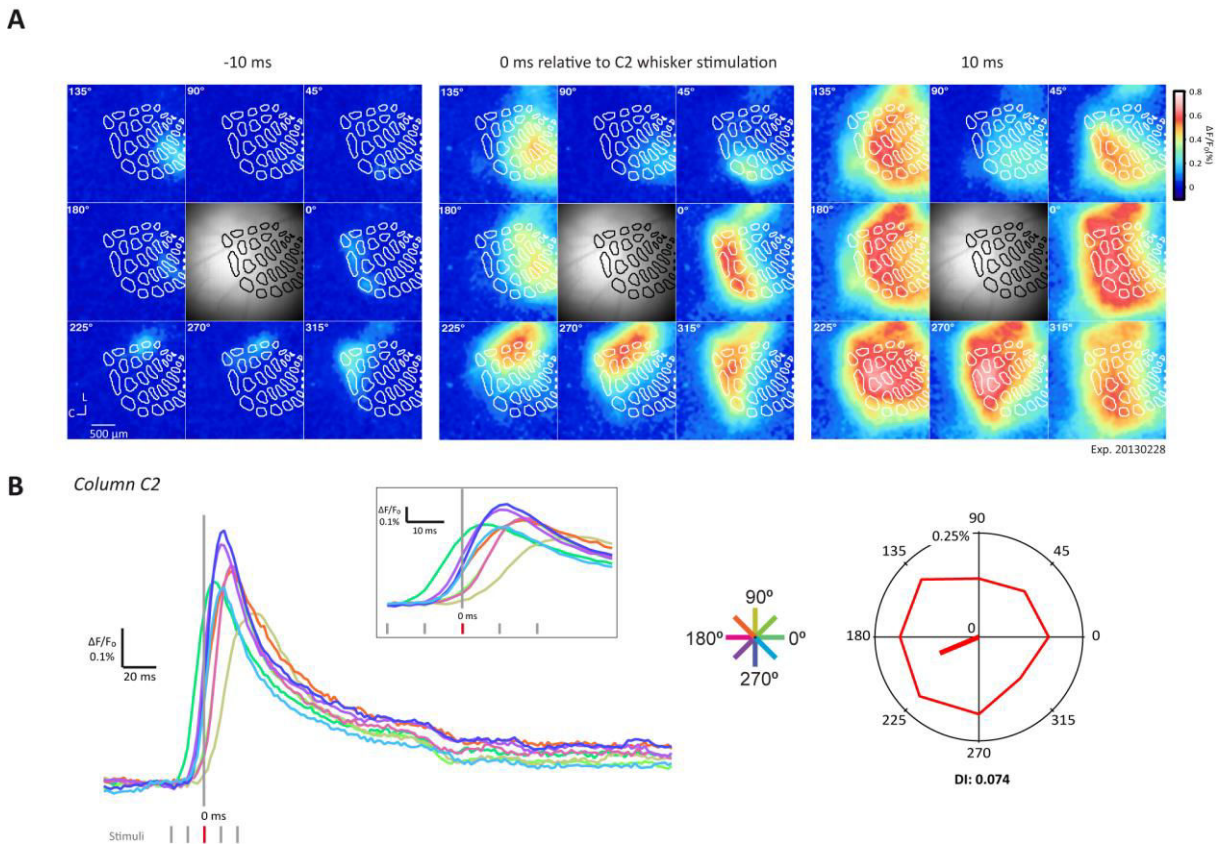


Figure 27: Responses depend on the spatio-temporal sequence of the multiwhisker deflections.

A: Snapshots of the averaged fluorescence signals (same case study of Figure 26C) for the eight global directions at three timings relative to the central whisker C2 deflection.

B: Fluorescent profiles measured from the C2 barrel for the eight directions of global motion. The inset is a zoom in of the profiles from -20 to 40 ms. The integral of each profile was calculated within the grey time-window (-20 ms to 240 ms) and represented in the tuning curve (right). The red thick vector shows the preferred angle and the length of the vector the angular summation of the responses. The direction index (DI) of the responses in this barrel is noted below.

For a movie of this case study, please check the supplementary file.

- *Barrels corresponding to the most rostral whiskers show significant direction selectivity towards caudoventral global angles.*

With the aim of depicting a spatial map of direction selectivity we did a pixel-by-pixel analysis in which we aligned the fluorescent signals on the time at which each whisker was stimulated. In Figure 28A we can observe this type of analysis for a representative experiment, aligned on the whisker C2 stimulation time. At 0 ms, which corresponds to the time at which the C2 whisker is stimulated (whatever the direction of the global stimulation), we can observe a pinwheel which is later inverted at 30 ms. These pinwheels are expected due to the architecture of the whisker pad and the stimulation protocol. Under the hypothesis that both pinwheels were going to compensate each other we chose to integrate the signals over a larger time window (-20 to 240 ms). We restricted the analysis to the area above the corresponding barrel, in this case C2 (Figure 28B), and did the same analysis independently for all the barrels.

The averaged Dpref and DI values for each barrel were calculated and represented in a 24-column matrix. Figure 28C shows such 24-column matrix for the same representative experiment where for each column the Dpref is color-coded and also indicated by the angle of the arrow, and the DI is represented by the length of the arrow. We will refer to this map as the “direction selectivity map”. We tested whether the Dpref was significant in each barrel by doing a Rayleigh test of uniform distribution of the angles. The columns with significant direction selectivity (anisotropic distribution of the Dpref for the 30 repetitions) are represented with high luminosity. We are also showing a 24-column matrix in a grey scale representing the significance of the Rayleigh test for each column (p-value), and the 24-column matrix with the DI values also on a grey scale. The histogram on the right shows the distribution of DI values for all the columns and the 30 repetitions.

We can notice for this representative experiment that the columns corresponding to the rostral whiskers show significant direction selectivity, and that this direction selectivity is towards the caudoventral axis, in agreement with the caudoventral biased reported by Jacob et al. (2008) in the C2 barrel-related column (further commented in the Discussion).

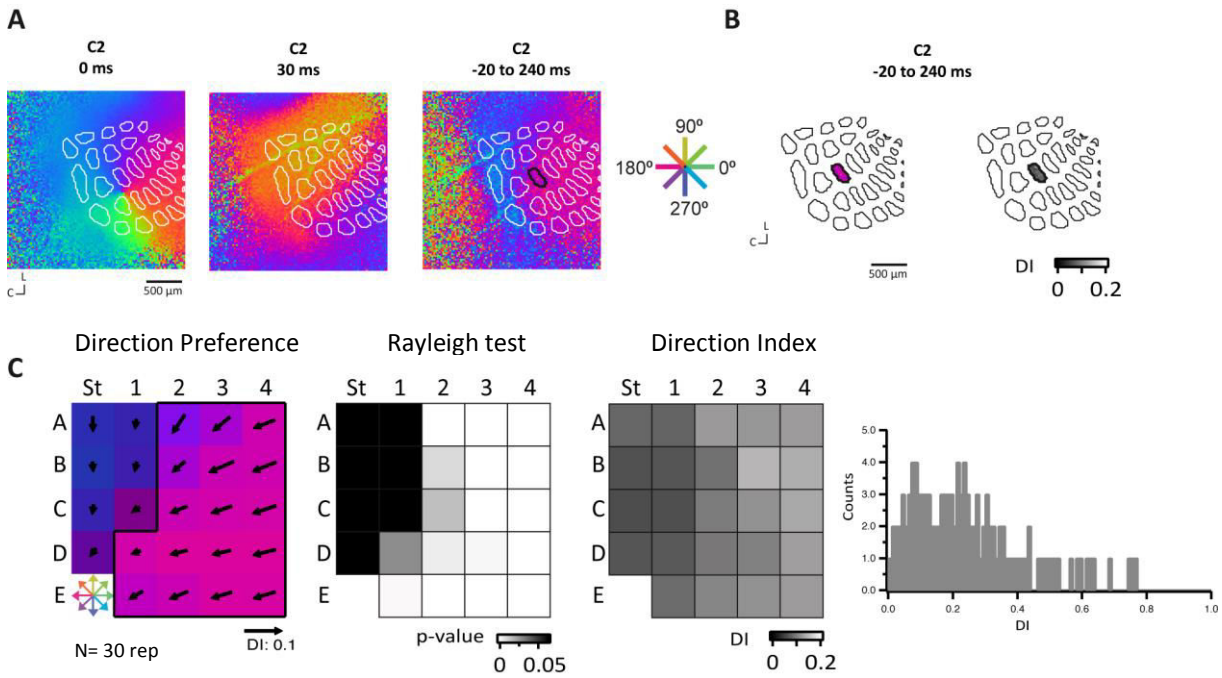


Figure 28: Spatial distribution of direction selectivity to global motion.

A: Direction preference computed for each pixel and each frame, and aligned relative to the time of whisker C2 deflection. Here are shown two examples corresponding to 0 and 30 ms. The third image of Dpref distribution has been computed by using a larger time window between -20 to 240 ms.

B: Direction preference maps and direction index maps have been computed whisker by whisker, by aligning the fluorescent signals relative to the time of the deflection of the corresponding whisker, and by restricting the analysis to the area above the corresponding barrel as in exemplified here with the column C2.

C: 24-whisker matrix of direction preferences obtained from the maps in B (left). For each barrel: Dpref is color-coded and represented by the angle of the arrow; the length of the arrow represents the direction index (DI). The anisotropy of the Dpref distribution was evaluated with a Rayleigh test and its significance ($p > 0.05$) is indicated by the higher luminosity. In the same way are represented 24-whisker matrices of anisotropy and DI on the right. On the far right is shown the histogram of the DI values calculated for the 30 repetitions of the protocol and for the 24 barrel-related columns ($n=720$ DI values; bin size: 0.01).

- *Global direction selectivity map is juxtaposed with the somatotopic map.*

Figure 29A shows the direction selectivity map obtained by averaging 8 independent mice experiments. The right matrix represents the DI values obtained by comparing the Dprefs from the eight experiments. The histogram on the right shows the distribution of averaged DIs for all the columns.

The direction selectivity map reveals that the mouse barrel cortex neurons are tuned to respond preferentially to caudoventral directions of global stimulation, consistently with previous results obtained in the rat barrel cortex for the whisker C2 (Jacob et al., 2008). This direction selectivity was significant for the more rostral whiskers (Arcs 2 to 4), and also for the whisker Alpha (StA) which showed a moderate but yet significant Dpref (see p-values in Figure 29A) towards the ventral direction.

In Figure 29B we represented the distribution of global direction vectors for the eight experiments (grey) and the average (color), for four barrel-related columns. If we pick three columns within the same row, for example row C, we can notice the strong anisotropy on the distribution of Dpref for the column corresponding to the rostral whisker C4, then a milder one for C2 and the isotropic distribution of the Dpref for the column corresponding to the most caudal whisker Gamma (StC). We are also showing the distribution of global direction vectors for the whisker Alpha that shows more distributed Dprefs, though with significant ventral direction selectivity.

From the eight experiments that were used to obtain the direction selectivity maps, half of them were done with a local direction of deflection of the whiskers towards caudal direction and the other half towards rostral direction. We split these data and calculated the average direction selectivity maps, this time with four experiments in each group. Figure 30A shows the two maps obtained with rostral and caudal local deflection of the whiskers. Given the reduced number of mice used to compute each map, less barrel-related columns show a significant global preferred direction. However, the significant columns are similar in both groups similar, suggesting that global direction selectivity is independent on the local direction of deflection of the whiskers, in agreement with Jacob et al. (further commented in the Discussion).

As already described in the Methods' section, the Dpref value was calculated by using the integral of the responses within a big time window (-20 to 240 ms). We computed the Dpref using the maximum value of the responses instead of the integral and we obtained similar global direction selectivity (Figure 30B). This indicates that the peak of the responses would be enough for the computation of the direction selectivity of a read-out stage.

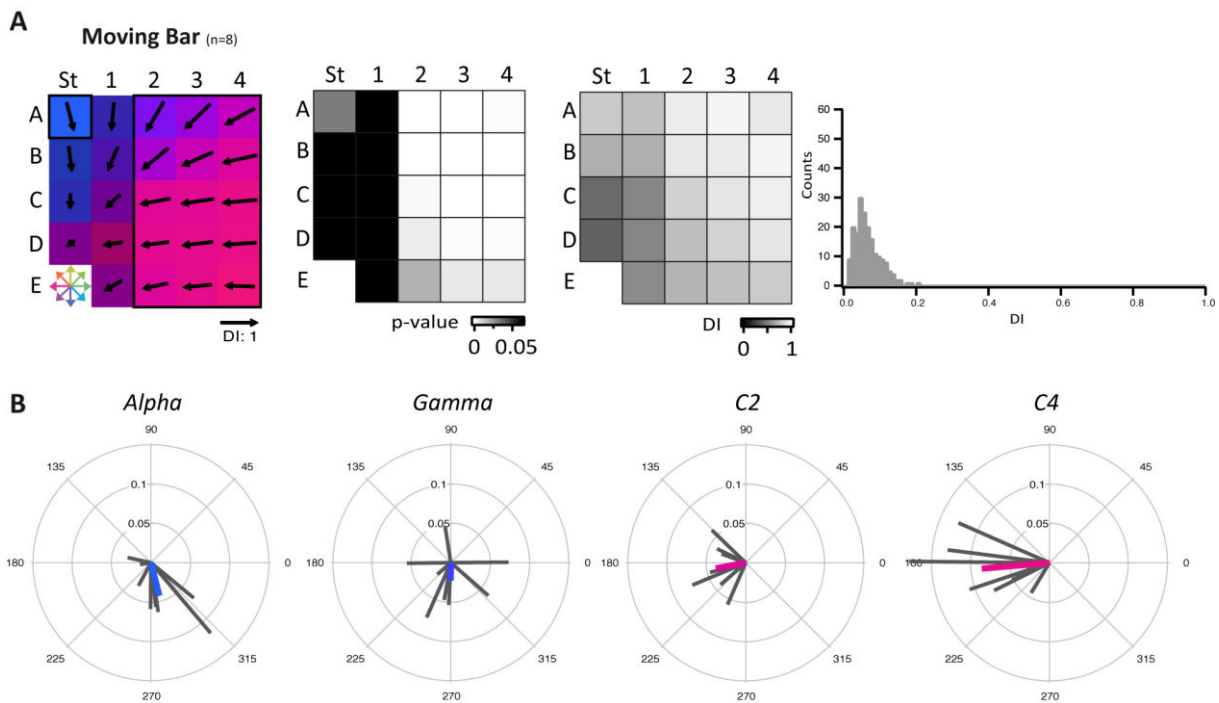


Figure 29: Averaged spatial distribution of global direction selectivity

A: Averaged 24-whisker matrix of direction preferences (n=8 mice, left). As with the case study, the Dpref is color-coded and represented by the angle of the arrows; the length of the arrow represents the DI between experiments; the significant anisotropic barrels (Rayleigh test, $p > 0.05$) are indicated by a higher luminosity. The histogram shows the DI distribution between experiments for each barrel-related column (n=192 DI values; bin size: 0.01).

B: Distribution of global direction vectors for each experiment (grey vectors) shown for barrel-related columns alpha, gamma, C2 and C4. The colored vector shows the averaged Dpref and DI for the 8 experiments.

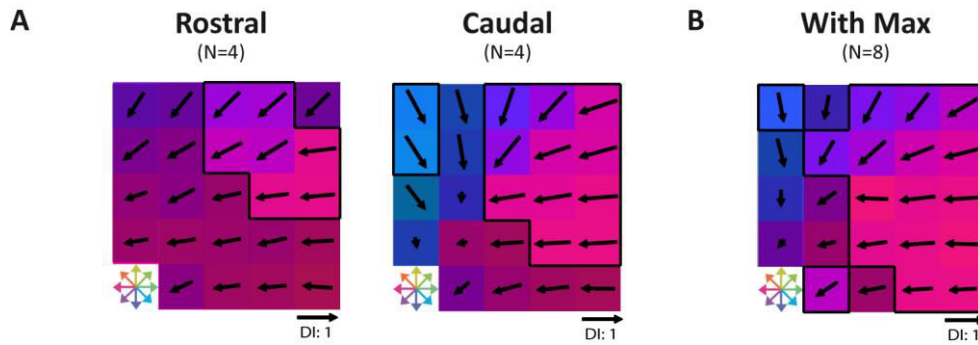


Figure 30: Global direction selectivity controls.

A: Global direction selectivity is independent of the local deflection angle of the whiskers. Averaged 24-whisker matrices of direction preferences obtained for experiments with rostral local whisker deflections ($n=4$ mice, left), or with caudal local whisker deflections ($n=4$ mice, right). The Dpref is color coded and represented by the angle of the arrows; the length of the arrow represents the DI between experiments; the significant anisotropic barrels (Rayleigh test, $P > 0.05$) are indicated by a higher luminosity.

B: Averaged 24-whisker matrix of direction preferences obtained for all experiments ($n=8$ mice), computed using the maximum values of the evoked responses instead of integrating the signal over a large time window. To be compared to Figure 29A.

- *Cortical responses to a moving bar are highly sublinear*

In 2007, Drew and Feldman showed that when they presented moving wavefronts (moving bars over 9-12 whiskers) in different directions to the rat whiskerpad, the starting position of these wavefronts had a big salience, mainly due to the suppressive interwhisker interactions. In some neurons that showed preference for a direction of the moving wavefront, suppression could also explain this selectivity: if the adjacent whiskers were deflected first giving a strong response, and the PW responses were suppressed, then the recorded unit will show a direction of preference depending on the balance of adjacent whiskers' responses/PW suppression is elicited for each direction. To further understand what might determine the global direction selectivity and its distribution on the barrel cortex, we first hypothesized that the global direction selectivity might be determined by the starting position of the moving bar given the big suppressive mechanism that might occur when adjacent whiskers are sequentially deflected.

To test this hypothesis we designed another stimulation protocol in which we alternate moving bars in 4 cardinal global directions with individual deflections of whiskers from the same row or arc, henceforth referred as “Static Bar” (Figure 31A). Figure 31B shows the snapshots of a representative experiment for the rostral global motion (0°) at 12 ms after the stimulation. If we compared the responses of the moving and static bar (Arc St) at this early stage and for this direction, we observe that the responses look very similar. By sequential linear summation of the responses to the static bars mimicking the moving bar, we constructed a linear prediction model. Comparing the evoked responses to the moving bar and the linear summation, we can notice that the linear summation is significantly larger (~ 3 times), strongly suggesting that suppressive mechanisms are involved in shaping the cortical responses to the moving bar (Figure 32A).

We next wanted to test whether these sublinearities depended on the direction of the moving bar. For five experiments we calculated the integral of the responses (moving bars or linear summation) by averaging signals from 24 ROIs corresponding to the L4 barrels, within a time window of -10 to 100 ms, for the four cardinal directions. Figure 32B shows that there were no significant differences on the ratio of these integrals for the different directions (One-Way ANOVA; $p=0.08$).

To quantify the differences in the responses for the moving/static bars we computed the integral of the responses from the same ROI and time window as before. Results are shown in Figure 32C. There were no significant differences between the responses to single arcs and the moving bars (One-Way ANOVA; $p=0.249$). Furthermore, when comparing the responses between the static and the moving conditions (i.e. Arc St and Moving 0° ; Arc 4 and Moving 180°) no significant differences were found either (t-test; $p=0.189$ and $p=0.084$, respectively). On the contrary, for the rows, there were significant differences between the responses for static and moving bars (One-Way ANOVA; $p=0.011$), but when doing a pairwise comparison we found that that difference is due mainly to the row E. Differences between the static and moving conditions (i.e. Row A and Moving; Row E and Moving 90°) were for both cases significant (t-test; $p=0.036$ and $p=0.003$, respectively).

To sum up, these results suggest that the information coming from the stimulation of the rows/arcs during the apparent motion protocol is not linearly integrated in the barrel cortex.

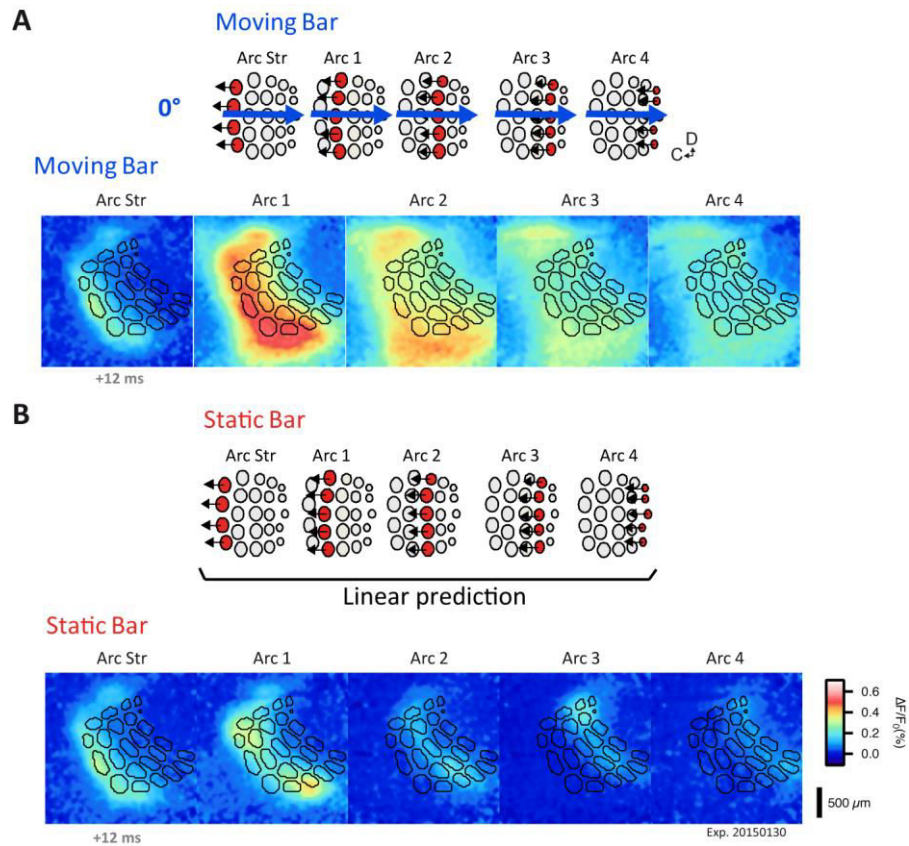


Figure 31: Cortical responses to a moving bar and to a static bar.

A: Moving Bar protocol. Apparent motions in 4 cardinal directions ("Moving Bar"), the scheme shows an example for the rostral global direction (0°). Snapshots of cortical activity evoked by a rostral moving bar for a case study, at 12 ms after the deflection of each arc.

B: Static Bar protocol. "Static Bar" multiwhisker stimuli consisting in whisker deflections delivered synchronously to individual arcs/rows of whiskers were intermingled pseudo-randomly with Moving Bar stimuli. "Linear prediction" is the summation of the static bars at times that matches the moving bar. Snapshots of cortical activity evoked individual arc deflections for the same case study, at 12 ms following the beginning of the stimulation.

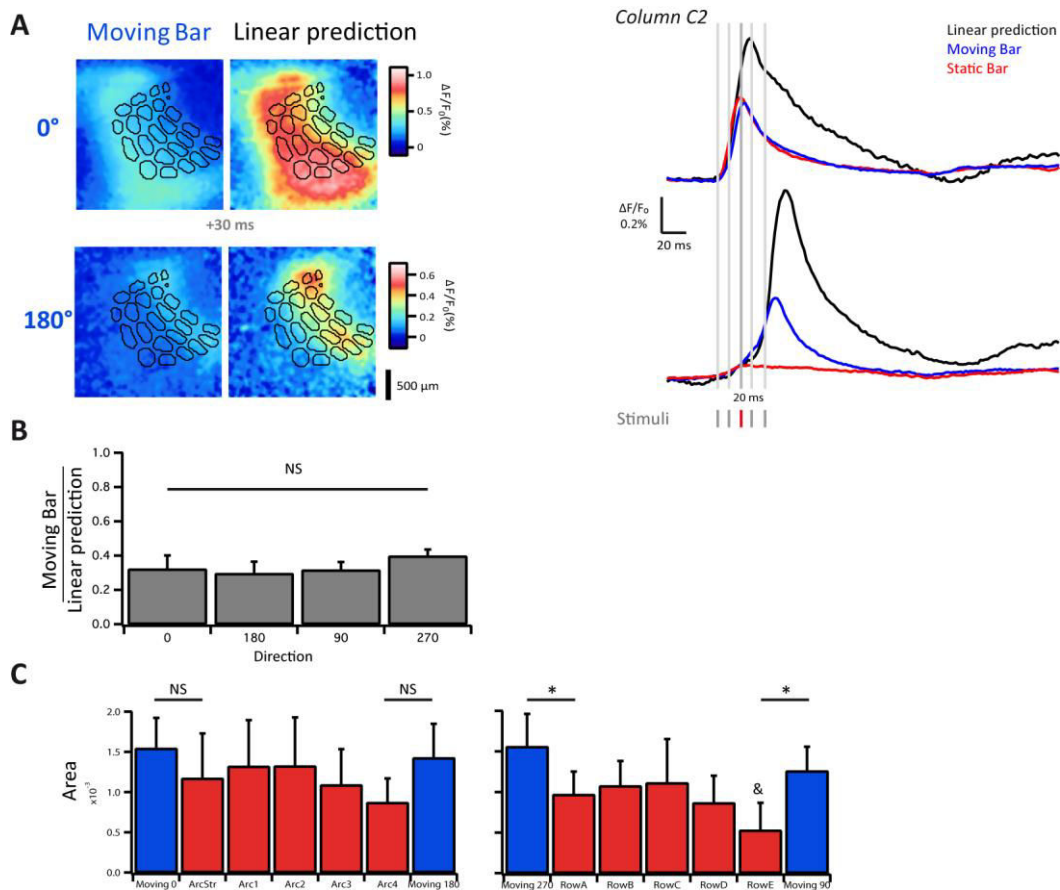


Figure 32: Cortical responses to a moving bar are highly sublinear.

A: Comparison of the cortical activity evoked by moving bars and their corresponding linear prediction. On the left are shown snapshots of the responses at 30 ms after the beginning of the stimulation for two global directions (0° and 180°). On the right are shown the profiles of activity calculated on the C2 barrel-related column for the linear prediction, moving bar and static bar corresponding to the first arc stimulated in the moving bar (Arc Str or Arc 4, respectively). The grey bars below the profiles indicate the time of stimulation of the Arc St, Arc 1, Arc 3 and Arc 4, while the red bar shows the stimulation of the Arc 2.

B: Population ratios (n=5 mice) of responses to the Moving Bar and the Linear Prediction averaged over 24 ROIs corresponding to the 24 barrels and over a time window of -10 to 100 ms and for the different directions. No significant differences were found between directions (ANOVA; p=0.08).

C: Population responses (n=5 mice) for the Moving Bar (blue) and the Static Bar (red) averaged over 24 ROIs corresponding to the 24 barrels over a time window of -10 to 100 ms, for the different directions. No significant differences were found between the arcs (One-way ANOVA; p=0.249) but the rows differed significantly (One-way ANOVA; p=0.011; &: significant treatment). No significant differences were found between the moving and static bars on the arcs, but there were significant differences between the moving and static rows (t-tests: NS no significant p>0.05; * significant p<0.05).

- *Global direction selectivity cannot be explained by the linear summation model*

In order to determine if these nonlinearities are used by the system to encode the direction of the global motion, we computed the direction selectivity maps for the linear prediction model, taking the data from the 5 experiments done with the Static Bar protocol. As we can see in Figure 33A, the direction selectivity map obtained with the linear prediction model is qualitatively different from the one obtained with the Moving Bar protocol (Figure 29A and repeated in Figure 33C). Only some columns – located mainly on the borders – showed significant Dpref, with angles distributed in an inverse pinwheel manner, pointing towards the exterior. The histogram below shows the distribution of the DIs for all the columns and all the experiments, confirming that most of them are close to zero. The Dpref spatial organization is expected given that the linear prediction responses are obtained by sequentially adding the responses of the static bars, then the border columns will have a bigger response for the directions that started on the opposite direction.

- *Despite of the high salience of the starting position of the moving bar, it is not enough to explain the global direction selectivity*

To test if the global direction selectivity could be explained by the salience of the starting position of the moving edge, we calculated the direction selectivity map using the responses to the static bars: Arc St, Arc 4, Row A, and Row E. The selectivity map shows a pinwheel-like distribution of the Dpref, with the center close to the column D3 (Figure 33B). The static bar direction selectivity map differs qualitatively from the moving bar selectivity maps, suggesting that the global direction selectivity is not due to the salience of the starting position of the moving bar, but rather due to a mechanism that builds up when the bar is moving across the whole whisker pad. We could have expected a perfect pinwheel as we are just considering the responses to the border arcs/rows, but why are the rostral and ventral directions more represented? In addition, the columns that correspond to caudal and dorsal whiskers showed significant direction selectivity. Both results might be due to the fact that deflecting the Straddlers and the whiskers in Row A produced larger responses than stimulating Arc 4 or Row E. Whiskers within a row have different diameters: caudal whiskers are thicker than rostral ones (Ibrahim and Wright, 1975; Voges et al., 2012), and a greater number of axons innervate their follicles (Welker and Van der Loos, 1986), which might correspond to the larger responses observed when deflecting the Straddlers. In contrast,

within an arc whiskers tend to increase their diameter from dorsal to ventral (Voges et al., 2012), being the whiskers in row A in average thinner and less innervated, than the ones in row E (Welker and Van der Loos, 1986), suggesting that different nonlinearities might shape the evoked responses in both rows.

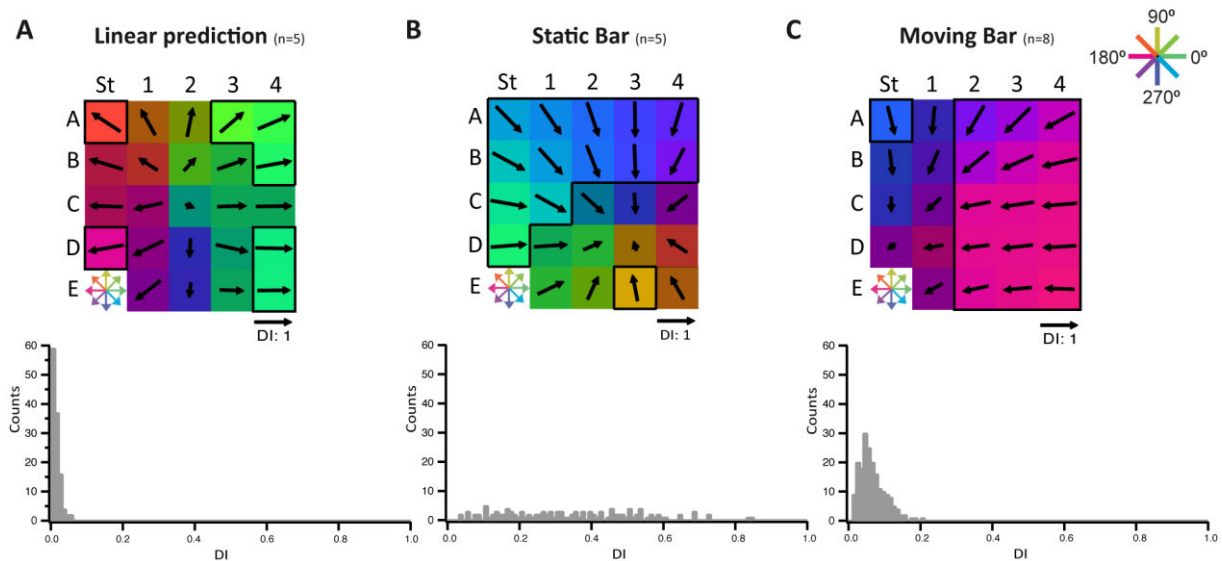


Figure 33: Global direction selectivity is neither explained by the linear prediction nor the starting position of the moving bar.

A: Averaged 24-whisker matrix of direction preferences (n=5 mice) for the linear prediction and histogram of the direction index between experiments (n=120 DI values; bin size: 0.01).

B: Averaged 24-whisker matrix of direction preferences for the Static Bar (starting point of the global motion), and histogram of the direction index between experiments (n=120 DI values; bin size: 0.01).

C: Moving Bar (same of Figure 29A)

Part IV – Discussion

To conclude this thesis, we will outline the results presented in this manuscript (Part II and Part III) and then discuss some aspects in more detail.

The main contributions of this thesis on the somatosensory system of the rodents are the following:

- The adaptation and optimization of the second generation 24-whisker stimulation matrix (Jacob et al., 2010) to the mouse whisker system.
- The development and validation, in collaboration with Lorraine Perronnet and Gabriel Peyré, of a technical method to link the recorded functional data (VSD) with the cortical structure (Perronnet, Vilarchao et al., 2015).
- The combination of the multiwhisker stimulation matrix with VSD imaging in the anesthetized mouse as a relevant experimental approach for studying the cortical responses to precise multiwhisker stimulations with a great temporal and spatial resolution. This experimental configuration allowed us to study the spatial distribution of the direction selectivity to local and global stimulation of the whiskers in the mouse.
- The observation that local direction selectivity is spatially distributed within the C2 barrel-related column. Although the responses are close to each other in the center of the column, they show a spatial distribution that is consistent from one animal to another. This distribution differs from the one that has been previously described in the rat barrel cortex, as it follows a pinwheel organization inverted on the lateral-medial axis.
- The demonstration of the existence of global directional responses in the mouse.
- The observation that global direction selectivity is distributed within the barrel cortex. Barrel columns that correspond to the more rostral whiskers showed significant direction selectivity while the barrel columns corresponding to the most caudal whiskers (except alpha) do not showed a preferred global direction.

- The observation of a caudoventral bias for global preferred directions, as previously reported by Jacob et al. (2008) for the C2 barrel-related column in the rat. This bias is also spatially distributed: more rostral columns preferred caudal global directions while the more dorsal tend to prefer ventral global directions.
- The confirmation that the global direction selectivity is independent from the direction of bending of individual whiskers, in agreement with previous results (in the rat) from our team (Jacob et al., 2008).
- The observation that global direction selectivity is neither explained by the linear summation of the responses to the progressive deflection of individual arcs/rows, nor by the salience of the starting position of the moving bar (i.e. border effect). Integration of the cortical responses during the global motion protocol is indeed highly sublinear, independently of its direction.

IV.1 VSD imaging: some aspects to keep in mind.

The VSD imaging technique brings the possibility to record the brain activity at a mesoscopic scale, covering large regions of the cortical surface with a great temporal and spatial resolution. It has proved to be a very useful technique not only for studying the spatial distribution of sensory evoked activity in the corresponding primary sensory area of primates, cats and rodents, but also, particularly in the mouse cortex, for revealing fast, complex, and bilaterally synchronized patterns of depolarization (Ferezou et al., 2007; Mohajerani et al., 2010).

In 2013, Mohajerani and collaborators recorded spontaneous activity with VSD imaging from a wide field that included the entire hemisphere (Mohajerani et al., 2013). They observed that hemisphere-wide and sensory-evoked motifs were present in the spontaneous activity of the anesthetized mouse, which reflected multiple sensory modes like vision, audition, and touch. When the activity was emerging from primary sensory areas, a common posterior-medial cortical sink, where sensory activity was extinguished, was observed in the parietal association area. In this study Mohajerani et al. showed that maps of intracortical monosynaptic connections predicted hemisphere-wide patterns of spontaneous and sensory-evoked depolarization, suggesting that an intracortical monosynaptic map of connections shapes the spread of spontaneous activity in the mouse cortex.

While imaging spontaneous activity in the anesthetized cat, Arieli and collaborators (1996), observed that spontaneous activity followed the same functional orientation maps evoked by visual stimulation (Arieli et al., 1996). At the moment, we are collaborating with Yann Zerlaut, a PhD student of the group of Dr. Alain Destexhe, analyzing together the spontaneous activity of the mouse barrel cortex to test if it resembles to the evoked activity in response to the global motion protocol. These analyzes are not finished yet at the time of writing this manuscript, but will be reported in a future publication.

Despite the multiple advantages of the VSD imaging technique, there are some limitations that should be taken into account when interpreting the VSD signals or designing

a VSD imaging experiment. One of the drawbacks of VSD imaging is that the amplitude of the signals are quite small, usually below $1\% \Delta F/F_0$, in comparison with calcium-sensitive dyes, which offer 100 times larger signals. Two-photon microscopy (Denk et al., 1990) and differential loading or expression of the calcium-sensitive probes in populations of cells (Stosiek et al., 2003), have allowed in vivo calcium imaging of networks with a single cell resolution. Nevertheless, calcium signals report almost exclusively spiking activity, masking the subthreshold changes. Conversely, it is not trivial to reveal spiking activity in VSD signals. An experimental approach combining wide-field calcium imaging with VSD imaging will enable to record both the sub- and suprathreshold responses (Berger et al., 2007).

When analyzing the VSD imaging data it is important to take into account the origin of the signals. In an article of great interest, Chemla & Chavanne reviewed the VSD imaging technique making a special focus on the different components of the VSD signal (Chemla and Chavane, 2010). As VSDs stain nonspecifically the cellular membranes, it has been impossible, until now, to differentiate the neuronal types from which the response originates. Thus, VSD signal reflects the activity of both excitatory and inhibitory cells. In the study done by Jacob et al. (2008) in the rat S1, excitatory and inhibitory cells were identified through their electrophysiological signature, and both populations showed selectivity to global direction.

Are we recording only neuronal activity? The glial cells, and specially the astrocytes, have important functions for the brain. As it has been reported in the visual cortex, astrocytes have response times close to 3-4 seconds after the stimulus onset (Schummers et al., 2008), making glial activity unlikely to contribute to the VSD signal, which is normally imaged within the first second after the onset of the response. Nevertheless, a recent study showed that there are also multiple astrocytic mechanisms (e.g. glutamate clearance) that contribute significantly to the fast VSD signal (Pál et al., 2015). The relative contribution of astrocytes to the total VSD signal has to be quantified.

To overcome the limitation of nonspecific staining, genetically-encoded voltage indicators (GEVIs) are being developed. As with genetically encoded calcium probes (Miyawaki et al., 1997), by adding the GEVI sequence downstream cell-specific promoters and using advanced strategies for gene regulation, it is possible to target the expression of

voltage sensitive proteins to chosen neuronal subtypes. The groups of Pr. Thomas Knopfel and Pr. Vincent Pieribone, major contributors in this domain, have used different molecular strategies to engineer efficient voltage sensitive proteins (Baker et al., 2008; Jin et al., 2012; Mishina et al., 2014). However, even if these probes work efficiently on in vitro cell cultures, and give promising results in vivo in the rodent cortex (Mutoh et al., 2015), they still suffer from major limitations, mainly related to their interference with hemoglobin absorption and low signal to noise ratios. Nevertheless, the next generations of GEVIs might constitute the best tools to read the cortical network activity.

The pharmacological side effects of VSDs have been studied both in vitro and in vivo. In 2010, Memmerick and collaborators analyzed the effect of different VSDs on the function of the receptor GABA_A (Mennerick et al., 2010). They showed a strong potentiation of GABA_A receptor function in vitro for several types of VSDs including RH1691 and di-4-ANEPPS. Later on, another study evaluated the pharmacological side effects of these two VSDs (RH1691 and di-4-ANEPPS) in vivo in the rat barrel cortex (intact dura preparation), showing that RH1691 causes a significant prolonged increase in the amplitude of the somatosensory-evoked potentials (Grandy et al., 2012). Unlike the results of Mennerick et al., the increment in the amplitude of the responses was only observed when using the dye RH1691, suggesting that it might be the main reason for the good signal to noise ratio of this dye. However, spontaneous activity was not affected by the staining for neither of the dyes. In fact, this might not affect our results given that our calculations of the direction selectivities were a relative value of the cortical responses.

In addition, VSD imaging is an invasive technique that requires a craniotomy, and this might perturb the structure and the function of the underlying brain surface. Kalmbach and Waters (2012) studied the changes of the temperature of the brain surface under a craniotomy (2 x 2 mm) in the anesthetized mouse, showing that heat loss is significant, about 10°C below body temperature, even when covering it with agarose and a glass coverslip. These temperature variations affect cellular and network function of the neocortex by increasing the excitability of the pyramidal neurons of L2/3 and by generating longer Up states (Reig et al., 2010; Hedrick and Waters, 2012).

To conclude, both the use of the VSD RH1691 and the necessary exposure of the brain in the craniotomy are likely to generate an increased response of the cortical neurons. In our experiments this was not a limitation, since we were comparing the evoked VSD signals for the different directions of stimulation, and based our analyses on relative values. Given our set-up configuration and scientific questions, VSD imaging was an optimal technique to capture real-time dynamics with a good spatiotemporal resolution over the whole barrel cortex.

IV.2 Intracolumnar spatial organization of direction selectivity in the mouse barrel cortex

The existence of a spatial organization for the local direction selectivity within the barrel column has been a controversial subject (Andermann and Moore, 2006; Kerr et al., 2007; Tsytsarev et al., 2010b; Kremer et al., 2011). We will discuss here some possible reasons for these discrepancies. As we can see in Table 1, there are many differences in the experimental conditions between these works, regarding the whisker stimulation protocols, the age of the rats, the type of anesthesia, and the recording techniques, among others.

Note that the results of Tsytsarev et al., even if they are present in Table 1, will not be further discussed here, mainly due to their lack of clarity, as their article shows results that contradict themselves regarding the location of the responses relative to the barrel column coordinates.

In 2011, Kremer and collaborators evaluated the existence of an intrabarrel pinwheel for two groups of rats: juveniles and adults, finding that the direction selectivity map was present in the adult rats, but not in the juveniles, reconciling the two previous studies (Andermann and Moore, 2006; Kerr et al., 2007). Therefore, the local direction selectivity map emerges long after the critical period for most other sensory cortical maps, e.g.: the barrel field and the somatotopic map of L2/3 are formed within a few days after birth, and two weeks postnatal, respectively (Stern et al., 2001). This suggests that the intrabarrel map might be due to experience-dependent plasticity, as it happens in the case of the mouse visual system, where the cell connectivity pattern and feature selectivity becomes stronger with visual experience (Ko et al., 2013).

In order to test whether synaptic plasticity can underlie the pinwheel structure in the adults, Kremer and collaborators constructed a model of nonselective L2/3 neurons based on the spatiotemporal correlations between the movement and the direction of the whisker. This model successfully predicted the emergence of an intrabarrel pinwheel in the rat barrel cortex after training. Another Hebbian learning model was developed by Wilson and collaborators (2010) to address the same question but it was based on the spatial

correlations between the whiskers when contacting an object. It successfully predicted the existence of an intrabarrel pinwheel in L2/3, and also predicted that neurons with similar tuning properties are interconnected by patterns of long-range lateral connections spanning distances of several whiskers (further discussed on the section: “3. Possible mechanisms of the emergence of global direction selectivity”).

It is important to notice that both the group of Andermann and Moore, and Kremer et al., used enriched environments for the rats. Three to six rats were housed together for a couple of weeks in large cages that included, as reported by Andermann and Moore: multilevel surfaces, rodent tubes, and a running wheel. These housing conditions and social environment enhance the use of the vibrissae, thus favoring the emergence of an intrabarrel direction selectivity map, if we consider that it is due to experience-dependent plasticity. The housing conditions were not reported in the article of Kerr and collaborators, suggesting that they were standard, as they were for our mice.

Another important difference between the groups that studied the spatial organization for the local direction selectivity is the choice of the stimulus shape. Kremer et al. used a sawtooth-like stimulus (amplitude 500 μm): a fast ramp (20 ms) followed by a slow decay (980 ms). While Andermann and Moore used a shark fin-like stimulus (amplitude 170 μm), which consisted of a half-sinusoidal fast rise (7 ms) and a slow decay (50 ms). Kerr et al., used a stimulus with faster deflections, consisting in a ramp-hold-ramp stimulus (R-H-R amplitude 500 μm) with very fast onset and offset ramps (10 ms, the whisker staying deflected for 500 ms).

In our experiments we used even a faster deflection of the whiskers with a trapezoid shape, R-H-R (2-2-2 ms), in order to obtain a good signal-to-noise ratio in VSD imaging. With such deflection we might be overstimulating the network and recruiting not only the neurons that are selective to the direction of the whisker deflection, but also other neurons that are direction-independent. We observed for most of the directions the arrival of the activity very close to the center of the barrel-related column; however, we could see a spatial distribution of the activity for the different directions. We hypothesize that by applying a slower stimulus (e.g. a R-H-R deflection of 10-10-10 ms) we might recruit less non-

direction-selective neurons and thus reveal more efficiently the spatial distribution of the direction-selective ones.

During these experiments we used the same optic configuration of our set-up for running both the local direction protocol and the global motion protocol in the same mouse. The spatial resolution was 25 $\mu\text{m}/\text{pxl}$, then the supragranular activity on the barrel-related column C2, whose barrel in L4 has a diameter of about 300 μm (Lefort et al., 2009), was imaged from about 5 pxls. We found that all the early responses (measured at 12 ms after stimulus onset) for the different directions of the whisker deflection were organized very close to the C2 column center, within a diameter of 100 μm (4 pxls). It would have been possible to do another series of experiments with a special focus on the intrabarrel organization of the local direction selectivity with a higher spatial resolution by changing the optics; however the FOV would not have covered the whole barrel field.

It is important also to consider that we are using here a different recording approach than tetrodes or 2-photon calcium imaging. With VSD imaging we are recording mainly the dendrite activity in L2/3, in contrast to the previous studies on the local direction selectivity in the barrel cortex in which the spiking activity was recorded with a single cell resolution. The dendrite disposition is diffuse within the supragranular layers and we can hypothesize that this could account for the differences between our results and the ones of Andermann and Moore, and Kremer et al.; i.e. while the somas of the L2/3 direction-selective neurons are distributed in a pinwheel manner, their dendrites are likely to be more diffuse and receive inputs very close to the center of the barrel. The mirror image pinwheel that we obtained might be due to neuronal morphologies with dendrites that might follow a different distribution than the somata. Nevertheless, we have done here the first study on the spatial distribution of the local direction selectivity in the mouse. The directional maps might differ from one species to another, thus it would be necessary to characterize the somata distribution of the direction-selective neurons of the L2/3 in the mouse barrel column.

Table 1: Comparison between experimental conditions for assessing the existence of a spatial distribution of the direction selectivity to a single whisker deflection.

	Andermann & Moore 2006	Kerr et al. 2007	Kremer et al. 2011	Tsytsarev et al. 2010	Our Results
Species	Sprague-Dawley rats	Wistar rats	Sprague-Dawley rats	Sprague-Dawley rats	C57BL6J mice
Age	Adults 392±35 gr.	Juveniles: 3 - 5 weeks	Juveniles: 4 - 5 weeks (100 gr) Adults: 11 - 16 weeks (350 gr)	Adults : 8 - 16 weeks (200-300 gr)	Adults : 6-10 weeks (20-30 gr)
Enriched environment	Yes	Not reported	Yes	Not reported	No
Anesthetics	Isoflurane (0.75%-1.125%)	Urethane (1.2 g/kg)	Isoflurane (1-1.5%)	Urethane (1.2 5 g/kg) Furosemide sulfate (0.1 mg/kg)	Urethane (1.7 mg/g)
Stimulus shape	Half-sinusoids fast rise (7 ms) and a slow fall (50 ms) Amplitude: 170 µm at 7 mm from skin	R-H-R: 10-500-10 ms Amplitude: 500 µm at 5 mm from skin	Sawtooth: 500 - 500 ms and 20 - 980 ms Amplitude: 500 µm at 5 mm from skin	R-H-R: 5-5-5 ms Amplitude: 200 -300 µm at 4-5 mm from skin	R-H-R: 2-2-2 ms Amplitude: 100 µm at 3 mm from skin
Whiskers	D3	E1	B1, B2, C2, D2, C3, D3	E2	C2
Recording technique	Tetrodes (L2/3 to L4)	Two-photon calcium imaging (Oregon Green BAPTA 1-AM) Patch-clamp	Two-photon calcium imaging (Oregon Green BAPTA 1-AM)	VSD imaging (RH1691 - 0.6 mg/ml)	VSD imaging (RH1691 - 1 mg/ml)
Intrabarrel spatial organization	Adults: Yes - Pinwheel	Juveniles: No	Juveniles: No Adults: Yes - Pinwheel	Adults: Yes - orthogonal deflection angles evoked responses located orthogonally	Adult mice: Yes - inverted pinwheel

IV.3 Possible mechanisms for the emergence of global direction selectivity

By using a 24-multidirectional stimulator matrix coupled with a VSD imaging camera, we recorded cortical responses to global stimuli in eight different directions. We showed that global direction selectivity is present in the superficial layers of the mouse barrel cortex, and is spatially organized within the barrel cortical space.

Is global direction selectivity emerging in the cortex or is the cortex reflecting a preference originating upstream? In our team, Ego-Stengel and collaborators (Ego-Stengel et al., 2012), showed that global direction selectivity is already present at the level of the thalamus, but it is highly amplified in the cortex: under cortical inactivation, selectivity in the VPM nucleus of the thalamus decreased on average but remained present.

The transformation of the sensory input from the vibrissae to the VPM involves several nonlinearities in order to generate anisotropic global receptive fields in the thalamic neurons. This goes against the classical view of the whisker system where projections from the whiskers to the cortex go along the lemniscal pathway with parallel fibers for each whisker, conserving the topography of the periphery with axons and dendrites that are restricted to small regions corresponding in general to only one whisker. Subcortical nonlinear interactions must exist between responses to different whiskers. Recordings done in our team from the trigeminal ganglion showed that the first-order neurons did not present a preferred direction for the global motion protocol (Ph.D. thesis of Julie Le Cam, Université Pierre et Marie Curie, 2010), suggesting that the global direction selectivity is not due to the mechanical coupling of the whiskers in the skin of the whisker pad.

A prospective relay where nonlinearities might occur is in the brainstem, in particular in the trigeminal nucleus PrV. The PrV neurons that project to VPM have multiwhisker receptive fields (Veinante and Deschênes, 1999). The responses to the PW are inherited from direct projections coming from the trigeminal ganglion (thus, non-selective to global direction), while the multiwhisker responses come from intratrigeminal connections between PrV and SpV nuclei. PrV receives excitatory inputs from the caudal subnucleus

(spVc) and inhibitory modulation from the interpolar subnucleus (spVi) (Minnery and Simons, 2003; Timofeeva, 2004; Furuta et al., 2008).

We would like in the future to record from the trigeminal nuclei in order to establish whether selectivity to global motion is already present at this stage. With this aim, I spent three months at the Weizmann Institute with the groups of Dr. Ehud Ahissar and Dr. Ilan Lampl, where I learnt to perform extracellular recordings from the different trigeminal nuclei. If we find neurons that are selective to the direction of the global motion already at this stage, it would be interesting to compare them with the ones obtained in the VPM to assess if nonlinearities are just transmitted to the thalamus or if the intrathalamic circuitry is also amplifying the anisotropy via intrinsic nonlinearities of the VPM cells (i.e.: spike thresholds and nonlinear summation of the inputs by the membrane or t-type Ca^{2+} currents).

As mentioned before, in 2010 Wilson and collaborators proposed a model to explain the emergence of direction selectivity maps in L2/3 of the rat barrel cortex. Their model was taking into account the spatial correlations between the whiskers when contacting an object. Besides from explaining the intrabarrel distribution of the local direction selectivity, their model also predicted that L2/3 neurons from different columns that share similar tuning properties are synaptically coupled. These long-range interactions are consistent with previous results showing that lateral interactions are stronger when whiskers are sequentially deflected in similar directions (Simons, 1985; Kida et al., 2005). These findings suggested that there might be a suprabarrel organization of the direction selectivity. Thus, there might be also a suprabarrel organization of the global direction selectivity. Indeed, we showed here that in the supragranular layers of the mouse barrel cortex the global direction selectivity is spatially organized: the barrel-related columns that correspond to more rostral whiskers are more selective to global motion directions than the ones that correspond to caudal whiskers.

In agreement with previous results obtained in our team in the rat barrel cortex by Jacob et al. (2008), we found that the preferred direction for global motion showed a bias towards caudo-ventral direction. In particular the caudal global direction was the most represented in our results. Another study done in our team by Ego-Stengel et al. (2012) showed that thalamic neurons of the VPM have a homogeneous distribution of the global

direction selectivities. Then how can we explain the cortical emergence of a bias? We can hypothesize that long-range intracortical connections (predicted by the model of Wilson et al., 2010) specifically along rows might interact with the thalamocortical input creating this bias. But which are then the mechanisms underlying the global direction selectivity?

Both in the barrel cortex and in the thalamus the extracellular response to global motion protocols were of a similar magnitude to the response obtained by deflecting only one whisker (Jacob et al., 2008; Ego-Stengel et al., 2012). This suggests that the nonlinearities involved in the global direction selectivity are likely to be suppressive rather than facilitatory, like the ones involved in cross-whisker suppressive interactions found both in VPM and cortex (Simons and Carvell, 1989; Ego-Stengel et al., 2005; Higley and Contreras, 2007).

The linear summation of the responses to single-whisker stimulation failed to explain the selectivity to global motion (Jacob et al., 2008). In addition, here we constructed a linear prediction by sequentially adding the responses to the stimulation of individual arcs or rows. If the spatial organization of global direction selectivity was only due to the lateral cortico-cortical connections we could have expected to obtain a map similar than with the moving bar protocol. We showed that the linear summation of the responses to a group of whiskers (arcs or rows), also failed to explain the global direction selectivity, and that the integration is highly sublinear.

In the article of Drew & Feldman (2007), a strong salience of the starting point of the bar on the cortical responses was reported. We can imagine then that the spatial distribution of the global direction selectivity could be influenced by the starting position of the moving bar. To test this hypothesis we compared the direction selectivity maps obtained with the moving bar with the ones obtained by just deflecting the first arcs or rows, in so-called “static bar”. The two maps differed: the rostral and ventral directions are more represented in the one that corresponds to the static bar protocol; while, for the moving bar, we found a bias in the opposite direction, caudoventral, as already mentioned. The bias in the case of the static bar can be due to the fact that the response to the deflection of Arc Str has a higher amplitude than when deflecting the Arc 4, and similarly the response to the deflection of Row A is larger than when deflecting Row E.

The differences in the two maps suggest that the global direction selectivity emerges when sequentially deflecting all the whiskers. These results are in agreement with the results obtained by Jacob et al. (2008) where they tested the cortical responses to the proximal (stimulating only 9 whiskers) and global protocols (24 whiskers). They reported that all the whiskers need to be deflected in order to obtain defined global direction selectivity. Drew & Feldman (2007) deflected only 9-12 whiskers, which might explain the lack of direction selectivity reported by them. Ego-Stengel et al (2012) reported that in the case of the thalamic neurons, applying the proximal protocol had little influence on the tuning curves. Indeed, these results suggest that the thalamus integrates vibrissal information from a narrower spatial domain than the cortical neurons.

In addition, another study done in our team in collaboration with the team of Dr. Alain Destexhe (Estebanez et al., 2012), used extracellular recordings and the 24-whisker stimulator to show that in the L4 to L6 of the rat barrel cortex there are at least two subpopulations of neurons: “local neurons” that respond more to uncorrelated stimuli tuned to center-surround local contrast, and “global neurons” that respond more to correlated stimuli encoding coherent motion at the whisker pad scale. Indeed, further studies done in collaboration with the team of Dr. Laurent Bourdieu showed that these two populations are also present in the L2/3, revealed with 2-photon calcium imaging (data not published). During the global motion protocol there are three correlations happening in simultaneous:

- Whiskers from the same row/arc are being deflected simultaneously;
- This deflection is in the same direction and with same stimulus shape;
- There is a time correlation: neighboring adjacent whiskers will be deflected within a coherent time (10 ms after or before).

We can hypothesize that when applying this protocol we are recording the responses of these two subpopulation of neurons. Local neurons are more likely to respond to the front edge of the moving bar, acting as contrast detectors, while global neurons would be more likely to respond to the coherent motion of the bar moving in a given direction. However, further studies need to be done in order to characterize how these two populations of cells respond to the global motion protocol.

Multiwhisker interactions were studied also by Hirata & Castro-Alamancos (2008), where they showed that multiwhisker stimulation enhances (reduction of spike latency in L4 and more spike probability in L2/3) short-latency responses and suppresses long-latency responses. This enhancement and suppression appear first at the L4 of the barrel cortex and were not present in the VPM. The enhancement caused by synaptic summation might be explained by synaptic cooperativity (convergence of synaptic activity evoked by different whiskers). On the other hand, multiwhisker suppression of the long-latency responses might be due to an increased recruitment of inhibition in the cortical network.

An alternative hypothesis that might explain the cortical mechanisms of amplification of the global direction selectivity is related with the second somatosensory cortex (S2). S1 and S2 are closely connected, and the latencies in which the responses arrive to S2 are compatible with the latencies in which the whiskers are stimulated (Benison et al., 2007; unpublished preliminary data from the team). We could test this hypothesis by recording the responses to the moving bar protocol before and after the inactivation of S2.

The same reasoning can be done for the primary motor cortex (M1), as sensory related activity reaches M1 within 8-10 ms (Ferezou et al., 2007) and there are monosynaptic projections that go back to S1, mainly to L1 synapsing with tuft dendrites of pyramidal neurons (Mao et al., 2011; Petreanu et al., 2012). Thus, within 16-20 ms tactile related activity coming from M1 could reach S1, compatible with the latencies of our stimulation protocol.

Indeed, the neurons in S1 that project to M1 show different membrane dynamics than the ones that project to S2, suggesting a different functional role of these projections: M1-projecting neurons are well-suited for stimulus detection, while the S2-projecting neurons might serve to encode object features (Yamashita et al., 2013; Clancy et al., 2015). Following this reasoning, S2 would be more likely than M1 to participate on the cortical amplification of global direction selectivity.

IV.4 Read-out: Advantages of direction selectivity maps?

The cortex extracts and amplifies features from the vast amount of information available to our senses. In higher mammals, stimulus representations are distributed in hierarchically arranged cortical areas, which process different features of the sensory scenes and integrate them in a progressively abstract manner. Conversely, in rodents, primary sensory cortices might present several multiplexed representations of the stimuli features (Estebanez et al., 2012). The cortical circuits might share the same general principles of cortical processing for the different sensory modalities, suggesting that they might share also similar organization strategies. For a further reading on this subject, see the review of (Harris and Mrsic-Flogel, 2013).

One role of intracortical connections might be to amplify thalamocortical input (Hull et al., 2009), although (Bruno and Sakmann, 2006) argued that synchronous TC input is large enough to drive the cortex and would not require any amplification. The preference to certain features of the stimulus found in the cortex could thus originate from the thalamus. We know that intracortical connections are not randomly organized, as the connection probability between supragranular nearby excitatory cells is higher for neurons that respond to similar features (e.g. direction selectivity), even if they are in distant regions (Gilbert and Wiesel, 1989; Ko et al., 2011). In contrast, local excitatory connections onto inhibitory interneurons are unrelated to feature preference (Bock et al., 2011; Hofer et al., 2011). This connectivity results in a recurrent excitatory subnetwork, which boosts sensory responses to certain preferred features.

In the visual cortices of cats and monkeys, the feedforward thalamocortical drive is amplified by a local recurrent intracortical loop that preserves the retinotopic mapping of visual inputs onto the cortex (Bringuier et al., 1999). Orientation preference is functionally and spatially organized as iso-orientation domains arranged as pinwheels (Bonhoeffer and Grinvald, 1991; Ohki et al., 2005; Blasdel, 1992). Within this organization the subthreshold tuning is sharper as neighboring neurons share the same orientation preferences (Figure 34), only at the center of the pinwheel the tuning will be broader (Schummers et al., 2002). An

important aspect of this organization is that both the excitatory and the inhibitory cells will be tuned to a certain orientation.

In the case of the visual system of the rodents, the primary visual cortex (V1) has a smaller volume and the representational maps are not present (Figure 34). Excitatory cells spatially distributed in a salt-and-pepper manner will have a broader subthreshold tuning, as the neighboring excitatory cells are likely to have different orientation tunings. Although, as already mentioned, the excitatory cells that share similar tuning are more likely to be synaptically connected (even through long-range connections) making the firing rate of these cells sharply tuned. Inhibitory cells embedded in this network will receive input from the surrounding excitatory cells which will have a large variety of orientation tunings, resulting in a broad inhibitory tuning. Remarkably, even if the mapping (e.g. a pinwheel) is not present, the final output of the cortex can be highly selective, as it has been observed in the visual system of the squirrels (Van Hooser et al., 2006), suggesting that mapping is not essential for accurate sensory function.

The barrel cortex of the rodents also covers a smaller cortical volume than the cat or primate visual systems. Hence, a higher processing of stimulus features, such as global direction selectivity, might occur in areas tightly connected with the barrel cortex, like S2 or M1, or another alternative could be that neurons within the barrel cortex code this higher order features. Indeed in our team, Jacob and colleagues showed that cortical neurons present direction selectivity to both the local deflection of the whisker and the global deflection of all the vibrissae. Moreover, these direction preferences are not correlated, meaning that the same neurons are able to code two different features of the stimulation through different mechanisms.

In our experiments of global motion (N=8) we used a direction of local whisker deflection that was the same for all the whiskers: on half of them (N=4) it was towards caudal and on the other half towards rostral directions. When computing the global direction selectivity for each group, the proportion of barrel columns with significant direction selectivity was lower than if taking all the experiments together, mainly given the reduction on the analyzed sample number. However, for the barrel columns that presented significant direction selectivity in both groups, the global directions had a similar distribution and were biased to caudoventral directions. In order to get rid of any effect that the local

direction of deflection of the vibrissae might have on the preferred direction of global deflection, we could run a similar protocol but with randomized local deflection directions for each whisker. In any case, these findings support our hypothesis that there are multiplexed representations of the stimuli on the barrel cortex.

As mentioned before, global direction selectivity is already present in the VPM, and thalamocortical projections convey this information to the cortex where it is sharpened (Ego-Stengel et al., 2012). One can hypothesize that, similar to the rodent visual cortex, this amplification process might be due to a recurrent excitatory subnetwork that could link neurons sharing similar preferences to a certain global direction. Thus, the subnetwork should contain long-range connections in order to link the global direction selectivity inherited by the thalamocortical projections of the different whiskers. We were interested in studying whether these multiplexed representations were spatially distributed in the cortical surface. With VSD imaging, we recorded responses that were likely coming from subthreshold dendritic activity of L2/3. We showed that both local and global direction selectivity were spatially distributed; however these selectivities might correspond to the subthreshold tuning.

It would be interesting to investigate whether the selectivity of the firing rate of the recorded population of neurons follows a similar spatial organization. A way of doing this would be to apply the same global motion protocol recording the suprathreshold activity by doing wide-field calcium imaging of the barrel cortex. Ai95D mice, a genetically modified strain that express GCaMP6f calcium indicator under the control of Cre recombinase, can be crossed with mice expressing Cre recombinase in cortical excitatory neurons ($Emx1^{Cre}$). With an appropriate set of filters, we would be able to record both VSD and calcium signals on the same animal.

An alternative way would be to couple the VSD imaging experiments with extracellular recordings of the cortical activity. By relating the VSD fluorescence signals with the spiking pattern of the neurons, spiking zones can be delimited from the high-amplitude VSD imaging signals (Jancke et al., 2004). By using one of these experimental approaches we might be able to compare spatial organization of the sub- and suprathreshold global direction selectivity in the mouse barrel cortex.

But what are the advantages of such spatial organization? By having a circuit of long-range connections distributed along the barrel cortex, whenever new whisker information arrives to the barrel-related column, it could be highly influenced by contextual information that was present a few tens of milliseconds earlier in the surrounding whiskers. We showed here that it is indeed the case in the barrel cortex. In fact, for the eight directions of global stimulation, the whiskers were deflected for the same amount of time, and with the same stimulus shape; however the amplitude of the responses were different depending on the stimulation sequence. The only thing that varied was the contextual information before the deflection of a certain set of whiskers, and intracortical connections are likely to provide this contextual information.

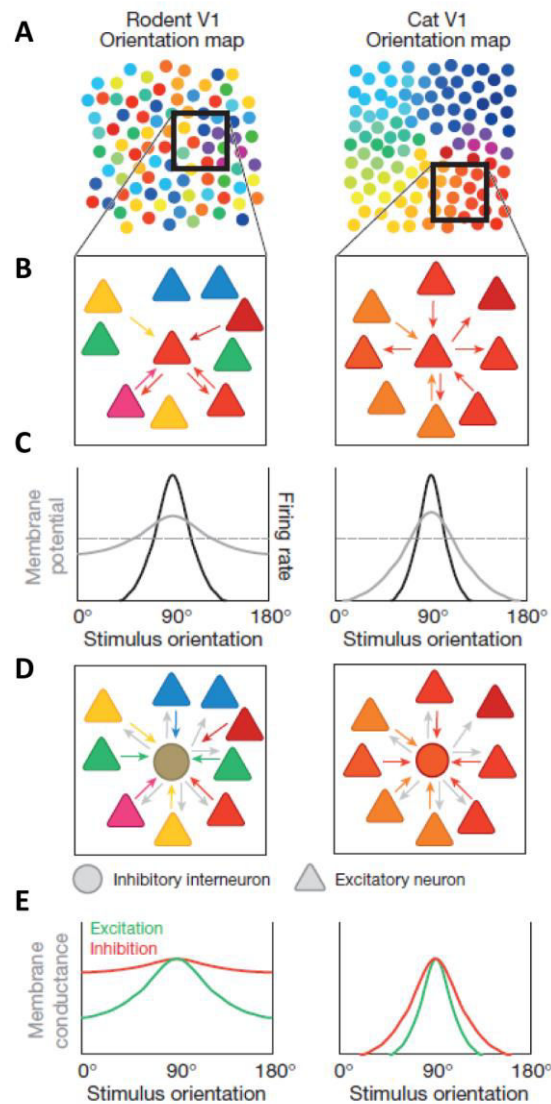


Figure 34: Relationship between feature mapping and coding in the visual cortex of the rodent and cat

A: Non-topographic arrangement of orientation preference in rodent V1 contrasts with spatially contiguous arrangement of orientation preference in cat V1.

B: In all cases, principal cells receive inputs preferentially from neurons with similar feature preference.

C: Incomplete functional specificity of connections for non-mapped features such as orientation in rodent V1 leads to broader subthreshold tuning. This is converted to sharp tuning of firing output by nonlinear neuronal amplification and synaptic inhibition.

D: Inhibitory interneurons receive dense and unselective input from all neighboring neurons.

E: The inhibitory and excitatory synaptic inputs received by a principal cell are both strongest for the same preferred stimulus, but inhibition is more broadly tuned than excitation, leading to sharpened tuning of spiking output.

From (Harris and Mrsic-Flogel, 2013)

IV.5 Sensory expectations

At odd with other sensory systems, the whisker system of the rodents is discrete from the periphery (the whiskers) up to the cortex (the barrels). In fact, the discreteness is not just spatial; it is also temporal as whisking produces repetitive whisker deflections when contacting an object. Thus, is the perception of the whisker space also discrete or is it perceived as continuous? The Gestalt theory proposes that perceptions are not isolated; we rather obtain a global perception of an object by combining all its perceptive attributes such as color, texture, shape, borders, etc., this makes the perception of an object invariant. Indeed, Gibson showed in humans that when presenting an object into different places of the palm of their hand, their perception was invariant to the location where the object was placed (Gibson, 1962). Moreover, in humans the haptic behavior is also discrete: when we walk in the dark we might touch a wall with our fingers, however, we perceive it as a whole.

In the visual system, a discrete sequence of stimulations in a spatiotemporal order can generate the perception of an apparent movement (Cavanagh et al., 1989), similar to what happens every time we watch a movie in the cinema. The apparent motion can be generated by many different stimuli, depending mainly on the time interval and the spatial distance of the stimulations; for instance, in the “line-motion” illusion a square is shown first followed by a flashed bar, which is perceived by the subjects as a line drawing (Hikosaka et al., 1993; Jancke et al., 2004). The study of Jancke et al. (2004) used this illusion in the anesthetized cat, showing that the spread of subthreshold activity evoked by presenting the first square could not be differentiated from the subthreshold activity evoked by the presentation of the real line drawing. They showed that the first square evokes a rapid spread of low-amplitude activity, but the high amplitude zone (spiking zone) followed the temporal dynamics of the moving bar, suggesting that an onset of any stimulus will create an intricate spatiotemporal pattern of spread of the subthreshold activity which might serve to perceive a motion.

When sequentially deflecting the whiskers we can hypothesize that two mechanisms occur: an early facilitation and a later suppression of the responses. According to Drew and Feldman (2007), suppression occurs with inter-arc deflection delays longer than 5 ms, and is maximal at 20 ms. Given that our interwhisker interval was 10 ms we expected to see suppressive responses. We can interpret a fast spread of activity as an anticipatory

mechanism, in which future locations of the arrival of thalamic inputs are pre-activated and then will be suppressed. In fact, in our experiments we showed that the activity from one barrel-column spreads to a neighboring one faster than the stimulation protocol, in other words, the barrel-related column is already active even before the deflection of its corresponding whisker. In agreement with this hypothesis, we also see that the responses to the neighboring arc/row were highly suppressed (see Figure 31). Hence, the lateral spread of the cortical activity would determine the integration area of the thalamocortical inputs.

IV.5.1 Direction selectivity in the awake mouse

As mentioned in the Part II, when the animal is whisking, the evoked responses to a whisker deflection are smaller and do not spread as much as when the animal is quiet. The reasoning then would be that in our anesthetized approach responses would be bigger and spread more than when the animal is awake and behaving, questioning the existence of global direction responses in the awake animal. However, even though the cortical responses might be larger in the anesthetized mouse, it should not affect the calculation of the global direction selectivity as it is a relative measure. Nevertheless, it is of our interest to study how these responses might differ in the awake animal, which is feasible in our experimental set-up. An extra step would need to be added: cutting the facial nerves branches in order to prevent whisking when running the protocol. The ramus temporalis, ramus zygomatico-orbitalis and ramus buccolabialis-superior together with the dorsal branch of the buccolabialis-inferior of the facial nerve would need to be transected in order to cut off inputs to both intrinsic and extrinsic muscles (Dörfl, 1982).

In addition, the awake configuration will allow us to study another interesting aspect: whether the mouse uses or not the global information in a behavioral task.

IV.5.2 Why a directional anisotropy?

But why are the caudal and ventral the two global directions of stimulation that elicit the biggest responses in the majority of the barrels? One might expect that the caudal direction could be more represented as when the animal encounters an object or is walking

along a corridor with a thigmotactic behavior; its whiskers are bent towards this direction. In addition, the preferred local direction of deflection is on the caudo-rostral axis. Why the ventral global direction gives a highest response is more difficult to explain. In fact the opposite results might be more intuitive: when walking the animal might encounter small obstacles in the floor, and the whiskers are bent on the dorsal direction, resulting in a bigger salience of this direction. However the ventral global direction is more represented. When looking to a running mouse's profile, one can see that the rows do not lie along the horizontal axis. Figure 35 shows snapshots of four high-speed videos where we recorded an adult naïve mouse running along a corridor (3.5 cm width). The snapshots reveal that the rows of the whiskerpad are not parallel to the dorso-ventral axis, and also that the whiskers are very protracted in all the cases. With such head position, the global direction of deflection of the whiskers is in the caudo-ventral axis. These preliminary observations suggest that the higher cortical representation of global caudo-ventral stimuli could reflect adaptive plasticity mechanisms leading to a higher sensitivity to the most frequent nature of the encountered stimuli. Further study of the mouse natural behavior and natural statistics might therefore be useful to understand the emergence of global direction selectivity.

Indeed, given that the intrabarrel direction selectivity maps emerge late in the development of the rats, and are likely to be shaped by experience-dependent plasticity (Kremer et al., 2011), we hypothesize that the same might happen to global direction selectivity maps. Further quantifications should be done in order to make a better estimation of the correlation between the angle of the head position and the preferred global angles of each barrel column.

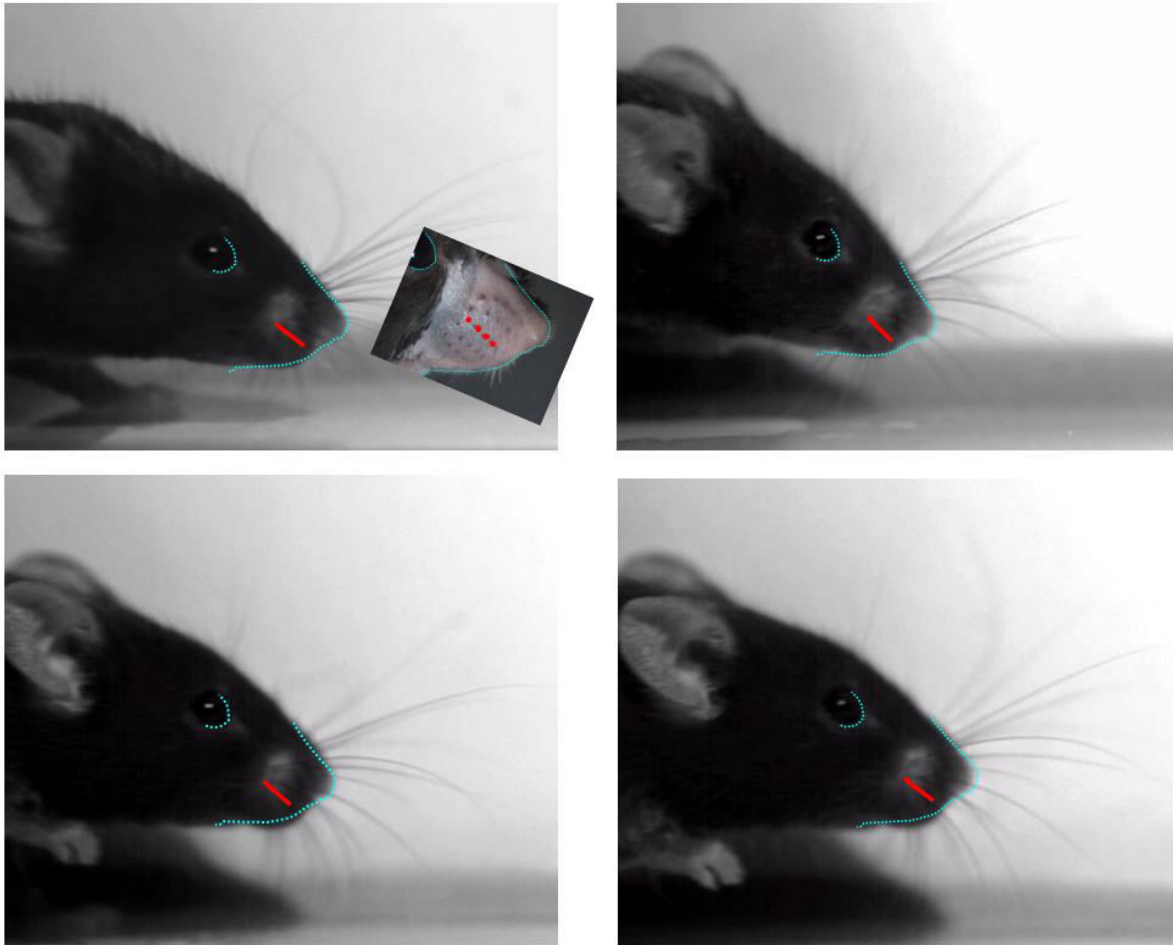


Figure 35: Head position of a mouse while running along a corridor.

The four panels correspond to snapshots of four movies of a mouse running through a 3.5 cm-width corridor. Since the implantation of the whiskers is not easy to determine on such high speed video frames, we compared these images with a high resolution photograph of a mouse with a shaved snout (inset, red dots have been placed on the C-row-whisker implantation sites). The mouse profile delineated in light blue from this photograph has been overlaid on the video snapshots to indicate the approximated position of the row C of the whisker pad.

IV.6 Conclusion

In summary, the main finding of this work is that the selectivity to the direction of local and global whisker stimulations are spatially distributed in the mouse barrel cortex, supporting the hypothesis that multiplexed representations of the stimuli can be found within this cortical volume.

Still, the questions of how these representations are read out, and whether this information is used by the behaving mouse, remain open. Indeed, when the mouse explores an object information coming from S1 and other areas, such as M1 and S2, is integrated with information coming from other sensory modalities, generating a more robust representation of it. Human beings go even further in abstraction by attaching to these perceptions a concept, a word.

Then, we might go back to the beginning of this thesis and re-ask the question: what is reality? Even though this work helps to further understand tactile sensory processing, we are still far from finding an answer to this question. Perhaps, as Nietzsche said, «*There are no facts, only interpretations*», and we can only know reality by studying how we interpret it. Or, perhaps, we will never find an answer to it. But aren't the unanswered questions the driving force of research? In my opinion, is worth it to keep trying.

Bibliography

- Ahissar, E., Sosnik, R., and Haidarliu, S. (2000). Transformation from temporal to rate coding in a somatosensory thalamocortical pathway. *Nature* 406, 302–306.
- Alitto, H.J., and Usrey, W.M. (2003). Corticothalamic feedback and sensory processing. *Curr. Opin. Neurobiol.* 13, 440–445.
- Alloway, K.D. (2008). Information processing streams in rodent barrel cortex: the differential functions of barrel and septal circuits. *Cereb. Cortex N. Y. N 1991* 18, 979–989.
- Andermann, M.L., and Moore, C.I. (2006). A somatotopic map of vibrissa motion direction within a barrel column. *Nat. Neurosci.* 9, 543–551.
- Arabzadeh, E., Panzeri, S., and Diamond, M.E. (2004). Whisker vibration information carried by rat barrel cortex neurons. *J. Neurosci. Off. J. Soc. Neurosci.* 24, 6011–6020.
- Arieli, A., Sterkin, A., Grinvald, A., and Aertsen, A. (1996). Dynamics of ongoing activity: explanation of the large variability in evoked cortical responses. *Science* 273, 1868–1871.
- Arieli, A., Grinvald, A., and Slovin, H. (2002). Dural substitute for long-term imaging of cortical activity in behaving monkeys and its clinical implications. *J. Neurosci. Methods* 114, 119–133.
- Arkley, K., Grant, R.A., Mitchinson, B., and Prescott, T.J. (2014). Strategy Change in Vibrissal Active Sensing during Rat Locomotion. *Curr. Biol.* 24, 1507–1512.
- Armstrong-James, M., and Callahan, C.A. (1991). Thalamo-cortical processing of vibrissal information in the rat. II. spatiotemporal convergence in the thalamic ventroposterior medial nucleus (VPM) and its relevance to generation of receptive fields of S1 cortical “barrel” neurones. *J. Comp. Neurol.* 303, 211–224.
- Armstrong-James, M., and Fox, K. (1987). Spatiotemporal convergence and divergence in the rat S1 “barrel” cortex. *J. Comp. Neurol.* 263, 265–281.
- Arsenault, D., and Zhang, Z. (2006). Developmental remodelling of the lemniscal synapse in the ventral basal thalamus of the mouse. *J. Physiol.* 573, 121–132.
- Ascoli, G.A., Alonso-Nanclares, L., Anderson, S.A., Barrionuevo, G., Benavides-Piccione, R., Burkhalter, A., Buzsáki, G., Cauli, B., DeFelipe, J., Fairén, A., et al. (2008). Petilla terminology: nomenclature of features of GABAergic interneurons of the cerebral cortex. *Nat. Rev. Neurosci.* 9, 557–568.
- Axelrad, H., Verley, R., and Farkas, E. (1976). Responses evoked in mouse and rat SI cortex by vibrissa stimulation. *Neurosci. Lett.* 3, 265–274.

- Bale, M.R., and Petersen, R.S. (2009). Transformation in the Neural Code for Whisker Deflection Direction Along the Lemniscal Pathway. *J. Neurophysiol.* *102*, 2771–2780.
- Beaulieu, C. (1993). Numerical data on neocortical neurons in adult rat, with special reference to the GABA population. *Brain Res.* *609*, 284–292.
- Benison, A.M., Ard, T.D., Crosby, A.M., and Barth, D.S. (2006). Temporal Patterns of Field Potentials in Vibrissa/Barrel Cortex Reveal Stimulus Orientation and Shape. *J. Neurophysiol.* *95*, 2242–2251.
- Benison, A.M., Rector, D.M., and Barth, D.S. (2007). Hemispheric Mapping of Secondary Somatosensory Cortex in the Rat. *J. Neurophysiol.* *97*, 200–207.
- Benshalom, G., and White, E.L. (1986). Quantification of thalamocortical synapses with spiny stellate neurons in layer IV of mouse somatosensory cortex. *J. Comp. Neurol.* *253*, 303–314.
- Berg, R.W., and Kleinfeld, D. (2003). Rhythmic Whisking by Rat: Retraction as Well as Protraction of the Vibrissae Is Under Active Muscular Control. *J. Neurophysiol.* *89*, 104–117.
- Berger, T., Borgdorff, A., Crochet, S., Neubauer, F.B., Lefort, S., Fauvet, B., Ferezou, I., Carleton, A., Lüscher, H.-R., and Petersen, C.C.H. (2007). Combined voltage and calcium epifluorescence imaging in vitro and in vivo reveals subthreshold and suprathreshold dynamics of mouse barrel cortex. *J. Neurophysiol.* *97*, 3751–3762.
- Bernardo, K.L., and Woolsey, T.A. (1987). Axonal trajectories between mouse somatosensory thalamus and cortex. *J. Comp. Neurol.* *258*, 542–564.
- Bernardo, K.L., McCasland, J.S., and Woolsey, T.A. (1990a). Local axonal trajectories in mouse barrel cortex. *Exp. Brain Res.* *82*, 247–253.
- Bernardo, K.L., McCasland, J.S., Woolsey, T.A., and Strominger, R.N. (1990b). Local intra- and interlaminar connections in mouse barrel cortex. *J. Comp. Neurol.* *291*, 231–255.
- Bobrov, E., Wolfe, J., Rao, R.P., and Brecht, M. (2014). The representation of social facial touch in rat barrel cortex. *Curr. Biol.* *24*, 109–115.
- Bokor, H., Acsády, L., and Deschênes, M. (2008). Vibrissal responses of thalamic cells that project to the septal columns of the barrel cortex and to the second somatosensory area. *J. Neurosci. Off. J. Soc. Neurosci.* *28*, 5169–5177.
- Bolori, A.-R., and Stanley, G.B. (2006). The Dynamics of Spatiotemporal Response Integration in the Somatosensory Cortex of the Vibrissa System. *J. Neurosci.* *26*, 3767–3782.
- Bourassa, J., Pinault, D., and Deschênes, M. (1995). Corticothalamic projections from the cortical barrel field to the somatosensory thalamus in rats: a single-fibre study using biocytin as an anterograde tracer. *Eur. J. Neurosci.* *7*, 19–30.
- Brecht, M. (2007). Barrel cortex and whisker-mediated behaviors. *Curr. Opin. Neurobiol.* *17*, 408–416.

- Brecht, M., and Sakmann, B. (2002). Dynamic representation of whisker deflection by synaptic potentials in spiny stellate and pyramidal cells in the barrels and septa of layer 4 rat somatosensory cortex. *J. Physiol.* *543*, 49–70.
- Brecht, M., Preilowski, B., and Merzenich, M.M. (1997). Functional architecture of the mystacial vibrissae. *Behav. Brain Res.* *84*, 81–97.
- Brecht, M., Roth, A., and Sakmann, B. (2003). Dynamic receptive fields of reconstructed pyramidal cells in layers 3 and 2 of rat somatosensory barrel cortex. *J. Physiol.* *553*, 243–265.
- Brumberg, J.C., Pinto, D.J., and Simons, D.J. (1996). Spatial gradients and inhibitory summation in the rat whisker barrel system. *J. Neurophysiol.* *76*, 130–140.
- Bruno, R.M., and Simons, D.J. (2002). Feedforward Mechanisms of Excitatory and Inhibitory Cortical Receptive Fields. *J. Neurosci.* *22*, 10966–10975.
- Bruno, R.M., Khatri, V., Land, P.W., and Simons, D.J. (2003). Thalamocortical angular tuning domains within individual barrels of rat somatosensory cortex. *J. Neurosci. Off. J. Soc. Neurosci.* *23*, 9565–9574.
- Bureau, I., Saint Paul, F. von, and Svoboda, K. (2006). Interdigitated paralemniscal and lemniscal pathways in the mouse barrel cortex. *PLoS Biol.* *4*, e382.
- Le Cam, J., Estebanez, L., Jacob, V., and Shulz, D.E. (2011). Spatial structure of multiwhisker receptive fields in the barrel cortex is stimulus dependent. *J. Neurophysiol.* *106*, 986–998.
- Cao, Y., Roy, S., Sachdev, R.N.S., and Heck, D.H. (2012). Dynamic correlation between whisking and breathing rhythms in mice. *J. Neurosci. Off. J. Soc. Neurosci.* *32*, 1653–1659.
- Carvell, G.E., and Simons, D.J. (1990). Biometric analyses of vibrissal tactile discrimination in the rat. *J. Neurosci. Off. J. Soc. Neurosci.* *10*, 2638–2648.
- Chakrabarti, S., and Alloway, K.D. (2006). Differential origin of projections from SI barrel cortex to the whisker representations in SII and MI. *J. Comp. Neurol.* *498*, 624–636.
- Chemla, S., and Chavane, F. (2010). A biophysical cortical column model to study the multi-component origin of the VSDI signal. *NeuroImage* *53*, 420–438.
- Chen, J.L., Carta, S., Soldado-Magraner, J., Schneider, B.L., and Helmchen, F. (2013). Behaviour-dependent recruitment of long-range projection neurons in somatosensory cortex. *Nature* *499*, 336–340.
- Chmielowska, J., Carvell, G.E., and Simons, D.J. (1989). Spatial organization of thalamocortical and corticothalamic projection systems in the rat Sml barrel cortex. *J. Comp. Neurol.* *285*, 325–338.
- Civillico, E.F., and Contreras, D. (2006). Integration of Evoked Responses in Supragranular Cortex Studied With Optical Recordings In Vivo. *J. Neurophysiol.* *96*, 336–351.

- Clancy, K.B., Schnepel, P., Rao, A.T., and Feldman, D.E. (2015). Structure of a Single Whisker Representation in Layer 2 of Mouse Somatosensory Cortex. *J. Neurosci.* *35*, 3946–3958.
- Constantinople, C.M., and Bruno, R.M. (2013). Deep cortical layers are activated directly by thalamus. *Science* *340*, 1591–1594.
- Cox, C.L., Huguenard, J.R., and Prince, D.A. (1997). Nucleus reticularis neurons mediate diverse inhibitory effects in thalamus. *Proc. Natl. Acad. Sci. U. S. A.* *94*, 8854–8859.
- Crandall, S.R., Cruikshank, S.J., and Connors, B.W. (2015). A Corticothalamic Switch: Controlling the Thalamus with Dynamic Synapses. *Neuron* *86*, 768–782.
- Crochet, S., and Petersen, C.C.H. (2006). Correlating whisker behavior with membrane potential in barrel cortex of awake mice. *Nat. Neurosci.* *9*, 608–610.
- Crochet, S., Poulet, J.F.A., Kremer, Y., and Petersen, C.C.H. (2011). Synaptic mechanisms underlying sparse coding of active touch. *Neuron* *69*, 1160–1175.
- DeFelipe, J., López-Cruz, P.L., Benavides-Piccione, R., Bielza, C., Larrañaga, P., Anderson, S., Burkhalter, A., Cauli, B., Fairén, A., Feldmeyer, D., et al. (2013). New insights into the classification and nomenclature of cortical GABAergic interneurons. *Nat. Rev. Neurosci.* *14*, 202–216.
- Denk, W. (1994). Two-photon scanning photochemical microscopy: mapping ligand-gated ion channel distributions. *Proc. Natl. Acad. Sci. U. S. A.* *91*, 6629–6633.
- Denk, W., Strickler, J.H., and Webb, W.W. (1990). Two-photon laser scanning fluorescence microscopy. *Science* *248*, 73–76.
- Deschenes, M. (2009). Vibrissal afferents from trigeminus to cortices. *Scholarpedia* *4*, 7454.
- Deschênes, M., Timofeeva, E., and Lavallée, P. (2003). The relay of high-frequency sensory signals in the Whisker-to-barreloid pathway. *J. Neurosci. Off. J. Soc. Neurosci.* *23*, 6778–6787.
- Deschênes, M., Moore, J., and Kleinfeld, D. (2012). Sniffing and whisking in rodents. *Curr. Opin. Neurobiol.* *22*, 243–250.
- Diamond, M.E., Armstrong-James, M., Budway, M.J., and Ebner, F.F. (1992). Somatic sensory responses in the rostral sector of the posterior group (POm) and in the ventral posterior medial nucleus (VPM) of the rat thalamus: dependence on the barrel field cortex. *J. Comp. Neurol.* *319*, 66–84.
- Diamond, M.E., Heimendahl, M. von, Knutsen, P.M., Kleinfeld, D., and Ahissar, E. (2008). “Where” and “what” in the whisker sensorimotor system. *Nat. Rev. Neurosci.* *9*, 601–612.
- Dombeck, D.A., Khabbaz, A.N., Collman, F., Adelman, T.L., and Tank, D.W. (2007). Imaging large-scale neural activity with cellular resolution in awake, mobile mice. *Neuron* *56*, 43–57.

- Dörfl, J. (1982). The musculature of the mystacial vibrissae of the white mouse. *J. Anat.* *135*, 147–154.
- Dörfl, J. (1985). The innervation of the mystacial region of the white mouse: A topographical study. *J. Anat.* *142*, 173–184.
- Drew, P.J., and Feldman, D.E. (2007). Representation of Moving Wavefronts of Whisker Deflection in Rat Somatosensory Cortex. *J. Neurophysiol.* *98*, 1566–1580.
- Ego-Stengel, V., Shulz, D.E., Haidarliu, S., Sosnik, R., and Ahissar, E. (2001). Acetylcholine-dependent induction and expression of functional plasticity in the barrel cortex of the adult rat. *J. Neurophysiol.* *86*, 422–437.
- Ego-Stengel, V., Mello e Souza, T., Jacob, V., and Shulz, D.E. (2005). Spatiotemporal characteristics of neuronal sensory integration in the barrel cortex of the rat. *J. Neurophysiol.* *93*, 1450–1467.
- Ego-Stengel, V., Le Cam, J., and Shulz, D.E. (2012). Coding of apparent motion in the thalamic nucleus of the rat vibrissal somatosensory system. *J. Neurosci. Off. J. Soc. Neurosci.* *32*, 3339–3351.
- Fanselow, E.E., and Nicolelis, M.A. (1999). Behavioral modulation of tactile responses in the rat somatosensory system. *J. Neurosci. Off. J. Soc. Neurosci.* *19*, 7603–7616.
- Feldmeyer, D. (2015). S1 microcircuits. *Scholarpedia* *10*, 7458.
- Feldmeyer, D., Lübke, J., Silver, R.A., and Sakmann, B. (2002). Synaptic connections between layer 4 spiny neurone-layer 2/3 pyramidal cell pairs in juvenile rat barrel cortex: physiology and anatomy of interlaminar signalling within a cortical column. *J. Physiol.* *538*, 803–822.
- Feldmeyer, D., Brecht, M., Helmchen, F., Petersen, C.C.H., Poulet, J.F.A., Staiger, J.F., Luhmann, H.J., and Schwarz, C. (2013). Barrel cortex function. *Prog. Neurobiol.* *103*, 3–27.
- Ferezou, I., Bolea, S., and Petersen, C.C.H. (2006). Visualizing the cortical representation of whisker touch: voltage-sensitive dye imaging in freely moving mice. *Neuron* *50*, 617–629.
- Ferezou, I., Haiss, F., Gentet, L.J., Aronoff, R., Weber, B., and Petersen, C.C.H. (2007). Spatiotemporal dynamics of cortical sensorimotor integration in behaving mice. *Neuron* *56*, 907–923.
- Fisher, N.I. (1995). *Statistical Analysis of Circular Data* (Cambridge University Press).
- Fitzgerald, O. (1940). Discharges from the sensory organs of the cat's vibrissae and the modification in their activity by ions. *J. Physiol.* *98*, 163–178.
- Fox, K. (2008). *Barrel Cortex* (Cambridge University Press).
- Furuta, T., Nakamura, K., and Deschenes, M. (2006). Angular Tuning Bias of Vibrissa-Responsive Cells in the Paralemniscal Pathway. *J. Neurosci.* *26*, 10548–10557.

- Furuta, T., Timofeeva, E., Nakamura, K., Okamoto-Furuta, K., Togo, M., Kaneko, T., and Deschênes, M. (2008). Inhibitory gating of vibrissal inputs in the brainstem. *J. Neurosci. Off. J. Soc. Neurosci.* *28*, 1789–1797.
- Gamzu, E., and Ahissar, E. (2001). Importance of temporal cues for tactile spatial- frequency discrimination. *J. Neurosci. Off. J. Soc. Neurosci.* *21*, 7416–7427.
- Ganguly, K., and Kleinfeld, D. (2004). Goal-directed whisking increases phase-locking between vibrissa movement and electrical activity in primary sensory cortex in rat. *Proc. Natl. Acad. Sci. U. S. A.* *101*, 12348–12353.
- Gao, P., Bermejo, R., and Zeigler, H.P. (2001). Whisker deafferentation and rodent whisking patterns: behavioral evidence for a central pattern generator. *J. Neurosci. Off. J. Soc. Neurosci.* *21*, 5374–5380.
- Gentet, L.J., Avermann, M., Matyas, F., Staiger, J.F., and Petersen, C.C.H. (2010). Membrane potential dynamics of GABAergic neurons in the barrel cortex of behaving mice. *Neuron* *65*, 422–435.
- Ghazanfar, A.A., and Nicolelis, M.A.L. (1997). Nonlinear Processing of Tactile Information in the Thalamocortical Loop. *J. Neurophysiol.* *78*, 506–510.
- Gibson, J.M., and Welker, W.I. (1983). Quantitative studies of stimulus coding in first-order vibrissa afferents of rats. 1. Receptive field properties and threshold distributions. *Somatosens. Res.* *1*, 51–67.
- Göbel, W., Kampa, B.M., and Helmchen, F. (2007). Imaging cellular network dynamics in three dimensions using fast 3D laser scanning. *Nat. Methods* *4*, 73–79.
- Goldreich, D., Peterson, B.E., and Merzenich, M.M. (1998). Optical imaging and electrophysiology of rat barrel cortex. II. Responses to paired-vibrissa deflections. *Cereb. Cortex N. Y. N 1991* *8*, 184–192.
- Golshani, P., Liu, X.-B., and Jones, E.G. (2001). Differences in quantal amplitude reflect GluR4- subunit number at corticothalamic synapses on two populations of thalamic neurons. *Proc. Natl. Acad. Sci. U. S. A.* *98*, 4172–4177.
- Gottlieb, J.P., and Keller, A. (1997). Intrinsic circuitry and physiological properties of pyramidal neurons in rat barrel cortex. *Exp. Brain Res.* *115*, 47–60.
- Grandy, T.H., Greenfield, S.A., and Devonshire, I.M. (2012). An evaluation of in vivo voltage-sensitive dyes: pharmacological side effects and signal-to-noise ratios after effective removal of brain-pulsation artifacts. *J. Neurophysiol.* *108*, 2931–2945.
- Grant, R.A., Mitchinson, B., Fox, C.W., and Prescott, T.J. (2009). Active Touch Sensing in the Rat: Anticipatory and Regulatory Control of Whisker Movements During Surface Exploration. *J. Neurophysiol.* *101*, 862–874.
- Grinvald, A., and Hildesheim, R. (2004). VSDI: a new era in functional imaging of cortical dynamics. *Nat. Rev. Neurosci.* *5*, 874–885.

- Grinvald, A., Anglister, L., Freeman, J.A., Hildesheim, R., and Manker, A. (1984). Real-time optical imaging of naturally evoked electrical activity in intact frog brain. *Nature* 308, 848–850.
- Grinvald, A., Lieke, E., Frostig, R.D., Gilbert, C.D., and Wiesel, T.N. (1986). Functional architecture of cortex revealed by optical imaging of intrinsic signals. *Nature* 324, 361–364.
- Guić-Robles, E., Valdivieso, C., and Guajardo, G. (1989). Rats can learn a roughness discrimination using only their vibrissal system. *Behav. Brain Res.* 31, 285–289.
- Guy, J., Wagener, R.J., Möck, M., and Staiger, J.F. (2015). Persistence of Functional Sensory Maps in the Absence of Cortical Layers in the Somatosensory Cortex of Reeler Mice. *Cereb. Cortex* 25, 2517–2528.
- Haidarliu, S. (2015). Whisking musculature. *Scholarpedia* 10, 32331.
- Haidarliu, S., and Ahissar, E. (1997). Spatial organization of facial vibrissae and cortical barrels in the guinea pig and golden hamster. *J. Comp. Neurol.* 385, 515–527.
- Haidarliu, S., Kleinfeld, D., Deschênes, M., and Ahissar, E. (2015). The Musculature That Drives Active Touch by Vibrissae and Nose in Mice. *Anat. Rec. Hoboken NJ* 2007 298, 1347–1358.
- Harris, K.D., and Mrsic-Flogel, T.D. (2013). Cortical connectivity and sensory coding. *Nature* 503, 51–58.
- Harris, K.D., and Shepherd, G.M.G. (2015). The neocortical circuit: themes and variations. *Nat. Neurosci.* 18, 170–181.
- Hartline, H.K. (1938). The Response of Single Optic Nerve Fibers of the Vertebrate Eye to Illumination of the Retina. *Am. J. Physiol. -- Leg. Content* 121, 400–415.
- Harvey, M.A., Sachdev, R.N., and Zeigler, H.P. (2001). Cortical barrel field ablation and unconditioned whisking kinematics. *Somatosens. Mot. Res.* 18, 223–227.
- Helmchen, F., Imoto, K., and Sakmann, B. (1996). Ca²⁺ buffering and action potential-evoked Ca²⁺ signaling in dendrites of pyramidal neurons. *Biophys. J.* 70, 1069–1081.
- Helmstaedter, M., Sakmann, B., and Feldmeyer, D. (2009a). Neuronal Correlates of Local, Lateral, and Translaminar Inhibition with Reference to Cortical Columns. *Cereb. Cortex* 19, 926–937.
- Helmstaedter, M., Sakmann, B., and Feldmeyer, D. (2009b). L2/3 Interneuron Groups Defined by Multiparameter Analysis of Axonal Projection, Dendritic Geometry, and Electrical Excitability. *Cereb. Cortex* 19, 951–962.
- Herkenham, M. (1980). Laminar organization of thalamic projections to the rat neocortex. *Science* 207, 532–535.

- Hestrin, S., and Armstrong, W.E. (1996). Morphology and physiology of cortical neurons in layer I. *J. Neurosci. Off. J. Soc. Neurosci.* *16*, 5290–5300.
- Higley, M.J., and Contreras, D. (2003). Nonlinear Integration of Sensory Responses in the Rat Barrel Cortex: An Intracellular Study In Vivo. *J. Neurosci.* *23*, 10190–10200.
- Higley, M.J., and Contreras, D. (2005). Integration of Synaptic Responses to Neighboring Whiskers in Rat Barrel Cortex In Vivo. *J. Neurophysiol.* *93*, 1920–1934.
- Higley, M.J., and Contreras, D. (2007). Cellular mechanisms of suppressive interactions between somatosensory responses in vivo. *J. Neurophysiol.* *97*, 647–658.
- Hires, S.A., Pammer, L., Svoboda, K., and Golomb, D. (2013). Tapered whiskers are required for active tactile sensation. *eLife* *2*, e01350.
- Hoeflinger, B.F., Bennett-Clarke, C.A., Chiaia, N.L., Killackey, H.P., and Rhoades, R.W. (1995). Patterning of local intracortical projections within the vibrissae representation of rat primary somatosensory cortex. *J. Comp. Neurol.* *354*, 551–563.
- Houades, V., Koulakoff, A., Ezan, P., Seif, I., and Giaume, C. (2008). Gap Junction-Mediated Astrocytic Networks in the Mouse Barrel Cortex. *J. Neurosci.* *28*, 5207–5217.
- Hubel, D.H. (1959). Single unit activity in striate cortex of unrestrained cats. *J. Physiol.* *147*, 226–238.
- Hubel, D.H., and Wiesel, T.N. (1959). Receptive fields of single neurones in the cat's striate cortex. *J. Physiol.* *148*, 574–591.
- Hubel, D.H., and Wiesel, T.N. (1962). Receptive fields, binocular interaction and functional architecture in the cat's visual cortex. *J. Physiol.* *160*, 106–154.
- Ito, M. (1981). Some quantitative aspects of vibrissa-driven neuronal responses in rat neocortex. *J. Neurophysiol.* *46*, 705–715.
- Ito, M. (1992). Simultaneous visualization of cortical barrels and horseradish peroxidase-injected layer 5b vibrissa neurones in the rat. *J. Physiol.* *454*, 247–265.
- Jacob, V., Le Cam, J., Ego-Stengel, V., and Shulz, D.E. (2008). Emergent Properties of Tactile Scenes Selectively Activate Barrel Cortex Neurons. *Neuron* *60*, 1112–1125.
- Jacob, V., Estebanez, L., Le Cam, J., Tiercelin, J.-Y., Parra, P., Parésys, G., and Shulz, D.E. (2010). The Matrix: a new tool for probing the whisker-to-barrel system with natural stimuli. *J. Neurosci. Methods* *189*, 65–74.
- Jacquin, M.F., Wiegand, M.R., and Renehan, W.E. (1990). Structure-function relationships in rat brain stem subnucleus interpolaris. VIII. Cortical inputs. *J. Neurophysiol.* *64*, 3–27.
- Jan, T.A., Lu, L., Li, C.-X., Williams, R.W., and Waters, R.S. (2008). Genetic analysis of posterior medial barrel subfield (PMBSF) size in somatosensory cortex (SI) in recombinant inbred strains of mice. *BMC Neurosci.* *9*, 3.

- Jancke, D., Chavane, F., Naaman, S., and Grinvald, A. (2004). Imaging cortical correlates of illusion in early visual cortex. *Nature* 428, 423–426.
- Jensen, K.F., and Killackey, H.P. (1987). Terminal arbors of axons projecting to the somatosensory cortex of the adult rat. I. The normal morphology of specific thalamocortical afferents. *J. Neurosci. Off. J. Soc. Neurosci.* 7, 3529–3543.
- Jin, T.-E., Witzemann, V., and Brecht, M. (2004). Fiber Types of the Intrinsic Whisker Muscle and Whisking Behavior. *J. Neurosci.* 24, 3386–3393.
- Jones, L.M., Depireux, D.A., Simons, D.J., and Keller, A. (2004). Robust temporal coding in the trigeminal system. *Science* 304, 1986–1989.
- Kaas, J.H., Nelson, R.J., Sur, M., Lin, C.S., and Merzenich, M.M. (1979). Multiple representations of the body within the primary somatosensory cortex of primates. *Science* 204, 521–523.
- Kampa, B.M., Göbel, W., and Helmchen, F. (2011). Measuring Neuronal Population Activity Using 3D Laser Scanning. *Cold Spring Harb. Protoc.* 2011, pdb.prot066597.
- Keller, A., and White, E.L. (1987). Synaptic organization of GABAergic neurons in the mouse Sml cortex. *J. Comp. Neurol.* 262, 1–12.
- Kenet, T., Bibitchkov, D., Tsodyks, M., Grinvald, A., and Arieli, A. (2003). Spontaneously emerging cortical representations of visual attributes. *Nature* 425, 954–956.
- Kerr, J.N.D., Greenberg, D., and Helmchen, F. (2005). Imaging input and output of neocortical networks in vivo. *Proc. Natl. Acad. Sci. U. S. A.* 102, 14063–14068.
- Kerr, J.N.D., de Kock, C.P.J., Greenberg, D.S., Bruno, R.M., Sakmann, B., and Helmchen, F. (2007). Spatial organization of neuronal population responses in layer 2/3 of rat barrel cortex. *J. Neurosci. Off. J. Soc. Neurosci.* 27, 13316–13328.
- Kida, H., Shimegi, S., and Sato, H. (2005). Similarity of direction tuning among responses to stimulation of different whiskers in neurons of rat barrel cortex. *J. Neurophysiol.* 94, 2004–2018.
- Kim, U., and Ebner, F.F. (1999). Barrels and septa: Separate circuits in rat barrel field cortex. *J. Comp. Neurol.* 408, 489–505.
- Kleinfeld, D., and Delaney, K.R. (1996). Distributed representation of vibrissa movement in the upper layers of somatosensory cortex revealed with voltage-sensitive dyes. *J. Comp. Neurol.* 375, 89–108.
- Kleinfeld, D., and Deschênes, M. (2011). Neuronal Basis for Object Location in the Vibrissa Scanning Sensorimotor System. *Neuron* 72, 455–468.
- Kleinfeld, D., Deschênes, M., Wang, F., and Moore, J.D. (2014). More than a rhythm of life: breathing as a binder of orofacial sensation. *Nat. Neurosci.* 17, 647–651.

- Ko, H., Cossell, L., Baragli, C., Antolik, J., Clopath, C., Hofer, S.B., and Mrsic-Flogel, T.D. (2013). The emergence of functional microcircuits in visual cortex. *Nature* *496*, 96–100.
- de Kock, C.P.J., Bruno, R.M., Spors, H., and Sakmann, B. (2007). Layer- and cell-type-specific suprathreshold stimulus representation in rat primary somatosensory cortex. *J. Physiol.* *581*, 139–154.
- Koralek, K.A., Jensen, K.F., and Killackey, H.P. (1988). Evidence for two complementary patterns of thalamic input to the rat somatosensory cortex. *Brain Res.* *463*, 346–351.
- Kremer, Y., Léger, J.-F., Goodman, D., Brette, R., and Bourdieu, L. (2011). Late emergence of the vibrissa direction selectivity map in the rat barrel cortex. *J. Neurosci. Off. J. Soc. Neurosci.* *31*, 10689–10700.
- Krubitzer, L.A., and Seelke, A.M.H. (2012). Cortical evolution in mammals: The bane and beauty of phenotypic variability. *Proc. Natl. Acad. Sci. U. S. A.* *109*, 10647–10654.
- Krupa, D.J., Matell, M.S., Brisben, A.J., Oliveira, L.M., and Nicolelis, M.A. (2001). Behavioral properties of the trigeminal somatosensory system in rats performing whisker-dependent tactile discriminations. *J. Neurosci. Off. J. Soc. Neurosci.* *21*, 5752–5763.
- Kyriazi, H.T., Carvell, G.E., Brumberg, J.C., and Simons, D.J. (1996). Quantitative effects of GABA and bicuculline methiodide on receptive field properties of neurons in real and simulated whisker barrels. *J. Neurophysiol.* *75*, 547–560.
- Lam, Y.-W., and Sherman, S.M. (2010). Functional Organization of the Somatosensory Cortical Layer 6 Feedback to the Thalamus. *Cereb. Cortex* *20*, 13–24.
- Land, P.W., and Erickson, S.L. (2005). Subbarrel domains in rat somatosensory (S1) cortex. *J. Comp. Neurol.* *490*, 414–426.
- Land, P.W., and Simons, D.J. (1985). Metabolic and structural correlates of the vibrissae representation in the thalamus of the adult rat. *Neurosci. Lett.* *60*, 319–324.
- Land, P.W., Buffer, S.A., and Yaskosky, J.D. (1995). Barreloids in adult rat thalamus: three-dimensional architecture and relationship to somatosensory cortical barrels. *J. Comp. Neurol.* *355*, 573–588.
- Lefort, S., Tómm, C., Floyd Sarria, J.-C., and Petersen, C.C.H. (2009). The excitatory neuronal network of the C2 barrel column in mouse primary somatosensory cortex. *Neuron* *61*, 301–316.
- Leiser, S.C., and Moxon, K.A. (2006). Relationship Between Physiological Response Type (RA and SA) and Vibrissal Receptive Field of Neurons Within the Rat Trigeminal Ganglion. *J. Neurophysiol.* *95*, 3129–3145.
- Lenschow, C., and Brecht, M. (2015). Barrel cortex membrane potential dynamics in social touch. *Neuron* *85*, 718–725.

- Leyton, A.S., and Sherrington, C.S. (1917). OBSERVATIONS ON THE EXCITABLE CORTEX OF THE CHIMPANZEE, ORANG-UTAN, AND GORILLA. *Q. J. Exp. Physiol.* *11*, 135–222.
- Li, L., and Ebner, F.F. (2007). Cortical Modulation of Spatial and Angular Tuning Maps in the Rat Thalamus. *J. Neurosci.* *27*, 167–179.
- Lichtenstein, S.H., Carvell, G.E., and Simons, D.J. (1990). Responses of rat trigeminal ganglion neurons to movements of vibrissae in different directions. *Somatosens. Mot. Res.* *7*, 47–65.
- Lichtman, J.W., Livet, J., and Sanes, J.R. (2008). A technicolour approach to the connectome. *Nat. Rev. Neurosci.* *9*, 417–422.
- Lippert, M.T., Takagaki, K., Xu, W., Huang, X., and Wu, J.-Y. (2007). Methods for voltage-sensitive dye imaging of rat cortical activity with high signal-to-noise ratio. *J. Neurophysiol.* *98*, 502–512.
- Livet, J., Weissman, T.A., Kang, H., Draft, R.W., Lu, J., Bennis, R.A., Sanes, J.R., and Lichtman, J.W. (2007). Transgenic strategies for combinatorial expression of fluorescent proteins in the nervous system. *Nature* *450*, 56–62.
- Van Der Loos, H. (1976). Barreloids in mouse somatosensory thalamus. *Neurosci. Lett.* *2*, 1–6.
- Lu, S.M., and Lin, R.C. (1993). Thalamic afferents of the rat barrel cortex: a light- and electron-microscopic study using *Phaseolus vulgaris* leucoagglutinin as an anterograde tracer. *Somatosens. Mot. Res.* *10*, 1–16.
- Lübke, J., Egger, V., Sakmann, B., and Feldmeyer, D. (2000). Columnar organization of dendrites and axons of single and synaptically coupled excitatory spiny neurons in layer 4 of the rat barrel cortex. *J. Neurosci. Off. J. Soc. Neurosci.* *20*, 5300–5311.
- Luhmann, H.J., Huston, J.P., and Hasenöhr, R.U. (2005). Contralateral increase in thigmotactic scanning following unilateral barrel-cortex lesion in mice. *Behav. Brain Res.* *157*, 39–43.
- Ma, P.M. (1991). The barrelettes--architectonic vibrissal representations in the brainstem trigeminal complex of the mouse. I. Normal structural organization. *J. Comp. Neurol.* *309*, 161–199.
- Ma, P.M., and Woolsey, T.A. (1984). Cytoarchitectonic correlates of the vibrissae in the medullary trigeminal complex of the mouse. *Brain Res.* *306*, 374–379.
- Manns, I.D., Sakmann, B., and Brecht, M. (2004). Sub- and suprathreshold receptive field properties of pyramidal neurones in layers 5A and 5B of rat somatosensory barrel cortex. *J. Physiol.* *556*, 601–622.
- Mao, T., Kusefoglou, D., Hooks, B.M., Huber, D., Petreanu, L., and Svoboda, K. (2011). Long-Range Neuronal Circuits Underlying the Interaction between Sensory and Motor Cortex. *Neuron* *72*, 111–123.

- Maravall, M., Petersen, R.S., Fairhall, A.L., Arabzadeh, E., and Diamond, M.E. (2007). Shifts in coding properties and maintenance of information transmission during adaptation in barrel cortex. *PLoS Biol.* *5*, e19.
- Markram, H., Toledo-Rodriguez, M., Wang, Y., Gupta, A., Silberberg, G., and Wu, C. (2004). Interneurons of the neocortical inhibitory system. *Nat. Rev. Neurosci.* *5*, 793–807.
- Mennerick, S., Chisari, M., Shu, H.-J., Taylor, A., Vasek, M., Eisenman, L.N., and Zorumski, C.F. (2010). Diverse Voltage-Sensitive Dyes Modulate GABA_A Receptor Function. *J. Neurosci.* *30*, 2871–2879.
- Meyer, H.S., Wimmer, V.C., Oberlaender, M., de Kock, C.P.J., Sakmann, B., and Helmstaedter, M. (2010). Number and laminar distribution of neurons in a thalamocortical projection column of rat vibrissal cortex. *Cereb. Cortex N. Y. N 1991* *20*, 2277–2286.
- Meyer, H.S., Schwarz, D., Wimmer, V.C., Schmitt, A.C., Kerr, J.N.D., Sakmann, B., and Helmstaedter, M. (2011). Inhibitory interneurons in a cortical column form hot zones of inhibition in layers 2 and 5A. *Proc. Natl. Acad. Sci. U. S. A.* *108*, 16807–16812.
- Meyer, H.S., Egger, R., Guest, J.M., Foerster, R., Reissl, S., and Oberlaender, M. (2013). Cellular organization of cortical barrel columns is whisker-specific. *Proc. Natl. Acad. Sci. U. S. A.* *110*, 19113–19118.
- Milani, H., Steiner, H., and Huston, J.P. (1989). Analysis of recovery from behavioral asymmetries induced by unilateral removal of vibrissae in the rat. *Behav. Neurosci.* *103*, 1067–1074.
- Minnery, B.S., and Simons, D.J. (2003). Response properties of whisker-associated trigeminothalamic neurons in rat nucleus principalis. *J. Neurophysiol.* *89*, 40–56.
- Minnery, B.S., Bruno, R.M., and Simons, D.J. (2003). Response transformation and receptive-field synthesis in the lemniscal trigeminothalamic circuit. *J. Neurophysiol.* *90*, 1556–1570.
- Mirabella, G., Battiston, S., and Diamond, M.E. (2001). Integration of Multiple-whisker Inputs in Rat Somatosensory Cortex. *Cereb. Cortex* *11*, 164–170.
- Miyawaki, A., Llopis, J., Heim, R., McCaffery, J.M., Adams, J.A., Ikura, M., and Tsien, R.Y. (1997). Fluorescent indicators for Ca²⁺ based on green fluorescent proteins and calmodulin. *Nature* *388*, 882–887.
- Mohajerani, M.H., McVea, D.A., Fingas, M., and Murphy, T.H. (2010). Mirrored Bilateral Slow-Wave Cortical Activity within Local Circuits Revealed by Fast Bihemispheric Voltage-Sensitive Dye Imaging in Anesthetized and Awake Mice. *J. Neurosci.* *30*, 3745–3751.
- Mohajerani, M.H., Chan, A.W., Mohsenvand, M., LeDue, J., Liu, R., McVea, D.A., Boyd, J.D., Wang, Y.T., Reimers, M., and Murphy, T.H. (2013). Spontaneous cortical activity alternates between motifs defined by regional axonal projections. *Nat. Neurosci.* *16*, 1426–1435.

- Moore, C.I., and Nelson, S.B. (1998). Spatio-temporal subthreshold receptive fields in the vibrissa representation of rat primary somatosensory cortex. *J. Neurophysiol.* *80*, 2882–2892.
- Mountcastle, V.B. (1957). Modality and topographic properties of single neurons of cat's somatic sensory cortex. *J. Neurophysiol.* *20*, 408–434.
- Mountcastle, V.B. (1997). The columnar organization of the neocortex. *Brain* *120*, 701–722.
- Mutoh, H., Mishina, Y., Gallero-Salas, Y., and Knöpfel, T. (2015). Comparative performance of a genetically-encoded voltage indicator and a blue voltage sensitive dye for large scale cortical voltage imaging. *Front. Cell. Neurosci.* *9*, 147.
- Narayanan, R.T., Egger, R., Johnson, A.S., Mansvelder, H.D., Sakmann, B., de Kock, C.P.J., and Oberlaender, M. (2015). Beyond Columnar Organization: Cell Type- and Target Layer-Specific Principles of Horizontal Axon Projection Patterns in Rat Vibrissal Cortex. *Cereb. Cortex N. Y. N* *1991*.
- Di Noto, P.M., Newman, L., Wall, S., and Einstein, G. (2013). The Hermunculus: What Is Known about the Representation of the Female Body in the Brain? *Cereb. Cortex* *23*, 1005–1013.
- Oberlaender, M., de Kock, C.P.J., Bruno, R.M., Ramirez, A., Meyer, H.S., Dercksen, V.J., Helmstaedter, M., and Sakmann, B. (2012). Cell type-specific three-dimensional structure of thalamocortical circuits in a column of rat vibrissal cortex. *Cereb. Cortex N. Y. N* *1991* *22*, 2375–2391.
- Orbach, H.S., Cohen, L.B., and Grinvald, A. (1985). Optical mapping of electrical activity in rat somatosensory and visual cortex. *J. Neurosci. Off. J. Soc. Neurosci.* *5*, 1886–1895.
- Pál, I., Kardos, J., Dobolyi, Á., and Héja, L. (2015). Appearance of fast astrocytic component in voltage-sensitive dye imaging of neural activity. *Mol. Brain* *8*, 35.
- Pantoja, J., Ribeiro, S., Wiest, M., Soares, E., Gervasoni, D., Lemos, N.A.M., and Nicolelis, M.A.L. (2007). Neuronal activity in the primary somatosensory thalamocortical loop is modulated by reward contingency during tactile discrimination. *J. Neurosci. Off. J. Soc. Neurosci.* *27*, 10608–10620.
- Pasternak, J.R., and Woolsey, T.A. (1975). The number, size and spatial distribution of neurons in lamina IV of the mouse Sml neocortex. *J. Comp. Neurol.* *160*, 291–306.
- Penfield, W., and Boldrey, E. (1937). Somatic Motor and Sensory Representation in the Cerebral Cortex of Man as Studied by Electrical Stimulation. *Brain* *60*, 389–443.
- Penfield, W., and Rasmussen, T. (1950). *The cerebral cortex of man; a clinical study of localization of function* (Oxford, England: Macmillan).
- Petersen, C.C.H. (2007). The functional organization of the barrel cortex. *Neuron* *56*, 339–355.

- Petersen, C.C.H. (2014). Cortical Control of Whisker Movement. *Annu. Rev. Neurosci.* 37, 183–203.
- Petersen, C.C.H., Grinvald, A., and Sakmann, B. (2003a). Spatiotemporal dynamics of sensory responses in layer 2/3 of rat barrel cortex measured in vivo by voltage-sensitive dye imaging combined with whole-cell voltage recordings and neuron reconstructions. *J. Neurosci. Off. J. Soc. Neurosci.* 23, 1298–1309.
- Petersen, C.C.H., Hahn, T.T.G., Mehta, M., Grinvald, A., and Sakmann, B. (2003b). Interaction of sensory responses with spontaneous depolarization in layer 2/3 barrel cortex. *Proc. Natl. Acad. Sci. U. S. A.* 100, 13638–13643.
- Petreaunu, L., Mao, T., Sternson, S.M., and Svoboda, K. (2009). The subcellular organization of neocortical excitatory connections. *Nature* 457, 1142–1145.
- Pierret, T., Lavallée, P., and Deschênes, M. (2000). Parallel streams for the relay of vibrissal information through thalamic barreloids. *J. Neurosci. Off. J. Soc. Neurosci.* 20, 7455–7462.
- Porter, J.T., Johnson, C.K., and Agmon, A. (2001). Diverse types of interneurons generate thalamus-evoked feedforward inhibition in the mouse barrel cortex. *J. Neurosci. Off. J. Soc. Neurosci.* 21, 2699–2710.
- Poulet, J.F.A., and Petersen, C.C.H. (2008). Internal brain state regulates membrane potential synchrony in barrel cortex of behaving mice. *Nature* 454, 881–885.
- Puccini, G.D., Compte, A., and Maravall, M. (2006). Stimulus Dependence of Barrel Cortex Directional Selectivity. *PLoS ONE* 1, e137.
- Qi, G., and Feldmeyer, D. (2015). Dendritic Target Region-Specific Formation of Synapses Between Excitatory Layer 4 Neurons and Layer 6 Pyramidal Cells. *Cereb. Cortex* bhu334.
- Ren, J.Q., Aika, Y., Heizmann, C.W., and Kosaka, T. (1992). Quantitative analysis of neurons and glial cells in the rat somatosensory cortex, with special reference to GABAergic neurons and parvalbumin-containing neurons. *Exp. Brain Res.* 92, 1–14.
- Reyes, A., and Sakmann, B. (1999). Developmental switch in the short-term modification of unitary EPSPs evoked in layer 2/3 and layer 5 pyramidal neurons of rat neocortex. *J. Neurosci. Off. J. Soc. Neurosci.* 19, 3827–3835.
- Rice, F.L., Kinnman, E., Aldskogius, H., Johansson, O., and Arvidsson, J. (1993). The innervation of the mystacial pad of the rat as revealed by PGP 9.5 immunofluorescence. *J. Comp. Neurol.* 337, 366–385.
- Rodgers, K.M., Benison, A.M., and Barth, D.S. (2006). Two-dimensional coincidence detection in the vibrissa/barrel field. *J. Neurophysiol.* 96, 1981–1990.
- Sachdev, R.N., Sellien, H., and Ebner, F. (2001). Temporal organization of multi-whisker contact in rats. *Somatosens. Mot. Res.* 18, 91–100.

- Sachdev, R.N.S., Sato, T., and Ebner, F.F. (2002). Divergent movement of adjacent whiskers. *J. Neurophysiol.* *87*, 1440–1448.
- Saig, A., Arieli, A., and Ahissar, E. (2010). What Is It Like to Be a Rat? Sensory Augmentation Study. In *Haptics: Generating and Perceiving Tangible Sensations*, A.M.L. Kappers, J.B.F. van Erp, W.M.B. Tiest, and F.C.T. van der Helm, eds. (Springer Berlin Heidelberg), pp. 298–305.
- Sato, T.R., Gray, N.W., Mainen, Z.F., and Svoboda, K. (2007). The functional microarchitecture of the mouse barrel cortex. *PLoS Biol.* *5*, e189.
- Schott, G.D. (1993). Penfield's homunculus: a note on cerebral cartography. *J. Neurol. Neurosurg. Psychiatry* *56*, 329–333.
- Schubert, D., Staiger, J.F., Cho, N., Kötter, R., Zilles, K., and Luhmann, H.J. (2001). Layer-specific intracolumnar and transcolumnar functional connectivity of layer V pyramidal cells in rat barrel cortex. *J. Neurosci. Off. J. Soc. Neurosci.* *21*, 3580–3592.
- Schubert, D., Kötter, R., and Staiger, J.F. (2007). Mapping functional connectivity in barrel-related columns reveals layer- and cell type-specific microcircuits. *Brain Struct. Funct.* *212*, 107–119.
- Sehara, K., Wakimoto, M., Ako, R., and Kawasaki, H. (2012). Distinct developmental principles underlie the formation of ipsilateral and contralateral whisker-related axonal patterns of layer 2/3 neurons in the barrel cortex. *Neuroscience* *226*, 289–304.
- Semba, K., and Komisaruk, B.R. (1984). Neural substrates of two different rhythmical vibrissal movements in the rat. *Neuroscience* *12*, 761–774.
- Shimegi, S., Ichikawa, T., Akasaki, T., and Sato, H. (1999). Temporal characteristics of response integration evoked by multiple whisker stimulations in the barrel cortex of rats. *J. Neurosci. Off. J. Soc. Neurosci.* *19*, 10164–10175.
- Shimegi, S., Akasaki, T., Ichikawa, T., and Sato, H. (2000). Physiological and Anatomical Organization of Multiwhisker Response Interactions in the Barrel Cortex of Rats. *J. Neurosci.* *20*, 6241–6248.
- Shoham, D., Glaser, D.E., Arieli, A., Kenet, T., Wijnbergen, C., Toledo, Y., Hildesheim, R., and Grinvald, A. (1999). Imaging cortical dynamics at high spatial and temporal resolution with novel blue voltage-sensitive dyes. *Neuron* *24*, 791–802.
- Shulz, D., and Ego-Stengel, V. (2012). S1 long-term plasticity. *Scholarpedia* *7*, 7615.
- Simons, D.J. (1978). Response properties of vibrissa units in rat SI somatosensory neocortex. *J. Neurophysiol.* *41*, 798–820.
- Simons, D.J. (1983). Multi-whisker stimulation and its effects on vibrissa units in rat S1 barrel cortex. *Brain Res.* *276*, 178–182.
- Simons, D.J. (1985). Temporal and spatial integration in the rat SI vibrissa cortex. *J. Neurophysiol.* *54*, 615–635.

Simons, D.J., and Carvell, G.E. (1989). Thalamocortical response transformation in the rat vibrissa/barrel system. *J. Neurophysiol.* *61*, 311–330.

Sims, R.E., Butcher, J.B., Parri, H.R., Glazewski, S., Sims, R.E., Butcher, J.B., Parri, H.R., and Glazewski, S. (2015). Astrocyte and Neuronal Plasticity in the Somatosensory System, Astrocyte and Neuronal Plasticity in the Somatosensory System. *Neural Plast.* *2015*, *2015*, e732014.

Sofroniew, N.J., and Svoboda, K. (2015). Whisking. *Curr. Biol.* *25*, R137–R140.

Sofroniew, N.J., Cohen, J.D., Lee, A.K., and Svoboda, K. (2014). Natural whisker-guided behavior by head-fixed mice in tactile virtual reality. *J. Neurosci. Off. J. Soc. Neurosci.* *34*, 9537–9550.

Staba, R.J., Ard, T.D., Benison, A.M., and Barth, D.S. (2005). Intracortical Pathways Mediate Nonlinear Fast Oscillation (>200 Hz) Interactions Within Rat Barrel Cortex. *J. Neurophysiol.* *93*, 2934–2939.

Staiger, J.F., Flaggmeyer, I., Schubert, D., Zilles, K., Kötter, R., and Luhmann, H.J. (2004). Functional Diversity of Layer IV Spiny Neurons in Rat Somatosensory Cortex: Quantitative Morphology of Electrophysiologically Characterized and Biocytin Labeled Cells. *Cereb. Cortex* *14*, 690–701.

Stern, E.A., Maravall, M., and Svoboda, K. (2001). Rapid Development and Plasticity of Layer 2/3 Maps in Rat Barrel Cortex In Vivo. *Neuron* *31*, 305–315.

Stosiek, C., Garaschuk, O., Holthoff, K., and Konnerth, A. (2003). In vivo two-photon calcium imaging of neuronal networks. *Proc. Natl. Acad. Sci. U. S. A.* *100*, 7319–7324.

Svoboda, K., Denk, W., Kleinfeld, D., and Tank, D.W. (1997). In vivo dendritic calcium dynamics in neocortical pyramidal neurons. *Nature* *385*, 161–165.

Swadlow, H.A., and Gusev, A.G. (2002). Receptive-field construction in cortical inhibitory interneurons. *Nat. Neurosci.* *5*, 403–404.

Szwed, M., Bagdasarian, K., and Ahissar, E. (2003). Encoding of vibrissal active touch. *Neuron* *40*, 621–630.

Szwed, M., Bagdasarian, K., Blumenfeld, B., Barak, O., Derdikman, D., and Ahissar, E. (2006). Responses of trigeminal ganglion neurons to the radial distance of contact during active vibrissal touch. *J. Neurophysiol.* *95*, 791–802.

Takagaki, K., Zhang, C., Wu, J.-Y., and Lippert, M.T. (2008). Crossmodal propagation of sensory-evoked and spontaneous activity in the rat neocortex. *Neurosci. Lett.* *431*, 191–196.

Takasaki, C., Okada, R., Mitani, A., Fukaya, M., Yamasaki, M., Fujihara, Y., Shirakawa, T., Tanaka, K., and Watanabe, M. (2008). Glutamate transporters regulate lesion-induced plasticity in the developing somatosensory cortex. *J. Neurosci. Off. J. Soc. Neurosci.* *28*, 4995–5006.

- Takata, N., Mishima, T., Hisatsune, C., Nagai, T., Ebisui, E., Mikoshiba, K., and Hirase, H. (2011). Astrocyte calcium signaling transforms cholinergic modulation to cortical plasticity in vivo. *J. Neurosci. Off. J. Soc. Neurosci.* *31*, 18155–18165.
- Timofeeva, E., Mérette, C., Emond, C., Lavallée, P., and Deschênes, M. (2003). A map of angular tuning preference in thalamic barreloids. *J. Neurosci. Off. J. Soc. Neurosci.* *23*, 10717–10723.
- Towal, R.B., and Hartmann, M.J. (2006). Right-left asymmetries in the whisking behavior of rats anticipate head movements. *J. Neurosci. Off. J. Soc. Neurosci.* *26*, 8838–8846.
- Towal, R.B., Quist, B.W., Gopal, V., Solomon, J.H., and Hartmann, M.J.Z. (2011). The morphology of the rat vibrissal array: a model for quantifying spatiotemporal patterns of whisker-object contact. *PLoS Comput. Biol.* *7*, e1001120.
- Tsodyks, M., Kenet, T., Grinvald, A., and Arieli, A. (1999). Linking spontaneous activity of single cortical neurons and the underlying functional architecture. *Science* *286*, 1943–1946.
- Tsytsarev, V., Pope, D., Pumbo, E., and Garver, W. (2010a). Intrinsic optical imaging of directional selectivity in rat barrel cortex: application of a multidirectional magnetic whisker stimulator. *J. Neurosci. Methods* *189*, 80–83.
- Tsytsarev, V., Pope, D., Pumbo, E., Yablonskii, A., and Hofmann, M. (2010b). Study of the cortical representation of whisker directional deflection using voltage-sensitive dye optical imaging. *NeuroImage* *53*, 233–238.
- Veinante, P., and Deschênes, M. (1999). Single- and multi-whisker channels in the ascending projections from the principal trigeminal nucleus in the rat. *J. Neurosci. Off. J. Soc. Neurosci.* *19*, 5085–5095.
- Veinante, P., Jacquin, M.F., and Deschênes, M. (2000). Thalamic projections from the whisker-sensitive regions of the spinal trigeminal complex in the rat. *J. Comp. Neurol.* *420*, 233–243.
- Vincent, S. (1912). The function of the vibrissae in the behavior of the white rat. *Behav. Monogr.* 1–76.
- Vincent, S.B. (1913). The tactile hair of the white rat. *J. Comp. Neurol.* *23*, 1–34.
- Vincent, J.L., Patel, G.H., Fox, M.D., Snyder, A.Z., Baker, J.T., Van Essen, D.C., Zempel, J.M., Snyder, L.H., Corbetta, M., and Raichle, M.E. (2007). Intrinsic functional architecture in the anaesthetized monkey brain. *Nature* *447*, 83–86.
- Waite, P.M. (1973). The responses of cells in the rat thalamus to mechanical movements of the whiskers. *J. Physiol.* *228*, 541–561.
- Waite, P.M.E. (2004). Chapter 26 - Trigeminal Sensory System. In *The Rat Nervous System* (Third Edition), G. Paxinos, ed. (Burlington: Academic Press), pp. 817–851.

- Webber, R.M., and Stanley, G.B. (2006). Transient and Steady-State Dynamics of Cortical Adaptation. *J. Neurophysiol.* *95*, 2923–2932.
- Welker, C. (1971). Microelectrode delineation of fine grain somatotopic organization of (Sml) cerebral neocortex in albino rat. *Brain Res.* *26*, 259–275.
- Welker, C. (1976). Receptive fields of barrels in the somatosensory neocortex of the rat. *J. Comp. Neurol.* *166*, 173–189.
- Welker, W.I. (1964). Analysis of Sniffing of the Albino Rat. *Behaviour* *22*, 223–244.
- Welker, C., and Woolsey, T.A. (1974). Structure of layer IV in the somatosensory neocortex of the rat: description and comparison with the mouse. *J. Comp. Neurol.* *158*, 437–453.
- Welker, E., and Van der Loos, H. (1986). Quantitative correlation between barrel-field size and the sensory innervation of the whiskerpad: a comparative study in six strains of mice bred for different patterns of mystacial vibrissae. *J. Neurosci. Off. J. Soc. Neurosci.* *6*, 3355–3373.
- Wilent, W.B., and Contreras, D. (2005). Dynamics of excitation and inhibition underlying stimulus selectivity in rat somatosensory cortex. *Nat. Neurosci.* *8*, 1364–1370.
- Wilson, S.P., Law, J.S., Mitchinson, B., Prescott, T.J., and Bednar, J.A. (2010). Modeling the Emergence of Whisker Direction Maps in Rat Barrel Cortex. *PLoS ONE* *5*, e8778.
- Wimmer, V.C., Bruno, R.M., de Kock, C.P.J., Kuner, T., and Sakmann, B. (2010). Dimensions of a projection column and architecture of VPM and POm axons in rat vibrissal cortex. *Cereb. Cortex N. Y. N 1991* *20*, 2265–2276.
- Wineski, L.E. (1983). Movements of the cranial vibrissae in the Golden hamster (*Mesocricetus auratus*). *J. Zool.* *200*, 261–280.
- Wolfe, J., Mende, C., and Brecht, M. (2011). Social facial touch in rats. *Behav. Neurosci.* *125*, 900–910.
- Woolsey, T.A., and Van der Loos, H. (1970). The structural organization of layer IV in the somatosensory region (SI) of mouse cerebral cortex. The description of a cortical field composed of discrete cytoarchitectonic units. *Brain Res.* *17*, 205–242.
- Yaksi, E., and Friedrich, R.W. (2006). Reconstruction of firing rate changes across neuronal populations by temporally deconvolved Ca²⁺ imaging. *Nat. Methods* *3*, 377–383.
- Yamashita, T., Pala, A., Pedrido, L., Kremer, Y., Welker, E., and Petersen, C.C.H. (2013). Membrane Potential Dynamics of Neocortical Projection Neurons Driving Target-Specific Signals. *Neuron* *80*, 1477–1490.
- Yu, C., Derdikman, D., Haidarliu, S., and Ahissar, E. (2006). Parallel thalamic pathways for whisking and touch signals in the rat. *PLoS Biol.* *4*, e124.

Yuste, R., and Simons, D. (1997). Barrels in the Desert: The Sde Boker Workshop on Neocortical Circuits. *Neuron* 19, 231–237.

Zhu, J.J., and Connors, B.W. (1999). Intrinsic firing patterns and whisker-evoked synaptic responses of neurons in the rat barrel cortex. *J. Neurophysiol.* 81, 1171–1183.

Zucker, E., and Welker, W.I. (1969). Coding of somatic sensory input by vibrissae neurons in the rat's trigeminal ganglion. *Brain Res.* 12, 138–156.